Transactions

of the

ASME

APRIL, 1951

VOL. 73, NO. 3

Transactions

of The American Society of Mechanical Engineers

Published on the tenth of every month, except March, June, September, and December

---

Published monthly by The American Society of Mechanical Engineers. Publication office at 20th and Northampton Streets, Easton, Pa. The editorial department is located at the headquarters of the Society, 29 West Thirty-Ninth Street, New York 18, N. Y. Cable address, "Dynamic," New York. Price $1.50 a copy, $12.00 a year for Transactions and the *Journal of Applied Mechanics* to members and affiliates, $1.00 a copy, $6.00 a year. Changes of address must be received at Society headquarters four weeks before they are to be effective on the mailing list. Please send old as well as new address. . . . By-Law: The Society shall not be responsible for statements or opinions advanced in papers or . . . printed in its publications (B13, Par. 4). . . . Entered as second-class matter March 2, 1928, at the Post Office at Easton, Pa., under the Act of August 24, 1912. . . .

Ultrasonic Flaw Detection in Pipes by Means of Shear Waves

By C. D. MORIARTY,[1] SCHENECTADY, N. Y.

This paper describes a procedure by which ultrasonic methods can be applied to the inspection of high-pressure piping. A description of the equipment used is included, together with some basic information by which the applicability to general pipe inspection can be evaluated. In the interest of accenting the application phases, a theoretical discussion of ultrasonic waves and their transformations has been omitted. Although this testing procedure is relatively new, the successful experience with it to date indicates its possibilities for providing additional insurance against hidden defects.

Introduction

THE annular cross section of pipes does not lend itself to adequate inspection for flaws by means of normal ultrasonic methods. This is especially true where it is suspected there are radial-type flaws extending axially, that is, defects whose dimensions are usually greater in a radial direction than in a circumferential direction, such as radial cracks or folds. The need for an ultrasonic method to detect this type of flaw in pipes is evident when it is realized that under internal pressure this orientation would weaken the pipe. The company with which the author is associated has recently developed a procedure by which ultrasonic shear waves can be used for such detection.

Without going into detail, there are three major types of ultrasonic waves which can be used in flaw detection: longitudinal, which is at present in most common routine use; shear, which has only recently been applied to inspection problems; and surface, which has not yet been applied to much routine inspection, at least to the author's knowledge. Of the three types, only longitudinal and shear waves penetrate into metal and become useful as a means of finding subsurface flaws. The present knowledge of these waves and their behavior in solids dates back to studies in seismology (1, 2).[2] A discussion of these waves has been condensed and related to ultrasonics by recent authors (3, 4, 5, 6).

By definition, a longitudinal wave is one in which the particle motion in the medium is parallel to the direction of sound travel. By definition also, a shear wave is one in which the particle motion is normal to the direction of travel. In the application described in this paper, the difference in particle motion of these two types of waves is of less importance than the difference in propagation velocities.

When a longitudinal wave is incident upon an interface between two materials at certain angles, four resultant waves may appear, of which two are transmitted, that is, a longitudinal and a shear wave. The shear wave travels at approximately one half the speed of the longitudinal wave. Taking into account this difference in velocity and the refraction laws of angular transmission from one medium to another, it is possible to take advantage of critical refraction angles to gain certain benefits. One of these benefits is so to choose the angle and materials as to have the faster longitudinal wave completely barred from entering the object under test, leaving only the slower shear wave. This single wave and single speed in the object under test is essential to proper interpretation of reflections from flaws. The shorter wave length as a result of this lower velocity is also conducive to detecting smaller flaws.

We are concerned here with the details in applying a shear wave to the practical problem of testing pipes, that is, equipment, method of test, and interpretation of results.

Equipment

For the testing of pipe with the shear-wave technique, the ultrasonic flaw-detection equipment used for forgings can be used, Fig. 1, provided it has a high sensitivity, and is equipped with an "angle searching unit." Throughout the author's investigations and tests, a Sperry reflectoscope of the UR type

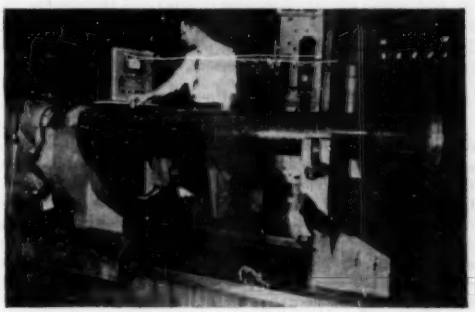

Fig. 1 Ultrasonic Flaw Detection in Pipes by Means of Shear Waves

was used, although any equivalent equipment with reject control facilities would be satisfactory. The modifications made by the author to adapt the unit to pipe testing are described in the following paragraph; corresponding modifications to equivalent equipment will be evident from this description. It is probable that other equipment and/or modifications will be developed for this application, but the author wishes to describe here merely the modifications he has found useful.

A modification of the searching unit that lends itself to testing various-diameter pipes is shown in Fig. 2. This modification was made as follows: Remove the Plexiglas wedge from the regular angle searching unit by removing the two stud bolts. Cut the wedge along the dotted line, as shown in Fig. 2(*a*), and polish the cut wedge face with polishing cloth. Take a 1¼-in-diam piece of Plexiglas approximately ⅞ in. thick and grind

[1] Schenectady Works Laboratory, General Electric Company. Mem. ASME.

[2] Numbers in parentheses refer to the Bibliography at the end of the paper.

Contributed by the Power Division and presented at the Fall Meeting, Worcester, Mass., September 19–21, 1950, of The American Society of Mechanical Engineers.

Note: Statements and opinions advanced in papers are to be understood as individual expressions of their authors and not those of the Society. Manuscript received at ASME Headquarters on June 9, 1950. Paper No. 50—F-14.

one face to the curvature of the pipe to be tested. Laying a sheet of emery cloth over the pipe makes this operation simpler. Several grades of cloth from coarse to polish may have to be used. Care should be taken that the grinding speed is not too great; otherwise the face of the plastic has a tendency to get soft and sticky. After grinding, the thinnest section of shoe should be $^3/_{16}$ in. As shown in Fig. 2(*b*), this curved shoe has a small bevel ground on one end of the flat face. This bevel, as we shall see, serves a useful purpose. The wedge is bolted back in position using a light oil as a conductor to transmit the sound waves between the crystal and the wedge, and the shoe is then set in the holder against the wedge.

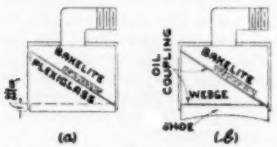

FIG. 2 ADAPTING ANGLE SEARCHING UNIT OT OBTAIN MAXIMUM SENSITIVITY ON CURVED SURFACES

The beveled edge on the Plexiglas shoe limits the rotational orientation of the shoe with respect to the holder by coinciding with the bakelite projection. The bevel is usually ground greater than necessary so that a slight rotational movement is possible to get the best directivity of the sound around the pipe. The shoe cannot be pulled off straight because of the suction of the oil seal between the wedge and the shoe. A quarter turn of the shoe causes the unbeveled part to ride up on the bakelite tip, thereby breaking the oil seal and permitting easy removal. Plexiglas shoes ground to different pipe curvatures can be interchanged quickly with this arrangement.

PREPARATION OF PIPE FOR TEST

Very little cleaning of the pipe for ultrasonic test is necessary on most pipes. The main requirement is that the pipe outside surface be free of loose material. Running a steel scraper over the surface removes loose scale and raised spots of paint, or tar. On pipe, as received from the mill, tight scale or smooth paint marks do not affect the test. If the pipe to be tested is a straight piece, this scraping operation is best performed by holding the scraper against the pipe surface as the pipe is rotated mechanically. Bent portions of pipe where scale may be excessive after heating and bending may require sandblasting.

After the cleaning operation, the pipe is coated on the outside surface with a heavy oil such as SAE No. 40, or even a light petroleum grease. This allows the sound to leave the crystal-holder face and enter the pipe surface, and at the same time permits smooth sliding action of the holder for scanning purposes. While the viscosity of the liquid coupling medium which transmits the sound wave is not critical, for the normal roughness of these pipe surfaces, the heavier oil is recommended.

SHEAR WAVES IN PIPE

Fig. 3 shows the propagation of a shear wave in flat-plate stock, or along the axial direction of a pipe if searching for transverse types of flaws. Angles and intensity per cents are only approximations. The angles are affected by the compositions of the materials and the intensities by the degree of coupling. The diagram serves to illustrate the importance of good coupling between the Plexiglas and the steel, in order not to reduce the low intensity of the shear wave (25 per cent) still further. Fig. 4 is a line diagram showing the center line of the path of the shear wave around a pipe. As can be seen, the shear wave, in a sense, ricochets off the inner and outer pipe-wall boundaries in its travel circumferentially. While a line is used in this diagram to depict the sound path, in reality it represents the center line of a continuously diverging beam. As can be appreciated, where a diverging beam is considered, there is a decrease in wave intensity per unit cross section with distance from the source. This divergence is further accented by the reflections from the convex and concave surfaces bounding the annular cross section of the pipe.

In Fig. 5 is an oscillogram taken on a good section of 8-in-diam pipe. It will be noted that the pulse length of the incident beam

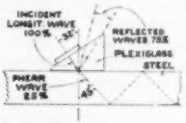

FIG. 3 PROPAGATION OF SHEAR WAVES IN FLAT PLATE

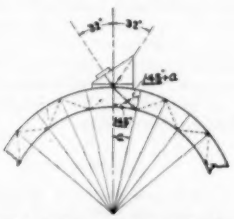

FIG. 4 PROPAGATION OF SHEAR WAVES IN ROUND PIPE

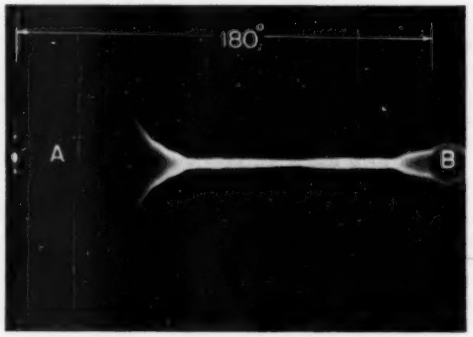

FIG. 5 ULTRASONIC OSCILLOGRAM TAKEN ON GOOD SECTION OF 8-IN-DIAM PIPE

(*A* is transmitted pulse, *B* is receiver indication after first revolution of pulse around pipe.)

A is quite long. This is not only permissible but advantageous in this application, since the sensitivity increases with the pulse length. Pulse length in shear-wave application is not detrimental from the standpoint of concealing a defect close to the source since the source can advance or recede with relation to a fixed flaw. This is not possible in normal longitudinal testing where there are fixed source-to-flaw distances.

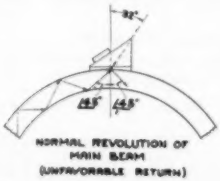

FIG. 6 ILLUSTRATING REASON FOR LOW-MAGNITUDE RECEIVER PICKUP OF SOUND AFTER REVOLUTION

(Sound is not directed at receiver crystal.)

Indication B is the reconversion of the shear wave into an electric pulse as the wave makes one complete revolution of the pipe and passes under the crystal holder. As can be seen in the diagram, Fig. 6,

this shear wave after revolution is approaching the crystal from the rear, or heel, of the Plexiglas shoe which is the most unfavorable approach for conversion to a longitudinal wave and subsequent electric reproduction. The net result is a relatively low-intensity sloping wave front not at all indicative of the strength of the shear wave that has completed one revolution.

It might be well to point out here that this first revolution return may vary somewhat in intensity on the screen, from one size pipe to another, since from the diagram, which is an ideal situation, it is readily understandable that the high-strength center-line portion of the beam may have a less favorable point of coincidence with the crystal upon its completion. The important factor is that the intensity and position on the screen remain fairly constant for a given-size homogenous pipe.

One of the difficult things for an ultrasonic operator, normally using longitudinal methods, to remember is that the oscillogram, Fig. 5, represents only 180 deg of the circumference of the pipe, yet the indication B is the result of a 360-deg travel. This paradoxical situation is brought about by the fact that there is no finite end to the sound path, that is, no end reflection, since the sound continues to circle the pipe until it is completely attenuated. If a notch were cut into the pipe diametrically opposite the sound source, its indication by reflection would coincide with indication B, since it is just as long from the source to the notch and back the same way, as it is from source to source by complete revolution. A notch located 270 deg from the source would show up some distance behind indication B, since the to-and-fro travel is greater than 360 deg.

Fig. 7 is an oscillogram taken on a 13-in-diam pipe, showing the indication from a notch about 60 deg ahead of the crystal. While

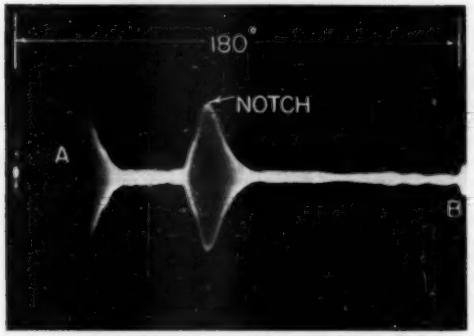

FIG. 7 ULTRASONIC OSCILLOGRAM TAKEN ON 13-IN-DIAM PIPE, WITH A NOTCH ABOUT 60 DEG IN FRONT OF CRYSTAL HOLDER
(Magnitude of indication by reflection, from small notch of definite depth, is used as sensitivity gage.

this is only a small notch about 5 per cent of the wall thickness, the intensity of its reflection is greater than that made by the main beam making a complete revolution and passing under the crystal in an unfavorable direction (indication B). A reflection from a notch, or defect, traverses the same path as the incident shear wave, except in the reverse direction, and thus strikes the Plexiglas shoe at a favorable angle for reconversion into a longitudinal wave which in turn will be directed at the crystal, Fig. 8.

A practical way to assist in locating the flaw region is for the operator to run his fingers over the surface of the pipe in line with the sound-beam direction. As his fingers travel away from the crystal holder, they will coincide with the points of sound reflection on the outside surface. Each of these points of reflection will be recognized by a slight drop in flaw-indication magnitude on the screen, since, in effect, it allows some of the

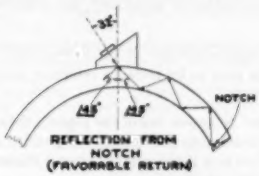

FIG. 8 ILLUSTRATING REASON FOR HIGH-MAGNITUDE RECEIVER PICKUP OF SOUND BY REFLECTION
(Reflected sound is directed at receiver crystal.)

sound energy to escape out of the pipe wall. When his fingers fail to affect the magnitude of the flaw indication, it is evidence that they are no longer between the source and the flaw.

ROTATION OF MATERIAL

In normal longitudinal-wave applications of ultrasonic testing, the operator may rotate the crystal about its axis with no detrimental effect on the test results. Such rotation is around the axis of symmetry of the crystal and therefore does not change the direction of the incident beam. This is not the case when using the angle-searching unit, since the axis of symmetry of the tipped crystal and that of the holder do not coincide. Therefore any rotation of the holder alters the direction of the incident beam and thereby places an added burden on hand operation to scan without rotating the holder.

An obvious solution to this would be to rotate the material to be tested about 5 to 10 rpm, holding the crystal steady, and advancing by successive steps along the length of pipe. On straight lengths of pipe, this is not only feasible but much more practical from the standpoint of assuring complete coverage in a short time. The main advantage, however, of rotating the pipe is the resultant ease of interpretation of the oscilloscope screen. Since the material is moving, any flaws therein have the same movement relative to the sound source and, therefore, the flaw reflection is perceived readily on the screen by its movement to the right or left, depending upon the direction of the pipe rotation. Spurious indications on the screen which accompany any wave-transformation phenomena, and which may vary in intensity although of low magnitude, remain fixed in position on the screen. The spurious indications are a function of the constants of the crystal holder, the uniform pipe thickness, and the variable of the oil coupling between crystal and pipe. The latter variable affects intensity but not time, or distance.

Where it is not feasible to rotate the pipe during test, the operator has to resort to hand-scanning. Although extra care has to be taken, and the test is slower under these conditions, the results are the same. An adequate procedure is to scan a 120-deg arc, with the beam aimed clockwise and then counterclockwise.

As before noted, each crystal position scans 180 deg ahead of that location so that movement through the 120-deg arc suffices to cover 300 deg around the pipe in the clockwise direction. Reversing the crystal direction covers 300 deg in the counterclockwise direction so that the entire circumference is scanned with 120-deg overlap. This is repeated throughout the length of the pipe in successive axial steps along this 120-deg arc. Around bends in pipes, the 120-deg scanning arc is chosen on the outside of the bend for better contact conditions.

INJURIOUS VERSUS NONINJURIOUS DEFECTS

Any understanding as to the distinction between noninjurious

and injurious defects need not be affected by the application of ultrasonic testing methods. In this connection, the company with which the author is associated, has adopted the following procedure:

Ultrasonic Depth Reference: 5 Per Cent Notch:

(*A*) On each pipe to be tested a reference notch is cut in the surface as follows:

1 Location: Near one end of the pipe on the outside or inside surface at the maximum wall thickness, specified as follows:

(*a*) Outside surface if the maximum wall thickness is less than 20 per cent of the inside diameter.

(*b*) Inside surface if the maximum wall thickness is greater than 20 per cent of the inside diameter.

2 Dimensions:

Depth: Approximately 5 per cent of the nominal wall thickness.

Width: Not more than twice the depth.

Length: Extending axially a distance equal to the nominal wall thickness.

Note: The sides of the cut must be smooth and radial, whether made by chisel, or cutter.

(*B*) On each pipe the maximum ultrasonic indication obtainable from this notch is known as the 5 per cent indication.

1 The maximum indication magnitude is determined by directing the sound circumferentially toward the notch with the crystal holder located at a radial arc displacement of about 90 deg each side of the notch.

Correlation of Defect Indications. Upon exploration of the pipe by ultrasonics, any defect indication on the screen, at approximately 90 deg displacement, that can be made to exceed in magnitude the 5 per cent indication calls for removal of the defect.

The foregoing procedure eliminates exploring the depth of minor defects by grinding. Such defects as die marks, tight scale breaks, shallow folds, and the like, do not come up to the 5 per cent indication and, therefore, require no further investigation. For purposes of correlation several indications were investigated by grinding or chipping, to determine their actual depth. Three of these defects are shown in Figs. 9, 10, and 11.

Present Limitations of Test

In initiating any new method of testing, it is well to recognize limitations, whether they be temporary, or permanent. One of these is the smallness of the pipe diameter that may be tested by this method. This limitation is partially the result of commercial equipment facilities and partially geometric inherent limitations. The pulse length and miscellaneous initial wave-transformation echoes limit the use of the first revolution of sound to circumferential travel of pipes greater than 4 in. OD. Of course, the second, third, or fourth-revolution indications may be used on smaller diameters with very little interpretation difficulty. We have tested 1¹/₄-in. pipe under these conditions. The geometrical limitation relates to wall thickness per diameter, with a fixed shear-wave entrance angle of 45 deg.

In Fig. 12 the diagram illustrates the point that if the wall thickness per diameter is too great, the center line of the shear-wave beam may not intercept the inside surface. This method of testing would suffer a loss in sensitivity on inside surface flaws, if the wall thickness exceeded 20 per cent of the inside diameter. If the calibration notch is placed on the inside surface, especially in doubtful cases, its ultrasonic detection gives assurance of test adequacy.

Another limitation pertains to the subject of flaw location. In spite of surface roughness, which may alter the shear-wave entrance angle of 45 deg, the position of the flaw usually may be localized to within a 10-deg arc. This in itself is not objectionable, but the uncertainty as to whether it is on the inside or outside, or somewhere in between, may cause delay in correlation. This is only a temporary limitation which, in time, may be corrected by the determination and use of a proper marking system.

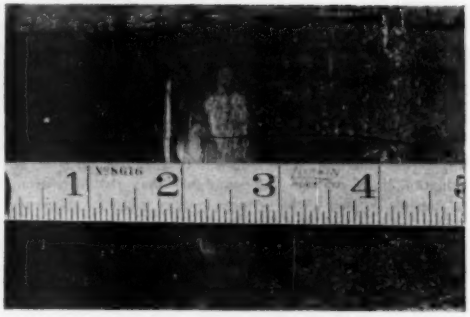

Fig. 9 Shallow Fold 1/32-In. Deep on 0.906-In. Wall Thickness
(Ultrasonic indication from this flaw was about 2/3 of that from a 5 per cent notch, i.e., flaw depth was about 2 per cent of wall thickness. Magnetic-particle means were used to make flaw visible.)

Fig. 10 Chipped Piece From a Pipe of 1.125 In. Wall Thickness, Showing Shallow Fold 1/16-In. Deep Which Was Invisible Before Chipping
(Ultrasonic indication magnitude from this flaw was slightly higher than that from the 5 per cent notch, i.e., flaw depth was slightly more than 5 per cent of wall thickness and therefore was removed.)

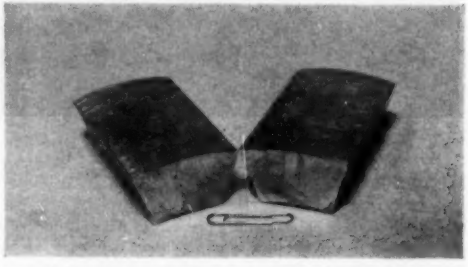

Fig. 11 Cross-Section View of Defective Area of Pipe With 0.940 In. Wall Thickness
(Disclosed crack penetrates 75 per cent of wall thickness. Ultrasonic indication magnitude from this flaw was several times greater than that from the 5 per cent notch. Crack was located ultrasonically in the middle of a 20-ft length of pipe. This pipe was rejected because of this defect.)

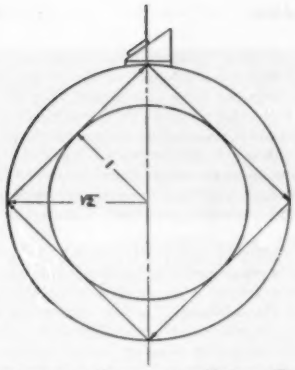

FIG. 12 ILLUSTRATING A LIMITATION OF PRESENT TEST, WHEREIN WALL THICKNESS EQUALS ID $(\sqrt{2}-1)/2$, OR APPROXIMATELY 20 PER CENT OF INSIDE DIAMETER
(Greater thickness than this does not permit high-strength center line of sound beam to intercept inside surface.)

Such a marking system, to be precise, would have to take into account the time of travel of the longitudinal wave in the Plexiglas shoe, the travel distance in the pipe being $\sqrt{2}$ times the circumferential distance, shear waves having one half the speed of longitudinal waves, and finally the conversion of the distance into degrees of arc.

Inherent in a test by instruments, such as present means of ultrasonic testing, is the inability to identify the nature of a flaw. Where the nature of the flaw is of academic interest only, the test may be performed on a magnitude basis. When testing pipes, "5 per cent of wall thickness" is the criterion between non-injurious defects and defects which must be removed.

The irregularities, or twists and turns of a natural crack prevent any accurate correlation of the depth with the magnitude of indication, hence the precaution to check doubtful indications from opposite directions. Actually, a 5 per cent notch with radial sides gives a smaller indication than one with 45-deg inclined sides, since the latter is perfect for reflecting the approximately 45-deg incident sound beam back to the source. It is theoretically possible to underestimate, as well as to overestimate the depth of a defect, when judging on reflection magnitude alone. This underestimation has occurred in practice on a defect whose ultrasonic indication was considerably greater than that from the 5 per cent notch, but not in proportion to the actual depth of the defect disclosed upon removal. Up to the present time, no defect giving an ultrasonic indication less than that from the 5 per cent notch has been found upon investigation to have depth greater than 5 per cent of wall thickness.

The sensitivity, or, in reality, signal-to-noise ratio inherent in the present equipment is more than adequate to meet the requirements of this test. Preliminary tests show that a barium-titanate crystal in place of the present quartz crystal, gives a higher usable sensitivity, permitting a still greater signal-to-noise ratio if material requirements should demand it in the future.

ACKNOWLEDGMENT

The writer takes pleasure in acknowledging the investigations of N. J. Lipstein on the theoretical and experimental aspects of the development described in this paper, and the contributions of M. K. Dennis in the problem of reducing the development to successful shop practice.

BIBLIOGRAPHY

1 "Introduction to Theoretical Seismology," by J. R. Macelwane and F. W. Sohon, Chapman & Hall, Ltd., London, England, 1936.

2 "On the Reflection and Refraction of Elastic Waves With Seismological Applications," by C. G. Knott, *Philosophical Magazine*, 5th series, vol. 48, 1899, pp. 64–97.

3 "Refinements in Supersonic Reflectoscopy, Polarized Sound," by F. A. Firestone and J. R. Frederick, *Journal of the Acoustical Society of America*, vol. 18, July, 1946, pp. 200–211.

4 "Ultrasonics," by Benson Carlin, McGraw-Hill Book Company, Inc., New York, N. Y., 1949.

5 "The Theory of Ultrasonic Materials Testing," by H. E. Van Valkenburg, *Mechanical Engineering*, vol. 71, October, 1949, pp. 817–820.

6 "Ultrasonics Bring 100% Inspection to Power Piping," by W. B. Bunn and W. J. Mitchell, *Power*, vol. 94, October, 1950, pp. 102–104, 164, 167 and 202.

Appendix

INSPECTION OF PIPE WELDS BY ULTRASONIC SHEAR WAVES

The question of ability to use ultrasonic means to inspect pipe welds is invariably raised whenever "pipes" and "ultrasonics" are discussed. As a result of the experience gained on the inspection of pipe material by ultrasonics, a renewed effort has been put forth to develop a procedure for ultrasonic inspection of circumferential pipe welds. The application is quite similar to that discussed in the foregoing paper, except that in inspecting circumferential welds the shear wave is directed axially of the pipe rather than circumferentially.

The major difficulty in the application of ultrasonic methods to the inspection of pipe welds is the false reflections that come from the irregularities at the inner and outer weld surfaces. At the outer surfaces there are the irregularities of the individual beads and the convex form of the weld-metal surface; at the inner surface there is the irregularity of the backing strip itself, or, if no backing strip is used, there are some irregularities due to the deposited metal. The false reflections from these irregularities do not affect the sensitivity of the ultrasonic test, but do make interpretation of the results extremely difficult, since it is usually impossible to distinguish a reflection caused by a surface irregularity (particularly on the inner surface) from one caused by a subsurface flaw. Obviously, this difficulty of interpretation could be considerably reduced by grinding the top and bottom surfaces flush with the parent metal, but the impracticability of so preparing the usual circumferential welds in pipe makes this solution somewhat academic.

In certain types of pipe welds used in some cases by the company with which the author is associated, this finish condition is feasible. After welding such items, the inside and outside surfaces are machined to remove all trace of weld location. These particular items then lend themselves to ultrasonic inspection by shear waves without interpretation difficulties.

It is recognized that in order for ultrasonic inspection of pipe welds to be practical, it must not demand a surface condition superior to that required for radiography. Preliminary tests with this goal in mind have been very encouraging. By concentrating efforts on the interpretation problem, we have been successful in detecting artificial defects of 2 per cent magnitude at various depth locations in the weld. By refinements in ability to pin-point the beam, and special depth location means on the screen, it is possible to differentiate between subsurface flaws and weld-surface irregularities. Investigations leading toward establishing an ultrasonic procedure for inspection of pipe welds are continuing.

Discussion

W. B. BUNN.[8] The author is to be congratulated on the presentation of so descriptive a paper on this important subject. The development of ultrasonic testing of pipe is of importance,

[8] Welding Engineer, The M. W. Kellogg Company, Jersey City, N. J. Mem. ASME.

because it brings into use a practical means of flaw detection in pipe becoming components of critical piping systems. Prior to this development the soundness of pipe entering high-pressure systems was judged by destructive tests from pipe ends, by visual examination of the surface, and by its withstanding satisfactorily a hydrostatic test. Service experience, and more recently the results of ultrasonic testing, has proved that the conventional methods of testing are inadequate.

The completeness of the paper presented leaves little latitude for comment on its substance. However, it would seem in order to present results of actual shop experience[4] in the testing of pipe, wherein the practice used follows exactly that set forth by the paper under discussion.

More than 300 pieces of ferritic-alloy pipe have been examined exceeding 7000 ft of total length, of which 10 pieces have had defects of greater depth than the 5 per cent of wall thickness set as a standard. Nine defects were of a lap or fold nature, while one had the characteristics of a crack. The most serious of these was 1/4 in. depth and approximately 3 1/2 in. long. The pipe examined was 1 per cent chromium–1/2 per cent molybdenum, 2 1/4 per cent chromium–1 per cent molybdenum, and 1 per cent chromium–1 per cent molybdenum–0.2 per cent vanadium. Pipe size was predominantly 6 in. to 10 in. of wall thickness from 0.432 in. to 1.125 in. The smallest pipe examined was 1 1/4 in. in size with a wall thickness of approximately 0.25 in. The thinnest was 0.148 in. wall in 4-in. OD pipe. The majority of defects were found in the heavy wall pipe, but one defect 2 in. long × 0.12 in. deep was found in the 0.25-in-thick pipe.

The incidence of defects has been much higher in the AISI type 347 austenitic pipe examined. Seven areas of defects have been disclosed in the inspection of slightly over 1100 ft of this pipe. Five of the defective areas were found in the inspection of 600 ft of 6 3/8-in-OD × 0.906-in-wall and 8 5/8-in-OD × 0.940-in-wall pipe. The lengths of the defective areas ranged from 3 in. to 9 ft 6 in. One internal system of defects found was 24 in. long, and had a depth exceeding one quarter of the wall thickness of the pipe. In some instances the areas were composed of laps or folds, together with cracks. In the testing of approximately 500 ft of lighter pipe, 0.148-in. wall to 0.456-in. wall, in pipe sizes of 2 1/8 in. OD to 5 in. OD, two defective areas have been disclosed, both in 4 1/2 in. OD × 0.148-in-wall pipe. These have not been sectioned for examination and are not visible on the outside of the pipe. However, radiographic examination of the areas shows heavy indications, probably approaching 50 per cent of the wall thickness for a length exceeding 1 in. in both areas.

Attention is called to the fact that all of the foregoing defects disclosed in the inspection of pipe were found in lengths which had passed mill inspection, most of it having been subjected to supplementary requirement tests, or their equivalent. Except for the possibility of chance disclosure of the defects during fabrication, the defective pipe would have entered service at high pressure with steam temperatures of 950 to 1050 F.

To determine if minor defects would grow in size when pipe is hot-bent we have examined more than 500 ft of arc in bends of 6-in. and 8-in. pipe. No defects were disclosed exceeding 5 per cent of the pipe wall thickness. In this examination approximately one half of the footage was austenitic material, the remainder being ferritic alloy.

Referring to the author's Appendix on the "inspection of pipe welds by ultrasonic shear waves," recently an inspection of twenty-five austenitic weld joints was made in an eastern generating station which has been in operation for approximately a year. Interpretation was difficult because the insides of the joints were not accessible for visual examination, and in some cases the welds were complex, joining pipe of different diameters with extensive weld deposits. One questionable area was marked for examination by other means. Radiographic examination and subsequent excavation disclosed a circumferential crack 3 in. long, 1/4 in. below the outer surface, with a depth of 5/16 in. It did not progress to either the inner or outer surface. The crack was inclined at such an angle that it is questionable if it would have been revealed by routine radiographic examination of the joint.

W. R. Hutchinson[5] and R. H. Frank.[6] In application, the reflectoscope is capable of detecting 2 per cent defects as readily as 80 per cent defects, particularly in wall sizes over 0.250 in. Even though the indication of a 2 per cent defect appears considerably smaller than the standard 5 per cent defect, it is easily detected by its movement along the screen, while the 80 per cent defect is of such magnitude that the sweep is all but amplified off the screen. Fig. 13 of this discussion shows a 7 per cent defect detected in a 12-in., Schedule 160 pipe, while Fig. 14 shows visual conformation. Similarly, Fig. 15 shows a reflectogram of a major defect in stabilized 2-in-OD Cr-Mo pipe, while Fig. 16 shows a section of this pipe containing two cracks 75 per cent and 80 per cent of wall thickness, respectively. Incidentally, this length of pipe was passed by visual inspection since nowhere were the cracks visible, while on the inside surface only magnaflux would have detected it.

[4] At the shop of the writer's company in Jersey City, N. J.

[5] Research Engineer, Pittsburgh Piping and Equipment Company, Pittsburgh, Pa.

[6] Technical Sales, Sperry Products, Incorporated, Pittsburgh, Pa.

Fig. 13 Seven Per Cent Defect in Schedule 160, 12-In. Pipe, 1.312-In. Wall

Fig. 14 Polished Pipe Section Showing 7 Per Cent Defect Located in Fig. 13

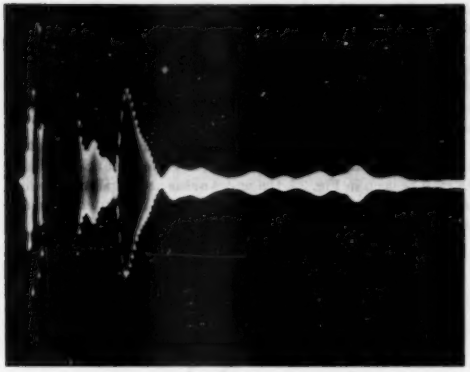

FIG. 15 REFLECTOGRAM OF 80 PER CENT DEFECT IN STABILIZED 2-IN-OD 0.240-IN-WALL CHROME-MOLY PIPE

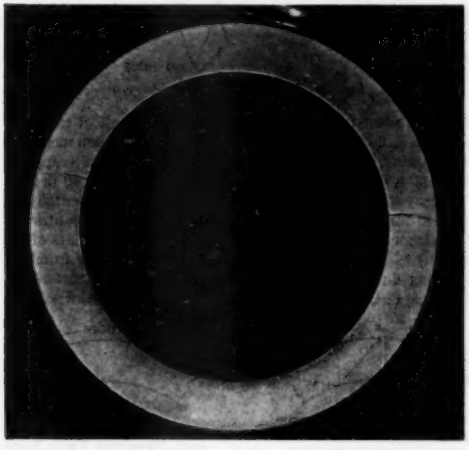

FIG. 16 STABILIZED 2-IN-OD 0.240-IN-WALL CHROME-MOLY PIPE, CONTAINING A 75 PER CENT AND 80 PER CENT DEFECT LOCATED IN FIG. 15

In our test procedure, calibration of the reflectoscope is accomplished by using a 5 per cent notch in a test ring of the same type material being investigated. The 5 per cent notch is clearly visible in Fig. 17, while its reflectogram is shown in Fig. 19. Since it was felt that any questionable defect detected on the outside surface could be examined visually, the notch was placed initially on the inside surface more fully to ascertain the magnitude of the inaccessible defect. However, a later investigation revealed no appreciable difference in indications from 5 per cent defects machined on both inside and outside surfaces. Therefore, ease of machining would appear to be the principal reason for the author's specification of notching the outside wall except where the wall is over 20 per cent of the inside diameter.

Theoretical Discussion. Ultrasonic testing of pipe is based upon the same principle as radar or sonar. A short pulse of high-frequency energy is emitted from the crystal and an echo returns. Then the length of time required for this pulse to reach

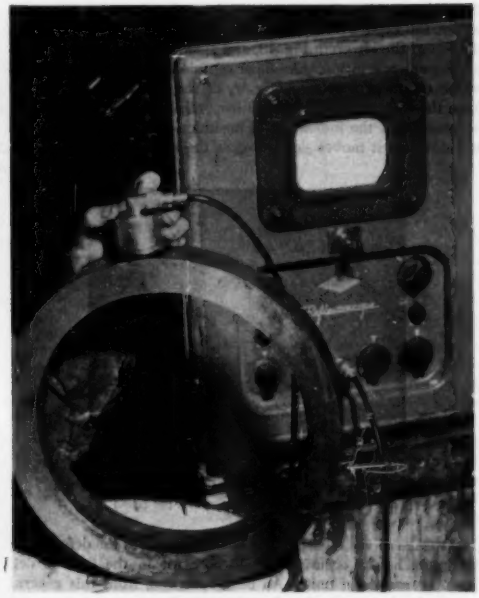

FIG. 17 TEST RING CONTAINING STANDARD 5 PER CENT NOTCH

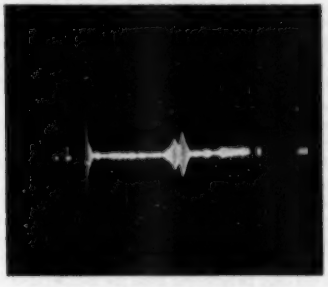

FIG. 18 REFLECTOGRAM OF 12-IN. SCHEDULE 160
(No defect. Initial pulse to left, return pulse to right.)

FIG. 19 REFLECTOGRAM OF 12-IN., SCHEDULE 160 TEST RING WITH STANDARD 5 PER CENT DEFECT

the discontinuity and return will determine how far across the screen the echo will appear. The initial pulse may be seen on the left of the screen in Fig. 18, and again on the right after completing one revolution. An 8 per cent defect is shown in Fig. 20, which occurred approximately 1/4 of the way around the pipe from the searching unit. When inspecting a piece of pipe it will be noted that the indication of an unknown defect will bob up and down as it moves slowly across the screen. This is due to

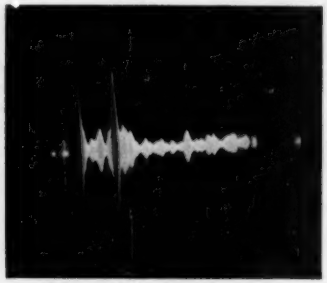

FIG. 20 REFLECTOGRAM OF 12-IN. SCHEDULE 160 PIPE
(Unknown defect estimated at 8 per cent.)

the passage of the zigzagging sound beam across the defect with maximum height occurring somewhere within the first 90 deg from the searching unit. An echo returning from this general area is clearly outside the obscuring initial pulse, yet not too far away from the crystal to be seriously attenuated.

Since the sound beam is bouncing back and fourth from alternate walls it might be assumed that a defect would be detected at a different angular distance from the crystal on different sizes of pipe. Actually, this is the case only if the schedule number varies with the pipe size. For a given schedule number, a defect will be picked up at the same angular distance from the crystal despite different pipe sizes since the diameter-to-wall-thickness ratio remains fairly constant. Conversely, a defect will be picked up at different angular distance for the same pipe size if the schedule number is varied.

It has been observed that at times a defect may be detected from one direction only, i.e., detected clockwise and not detected counterclockwise. The occurrence of a lap or fold in the surface could produce such a condition as may be seen from Fig. 21. A signal would only be reflected from the counterclockwise direction due to a corner effect produced between the lap and the outside wall. If a subsurface crack would occur at the same orientation or parallel to the walls as in Fig. 22, the search beam would bounce off and continue its circumferential path. Thus, it is possible for a subsurface defect to be so oriented as to be just as invisible to ultrasonic testing as an angular crack is to gamma-ray or x-ray radiography.

The return pulse, or back reflection as it is commonly called, is a clear measure of the searching unit to pipe sound transmission. Should the return pulse appear smaller than usual, the test sensitivity is lowered, and the estimation of the size of an unknown defect will be inaccurate. The normal return pulse is clearly visible in Figs. 13, 18, 19, and 20. In the case of a gross crack or major defect, the return pulse would reduce or disappear since most of the signal would be reflected rather than transmitted. In this case, the size of the back reflection would be of little consequence since the size of the echo alone would indicate a harmful condition.

FIG. 21 ECHO RETURNED FROM COUNTERCLOCKWISE DIRECTION ONLY

FIG. 22 DEFECT NOT DETECTED

Location of an Unknown Defect by Finger Attenuation. Let us consider the location of a defect by the use of node points. As may be seen in Fig. 23, the nodes occur at the points at which the sound reflects off the outside surface. It is of interest to note that the distance between these nodes (points of reflection) was

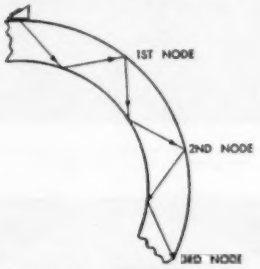

FIG. 23 LOCATION OF NODE POINTS

less than calculated using 45 deg as the basic angle of transmission, especially on the higher frequencies. Based upon measured node spacing, the transmission angle in chrome-moly pipe appears to be 43 1/2 deg from the vertical for 0.5 megacycle, 40 deg for 1 megacycle, and 38 deg for 2.25 megacycles. Incidentally, it was also observed that node spacing varies with pipe eccentricity. The author has described how these node points (points of reflection) can be established by moving a finger away from the searching unit toward the defect. Now assuming a surface defect as in Fig. 24, the last clockwise and counterclockwise node

FIG. 24 SURFACE DEFECT DETECTED FROM CLOCKWISE AND COUNTERCLOCKWISE DIRECTIONS

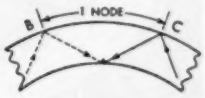

FIG. 25 INSIDE-SURFACE DEFECT DETECTED FROM BOTH DIRECTIONS

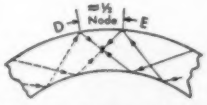

FIG. 26 SUBSURFACE DEFECT DETECTED FROM BOTH DIRECTIONS

points at which the defect indication is visibly attenuated by the finger, coincide at point A. Again assuming a defect on the inside surface as in Fig. 25, the last clockwise and counterclockwise node points at which the defect indication is visibly attenuated occur at points B and C, or one node apart. Similarly, assuming a center defect as in Fig. 26, the last clockwise and counterclockwise node points occur at points D and E, or approximately 1/2 node apart. Therefore the separation of the last clockwise and counterclockwise node points may be used to determine both depth[7] and location of an unknown de-

[7] Depth and node spacing do not vary exactly linearly. However, as may be seen in Fig. 27, this nonlinearity will produce only a maximum error at mid-wall of 10 per cent in the heaviest-schedule high-pressure steam pipe made. Of course, the lower the schedule number, the smaller is the error.

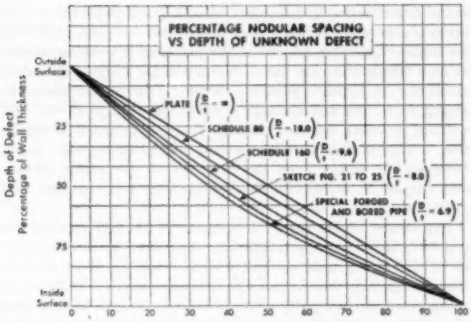

FIG. 27 PERCENTAGE NODULAR SPACING VERSUS DEPTH OF UNKNOWN DEFECT

fect, since the depth of an unknown defect is proportional to the distance between last clockwise and counterclockwise node points, while the location is midway between these node points.

Location of an Unknown Defect by Visual Node Technique. In the event the unknown defect cannot be detected from both sides, another interesting method of location is by the use of a calibrated screen referred to as the "visual node technique." Here an artificial defect of Plexiglas with one edge enclined 40 deg from the vertical is placed on the pipe surface thereby enabling the sound beam to pass out of the pipe wall and be reflected by the inclined plane. The approximate location of an unknown defect may be determined by sliding the artificial defect over the surface of the pipe until the two indications coincide on the screen.[9]

An artificial defect used for 0.5 megacycle testing is shown in Fig. 28. For 1-megacycle and $2^1/_4$-megacycle testing, similar artificial defects were used, except that they were tapered down to $^3/_{64}$ in. and $^1/_{64}$ in., respectively, at the trailing edge. In cali-

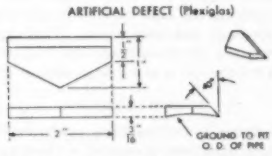

FIG. 28 ARTIFICIAL DEFECT; PLEXIGLAS

brating the screen with the artificial defect, 2.25 megacycles were used on 12-in. schedule 160 pipe, since this frequency produced the most distinct node points. One megacycle was used with some difficulty in calibration, while dispersion at 0.5 megacycle was too great for accurate calibration.

To calibrate the screen as in Fig. 29, the artificial defect was placed in the general locality of the unknown defect, and the crystal was moved away from the artificial defect until at least two successive node points were located. The peaks of these indications were inked on the screen above the sweep, and these artificial defect-to-crystal distances recorded. It is believed that the most accurate location is achieved when the calibrating node points straddle the unknown defect. This calibrates the screen for that particular locality despite eccentricity and out-of-roundness. Since these two ink marks correspond to the outside-surface defects, a third ink mark halfway between corresponds to an inside-surface defect. The sawtooth wave or a ruler may

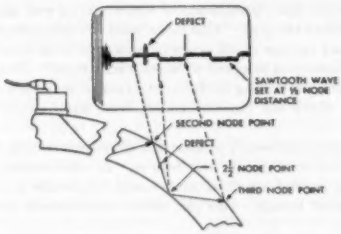

FIG. 29 CALIBRATED SCREEN

be used to determine this mid-point. Consequently, that segment on the screen between an inside ink mark and an outside ink mark is equivalent to the pipe wall.

Therefore it may be seen that by the use of the visual node technique, the depth of a defect between inside and outside surfaces of a pipe wall is proportional to the location of its indication between inside and outside ink marks on the screen.[9] Similarly, having redetected the unknown defect and marked the node points on the pipe,[10] the position of the unknown defect between these node points is proportional to the location of its indication between the outside ink marks.

J. J. MACISAAC[11] AND H. A. WAGNER.[12] Users of pipe, particularly where heavy wall thicknesses are involved, have long felt the need for a satisfactory means of examining more than merely the ends of a piece of pipe intended for high-pressure high-temperature service. Despite so-called "hidden" factors of safety which may or may not exist in any given case, pressure is continually being exerted to increase allowable design stresses at high temperatures. The pipe designer will doubtless rest easier if he can be assured by a test such as this that the pipe, throughout its length, is entirely devoid of significant defects so that the material may be counted on to develop its full capabilities. The author and his company are to be congratulated for the development of this test as applied to pipe, and for their willingness to publish the results of their work.

Some question has been raised heretofore as to reliability of interpretation of results of sonic tests. Is this procedure of sonic testing essentially a laboratory tool which may be effective only on short lengths of pipe such as might be found between the throttle valve and steam chest of a turbine? Or could the test be made satisfactorily in the hands of the pipe manufacturer or pipe fabricator? If the test is made by the manufacturer, would the author advocate eliminating the usual hydrostatic test?

If the test is carried out by the pipe manufacturer or fabricator, the question is raised as to what is needed in the way of personnel and experience for a satisfactory evaluation. To what extent,

[8] If interference between the two indications occur, the crystal and artificial defect may be moved sideways until the unknown defect disappears. In this case, it is advantageous to mark the location of the unknown defect on the screen.

[9] Here too, some nonlinearity exists as in the finger-attenuation method. However, the maximum error for the heaviest-schedule pipe is only 3 per cent, while the maximum error for the heavier forged and bored pipe is only 6 per cent. Of course the lower the schedule number, the smaller is the error.

[10] These node points or distances are those measured from artificial defect to crystal, and these distances from the crystal are marked on the pipe surface after redetection of the unknown defect.

[11] Engineering Department, The Detroit Edison Company, Detroit, Mich. Jun. ASME.

[12] Engineering Department, The Detroit Edison Company, Detroit, Mich. Mem. ASME.

for instance, is the test dependent on the skill and application of the operator? It would be of interest to know also how costly a test this is. In the hands of an experienced operator, for instance, how long would it take to completely test a 30-ft length of 12-in. schedule 160 pipe?

It appears that throughout the test work, oil was used to coat the outside of the pipe. Can oil be used to correct impedance of the contact surface of all types of materials to be tested, or are certain fluids best adapted to certain materials? Also, to what degree does the testing of different types of materials affect the angle at which the incident longitudinal wave enters the pipe surface?

It has been previously observed in ultrasonic testing that grain size appears to affect the test results. In other words, it seems that large crystal structure makes some materials impenetrable to ultrasonic beams. Has the author experienced such a phenomenon?

W. A. Pollock.[13] Creep can cause failures that hydrostatic testing does not detect. The author and his company provide an invaluable service in developing this rapid, nondestructive test which permits examination of every square inch on important piping at a reasonable cost. Also important is the fact that the test was made available to the industry as soon as it was developed.

This test method importantly supplements other nondestructive tests such as zyglo and magnaflux. It is especially valuable because it detects subsurface as well as surface flaws and permits repair or replacement of questionable sections of piping before serious accidents occur.

The writer's company has employed the Sperry Company on two occasions to conduct tests employing this method with the reflectoscope. The results obtained were satisfactory.

On the first occasion all of the pipe ends of the high-pressure and high-temperature steam piping for an addition to one of the stations were examined for defects. One longitudinal crack 3 in. long and 8 per cent of the wall thickness was found in an elbow in a 450-psi 950-F steam line that had been tested hydrostatically. This defect was just under the surface and even after location with the reflectoscope defied detection by zyglo, magnaflux, and heating with an acetylene torch. This crack was repaired by grinding it out. It is not intended to imply that this test can replace the other tests mentioned because it has limitations and should be used by well-trained operators who can interpret properly the indications on the scope.

The second experience was in testing 3-in. boiler-screen tubes for corrosion. Because the general pattern of corrosion was known, sample tubes were made up as reference pieces. The results obtained were satisfactory but not as positive as was the case with the larger pipe. This was due to the actual corrosion pattern not being exactly like the reference pieces. Also, the small tube size made the testing difficult. Speed of testing by this method was in its favor when compared to other methods.

A. W. Rankin.[14] In the manufacture of turbine-generator sets, the component parts such as turbine shells, rotors, buckets, etc., are subjected to frequent inspection by visual, magnetic-particle, dye, and x-ray tests. Prior to the development described in this paper, however, the inspection of piping for steam leads between the emergency stop valve and the turbine shell was by visual and hydrostatic tests only. A tight radial crack on the inside surface of a pipe would be difficult to locate by visual examination, and a hydrostatic test at 1.5 or 2 times the normal operating pressure is not a very severe test for piping intended for high-temperature service as the permissible working stresses at high temperature are only a fraction of the room-temperature strength. It appears possible, therefore, for high-temperature piping to be cracked through a major percentage of the wall without its being detected through visual or hydrostatic inspection. The ultrasonic test method described in this paper, however, can detect even the diemarks on the inside surface, and equals in sensitivity any practicable test method now available.

Experience of the writer's company with this method has proved it to be entirely practicable, and, since its development, all of the piping used for main steam leads on large turbines manufactured by this company have been so tested. Such piping is inspected ultrasonically while in straight lengths before being placed in production stock, and, in addition, piping of one alloy is given a second ultrasonic test after hot-bending. Ultrasonic inspection of installed piping is also possible, but is more difficult than the examination of straight lengths which can be rotated. We have gained experience in the ultrasonic inspection of installed piping by the examination of the steam leads on four turbine installations. Such inspection is high in cost and man-hours demand, and probably would be commercially acceptable only in critical cases, at least in the present state of the art.

In ultrasonic inspection, the interpretation of the results is usually quite difficult. The use of a 5 per cent calibration notch in pipe inspection, however, simplifies considerably such interpretation. Flaws exceeding 5 per cent on either the inside or outside surfaces can be investigated by grinding, but flaws within the wall require cutting the pipe in two. This is not a major disadvantage since the ultrasonic inspection will locate exactly the point at which the pipe should be cut. After investigation, and removal of the defective area if necessary, the pipe can be rejoined by welding. Our own experience indicates that such action would not be required very frequently except in a defective heat of steel.

On the basis of the successful results obtained on pipe inspection by the method described in this paper, the writer's company is now applying the same method to the inspection of retaining rings for large generator rotors. It is expected that as further opportunities are recognized, this inspection technique will be applied to other parts of our large turbine sets.

Author's Closure

The author wishes to express his appreciation of the various discussions which have been presented of this paper, and of the extent to which they have improved the paper by amplifying both the theoretical and practical aspects of ultrasonic testing.

W. H. Bunn's discussion relating to their shop experience is revealing from the viewpoint of incidence of injurious defects. If averages may be applied, it would indicate one injurious defect per 700 feet of ferritic-alloy pipe, and one injurious defect per 160 feet of austenitic pipe. These figures appear rather high, but undoubtedly will be reduced as inspection, in general, is improved.

W. R. Hutchinson and R. H. Frank have presented a very interesting procedure for determining the depth of a defect that does not come to either surface. Their discussion shows they have done considerable work on the fundamentals of ultrasonic testing of pipe. The reference to the use of an artificial defect recalls our similar use of a small Alnico magnet. On some finished surfaces where notching was not permissible, we were able to substitute the reflection from an Alnico magnet which had previously been correlated with that from a notch. While the theoretical limitations on detection of certain oriented types

[13] Technical Engineer of Power Plants, Wisconsin Electric Power Company, Milwaukee, Wis. Mem. ASME.

[14] Assistant Division Engineer, Steam Turbine Engineering Division, General Electric Company, Schenectady, N. Y. Mem. ASME.

of defects is correct, there are extenuating circumstances that prevent a positive prediction. For example, the jagged condition of a natural crack may reflect sound favorably or unfavorably, while a curved defect may form a concave focusing reflector in one direction and a convex dispersing reflector in the other. Unfortunately, it is difficult to artificially reproduce many types of natural defects.

J. J. MacIsaac and H. A. Wagner have asked questions that are pertinent to any discussion on the practical aspect of an ultrasonic test. It is true that there are ultrasonic tests in the embryonic stage that are, and rightfully should be, limited to laboratory use. However, this particular application on piping is relatively simple because of the relatively low sensitivity of 5 per cent that is required. The shop experience by Bunn testifies to the practicability of the test. With respect to the hydrostatic test, it is the opinion of the author and his associates that hydrostatic testing is not necessary if the ultrasonic test has previously been used, although some engineers may still require a hydrostatic test of installed piping simply to check the tightness of flanged joints.

It was the author's intention in the writing of the paper to present it in a form consistent with the simplicity of the test and for the purpose of encouraging its wider use. The simplicity of a test may be measured somewhat by the speed with which it may be carried out. In this respect we recommend a scanning speed not in excess of 6 inches per second.

The use of oil as a coupling medium is fundamentally one of convenience. Nearly any fluid material would be satisfactory from a sound transmission standpoint. In regard to angle of entrance of the shear wave, it would not vary appreciably within the range of compositions of alloy steels, certainly not enough to affect testing results. Large crystal structure does definitely affect the ability to ultrasonic test. For example, in using the shear-wave test on ferritic retaining rings, we can not test them until after they are heat-treated. We have experienced no grain difficulties on any seamless pipe, whether ferritic or austenitic.

Joints for High-Pressure High-Temperature Piping

By I. H. CARLSON[1] and W. S. BLACK,[2] CHICAGO, ILL.

This paper outlines briefly the difficult problem of obtaining leakproof joints for high-pressure high-temperature piping. It includes the results obtained from an extensive test on three full-sized joints for connecting ferritic-alloy main steam piping to austenitic-alloy turbine equipment of 150,000-kw capacity. The scope of the tests was limited by the amount of steam available, but the information secured should be of value to others having similar problems. It is hoped that others having experience or knowledge in this field will contribute additional information concerning this problem which is important to the continued progress of the power industry.

Introduction

OPERATING engineers have long been troubled with leaks in pipe joints and, as a direct result, wherever possible, welding has become an answer in most cases. However, it is the judgment of some that piping of different expansion characteristics whether of the same material or of different materials shall not be welded to form the joint. There is also a need for mechanical joints where the piping must be disconnected from equipment.

It may not be generally appreciated that temperature stresses are often several times as much as those permitted by code formulas which are based on pressure forces alone and have not yet included factors to indicate the extent of stresses created by differential expansion. The importance of this problem has been emphasized in at least two papers which have appeared before the Society.[3,4] A temperature differential of only 150 F between two points in a steel mass may produce a stress of 30,000 psi.

For these reasons a series of joints have been considered which will permit relative motion between the two parts of the joint having differences in expansion due either to variation in operating temperatures or coefficients of expansion.

The most troublesome kind of problem with pipe joints arises from rapid changes in temperatures. Differences in temperature, differences in rigidity, differences in coefficients of expansion and of heat conductivity result in relative movements of sealing surfaces so that leakage may occur in the joints. Earlier tests, on 1200-psi 925 F steam,[5] have shown that standard tongue-and-groove ASA flanged joints leaked under temperature differences less than encountered under actual operating conditions. Operating trouble also has been experienced with ring-joint-type gaskets. In the latest series of tests, three special joints intended to permit relative movement of parts differing in thermal expansion ($2^1/_4$ per cent Cr, 1 per cent Mo to 18 per cent Cr, 8 per cent Ni Cb steel) were investigated. These joints, the pressure-seal, the bellows type, and a spiral-wound metal, asbestos-filled gasket joint designed for 1900-psi 1050 F steam service are shown in Figs. 1, 2, and 3.

Description of Joints

The "pressure-seal" joint utilizes the fluid pressure acting against the full gasket circle area to obtain its sealing force between the conical surface of the stub end and the cylindrical surface of the socket flange, and is assisted by moderate initial bolt loading in the case of joints subjected to bending loads or operating on vacuum or low-pressure service. A seal is also obtained at the inner cone surface of the stub end by using sufficient initial bolt load to carry the pressure load on that circle area plus enough to secure the equivalent "valve seating" tightness for the joint. A third seal is effective in series with the foregoing two seals when the stub end is made of a metal having a higher coefficient of expansion than that composing the socket, and the initial clearance at assembly temperature is made less than the differential expansion so as to secure a "shrink fit" under the higher-operating-temperature conditions.

The pressure-seal joint remains tight irrespective of the bolt elongation or adjustment because the conical seating surface maintains the same relative position to the cylindrical seating surface. The two conical surfaces of the stub end have the same apex, a geometrical relation which permits one pipe end of the joint to expand or contract freely with respect to the other without change in the relative positions of either pair of mating conical surfaces.

The "bellows-type" gasket is intended to care for both axial and radial relative movements of the opposed flange faces. When the pipe is being heated, the inner rims of the faces are hotter and approach each other closer than the outer diameters of the same gasket chamber. When cooling, the opposite occurs tending to open the joint, but as long as the gasket seals against the flanges, the pressure acting on the interior faces of the gasket tends to hold the gasket against the flanges in sealing engagement.

At the time the bellows-type test joint was designed, it was decided to maintain a metal thickness on the 18-8 Cb end of $1^3/_8$ in., whereas the metal thickness of the $2^1/_4$–1 chrome-moly piping was $2^1/_8$ in. This was desired because of increased problems that would be encountered in welding heavier austenitic material. The reduced wall on the austenitic pipe made it possible to reduce the bolt circle and total flange mass considerably. In an effort to minimize the effect of the difference in expansion of the two flange materials, the drilled holes in the austenitic flange were

---

[1] Supervising Engineer, Engineering Division, Crane Company.

[2] Assistant Supervising Engineer, Engineering Division, Crane Company. Jun. ASME.

[3] "Cyclic Heating Test of Main Steam Piping Joints Between Ferritic and Austenitic Steels—Sewaren Generating Station," by H. Weisberg, Trans. ASME, vol. 71, 1949, pp. 643–664.

[4] "Thermal Shock and Other Comparison Tests of Austenitic and Ferritic Steels for Main Steam Piping," by W. C. Stewart and W. G. Schriets, ASME Paper No. 50—S-23, presented at the Spring Meeting, Washington, D. C., April 12–14, 1950, of The American Society of Mechanical Engineers.

Contributed by the Power Division and presented at the Fall Meeting, Worcester, Mass., September 19–21, 1950, of The American Society of Mechanical Engineers.

Note: Statements and opinions advanced in papers are to be understood as individual expressions of their authors and not those of the Society. Manuscript received at ASME Headquarters, August 3, 1950. Paper No. 50—F-32.

[5] "Performance Tests of Pressure-Seal Pipe Joints," by I. H. Carlson and W. S. Black, *Valve World*, vol. 44, April-May, 1947, pp. 34–44.

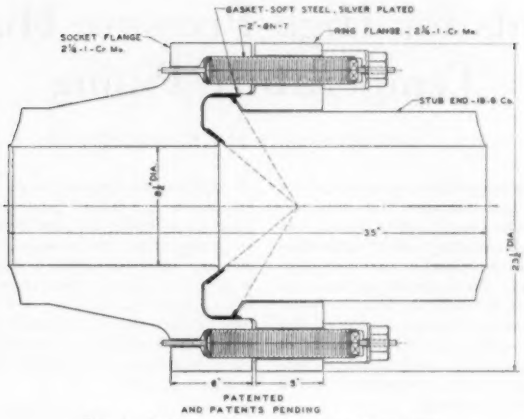

FIG. 1 SECTIONAL VIEW OF PRESSURE-SEAL JOINT
(Patented and patents pending.)

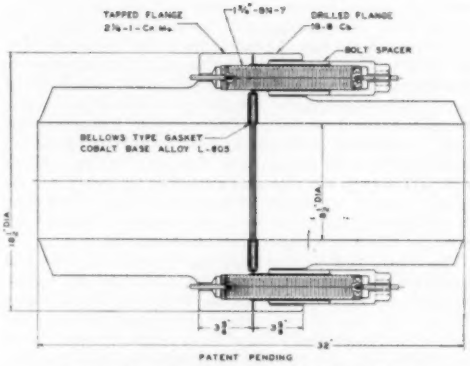

FIG. 2 SECTIONAL VIEW OF BELLOWS-TYPE JOINT
(Patent pending.)

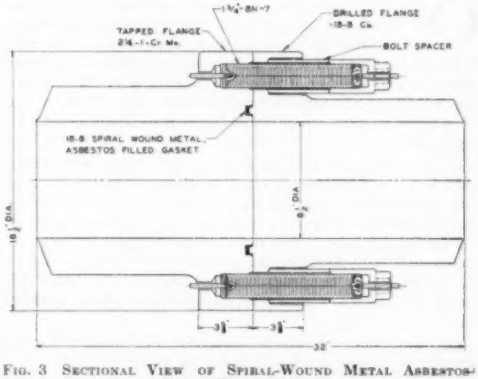

FIG. 3 SECTIONAL VIEW OF SPIRAL-WOUND METAL ASBESTOS-FILLED GASKET JOINT

counterbored for sleeves of the same material as the bolts, which acted as spacers between the nuts and flanges. This construction increased the effective length of bolt for absorption of strain caused by the differential expansion by an amount equal to twice the length of the sleeves.

The spiral-wound gasket joint was made by remachining the bellows-type joint flanges to accommodate the spiral-wound metal asbestos-filled gasket. It will be noted that in this assembly the flange faces are brought into contact over their entire width, thus limiting the amount of gasket compression.

It is appreciated that some differences in properties between castings and forgings must be considered in the case of austenitic chromium-nickel alloys. For this reason it should be noted that all tests were made on joints having cast pipe and flange members.

The use of superalloy for the bolting on the joints eliminated the troubles prevalent in former high-temperature flange joints in which the bolts themselves relaxed and unloaded the gasket during the cyclic temperature conditions. In all cases of decrease of bolt loading, as found by direct measurements using the elongation method, the decrease was due to deformation of the

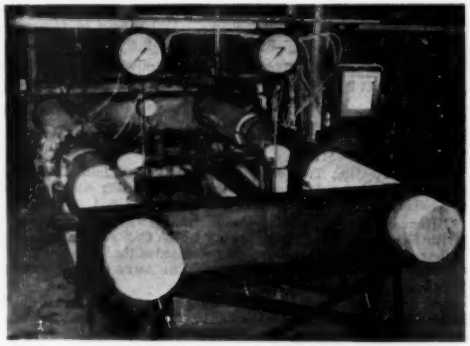

FIG. 4 APPARATUS FOR TESTING 10-IN. 1900-PSI, 1050 F FLANGED PIPE JOINTS
(Pressure-seal joint shown at left.)

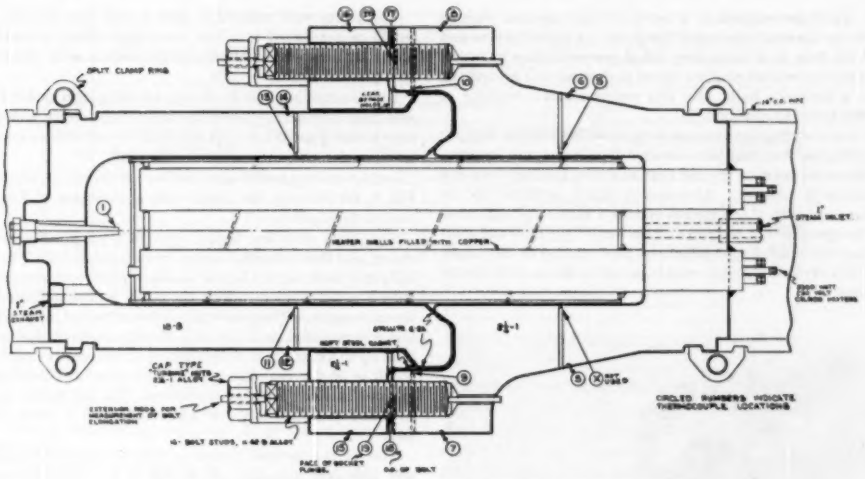

FIG. 5 SECTIONAL VIEW OF PRESSURE-SEAL JOINT AS ASSEMBLED FOR TEST

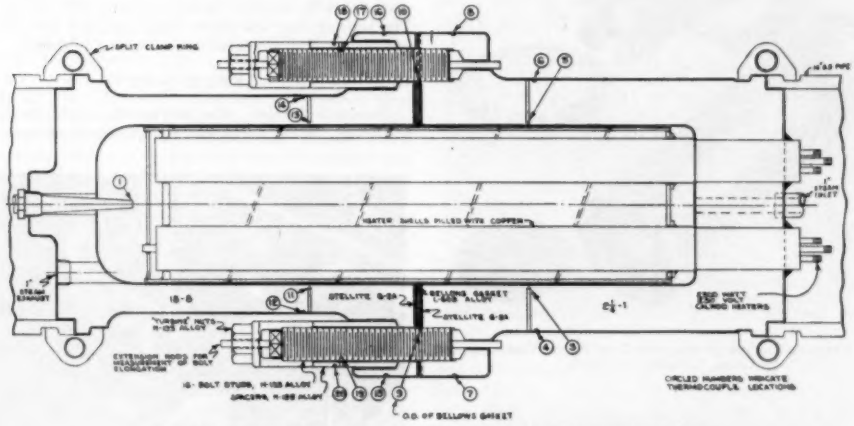

FIG. 6 SECTIONAL VIEW OF BELLOWS-TYPE JOINT AS ASSEMBLED FOR TEST

gasket and/or the flanges. None of the bolts was stretched permanently.

PERFORMANCE TESTS—PROCEDURE

In order to compare performance of the three types of joints—the pressure-seal, bellows-type, and spiral-wound gasket joints—laboratory tests were conducted to ascertain the relative ability of the joints to remain tight when heated to 1050 F and then cooled with saturated steam entering at 575 F. This was done 25 times on the pressure-seal, 23 times on the bellows-type, and 2 times on the spiral-wound gasket joint. The joints were tested in the apparatus illustrated in Figs. 4, 5, and 6, in which a bending moment 50 per cent greater than expected in service was applied by means of a hydraulic cylinder.

Since the superheater was rated at 1000 F maximum, it was necessary to supply additional heat to the steam in order to raise the metal temperatures of the joints to the required 1050 F. For this purpose four electric heater units, Fig. 7, with a total output of 20 kw were inserted in each joint. The heater capacity was calculated to be that required to boost the temperature of the steam 200 F (to total temperature of 1100 F).

For measuring exhaust-steam temperature a 5-in. thermocouple well was installed in the 18–8 end of each joint. Metal temperatures at top and bottom were measured with No. 20 gage iron-constantan thermocouples and a high-speed recorder at positions shown in Figs. 5 and 6.

In order to approach the steam velocity and heat-transfer conditions occurring in the field, a steel liner was inserted over the electric heaters, as shown in Figs. 7 and 8, so that the limited amount of saturated steam available for cooling, 4300 lb of steam

per hr, would be confined to a narrow $^1/_{16}$-in. annular passage between the liner and the wall of the joint. A $^1/_8$-in. wire wound around the liner in a $^1/_{16}$-in-deep spiral groove further increased the velocity by constricting the steam to flow spirally around the liner in a 6-in-wide path. By this means a steam velocity of over 9000 fpm was obtained.

It is believed that the attempt to produce high steam velocity by spiraling the flow may have resulted in a less severe temperature differential between top and bottom during heating or cooling than occurs in practice. Attention is called, however, to the fact that even with $4^1/_2$ complete spirals, a significant difference in the temperatures at the top and bottom of the pipe and joint was observed which might affect the performance of the joints. A joint in a vertical pipe line would operate under more favorable conditions.

FIG. 7 STUDDED FLANGE OF BELLOWS-TYPE JOINT WITH ELECTRIC HEATERS, GASKET, AND LINER

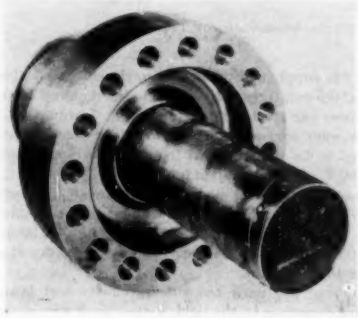

FIG. 8 SOCKET FLANGE OF PRESSURE-SEAL JOINT WITH LINER AND END BAFFLE PLATE ASSEMBLED

The joints were covered in such a way that leakage, if any, would be conducted to a 1-in. drain pipe where it could be detected by means of an electric thermoswitch or by condensation on a piece of glass.

For determining bolt stress by the elongation method, extension rods were screwed into the ends of the studs, and the rods were center-punched at opposite ends for use with an extensometer equipped with a $^1/_{1000}$-in. indicating dial.

Insulation boxes were installed on the joints, as illustrated in Fig. 9, for covering the joints with a minimum of 9 in. of expanded vermiculite.

The joints were first heated with 1450-psi 910-F superheated steam, and then, with the electric heaters set at 1350 F to 1500 F, the joints were further heated to near equilibrium temperature of 1050 F metal temperature on the inside wall as indicated by the thermocouples. They were then allowed to cool, after which the test was repeated, but this time bending moment was gradually built up to a maximum of 30,800 lb-ft at temperature equilibrium, which is 50 per cent in excess of the calculated bending stress expected under operating conditions. To this point, the joints were not quenched but were allowed to cool to room temperature.

The joints were then heated to 1050 F while the bending load was increased gradually to 30,800 lb-ft. When temperature equilibrium was practically attained, the electric heaters and the flow of superheated steam were turned off and the joint was quenched with saturated steam at about 1300 psi and 575 F. The bending load was released and reapplied once just before quenching. This also was done once during quenching.

RESULTS OF TESTS

Pressure-Seal Joint. The pressure-seal joint remained tight on all tests, namely, a 0 to 4000-psi hydrostatic-pressure test, the

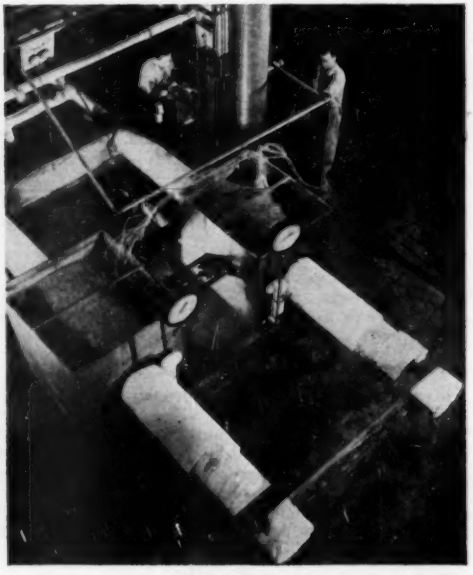

FIG. 9 VIEW OF APPARATUS DURING QUENCH TESTS

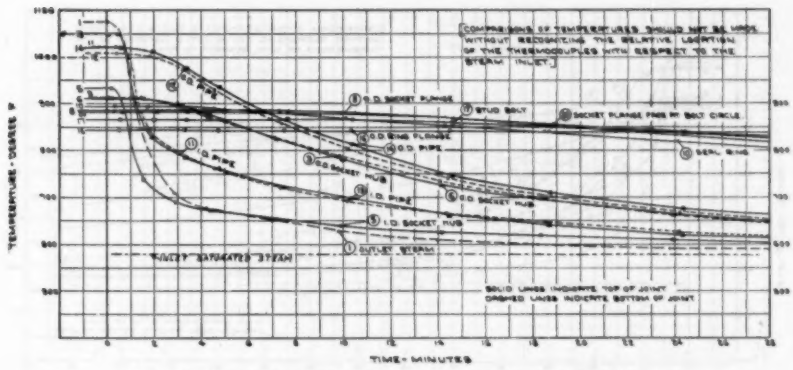

FIG. 10 TEMPERATURES ON PRESSURE-SEAL JOINT DURING QUENCH NO. 20

normal heating and cooling tests, and 25 cycles of quenching with 575 F steam.

Fig. 10 represents a typical quench and demonstrates the manner in which various thermocouple locations cooled during the 25 quenches. Extreme caution should be used in comparing temperatures because of the relative axial as well as radial positions of the thermocouple points. Comparison should be made only after recognizing that the temperature of the steam passing through the joint varies from point to point and also that there may be other factors which make direct comparisons misleading. The information as obtained does show large differences of temperatures and is presented mainly for that purpose rather than for any direct comparison or for substantiating inferences based upon temperature differences. A great many more thermocouple points are needed to determine the detailed behavior of the various parts of the joints.

In order to avoid a confusion of lines on the temperature graphs, all the temperatures measured at the top of the joints and pipe were plotted, but only those measured at the bottom which showed a considerable spread existing at some moment between corresponding parts of top and bottom were plotted. Temperature differences between corresponding parts of the joints at top and bottom, which are not shown by curves, did not exceed 30 F and usually were not more than 5 to 10 F on the three joints.

Upon disassembly it was noted that once the nuts, which had been lubricated with high-temperature thread compound, were broken loose they could be unscrewed from the bolt studs by hand. The bolt studs, similarly lubricated, also unscrewed easily and required only hand power for breaking loose. All nuts and bolts were found to be in excellent condition with no evidence of galling. The flanges were still flat at the end of the test. There was some extrusion of the gasket, because in the design it is intended that the gasket initially be stressed beyond the yield point.

Bellows-Type Joint. The bellows-type joint was tight from 0 to 4000 psi hydrostatic pressure with 20,500 psi initial bolt stress. It was also tight during the normal heating and cooling tests, although the bolt stress decreased to 12,800 psi as a result of slight yielding of the 18–8 flange.

With the bolt studs restressed to 20,300 psi, the bellows-type joint remained tight during the first six cycles of heating and quenching but leaked very slightly on quenches No. 7, No. 11, and No. 12. After quench No. 13, which produced no leakage, the bellows-type joint was restressed from a residual bolt stress of 16,100 psi to 19,900 psi. Ten more quench tests were conducted and leakage was detected 8 times. Whenever the bellows-type joint leaked, the amount of leakage was minor and would probably have passed unnoticed without the aid of the special leak detector. The joint sealed itself in every case. A résumé of all 23 quenches is contained in Table 1, and the curves in Fig. 11 illustrate the cooling rates at the various thermocouple locations shown in Fig. 6.

TABLE 1 EFFECT OF QUENCHES UPON TIGHTNESS OF BELLOWS-TYPE JOINT

Quench no.	Comment	Quench no.	Comment
1	Tight	13	Tight
2	Tight	14[a]	Leaked for 3 min
3	Tight	15	Leaked for 3 min
4	Tight	16	Leaked for 3 min
5	Tight	17	Leaked for 1 min
6	Tight	18	Tight
7	Leaked for 6 min	19	Leaked for 3 min
8	Tight	20	Leaked for 5 min
9	Tight	21	Leaked for 2 min
10	Tight	22	Leaked for 3 min
11	Leaked for 8 min	23	Tight
12	Leaked for 15 sec		

[a] Bolt studs were restressed before quench No. 14.

At the conclusion of the quench tests of the bellows-type joint the residual bolt stress was 19,400 psi. When the joint was disassembled it was found that the bolt-stud threads were free enough to permit turning the bolt studs by hand and showed no signs of galling. Final inspection revealed the 18–8 flange to be dished 0.010 in. at the OD of the bolt-circle face and 0.004 in. at the OD of the stellite-faced gasket chamber. The face of the studded flange was still flat at the end of the test.

Spiral-Wound Gasket Joint. Initial thickness of the spiral-wound metal, asbestos-filled gasket was 0.175 in. The tongue and groove in the flanges were machined so that when the bolts were tightened, the flange faces came into contact, and the gasket compressed 0.050 in. to a thickness of 0.125 in. With the spiral-wound gasket placed dry in the groove of the $2^1/_4$–1 chrome-moly flange, the joint was assembled with an average initial bolt stress of 29,900 psi. While tightening the bolt studs in increments of stress, the average bolt stress required to just bring the two flanges together was noted to be 11,500 psi. This was the stress required to compress the gasket the desired 0.050 in.

After determining that the joint was tight on 4000 psi hydrostatic pressure, it was heated at a normal rate to equilibrium metal temperature of 1050 F as indicated by the thermocouples $^1/_8$ in. from the inside wall. No leakage was observed during heating or cooling. Residual bolt stress averaged 25,800 psi.

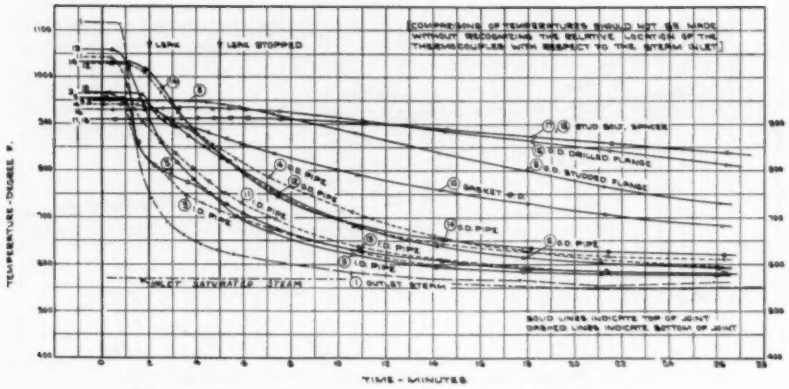

FIG. 11 TEMPERATURES ON BELLOWS-TYPE JOINT DURING QUENCH NO. 14

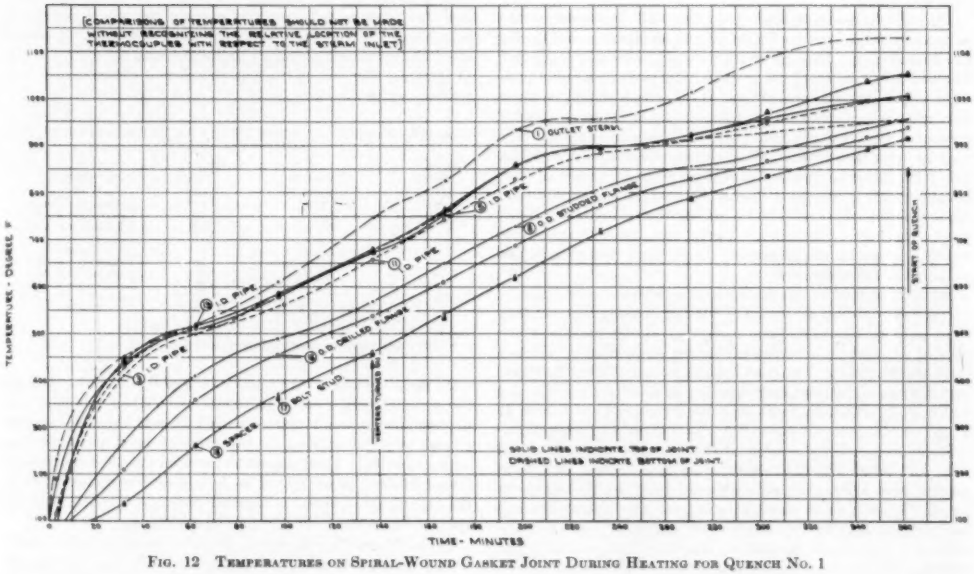

FIG. 12 TEMPERATURES ON SPIRAL-WOUND GASKET JOINT DURING HEATING FOR QUENCH NO. 1

With the average bolt stress of 25,800 psi, the joint was again heated and then quenched. Fig. 12 shows that just before the quench the metal temperatures ranged from 918 F for the top bolt spacer to 1055 F for the top inside wall of the pipe. After quenching for 5 min, the joint began to leak moderately. Leakage lasted for 15 min, after which the joint became tight, Fig. 13.

During quench No. 2, the joint began to leak 2 min after starting the quench. For the first minute the leak was moderate, after which it increased suddenly to the extent that part of the insulation blew out of the box exposing the 4 top bolts. The saturated-steam supply was turned off for 15 min, then it was again turned on gradually until a pressure of 1450 psi was reached. The joint was tight at this pressure and the test was discontinued after 8 min.

Since the flange faces were in contact, there was no easy path by way of which the steam that leaked past the gasket could escape to the atmosphere because the boltholes in this design of joint are virtually sealed by the smoothly machined bearing surfaces at the face of the nuts and at the ball-type seat of the bolt-stud spacers. When leakage occurred, the steam traveled along the top bolt containing thermocouple No. 17, Fig. 6, and out of the $^{9}/_{32}$-in-diam hole that had been drilled through the spacer into the bolt for thermocouple No. 17.

The residual bolt stresses averaged 19,800 psi. Disassembly of the joint revealed that from an initial compression of 0.050 in.,

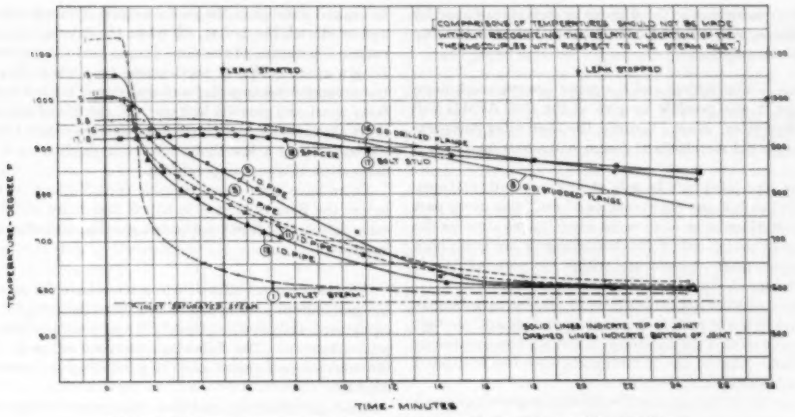

FIG. 13 TEMPERATURES ON SPIRAL-WOUND GASKET JOINT DURING QUENCH NO. 1

the gasket had taken a permanent set of 0.043 in., leaving a spring resiliency or final gasket compression of only 0.007 in. The gasket had flattened so that the radial clearance between the gasket and the groove decreased from 0.020 to 0.002 in. at the outer periphery of the gasket. No clearance remained at the inner periphery, and the gasket was very difficult to remove. The flange faces were flat at the end of the tests.

SUMMARY OF TEST RESULTS

1 The special 10-in. 1900-psi pressure-seal flanged pipe joint remained tight throughout 25 cycles of heating to 1050 F and quenching with saturated steam at approximately 575 F.

2 The special 10-in. 1900-psi bellows-type flanged pipe joint leaked 11 times out of a total of 23 quench tests. The amount of leakage was extremely slight, and the length of time of leakage varied from 15 sec to 8 min. The joint sealed itself in every case. Final inspection showed the drilled 18–8 flange deformed 0.010 in. at the outer edge and 0.004 in. at the OD of the stellite-faced gasket chamber.

3 Performance of the special 10-in. 1900-psi spiral-wound metal asbestos-filled gasket flanged pipe joint in this application was unsatisfactory. During the first quench the spiral-wound gasket leaked moderately for 15 min after which time the joint sealed itself. During the second quench the joint leaked severely.

ACKNOWLEDGMENTS

These tests were undertaken at the request of Sargent & Lundy, and the Commonwealth Edison Company.

Discussion

L. M. GOLDSMITH.[6] This paper is interesting, not only because of the comparison it presents between three quite dissimilar types of closures, but because of the bolting arrangement which permits the use of flanges which are much smaller than standard. The enormous mass of present high-pressure standard flanges is a very definite handicap to good piping design, and any attempt at reduction is a step in the right direction and should be given every encouragement.

The pressure-seal joint which gave the best results in the experiments reported is open to the obvious objection of high cost. We also wonder whether over a long period of time the greater expansion of the 18–8 male end will not cause the socket flange to spread as a result of concentration of stress in the narrow section under the shoulder.

We note that both of the gasketed joints leaked as a result of the severe shock-quenching to which the joints were subjected. This quench was apparently designed to simulate what happens in a pipe line as a result of water carry-over through the superheater of a boiler. It is our belief that such carry-over is of relatively infrequent occurrence in modern boilers and the test was therefore not entirely fair to the gasketed joints which would probably have remained perfectly tight under cooling and heating conditions such as are normally encountered in shutting down and starting up of power-plant machinery.

With particular reference to the spiral-wound gasket, we would be interested in knowing why the joint was designed so as to obtain a full contact over the ungasketed faces of the flanges. We note that this resulted in a final cold gasket compression of only 0.007 in., and it is probable that there was no compression whatever during the period when the joint was distorted by rapidly changing temperatures. The writer's company has been using spiral-wound gaskets in standard large male and female joints in its Van Dyke class steamships with very great success since 1937. Nine of these ships were built, so that we feel we have had considerable experience with these gaskets and joints in actual service. The temperatures and pressures are admittedly not as severe as those used by the authors in their tests, being only 625 psi at 910 F. However, the joints are subjected to weekly shutdowns while the ships are in port, so that the service required of the gaskets is unusually severe as compared to most power-plant services. As a result of our successful experience with these spiral-wound gaskets on our Van Dyke ships, we are using them again together with the same type of joint on the three supertankers which we are now building, which are designed for steam at 650 psi pressure at 1020 F.

We hope that if the authors intend to continue their studies, they will include a joint where the entire responsibility for the closure is placed upon the spiral-wound gasket. We are reasonably certain that such a gasket will remain tight under the pressure and temperature conditions imposed by the test, if the opposing flanges are of similar metals. But whether it would re-

[6] Chief Engineer, The Atlantic Refining Company, Philadelphia, Pa. Fellow ASME.

main tight when subjected to the slippage or distortion caused by a wide difference in coefficient of expansion between the two flanges is open to question.

J. C. Hobbs.[7] The subject and the paper deserve much more attention than it was possible to give at the 1950 ASME Fall Meeting at Worcester, Mass., because the increasing temperatures have made old standards of design dangerous under some conditions.

Almost any pipe joint may be safe at ordinary temperatures. Most joints are safe if the temperatures of each and every part are always maintained at or close to the same temperature as the other component parts, even if the temperatures are quite high and the pressure-made stresses are within the permissible safe limits of the materials used for the specific structure.

The condition which is not generally recognized as very dangerous is that in which one part is at one temperature and another at a different one so that the difference in the relative expansions exceeds the elastic limit of one or both parts—not free to expand to their normal condition.

Even very small differences of a few hundred degrees compared to the temperatures around 1000 F quite common today, may cause complete failure of piping or tubing of homogeneous structure.

The fact that most materials have a considerable amount of plasticity, and many materials of construction may be deformed beyond their respective elastic limits many times, is the only reason more disastrous failures have not occurred.

The behavior of structures is so complex that a leading world authority recently stated: "Two generations will be required before engineers generally recognize the full significance and effect of temperature differences."

It is a hopeful sign when leaders like the sponsors of this project recognize the need for research and follow through even at great expense to themselves. Full-size tests are very costly, particularly when expensive alloys constitute the structures, such as in the joints described, joining 18–8 to ferritic alloy.

This subject is entirely too great to cover in a limited discussion but briefly, the following comments are contributed to explain the poor behavior of two of the joints even under conditions much more favorable than often exist in practice:

Operating men know that the vertical joint in a horizontal line or the bonnet joint in a valve having a horizontal stem are the ones that leak when a "shot of water carry-over" passes through the pipe line. Furthermore, the leak is almost always at the bottom. The reason is evident; the lower part of the pipe is cooled enough to contract beyond the ability of the gasket to expand and maintain the seal. The hot top, perhaps three-quarters of the pipe circumference, acts as a very strong strut to keep the leak open, stretch the bolts, and even dish the face of the solid pipe end itself as it did on one of the flat face joints tested. The forces are so large that some part must yield beyond the elastic limit.

This occurred on this test even though the steam contained no water and it was caused to flow equally across the inside pipe face by the spiral passage around the solid core, tending to equalize top and bottom.

The thermocouples still indicated a considerable difference in temperature as they always do on a horizontal line due to convection cooling on the outside of the piping.

The spiral-wound metal asbestos-filled gasket failed to meet more of nature's fundamental laws than the other flat-faced joint because (1) the entire faces of the two flanges were in contact with each other so that when the interior lining of the pipe wanted to expand more than the cooler outside it would either upset its end or stretch the bolts; (2) when the interior of the pipe was cooled, the outside of the same flanges held the inner parts of the flanges apart. This is particularly true when only a part of the circumference is cooled and that remaining hot holds the cool faces apart and permits leakage; (3) the life of asbestos is very short above 750 F, and the useful resilience of this type of gasket limited to only a few thousands, perhaps three or four in most cases, even at lower temperatures.

There have been other valuable contributions on this subject before the Society, and it is hoped that more will follow at an early date so that it will not be two generations before more safety is assured.

S. S. Lippincott.[8] Introductory remarks in the paper recognize the problems of joining dissimilar alloys, the need for mobility of equipment, and provision for relative movement of the parts of the joint assembly. The following comment refers to the test of the spiral-wound gasket and the joint design in which it was assembled.

Although it is recognized that relative movement of the parts of the joint assembly are essential to a successful design, it appears to the writer that this feature was not given sufficient consideration in the design of the joint used in this test. Reference to Fig. 3 of the paper, indicates that flange faces will be in contact over their entire width to the outside diameter of the flange when the joint is made up, thus preventing freedom of movement necessary for successful performance.

A review of the test data indicates that leaks occurred during the quenching cycle at the high peak of temperature difference between the inside and outside of the flange faces and that leaks ultimately stopped as the outer portions of the flanges had the opportunity to cool and approach the reduced temperature at the inner flange faces. During those periods when the temperatures at the flange ID and OD were substantially the same no leaks are reported.

The nature of the leak at thermocouple No. 17 implies that the outside lips of the flanges were still in contact when the leak occurred, whereas the inner portions from the pipe orifice out to the boltholes were obviously separated. It is believed reasonable to assume that separation of the flanges was much more at the pipe bore than at that point immediately adjacent to the boltholes. Since the gasket was located as close to the pipe bore as appears conveniently possible and as illustrated in Fig. 3, a considerable loss in gasket-face load would occur due to relaxation in the flanges themselves and without consideration to the compressive force applied through the bolt studs. Spiral-wound gaskets have been supplied for service conditions up to 2000 psi 1050 F and for many installations at 1050 F and lower pressures. Numerous installations at pressure ranges of 1000 to 1500 psi and temperature ranges up to 1050 F have operated successfully for a number of years. No reports of operating failures have been received.

Many of these installations are with conventional flange designs, including clearance between the outer portion of the flange faces for movement due to expansion differences between the inside and outside of the fittings of like or unlike alloys. Where conventional large tongue-and-groove joints have been used, gaskets similar to the one used in the test under discussion have performed successfully. Where raised-face flanges have been used, similar gaskets, encased in outer gage rings, have performed successfully. In this design a radial contact $^1/_8$ in. nominal width is made with the face of the fitting. All portions of the flange beyond the standard raised face OD are free.

[7] Proprietor, Hobbs Science Services, Painesville, Ohio. Fellow ASME.

[8] Flexitallic Gasket Company, Camden, N. J.

It is realized that thermal-shock conditions normally encountered do not approach those used by the authors. It is indicated, however, that spiral-wound gaskets will give satisfactory service for peak temperatures and pressures, provided provision is made for flange movement due to thermal shock or other stresses resulting from pipe-line design.

In conclusion, it is believed the joint design used for the spiral-wound gasket test did not permit the desired movement of the flange faces and does not parallel actual service results obtained.

R. SHEPPARD.[9] The following remarks pertain to the spiral-wound gasket tests and in particular to the construction of the flanges containing the gasket.

Referring to Fig. 3 of the paper, it is evident that when the flanges are drawn together initially they contact over their entire face all the way to the outside diameter. Such a design must rely entirely upon the elasticity in the gasket with practically zero utilization of stud elasticity in order to keep adequate unit pressure on the gasket during the transient conditions induced by sudden temperature decrease of the steam flowing in the pipe.

This is confirmed if one studies the thermocouple temperatures of Fig. 13.

The temperature (16) at the OD of the drilled flange $7^1/_2$ min after the quench began had decreased practically none, whereas the flange inner-bore temperatures (11) and (13) had decreased approximately 350 F. Suppose we proportion this differential radially across the flange face hyperbolically. It can be calculated easily that the flange faces at the inside bore in the region of the gasket simply part company by about 0.010 in., which is greater than the 0.007 elasticity in the gasket; hence the gasket joint leaks until temperature equilibrium is reestablished.

It is the opinion of the writer that the spiral-wound gasket performance during such shop tests would have been surprisingly improved had the flange faces been relieved as shown in Fig. 14 of this discussion. With such a relief extending from the gasket

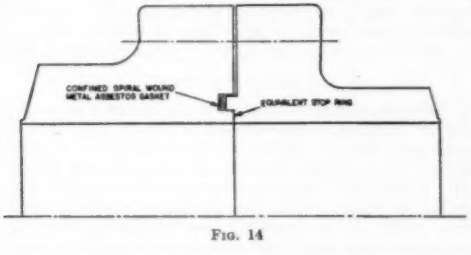

FIG. 14

to the OD of the flange, the faces are permitted to close up several mils by virtue of the temperature differential existing radially across the flange face. Such closure of the flanges at the OD would utilize to some degree the elastic stretch in the studs and greatly decrease the estimated 0.010-in. parting of the flanges in the region of the gaskets.

Perhaps the well-known and widely used type of spiral-wound gasket with its integral "stop ring" owes its success in part to the relieved faces of the raised-face-type flange in which it is commonly used.

The company with which the writer is associated has to date experienced completely satisfactory service with spiral-wound asbestos-filled gaskets in 24 flanged joints operating in five central-station steam turbines at 500 psi pressure and 1050 F. Some of these flanges have been in service nearly 2 years. These applications have about the same gasket proportions and diameters as were tested herein and in all cases one flange half is 18–8 steel and the other is ferritic steel. The spiral-wound gasket was selected primarily because it was believed capable of adjusting itself to the expansion movements occasioned by the different coefficients of expansions of the two materials. These expectations have been realized so far. It is very probable that none of these flanges has been subjected to sudden steam temperature decreases of over 50 deg per min for a total change of 200 F, whereas these laboratory tests approached 300 deg per min with a total change of 500 F. Twelve additional flanges with about 7-in-OD gasket continue to give trouble-free service at 1050 F at a pressure of 1500 psi in large tongue-and-groove flanges after 1 to 2 years. However, these applications had similar materials in both mating flanges. Satisfactory service at 1250 psi 1000 F

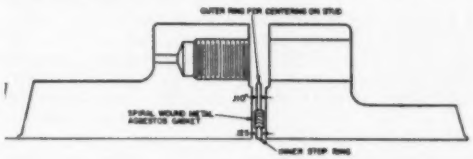

FIG. 15

has been experienced on other spiral-wound gasket applications.

It is hoped that the authors' single laboratory test will not give the impression that spirally wound gaskets are unsatisfactory for steam-service duty at 1000 to 1050 F and high pressures, for this certainly is not the case, on the basis of the writer's present experience.

The spiral-wound gasket used in the laboratory test was wound for a unit gasket pressure of approximately 15,000 psi when compressed to a thickness of 0.125 in. Flexible gaskets of such a density, when used with a "stop" have an advantage that high concentrated pressures on the tongue and groove in the region of the gasket seal area are not possible. Subsequently less distortion and creep of the flange faces, tending to mushroom edges under long-time high-temperature service, may yield a dividend not previously appreciated.

The relative simplicity of the spiral-wound gasket and its flange warrants further development to improve its shock characteristics. The writer suggests that further experiments and shock tests be conducted with spiral-wound asbestos gaskets with the flange-face reliefs similar to that shown in Fig. 14, or the stop-ring type illustrated in Fig. 15 of this discussion.

AUTHORS' CLOSURE

It is interesting to note that three of the four discussers are generally of the opinion that the tests of the joints were unfairly or abnormally severe. The quench was intended to simulate what happens in a pipe line when the steam temperature suddenly drops, for some reason, from superheat to saturation temperature. While it is asserted that this condition is of relatively infrequent occurrence in modern steam generators, yet some operators of both stationary power plants and ship power plants have experienced serious leakage from such causes frequently enough to consider it worth while to endeavor to develop a pipe joint that will remain tight even under such occurrences.

As indicated in the paper, the spiral-wound gasketed joint that was tested was constructed so as to obtain full contact over the

[9] Assistant Division Engineer, Steam Turbine Engineering Division, General Electric Company, Schenectady, N. Y. Mem. ASME.

entire faces of the flanges. This design was not originally included in the test program with the other two types of joints. After the program was under way, it was decided to also test the spiral-wound gasket joint in accordance with a request of the turbine manufacturer. The flanges were made by remachining the bellows-type joint flanges. When the joint leaked it is very probable that there was no compression of the gasket whatsoever as the joint distorted by rapidly changing temperatures. If the joint were to be redesigned it is possible that performance might be somewhat improved if the flange faces were relieved from the gasket out to the OD of the flanges, as has been suggested, so as to utilize the flexibility of the flanges, bolts, and gasket to the fullest extent.

In answer to Mr. Goldsmith's question concerning the strength of the socket flange of the pressure-seal joint, it may be pointed out that this joint is designed so that the amount of interference due to radial expansion of the 18-8 stub end (male end) relative to the socket is insufficient to cause high enough stress in the section under the shoulder of the socket flange to result in permanent deflection.

The authors wish to express their appreciation to those who submitted comments and discussion on the paper.

Investigation of Steam Separation in Boiler Drums Through Studies on a Model

By E. A. FARBER,[1] MADISON, WIS.

This investigation shows a method by which the performance of steam-boiler drum internals can be compared. The method is based on tests carried out with a model filled with Freon 12 liquid and vapor and gives the same density ratio between liquid and vapor which exists in the boiler. When the velocity of the liquid-vapor mixture in the model drum is adjusted to the proper value, then the separation forces in the model and boiler are the same. Freon 12 was selected after tests with water and air had been made but proved to be insufficient. The experiments were performed at different loads, pressures, and liquid levels in the drum. Several different drum internal arrangements were tested, and results and conclusions based on these tests are reported in this paper.

Introduction

THE present trend of increasing the output, operating temperature, and pressure of steam generators or boilers has caused steam separation to become one of the leading problems in power-plant engineering.

Steam generators are designed by men with years of experience drawing on actual performance data of similar units. After a steam generator is built, any changes which have to be made to improve its performance are very costly. A method based on model studies, by which the performance of drum internals can be compared, is explained in this paper. This method allows investigation of different and radically new drum internals which on the steam boiler is prohibitive because of risk and cost involved. These model tests can be carried on while the steam generator is still in the design stage, and from the results of these tests the best arrangement of drum internals can be selected.

Previous Investigation

The only tests with which the author is familiar, and which can be considered as being in the same general group are the ones made by R. A. Lorenzini of the Foster Wheeler Corporation. Mr. Lorenzini tested full-size drum internals in a half-drum with water and air at atmospheric temperature and pressure. Mr. Lorenzini was interested primarily in the entrainment and did not measure the carry-over. "Entrainment" is defined as the amount of vapor which is recirculated through the downcomers; "carry-over" as the amount of moisture being carried through the vapor tubes. Mr. Lorenzini's tests can be compared with the air and water tests at atmospheric condition which are included in the first part of this investigation.

Scope and Purpose of Present Investigation

In producing similar conditions in a model and its prototype it is seldom possible to have complete similarity as indicated by equal values for each dimensionless ratio involved. This investigation too, required a compromise in obtaining similar conditions.

Separation of liquid and vapor is accomplished by centrifugal and inertia forces. These forces acting on the liquid and on the vapor are adjusted in the model to be the same as the forces in the boiler. Viscosity and surface tension were considered to be of secondary importance. These two quantities were matched as well as could be done with different fluids.

First the possibility of using water and air was investigated. The tests were started at atmospheric conditions and then improved by going to higher pressures. The similarity between the boiler and the model improved with the increase in pressure, but is still rather poor at 200 psig, close to the maximum allowable operating pressure of the model.

Freon 12, as liquid in equilibrium with its own vapor (like water and steam in the boiler) seems to be the best choice of medium for the operation of the model since it allows testing at reasonably low temperatures and pressures. At the proper temperature and pressure, Freon 12 in the model gives the same liquid-to-vapor density ratio as the ratio which exists in the boiler drum, Figs. 1 and 2. Then by adjusting the velocity of the liquid-and-vapor mixture in the model, the separation forces can be made to be the same in the model and boiler.

The purpose of this investigation was to compare various arrangements and designs of drum internals and to select the internals which give the least amount of carry-over (moisture in the steam leaving the drum), and the minimum amount of entrainment (vapor recirculated in the downcomers).

Design of the Model

This research project was undertaken in connection with a new Foster Wheeler dual-circulation boiler which at the time was under construction at the Standard Oil Refinery, Whiting, Ind.

The method developed here is entirely general but since the work referred directly to the new boiler, the drum of the model, the heart of this investigation, is a true image of a typical section of the boiler drum but reduced in size to about one third. A model drum of this size allowed the use of standard tubes for the risers and downcomers of the model. The section of the drum was 12 in. from end plate to end plate so that three separators or desteamers can be installed on each side contiguous to each other. Each end flange was designed with a 6 in. clear-vision observation window, located eccentrically. When the end flanges are rotated, any section of the drum can be observed in turn. This design of the drum section allows visual observation of the separation process as it occurs in different parts of the drum, Fig. 3.

The rest of the equipment can be classified as auxiliary since its purpose was only to mix the liquid and vapor in any amount or ratio desired and to pump it into the drum. To accomplish this, two independent circuits, one for vapor and one for liquid, were required. Fig. 3 shows the vapor leaving the drum, flowing through a compressor into the mixing header and through the riser tubes back into the drum. The liquid is leaving the drum through the downcomers, flows through a variable-speed pump

---

[1] Assistant Professor of Mechanical Engineering, University of Wisconsin. Jun. ASME.

Contributed by the Power Division and presented at the Fall Meeting, Worcester, Mass., September 19–21, 1950, of The American Society of Mechanical Engineers.

Note: Statements and opinions advanced in papers are to be understood as individual expressions of their authors and not those of the Society. Manuscript received at ASME Headquarters, July 25, 1950. Paper No. 50—F-25.

into the mixing header, and then through the risers back into the drum. By throttling the vapor at the inlet of the constant-displacement compressor, the vapor flow can be controlled. The flow rate of the liquid can be controlled by varying the speed of the pump.

Measuring and Control Instruments

Fig. 4 shows the arrangement of the control instruments. The pressure in the drum of the model is determined with a Bourdon pressure gage and gives the condition under which the separation process takes place.

The pressure drop across calibrated orifices, which were installed in the vapor lines leaving the drum, measures the vapor flow rate.

When water is used in the model, the carry-over has to be measured by homemade separation calorimeters. The carry-over when Freon 12 is used can be determined from measurements of pressure and temperature ahead of the orifices in the vapor tubes and the pressure drop across the orifices. As a check of the results which were found from vapor tables, the temperature of the vapor, after it was throttled through the orifices, was also recorded.

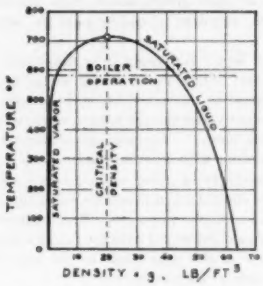

Fig. 1 Density of Water-Steam

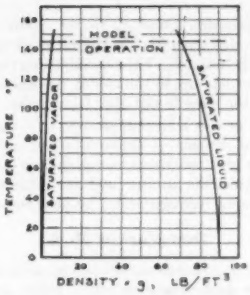

Fig. 2 Density of Freon 12 Vapor and Liquid

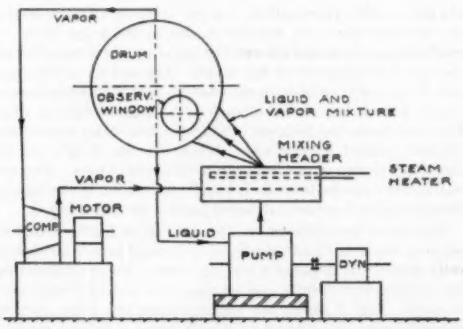

Fig. 3 Schematic Arrangement of Model Boiler and Accessories

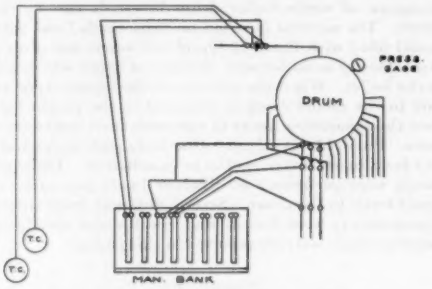

Fig. 4 Arrangement of Control Instruments

Calibrated nozzles in the downcomers are used to determine the flow rate of the liquid in terms of the pressure drops across the nozzles.

Static pressure taps located 3 ft apart in each downcomer measured the actual density in the downcomers. Since the density of the pure liquid can be found from the liquid tables, the amount of vapor in the downcomers can be calculated by simple ratios, from the density of the liquid and the actual density in the downcomers.

Figs. 5 and 6 show the model with the control instruments. Fig. 7 gives one arrangement of drum internals. Fig. 7(a) shows the position of the desteamers in the boiler-model drum. The inserts can be seen clearly. The inserts were removed later in the experiments leaving only a box of square cross section. As the liquid-vapor mixture enters the box tangentially through a nozzle, a vortex (without a guide) is formed inside the box, separating the liquid from the vapor. The liquid drains off in the corners while the vapor leaves the separator through the top center.

Experimental Procedure

The experimental procedure consisted of the determination of carry-over as well as entrainment at different (1) loads, (2) pressures, (3) liquid levels. The arrangements of drum internals tested were as follows:

1 No drum internals.
2 Cyclone separators with inserts.
3 Cyclone separators without inserts.
4 Cyclone separators without inserts and with spiders over the downcomers.

All these arrangements were tested with Freon 12 but only the first three with water and air.

The air and water tests were made at 0, 100, and 200 psig, at 80 per cent full, and 120 per cent normal load. The Freon 12

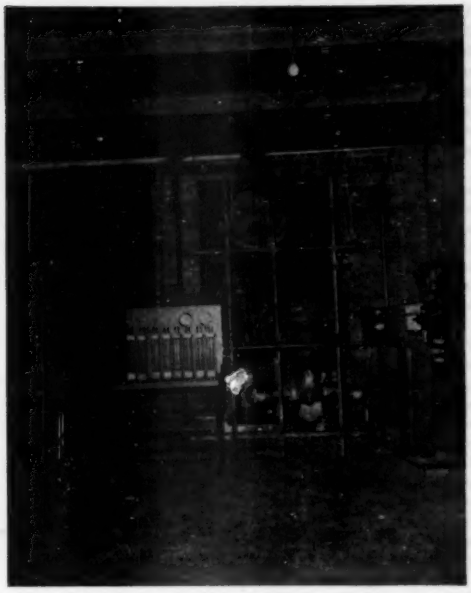

FIG. 5 APPARATUS COMPLETE WITH CONTROL INSTRUMENTS AND CONTROL BOARD

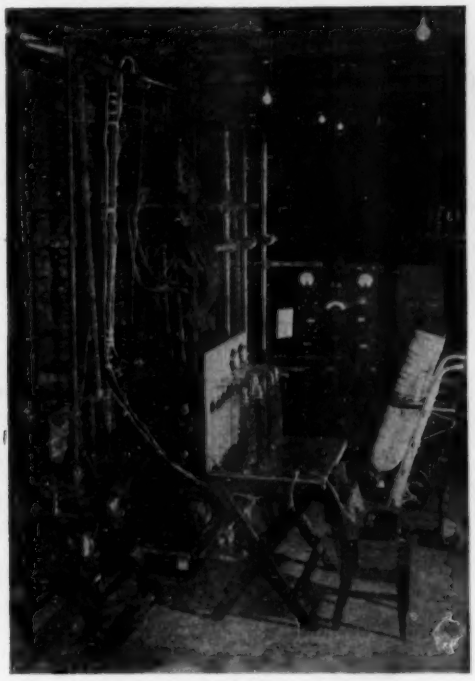

FIG. 6 CHARGING MODEL BOILER WITH FREON 12

tests were made at 175, 200, and 225 psig, at 80 per cent full, and 120 per cent normal load.

Normal load in the model is defined as follows: The same volume of vapor and liquid (volumetric ratio of 1 to 1) is circulated through the model at a velocity which gives separation forces of the liquid and vapor which are numerically equal to the forces in the boiler drum under normal operation. This volumetric ratio of 1 to 1 was maintained at 80 per cent and 120 per cent normal load.

The density ratio of water to air at 200 psig is 62 to 1 as compared with 12.4 to 1 for water and steam in the Foster Wheeler boiler drum at 1450 psia. The density ratio in the model filled with Freon 12 at 218 psig (145 F), as well as the separation forces, are the same as in the boiler.

The boiler velocities used in determining the separating forces were estimates supplied by the Foster Wheeler Corporation. The performance of the drum internals was also tested at lower and higher velocities, but the results are not reported here.

Normal liquid level in the model corresponds to normal water level in the boiler, low liquid level to the minimum allowable water level in the boiler, and high liquid level to the maximum allowable water level in the boiler.

DISCUSSION AND EVALUATION OF THE RESULTS

General Discussion of Results. The individual results of each tube were averaged, and the average values are reported here rather than the results of each tube. This was done to prevent the listing of a great amount of data or to draw an unreasonable number of curves. The averaged results follow the same trend as the individual results and are numerically almost the same, but it was believed that the averages are a better representation than the results of a specific tube. The results are presented here graphically in such a way that they can be applied directly to the actual boiler.

A superficial glance at the results obtained, Figs. 8 through 14, shows that some factors will increase carry-over and entrainment independently from the particular arrangement of drum internals. The magnitude of the increase of carry-over and entrainment can, however, to some extent be controlled by the drum internals.

Factors Inducing Carry-Over and Entrainment. A closer check of the results reveals that carry-over increased with increase in load or pressure or liquid level. On the other hand the entrainment increased with an increase in load or pressure but with a decrease in liquid level.

Modifying Effect of Drum Internals. The drum internals modify the influence of load, pressure, and liquid-level changes according to the effectiveness of the particular arrangement tested. Step by step therefore, a set of drum internals can be changed until best results are obtained.

Water and Air Versus Freon 12. As the boiler pressure increases, the density ratio of the liquid to vapor decreases making the separation process more difficult. This fact could be observed in the results of the model as the density ratio decreased. With this decrease of the density ratio the amounts of carry-over and entrainment increased. The lowest density ratio which could be obtained with water and air was 62 to 1, while the boiler was intended to operate normally at a ratio of 12.4 to 1. Visual observation of the separation process in the drum showed that at higher pressures more thorough mixing existed, as evidenced by smaller and more numerous vapor bubbles in the liquid in the drum.

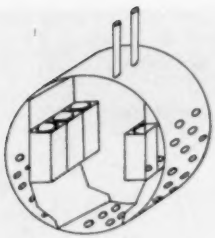

FIG. 7(a)

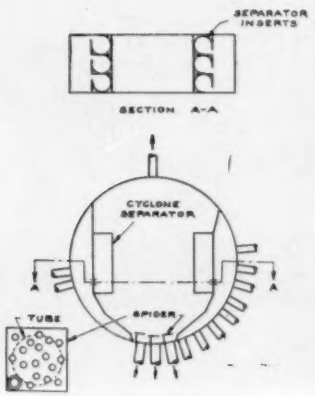

FIG. 7 DRUM INTERNALS

Since the separation was accomplished comparatively easily at higher density ratios as 62 to 1, finer differences in drum internals, or better, their effectiveness, could not be detected. Freon 12, however, brought out those differences. This last fact also seems to be a very strong support of the belief that the density ratio is one of the most important dimensionless ratios in steam-separation similarity of this type.

Water-and-Freon-Vapor Mixture. The possibility of using a liquid and a different vapor such as water and Freon 12 vapor was investigated, but the determination of carry-over proved to be rather difficult.

Relative and Absolute Value of These Results. This investigation leaves little doubt as to the value of the method described here in distinguishing between different types of internals, and it permits a choice of the best arrangement. In other words, this method gives a relative comparison. It was also noticed that the numerical values of carry-over and entrainment were of the same order of magnitude as the results of some field tests with respect to entrainment made by the Foster Wheeler Corporation on similar boilers.

Effect of Load Changes Upon Carry-Over and Entrainment. An increase in load forces more vapor to leave the drum, causing more turbulence in the drum, which results in higher carry-over and entrainment.

Effect of Pressure Changes Upon Carry-Over and Entrainment. An increase in pressure decreases the density ratio and, therefore, lessens the difference between the separation forces on the liquid and on the vapor, and less complete separation results.

Effect of Liquid Level Changes Upon Carry-Over and Entrainment. An increase in liquid level lessens the vapor space in the drum, thus giving a wet sample less time to remain there and to lose the liquid carried along. The inherent increase in velocity will also carry larger liquid drops into the vapor tubes. This increase in liquid level, however, increases the liquid space in the drum and, following the same reasoning as before, will give more time for separation, lower velocity, and therefore decreases the entrainment.

Carry-Over and Entrainment With No Drum Internals. When no drum internals were used, it could be seen that the mixture entered the drum from the riser tubes in irregular gushing jets sending liquid spray right into the vapor tubes. Some of these jets entering below the liquid level, others impinging upon the liquid-vapor interface produced violent mixing of the liquid and the vapor in the drum. This continuous turbulent action resulted in very large amounts of carry-over and entrainment.

Carry-Over and Entrainment With Drum Internals. Separators with inserts were installed first since they are standard and were intended to be used in the boiler at Whiting. The results obtained were much better. No open jets could carry large droplets directly into the vapor tubes. No jets entered the drum below the liquid level, the mixing in the drum was much less violent, and less vapor content could be noticed in the liquid in the drum. The entrainment, however, did not decrease as much as it should have and close observation revealed that (especially at low liquid levels) vortexes were formed over some downcomers carrying vapor from the vapor-liquid interface into the downcomers, thus increasing the entrainment. Spiders were put over the downcomers, Fig. 7, which prevented these vortexes from forming.

Then the separator inserts were taken out. No difference in the results with water and air could be noticed, but Freon 12 showed better performance without inserts, Figs. 12 and 13. If Figs. 13 and 14 are compared with respect to the entrainment, the effectiveness of the spiders can be appreciated.

CONCLUSIONS

1 An increase in load, keeping pressure and liquid level constant, increases the amount of carry-over and entrainment.

2 An increase in pressure, keeping load and liquid level constant, increases the amount of carry-over and entrainment.

3 An increase in liquid level, keeping load and pressure constant, increases carry-over and decreases entrainment.

4 Load and liquid-level changes have a much greater effect upon carry-over and entrainment than pressure changes.

5 Water and air tests cannot be used to bring out finer differences in performance of drum internals.

6 The possibility of using mixtures such as water and Freon 12 vapor has to be investigated further.

7 Carry-over is caused by the following:

(*a*) Direct spray.

(*b*) Entrained spray carried because of the high vapor velocities.

8 Entrainment is caused by the following:

(*a*) Direct mixing of liquid and vapor in the drum.

(*b*) The formation of vortexes over some downcomers.

9 Any condition which reduces the difference between liquid and vapor density will make the separation more difficult. The present trend of increasing the steam-generator pressure is one of those factors.

10 The determination of the performance and the distinction between the performance of different drum internals has been established by this new method of model testing.

11 An increase in velocity of the separators or a decrease in diameter increases the separation forces and causes more complete separation. There is, however, a practical limit to the maximum velocity at which either the mixture starts spilling

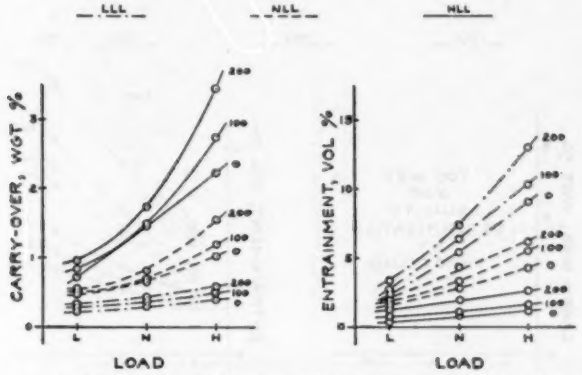

FIG. 8 CARRY-OVER AND ENTRAINMENT; NO DRUM INTERNALS; WATER-AIR

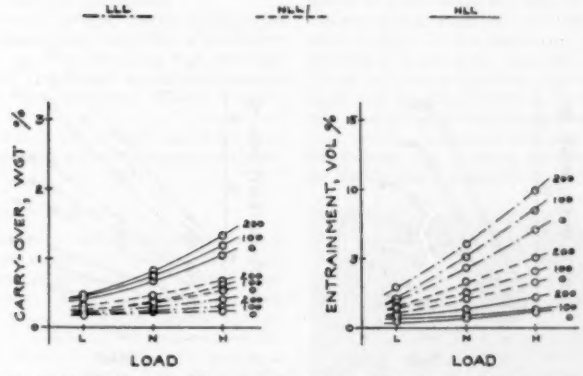

FIG. 9 CARRY-OVER AND ENTRAINMENT; CYCLONE SEPARATORS WITH INSERTS; WATER-AIR

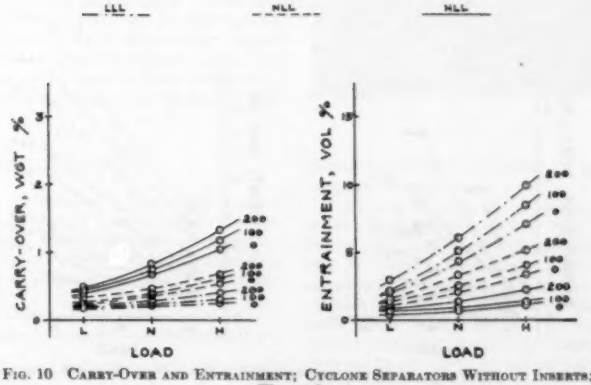

FIG. 10 CARRY-OVER AND ENTRAINMENT; CYCLONE SEPARATORS WITHOUT INSERTS; WATER-AIR

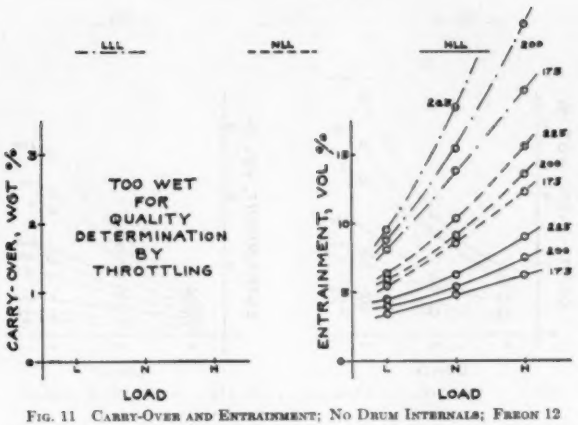

FIG. 11 CARRY-OVER AND ENTRAINMENT; NO DRUM INTERNALS; FREON 12

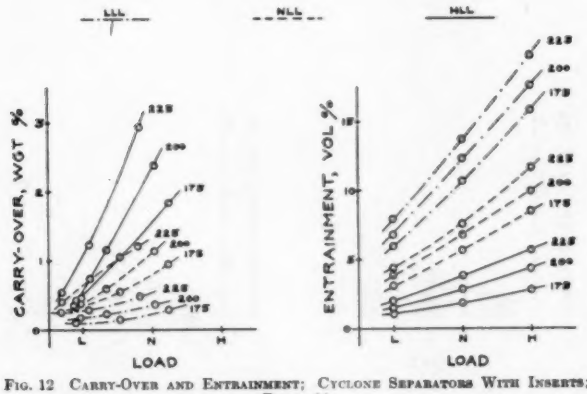

FIG. 12 CARRY-OVER AND ENTRAINMENT; CYCLONE SEPARATORS WITH INSERTS; FREON 12

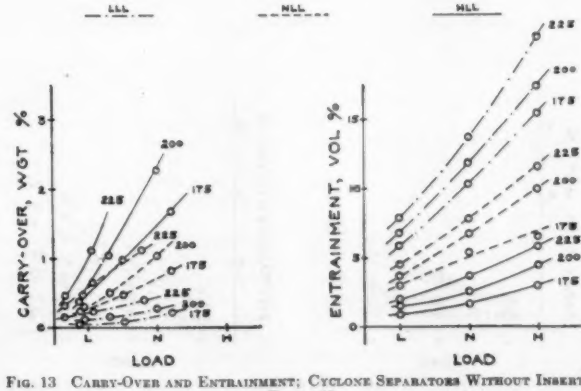

FIG. 13 CARRY-OVER AND ENTRAINMENT; CYCLONE SEPARATORS WITHOUT INSERTS; FREON 12

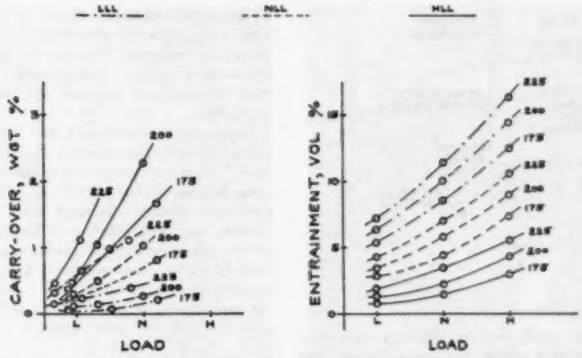

FIG. 14 CARRY-OVER AND ENTRAINMENT; CYCLONE SEPARATORS WITHOUT INSERTS; SPIDERS OVER DOWNCOMERS; FREON 12

over the top of the separator or the pressure drop across the separator is too great to allow proper functioning.

12 The absolute relationship between the numerical results of the model and boiler tests and their correlation will still have to be investigated further. However, the results, Figs. 8 through 14, of this investigation are of the same general magnitude as those of field tests conducted by the Foster Wheeler Corporation on similar boilers.

13 The author believes that this method, using Freon 12 or similar fluids, will aid appreciably in the development of simpler and better drum internals.

ACKNOWLEDGMENTS

Herewith the author wishes to express his indebtedness to Dean H. O. Croft, University of Missouri, Columbia, Mo., under whose guidance this project was undertaken and carried to completion. His advice, assistance, and judgment were highly valued.

The valuable advice of Mr. G. W. Watts, Director of Engineering, Mr. A. T. Milbrook, Assistant Chief Engineer, and Mr. Rank, Designer, all of the Standard Oil Company of Indiana, is gratefully acknowledged and, in particular, their help with the design and actual construction of the model boiler was appreciated.

Acknowledgment is made to the Foster Wheeler Corporation which furnished blueprints and data of one of its new-type boilers which was being built at the time for the Standard Oil Company at Whiting, Ind., and to Mr. R. A. Lorenzini, research engineer, for his assistance and for giving valuable information.

This research project was carried on at the State University of Iowa, Iowa City, Iowa, under a Fellowship of the Standard Oil Company of Indiana.

Discussion

R. U. BLASER[2] AND F. G. RAYNOR.[3] The author has presented a very interesting account of a new testing technique. The laboratory duplication of mixture densities, velocities, and separating forces has always been difficult and the author's use of Freon 12 under pressure is an excellent contribution toward solving the problem.

The writers' company has for more than 20 years used full-scale models in a laboratory test drum to develop new designs and improve existing steam and water separators. This apparatus, shown in Fig. 15 of this discussion, has full glass ends and access openings to admit actual production models for test purposes. The air and water used in these tests are supplied by a blower and pump and complete instrumentation is provided to measure quantities and other variables. Various testing techniques have been used in the past for investigation of different problems. For example, Fig. 16 shows a device for measuring carry-over. By maintaining a measured chemical concentration in the test

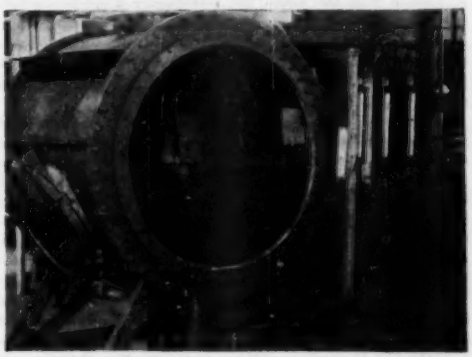

FIG. 15

drum, the increase in conductivity in the upper water chamber is a measure of carry-over.

Conversion of such laboratory results to steam and water conditions with factors derived from Stokes' law has been correlated with many tests on steam boilers in service. The Babcock & Wilcox cyclone steam separator and corrugated steam scrubbers are outstanding examples of the successful application of laboratory developments to operating boilers. Progress in boiler design during the past 10 years has improved the efficiency of separation such that steam containing less than 0.5 ppm can be obtained from a drum into which is discharged more than 1,000,000 lb per hr of steam and 12,000,000 lb per hr of water.

[2] Babcock & Wilcox Company, Research and Development Department, Alliance, Ohio.

[3] Babcock & Wilcox Company, Staff Engineering Department, New York, N. Y. Jun. ASME.

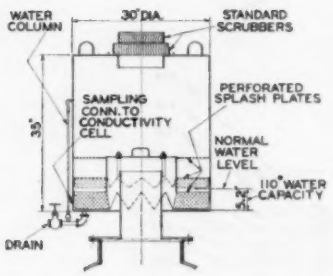

FIG. 16

This high degree of steam purity can be obtained over wide ranges in pressures, fluctuating steam flow, water levels, and boiler-water concentrations.

The separation of steam and water can be broken down into several phases. First is the primary separation which must be accomplished on the mixture of steam and water entering the drum. The first function of a primary separator is to remove the steam from the water to be recirculated. The Babcock & Wilcox cyclone separator uses a tangential inlet to a cylinder to provide the centrifugal forces used for separation. The author's test results indicate an improved performance with the "inserts" removed from the primary separators. Since the centrifugal forces are then no longer present, it would seem that the application of the term "cyclone separator" to that particular design is a misnomer.

The second phase of the separating process should be designed to remove from the steam the boiler-water droplets resulting from incomplete primary separation. Of particular concern here is the necessity of keeping the steam velocity low enough to avoid carrying the droplets along. Both secondary and primary separators should be so arranged that variations in water level in the drum will not affect their performance.

An efficient primary separator must function over 12 to 15 in. variation in water level. For example, the Babcock & Wilcox cyclone separator develops enough kinetic energy to impel the separated water through directing vanes at a velocity sufficient to overcome the head of water in the drum, even though the separator may be partly submerged. In evaluating the relatively large effect of changes in water level reported by the author, it would be helpful to know the actual levels represented by the curves labeled low, normal, and high liquid level.

The author defines normal load as a one-to-one volume ratio of vapor and liquid at a definite velocity. Since he indicates that the tests at lower and higher velocities are not reported, does the "load" abscissa on the curves of his Figs. 8 through 14 represent a variation in the volume ratio, total vapor flow, or some other variable? During operation of natural-circulation boilers, the steam load in terms of volume or weight varies over a considerable range without changing the water circulation a proportionate amount. In the test work a complete schedule of variables must be covered since some types of separators in special applications can lose efficiency at low loads as well as high.

Another factor which should be controlled closely is the one-third scale used in the author's tests. We agree with the author that model similarity is difficult to achieve, and it would seem worth while to use full-size equipment in such development work.

In addition to the variables which can be investigated in laboratory tests, there are other factors which have adverse effects on separation efficiency. Foaming may be caused by excessively high boiler-water concentration or considerable amounts of other contaminants. The layer of steam bubbles will vary with boiler-water analysis and pressure as well as concentration. Such a foam layer decreases the space available for secondary separation.

Experience has indicated that a satisfactory test method of measuring steam purity below 1 ppm does not exist at the present time. Even with carry-over values of such a low order, troublesome turbine fouling with both soluble and insoluble deposits sometimes occurs. Although conductivity of condensed-steam samples may give relative indications, it seems necessary for further improvements in separator designs to be judged on the basis of turbine performance. At least some of these turbine deposits are concerned with the equilibrium condition of chemical compounds in boiler water and steam at operating temperature and are very difficult to duplicate in laboratory tests.

It is encouraging to find others who are doing work in this field, and we would again like to commend the author for his use of Freon 12. We have presented a number of additional factors in the hope that other research investigations may be encouraged. Continued research and development work is certainly necessary to eliminate the last fraction of troublesome carry-over which now plagues the industry.

A. P. BOEHMER.[4] The author is to be congratulated on his unique approach to the problem of investigating high-pressure high-temperature equipment under conditions of relatively low pressures and temperatures. The fact that it is possible to determine what happens and to make changes inexpensively and rapidly makes the model technique important and useful.

The approach by dimensional analysis, however, requires that all variables be accounted for. The author states that once the density ratios of the fluids are equal, "Then by adjusting the velocity of the liquid and vapor mixture in the model the separation forces can be made to be the same in the model and boiler."

This writer cannot agree that separation forces are independent of the surface tension of the fluids. It is likely that as the surface tension increases, there is probably an increase in both carry-over and entrainment, although this is a question.

The viscosity too has not been considered. A Reynolds criterion might be more important than simply velocity comparisons in so far as fluid characteristics are concerned.

A check on these two properties is possible by use of a fluid other than Freon 12. Either Freon 11 is recommended, which will give proper density ratios corresponding to Freon 12 at lower pressures than the latter, or Freon 114 which will operate at lower temperatures than Freon 11 but at high pressures, although lower than Freon 12.

Another suggestion, to make the data more universal in application, would be to establish a quantitative yardstick with regard to the fluid level in the drum. This either could be a diameter ratio or depth of submergence of the tubes.

A true model study requires a check of the actual equipment for accurate comparison. The author simply has indicated that "... the numerical values of carry-over and entrainment were of the same order of magnitude as the results of some field tests with respect to entrainment..." This could hardly be considered corroborating evidence. It is realized that there are difficulties in testing on the prototype boiler, but it is hoped that at some time data can be taken to confirm or deny similarity.

[4] Associate Professor of Mechanical Engineering, State University of Iowa, Iowa City, Iowa.

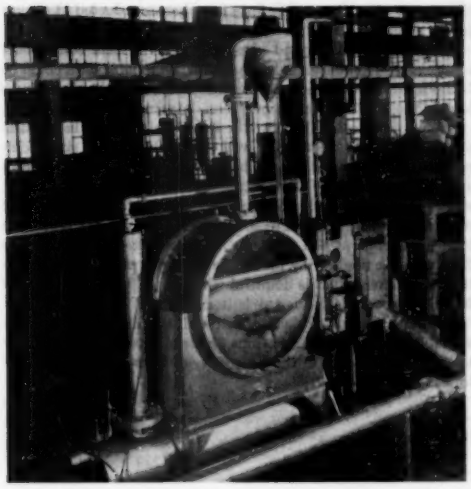

FIG. 17 AIR-WATER TEST APPARATUS—FRONT VIEW

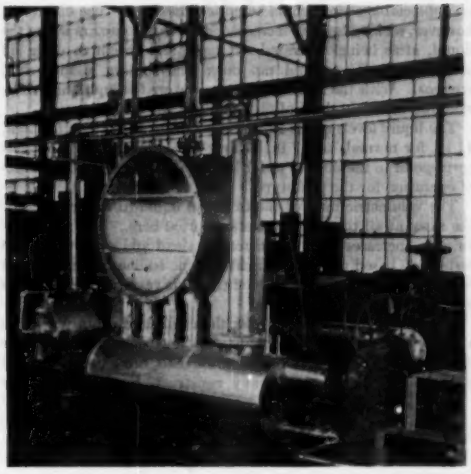

FIG. 18 AIR-WATER TEST APPARATUS—REAR VIEW

It would add to the paper to mention that the density ratios of Freon 12 at 175, 200, and 225 psig correspond approximately to boiler pressures of 1200, 1350, and 1500 psia.

R. A. LORENZINI.[8] The organization with which the writer is associated has used atmospheric air and water exclusively in the development of separators for use in steam drums of boilers. Full-size separators in full-diameter drums have been and are being tested at volumetric rates of air and water flows comparable to the steam and water flows encountered in actual boilers. Transparent plastic heads have been used, and the separators tested contain "windows" so that the flow mechanism can be studied and photographed for future reference.

Visual observation is perhaps the most important phase of these investigations, but since the imagination is known to play pranks on one's memory, a photographic record is kept so that various devices may be readily and accurately compared at some future time.

While the use of air and water has serious shortcomings, it furnishes much valuable information to the boiler manufacturer and, in general, a device which shows promise with air and water will usually be more successful in the boiler than one which does not perform satisfactorily in the air-water test apparatus. Aside from the fact that the density ratio of air and water differs greatly from that of steam and water in the boiler, the various thermal properties such as viscosity and surface tension which are known to affect separation are also different. Through the choice of another medium such as Freon 12 liquid and its vapor, density ratios comparable to those existing in high-pressure boilers can be attained at moderate pressures and temperatures. However, any simultaneous agreement of the other thermal properties would be fortuitous. Aside from the requirement of similarity of these thermal properties, similarity of the physical factors such as lengths and forces must also be satisfied. In a device which relies on centrifugal force for separation, physical similarity is partly achieved when the separating factor V^2/rg is the same for the model and prototype. Since complete similarity cannot be attained or even closely approached, it is not possible to predict exactly in a quantitative sense the performance of a device in a boiler drum from tests made in a model with a different fluid. Evidence of this lies in the fact that the author's tests with Freon 12 gave appreciable downcomer entrainment, whereas tests on the actual boiler at full load over a range of gage glass levels varying from a point 8 in. below normal to a level 8 in. above normal resulted in no measurable downcomer entrainment.

Aside from obtaining valuable information on separating effectiveness through the use of the air-water test apparatus, pressure-drop data which are directly applicable to the boiler installation can be obtained. A knowledge of the pressure drop of the separating device is important because of its effect on the circulation in the boiler.

Figs. 17 and 18, herewith, show two views of one of several air-water test drums which are being used in our laboratory for the study of steam-water separation. The air and water loadings can be varied over wide ranges and, for any level and rating, the performance of the separating device is established by collecting and metering the air which is entrained in the downcomers and by measuring the moisture carry-over. The photographs demonstrate the ease with which the flow phenomena and separating mechanism may be observed and the ready accessibility of the drum-internals for changes.

[8] Mechanical Engineer, Research Department, Foster Wheeler Corporation, New York, N. Y. Jun. ASME.

AUTHOR'S CLOSURE

The author wishes to thank all the discussers for their interest in this subject and their helpful comments. It was especially interesting to have representatives of the two largest boiler manufacturing companies discuss this paper and to hear about experiments they are conducting in their research and development laboratories.

The author wishes next to answer some of the questions raised by the discussers. He cannot agree with Mr. Blaser and Mr. Raynor that, when the inserts are taken out of the separator boxes, the centrifugal or separation forces disappear. The vortexes were still present as could be seen by visual observation and

no appreciable change could be noticed in them. The difference, however, seemed to be in increased space in the corners where the liquid, after being separated out had ample room to drain off undisturbed. The liquid ran down the corners in four even streams. With the inserts in the separators the liquid had to be removed as a thin sheet of film all along the inserts.

The liquid levels in the 24-in. model drum were 15 in. for high, 11 in. for normal, and 7 in. for low liquid levels. These levels correspond to the normal water level, and upper and lower limits of operation for the prototype.

The volumetric ratio of one to one of liquid to vapor was kept the same at all times in the tests reported here. The water circulation increases with the increase in load and since the model tests were based upon an estimate of one to one vapor to liquid ratio at normal load it is believed that this variation is as good as other changes of the variables.

The reason for using a smaller than full-sized drum was to be able to use a lighter design and tube dimensions practicable for laboratory use. If a full-sized drum had been used it would have had to be of very heavy construction. This is partly the reason why all previous tests have been conducted at atmospheric conditions.

The surface tension and viscosity also will have some effect upon the results of the model; however, no reliable data could be found for water and steam at the high pressures and temperatures used in the boiler. In addition Freon data was rather incomplete.

Undoubtedly other fluids will be found which fulfill the requirements for model tests equally well or even better but since comparatively large quantities of fluid are being used and a certain amount is lost during the filling and emptying processes, a fluid easily and economically obtainable must be found. Freon 12 was the cheapest of the Freons and could be obtained easily in large quantities at the time the tests were conducted. Other Freons can be used giving the required density ratios at somewhat lower pressures but it is doubtful whether the viscosity and surface tension correlation is any better.

The author again wishes to thank all the discussers for their valuable comments and questions which he hopes can be solved by tests being continued at the University of Iowa and other laboratories.

Flow of a Flashing Mixture of Water and Steam Through Pipes and Valves

By W. F. ALLEN, JR.,[1] BOSTON, MASS.

A simple method is presented of designing piping and valves, particularly heater drain piping, to carry a flashing mixture of water and steam. Rational design formulas are derived from the energy, continuity, and dynamic equations on the basis of an assumed uniform mixture at any point in the path of flow. Earlier papers have predicted and verified experimentally the existence of a critical pressure, under certain conditions at the end of a pipe carrying a flashing mixture. Results calculated from the derived formulas compare favorably with these published test data. It is noted that if the initial assumption of a uniform mixture is not fulfilled, the limitations imposed on the piping are less severe than for the uniform-mixture case, as the capacity of both valves and pipes will be greater than predicted by formulas. A scheme is suggested for eliminating flashing completely in heater drain systems employing drain coolers.

Nomenclature

The following nomenclature is used in the paper:

p = absolute pressure, psf
v = specific volume, cu ft per lb
h = enthalpy, Btu per lb
V = velocity, fps
W = mass rate of flow, lb per sec
A = area of cross section, sq ft
z = height, ft
L = total equivalent length, ft
D = diameter, ft
Y = perimeter of duct, ft
g = acceleration given to unit mass by unit force, ft per sec^2
f = coefficient of friction
Q = heat transfer, Btu per lb
Subscript f = refers to property of saturated liquid
Subscript g = refers to property of saturated vapor
Subscript fg = refers to property change due to change of state from saturated liquid to saturated vapor

Introduction

The design of piping, such as the cascade drain lines between feedwater heaters, which convey initially saturated liquid from a source at one pressure to a receiver at a lower pressure has been a perplexing problem. Experience has proved that sizing valves and piping for this service by the usual criteria for liquid flow is unsatisfactory. The alternative procedure of sizing by empirical formulas or arbitrary selection not only is costly but, more important, offers no guarantee that the resultant capacity of the piping system will be adequate.

Earlier writers have predicted that the vaporising liquid will exhibit a maximum in the curve of flow per unit area versus pressure drop as does a vapor. Subsequent papers have verified this prediction experimentally for pipes by measurement of a pipe exit or critical pressure above the pressure in the receiver; however, the proposed method of numerical integration of the combined dynamic and continuity equations to determine this maximum is so tedious and time-consuming as to be impractical for everyday engineering use.

The primary objective of this paper is to present simple rational formulas that may be used in design, with the assurance that the resultant capacity of both valves and pipes will be adequate.

Results calculated from the derived formulas are compared with published test data. Additional data from operating steam power stations, although not taken with the precision required of experimental data for exact conformation of the formulas, confirm the existence of the critical-pressure phenomena in cases predicted by formulas. Several alternative designs of heater drain systems are discussed and specific instructions are included for application of the formulas to each case.

Development of Formulas

Any analysis undertaken to predict the flow characteristics of a two-phase mixture, such as water and steam, necessitates an assumption concerning the nature of the flow. Several possible assumptions are as follows:

1 The water and steam flow as a finely divided mixture with equal average velocities.

2 The water and steam travel separately with equal average velocities and with a continuous interface between them.

3 The water and steam travel separately with unequal velocities and with a continuous interface between them.

4 The water and steam travel as a mixture with unequal velocities.

Of these possible assumptions the first offers the most opportunity for analysis and is the one followed herein. It is also assumed that the properties of the mixture are as given in the Steam Tables (1).[2] The degree of validity of these assumptions can be determined only by a comparison of test data with results obtained from formulas.

For any problem involving the one-dimensional steady flow of fluids, the applicable fundamental relations are

Energy equation*

$$dh + d\left(\frac{V^2}{2g}\right) + dz - dQ = 0 \quad \ldots\ldots\ldots [1]$$

Dynamic equation

$$vdp + d\left(\frac{V^2}{2g}\right) + dz + \frac{fYV^2}{2Ag}\,dL = 0 \quad \ldots\ldots\ldots [2]$$

---

[1] Engineer, Mechanical Division, Stone & Webster Engineering Corporation. Jun. ASME.

Contributed by the Power Division and presented at the Fall Meeting, Worcester, Mass., September 19–21, 1950, of The American Society of Mechanical Engineers.

Note: Statements and opinions advanced in papers are to be understood as individual expressions of their authors and not those of the Society. Manuscript received at ASME Headquarters, August 14, 1950. Paper No. 50—F-27.

[2] Numbers in parentheses refer to Bibliography at end of paper.

* The dimensional constant $J = 778$ is purposely omitted in this expression.

Continuity equation

$$W = \frac{VA}{v} \quad \ldots\ldots [3]$$

Heat transfer and the influence of static head are assumed to be negligible in the analysis which follows.

The three fundamental relations alone will not suffice for a solution of the flow conditions. An additional relation for the fluid is needed between any two of the four variables which may be found from a table of properties or, if capable of algebraic representation, in the form of an equation of state.

Theory of Flow Through Pipes

For flow through pipes of constant cross-sectional area the dynamic Equation [2] may be combined with the continuity Equation [3] as follows: For a pipe of uniform section, Y/A may be expressed in terms of the diameter and W/A is a constant; hence $dV = (W/A)dv$ and Equation [2] may be rewritten as

$$v\,dp + \left(\frac{W}{A}\right)^2 \frac{v\,dv}{g} + \left(\frac{W}{A}\right)^2 \frac{4f}{2Dg} v^2 dL = 0 \quad \ldots\ldots [4]$$

Dividing through by v^2 and integrating, Equation [4] becomes

$$\int_{p_1}^{p} \frac{dp}{v} + \left(\frac{W}{A}\right)^2 \frac{1}{g} \log_e \frac{v}{v_1} + \left(\frac{W}{A}\right)^2 \frac{2fL}{gD} = 0 \quad \ldots [4a]^{**}$$

Equation [4a] may be rearranged

$$\left(\frac{W}{A}\right)^2 = g \frac{\int_{p_1}^{p} -\frac{dp}{v}}{\log_e \frac{v}{v_1} + \frac{2fL}{D}} \quad \ldots\ldots [4b]^{2}$$

This equation may be solved by assuming a friction factor, an equivalent length of pipe, and evaluating the integral

$$\int_{p_1}^{p} -\frac{dp}{v}$$

numerically by taking small pressure increments and summing the values of $\Delta p/v$. For the case of flow through a line without a throttling or control device, the initial pressure p_1, is known.

A calculation of this type extended down to a suitably low value of pressure will indicate the existence of a maximum value of W/A for an optimum downstream end pressure; this end pressure depends on the equivalent length of piping, the friction factor, and the initial saturation pressure. If the pressure in the receiver is less than this optimum end pressure, the pressure at the end of the line will be the optimum pressure. This optimum end pressure will be referred to henceforth as a critical pressure.

In heater drain lines the flow is restricted to maintain a predetermined level in the upstream source, and across the throttling device in the drain line the pressure drops automatically to that required to force the fluid into the receiver.

In order to apply Equation [4b] to determine a critical pressure at the end of a heater drain line, it is necessary first to assume a pressure after the drainage control valve or other control device. If this assumption is not correct, and the possibility of its being exactly correct is remote, it is necessary to repeat the entire numerical summation process at least twice in order to plot a curve from which the correct value of W/A can be determined; W/A is a known or desired quantity from the heat balance or other data. For a different value of W/A, which would be a trial with a different pipe size, all other conditions remaining the same, the calculation has to be repeated three more times.

This lengthy calculation may be obviated if it is possible to find a direct solution for critical pressure. The direct solution can be obtained if mixture volume can be expressed algebraically in terms of pressure.

The nature of the expansion is more nearly isenthalpic than isentropic for flow through pipes, although the difference in volume whether isenthalpic or isentropic will not be large; hence volume of the fluid may be expressed thus as for an isenthalpic expansion.

$$v = v_f + (h_{f1} - h_f)\frac{v_{fg}}{h_{fg}} \quad \ldots\ldots [5]$$

Inspection of properties as tabulated in the "Steam Tables" (1) reveals useful relationships between enthalpy, pressure, and volume over limited pressure ranges.

The liquid volume and the enthalpy of vaporization may be taken as constants of average value over wide ranges of pressure with only small-percentage deviations from the respective actual values. Thus

$$v_f = \frac{v_{f1} + v_{f2}}{2}, \quad \text{and} \quad h_{fg} = \frac{h_{fg1} + h_{fg2}}{2}$$

Also, over limited ranges of pressure

$$h_{f1} - h_f = k_1 (p_1 - p), \quad \text{and} \quad v_{fg} = \frac{k_2}{p}$$

where k_1 and k_2 are constants.

Rewriting Equation [5] and substituting the foregoing expressions

$$v = \frac{v_{f1} + v_{f2}}{2} + \frac{k_1 (p_1 - p) 2k_2}{(h_{fg1} + h_{fg2})\,p} \quad \ldots\ldots [5a]$$

For the purpose of evaluating the constants, a lower limit of pressure is assumed. In most cases it is not necessary to recompute the constants unless the value of pressure found differs greatly from the assumed pressure.

Expressing k_1 and k_2 as

$$k_1 = \frac{h_{f1} - h_{f2}}{p_1 - p_2}, \quad \text{and} \quad k_2 = p_1 v_{fg1}$$

Equation [5a] may be written as

$$v = \frac{v_{f1} + v_{f2}}{2} + \left(\frac{h_{f1} - h_{f2}}{p_1 - p_2}\right)\left(\frac{2p_1 v_{fg1}}{h_{fg1} + h_{fg2}}\right)\left(\frac{p_1}{p} - 1\right) \quad [5b]$$

Using

$$C_1 = \frac{v_{f1} + v_{f2}}{2} - \left(\frac{h_{f1} - h_{f2}}{p_1 - p_2}\right)\left(\frac{2p_1 v_{fg2}}{h_{fg1} + h_{fg2}}\right)$$

and

$$C_2 = \left(\frac{h_{f1} - h_{f2}}{p_1 - p_2}\right)\left(\frac{2p_1 v_{fg2}}{h_{fg1} + h_{fg2}}\right) p_1$$

Equation [5b] may be written as

$$v = C_1 + \frac{C_2}{p} \quad \ldots\ldots [5c]$$

Equation [4b] may now be written in terms of a single variable by expressing volume in terms of pressure

** In order to reserve the subscript 2 for subsequent use the upper limit of integration is written without subscript.

[2] A similar equation is presented in the Bibliography (3).

$$\left(\frac{W}{A}\right)^2 = \frac{g\displaystyle\int_p^{p_1} \frac{pdp}{C_1p + C_2}}{\log_e\left[\left(\frac{p_1}{p}\right)\left(\frac{C_1p + C_2}{C_1p_1 + C_2}\right)\right] + \frac{2fL}{D}} \quad \ldots\ldots [6]$$

Integrating

$$\left(\frac{W}{A}\right)^2 = \frac{\dfrac{g}{C_1^2}\left[C_1(p_1 - p) - C_2\log_e\left(\dfrac{C_1p_1 + C_2}{C_1p + C_2}\right)\right]}{\log_e\left[\left(\dfrac{p_1}{p}\right)\left(\dfrac{C_1p + C_2}{C_1p_1 + C_2}\right)\right] + \dfrac{2fL}{D}} \quad \ldots [6a]$$

This is the desired equation in terms of pressure for the rate of flow per unit area. The direct solution for critical pressure may be obtained by differentiating Equation [6a] with respect to pressure and equating to zero. However, as a uniform-mixture average-velocity condition is assumed, it is easier to use the fact from thermodynamics that the velocity at the end of a pipe of constant cross section or at a section of minimum area in the piping (throat of control device) may be expressed as

$$V = v\sqrt{-\frac{gdp}{dv}} \quad \ldots\ldots [7]$$

from [5c]

$$\frac{dv}{dp} = -\frac{C_2}{p^2}$$

and Equation [7] may be restated as

$$V = pv\sqrt{\frac{g}{C_2}} \quad \ldots\ldots [7a]$$

or as

$$p = \frac{V}{v}\sqrt{\frac{C_2}{g}}$$

From Equation [3] $V/v = W/A$ and hence Equation [7a] becomes

$$p_c = \frac{W}{A}\sqrt{\frac{C_2}{g}} \quad \ldots\ldots [8]$$

This may be written in a more convenient form for interpretation

$$p_c = \frac{W}{A}Cp_1 \quad \ldots\ldots [8a]$$

with

$$C = \left[\left(\frac{h_{f1} - h_{f2}}{p_1 - p_2}\right)\left(\frac{2v_{fg1}}{h_{fg1} + h_{fg2}}\right)\frac{1}{g}\right]^{1/2}$$

Equation [8a] shows the relationship between critical pressure, initial pressure, and rate of flow, and is a valuable tool in the interpretation of the critical-pressure phenomena for flow through pipes. Clearly, for a given initial pressure corresponding to the initial saturation temperature of the liquid, there are an infinite number of values of the critical pressure each corresponding to a different value of W/A. However, Equation [8a] can be valid only when the size and length of pipe do not determine the flow rate, that is, Equation [8a] gives a value of pressure that will exist if the capacity of the piping system is adequate to pass the given rate of flow.

In addition to the equation being simple to solve, it does not involve the assumption of a friction factor, although it is assumed throughout that volume may be computed on the basis of an isenthalpic expansion. If it is desired to find the pressure drop from the outlet of the drainage control device to the pipe discharge, Equation [6a] may be used. Here a friction factor has to be assumed; p in this case is already known as either downstream receiver pressure or calculated critical pressure, and p_1 is the only unknown. The equation has to be solved by trial for p_1, but this is simple by comparison with numerical integration of Equation [4b].

The previous paragraphs deal with flow conditions where the pipe resistance is not the factor limiting the flow. In cases where a throttling device is not in the line, the equation for critical pressure may be used in conjunction with the equation for the rate of flow, in order to determine the amount that will flow and the pressure at discharge. The equations may be combined as follows

$$p^2\left[\log_e\left(\frac{p}{p_1}\right)\left(\frac{C_1p_1 + C_2}{C_1p + C_2}\right) - \frac{2fL}{D}\right] = \frac{C_2}{C_1^2}\left[C_1(p - p_1) - C_2\log_e\left(\frac{C_1p + C_2}{C_1p_1 + C_2}\right)\right] \quad \ldots\ldots [9]$$

This transcendental equation is difficult to solve, and hence it may be easier to solve each independently and compare the results, or solve the rate-of-flow equation for a maximum value.

Flow Through Control Devices

The critical-pressure equation applies not only to flow through a duct of uniform cross-sectional area but also to flow through the restricted openings of control devices as long as the assumption of volume calculated on the basis of an isenthalpic expansion is admissible.

In order to determine the rate of flow through the control device, it is assumed the flow is isentropic. Equation [1] becomes

$$dh + \frac{VdV}{g} = 0$$

With negligible inlet velocity, velocity through the control device is given by

$$V = \sqrt{2g(h_1 - h)} \quad \ldots\ldots [1a]$$

or since Equations [1] and [2] are equivalent for an isentropic expansion

$$V = \sqrt{2g\int_p^{p_1} vdp} \quad \ldots\ldots [2a]$$

and the rate of flow becomes

$$\frac{W}{A} = \frac{1}{v}\sqrt{2g\int_p^{p_1} vdp} \quad \ldots\ldots [10]$$

By virtue of the small difference in isenthalpic and isentropic volumes Equation [5c] may be used for volume, and Equation [10] becomes

$$\frac{W}{A} = \frac{p}{C_1p + C_2}\sqrt{2g\int_p^{p_1}\left(C_1 + \frac{C_2}{p}\right)dp} \quad \ldots [10a]$$

This expression may be integrated to give

$$\frac{W}{A} = \frac{p}{C_1p + C_2}\sqrt{2g\left[C_1(p_1 - p) + C_2\log_e\left(\frac{p_1}{p}\right)\right]} \quad [10b]$$

In order to find the capacity, the critical-pressure expression may be combined with the equation for W/A and stated as follows

$$2C_3\left[C_1(p_1 - p) + C_3 \log_e\left(\frac{p_1}{p}\right)\right] - (C_1 p + C_2)^2 = 0 \quad [11]$$

In this case also, it may be easier to solve the two equations independently by trial or solve Equation [10*b*] for a maximum rather than endeavor to solve the foregoing equation.

The foregoing analysis is based on saturated liquid entering the control device. If a mixture of water and steam enters the control device, the form of equation for W/A is the same as Equation [10*b*], but the constants are evaluated on the basis of an initial saturated state while the pressure p_1 will correspond to the pressure at the inlet of the control device.

Comparison of Formulas With Test Data

The foregoing analysis, predicated on the assumption that the water and steam flow as a finely divided mixture with equal average velocities, indicates that a critical pressure will exist at the throat of throttling restrictions and under certain conditions at the end of pipes conveying initially saturated liquid. In order to ascertain the validity of this analysis, results calculated from formulas will be compared with test data previously published in the literature.

Data Pertaining to Pipe Exit Pressures

In Table 1 are listed test data from a study of several cascade drain lines at the Connor's Creek Station of The Detroit Edison Company (3) and one drain line in the Barking B Power Station (4), England.

The data on the one drain line, No. 5 in Table 1 at the Barking B Power Station, were obtained by direct pressure measurement and from heat-balance calculation.

The calculated critical pressures were determined by the formula $p_c = (W/A)\,Cp_1$.

Clearly, from the test data, a critical pressure may exist at the end of pipes conveying a flashing mixture of water and steam. The agreement between the calculated critical pressure and the actual measured pressure is probably within the limits of the accuracy of test results in a power plant for lines 1, 3, and 5. The four test runs for line 2 are slightly higher than the calculated critical pressures. Possibly the flows from the heat-balance calculation were slightly low or the temperature measurements with the thermocouple were such as to give some slight stagnation effect.

Line 4 has a measured end pressure slightly above receiver pressure. This result is evidently erroneous because the calculated critical pressure is much less than the receiver pressure.

All of these tests were conducted on 4-in-diam heater drain lines, each containing a number of bends in the piping arrangement.

A number of tests on straight lengths of piping are also reported in the literature (5). The lengths varied from 5 to 76 ft of piping, and the diameters from 0.53 in. to 1.5 in. A critical pressure was observed in all of these tests but the critical pressures reported are lower than the calculated critical pressures and the rates of flow exceeded the calculated rates of flow in all cases.

TABLE 1 TEST DATA AND CALCULATED RESULTS FOR FLOW THROUGH CASCADE DRAIN LINES

Line no.	Nominal pipe diam, in.	Flow, lb/sec/sq ft	Upstream heater saturation pressure, psia	Downstream heater pressure, psia	—End of line pressure— Measured, psia	Calculated, psia	Equivalent length of line, ft
1*a*	4	266	37.0	8.0	18.2	17.8	58
1*b*	4	144	29.8	6.5	13.2	12.6	58
1*c*	4	116	23.9	5.1	10.6	9.7	58
1*d*	4	82.5	18.2	3.8	6.7	6.8	58
2*a*	4	286	42.8	10.5	27.4	24.6	49
2*b*	4	239	38.2	9.0	23.0	20.4	49
2*c*	4	198	32.5	7.6	18.8	17.1	49
2*d*	4	157	27.4	6.5	14.5	13.4	49
3	4	251	41.4	8.4	22.0	21.8	90
4	4	158	152	45.8	47.2	20.2	
5	4	260	41	16	22	22.5	100

Note: Lines 1–4, reference (3). Line 5, reference (4).

The Detroit Edison Company data include test results on a total of four heater drain lines on 30,000-kw and 60,000-kw turbine installations. These are numbered 1, 2, 3, and 4 in Table 1. During these tests, temperature measurements were taken at various points along the drain-line piping, and the corresponding saturation pressures were obtained from the Steam Tables (1) The quantity of drains flowing through the lines was determined by heat-balance calculation. Temperatures were determined with iron-constantan thermocouples and a potentiometer-type temperature indicator. Benjamin and Miller stated in their paper (3) that they believe the measured temperatures were in error by no more than ±1 F. Previously, in tests of flow through throttling orifices (6), they had observed both temperature and pressure along lines carrying a flashing mixture. In all cases the saturation pressure corresponding to the observed temperature checked the observed pressure within 0.5 psi. Burnell (5) also has reported taking simultaneous pressure and temperature observations and detected little if any difference, in all cases. This is noted because the properties in the Steam Tables are based on water and steam in equilibrium with a plane continuous interface between them, whereas in the analysis it was assumed that the water was finely divided. Evidently the effect of surface tension is not of sufficient magnitude to invalidate the analysis for design purposes.

In the development of the formulas, it was assumed that the water and steam flow as a finely divided mixture with equal average velocities. This statement contains two separate assumptions: (*a*) the water and steam flow as a finely divided mixture, (*b*) the average velocities over a cross section of the pipe are equal.

The effect of friction in creating an unequal velocity distribution over a cross section will be more pronounced with small-diameter pipes than with those of larger diameter, and the absence of bends in the piping will tend to perpetuate the unequal velocity distribution. An actual layout of heater drain piping of larger diameter than the $\frac{1}{2}$ to $1\frac{1}{2}$ range of sizes tested by Burnell, and containing bends, valves, and other irregularities, will have a much more pronounced tendency to create turbulence and thoroughly mix the two phases of the fluid than would the straight pipe of small diameter. The probability of both assumptions (*a*) and (*b*) being good approximations is greater for an actual drain-piping arrangement than for the piping tested by Burnell.

The less finely the liquid is divided in the vapor, the more probable it is that the average water velocity is less than the average steam velocity because of the difference in forces necessary to accelerate the respective masses of water and steam by the same amount. It may be shown that the effect of a steam velocity

greater than the water velocity would be to increase the maximum rate of flow over that for equal velocities, and decrease the critical pressure from the value for equal velocities (5). For the actual critical pressure to be higher than calculated by formula it would be necessary for the water to have a velocity higher than the steam. As this appears impossible, the discrepancy between measured and calculated pressures for line 4 was attributed to experimental inaccuracies and not to the calculated result.

Evidently the most severe limitations are imposed on piping in which the mixture distribution is uniform and the average velocities of the two phases are equal. In other words, for piping without a throttling device the rate of flow will be a minimum, all other conditions remaining fixed; and, for any pipe, all other conditions remaining fixed, the critical pressure will be a maximum. Hence for design purposes, the derived formula for critical pressure $p_c = (W/A)Cp_1$ may be used, although for small-diameter straight pipe the critical pressure may be lower than calculated by this formula. In the design of unthrottled piping such as boiler blow-off lines the formula for weight of flow may be used, although for straight runs of small-diameter pipe the weight of flow may exceed the value calculated by the formula.

Additional experimental evidence verifying the existence of a critical pressure was obtained from operating data on the 14th-stage heater drain line on Unit No. 1, Potomac River Generating Station of the Potomac Electric Power Company.

This line discharged through a drain cooler and regulating valve to the condenser. At overloads on the unit it was necessary to open the by-pass around the regulating valve and drain cooler in order to pass the flow. Calculations indicated that the fluid could not flash before the regulating valve because of the static head on the valve inlet. (It is noted later in the paper that the fluid will not flash prior to passage through the valve throat if sufficient static head is imposed on the valve inlet.) The pressure available across the valve was calculated to be greatly in excess of that required for the actual flow if the fluid flashed in the upward discharge leg to the condenser. However, the calculated pressure at the pipe discharge was found to be above the saturation pressure corresponding to the temperature at the drain cooler outlet thus indicating that the liquid could not flash in the discharge leg. The capacity as stated by the manufacturer for the pressure differential available across the valve under this condition was 35,000 lb per hr. The flow that the valve failed to pass was 39,000 lb per hr. This condition was corrected completely by increasing the size of the discharge leg, thus lowering the critical pressure at the pipe exit and allowing the fluid to flash.

Data Pertaining to Valve Capacity

In Table 2 are listed data pertaining to the 8th-stage heater drain line, 1948 Extension—Chesterfield Power Station of the Virginia Electric and Power Company. This line was investigated because the 2-in. regulating valve as originally furnished would not pass the flow from the 8th-stage heater to the 12th-stage deaerating heater under any load condition, although the valve capacity of 70,000 lb per hr under the given conditions as stated by the manufacturer was almost double the actual flow from the heater. The drain line is $2^1/_2$ in. diam, and the valve is located adjacent to the deaerator 55 ft above the water level in the 8th-stage-heater hot well.

The valve passed 17,000 lb per hr in the wide-open position whereas the total heater drain flow was 38,000 lb per hr as determined from the heat balance. The quantity passed by the valve was determined by observing the rise of the water level in the 8th-stage heater while measuring time with a stop watch. The results of several such runs were averaged to give the result mentioned. Readings were taken of initial saturation temperature, pressure at the valve inlet, and the 12th-stage deaerating-heater pressure. The maximum valve-orifice area, as stated by the manufacturer, was 0.56 sq in. The valve had a well-rounded scroll inlet and a Venturi-type outlet. The cold-water coefficient of discharge for the valve should approach unity because of the gradual curvature of the internal surfaces.

In the calculation, values of the critical pressure at the valve throat were assumed ranging from 100 psia to 120 psia in 5-psi increments. The maximum rate of flow was computed using Equation [10*b*]

$$\frac{W}{A} = \frac{p}{C_1 p + C_2} \sqrt{2g\left[C_1(p_1 - p) + C_2 \log_e\left(\frac{p_1}{p}\right)\right]}$$

In solving this equation the values of pressure and other properties used in computing the constants C_1 and C_2 are those corresponding to the initial state of the liquid in the 8th-stage-heater hot well, as it is the initial saturation state that determines the volume at any pressure. The value of p_1 used, as it appears singly under the square-root sign, corresponds to the pressure at the valve inlet since it is the valve-inlet pressure which determines the energy available for accelerating the fluid through the valve.

Values of p_c were computed as a check using the calculated values of W/A, and the equation $p_c = (W/A)Cp_1$.

According to the calculation, the maximum value of W/A occurs when the pressure at the valve throat is approximately 108 psia. The agreement between measured and calculated results is sufficiently close to verify the existence, but not the exact value, of a critical throat pressure. Due to the adverse conditions under which the flow measurement was obtained it is impossible to state definitely whether the approximately 13 per cent difference between the measured and calculated flows should be attributed to experimental inaccuracy or to other causes. It is worthy of note that the pressure at the valve inlet is 20 psi below the initial saturation pressure, and that a large volume of vapor has been formed prior to passage through the valve.

Unfortunately, test data on valve capacities for initially saturated water appear to be nonexistent in the literature. However, several investigators (4, 5, 6, 7) have reported data on the flow of saturated liquid through orifices and nozzles. In the absence of additional direct observations on valves, these data on orifices and nozzles are significant.

All the results reported indicate that the actual flows of in-

TABLE 2 TEST DATA AND CALCULATED RESULTS; 2-IN. REGULATING VALVE

Initial saturation temperature, 8th-stage heater, deg F 361
Initial saturation pressure, 8th-stage heater, psia 154.9
Pressure at valve inlet, psia 135
Receiver pressure, 12th-stage heater, psia 63.2
Flow, lb per hr, 17000
Valve-throat area, sq-in., 0.56

Assumed P_c, psia	Calculated P_c, psia	C_1	C_2	$\frac{W}{A}$ Calculated, lb/sec/sq ft	$\frac{W}{A}$ Actual, lb/sec/sq ft
100	107	0.306	$0.324p_1$	1080	1210
105	108	0.301	$0.319p_1$	1048	1210
108	108	0.298	$0.316p_1$	1056	1210
110	108	0.296	$0.314p_1$	1054	1210
115	106	0.292	$0.310p_1$	1038	1210
120	100	0.288	$0.306p_1$	983	1210

itially saturated liquid through orifices and nozzles are greater than would be expected from theory, although the existence of a critical throat pressure is noted in several cases. The excess of capacity over that theoretically predicted is attributed by the investigators to the failure of the fluid to attain thermodynamic equilibrium at the orifice throat, due principally, perhaps, to surface tension and is noted as analogous to the phenomena of supersaturation in steam nozzles.

Almost all of these data dealt with arrangements such that flashing could not occur before the device. Many heater drain-piping arrangements, including the one containing the 2-in. valve at the Chesterfield Station, are such that a large volume of vapor is formed prior to passage through the valve. This volume of vapor may tend to form a nucleus for additional expansion. Furthermore, the internal surfaces of regulating valves would tend to create more turbulence than would the simple outline of an orifice or nozzle, and it appears that increased turbulence would produce a more nearly stable equilibrium condition.

Although the condition of "metastable" equilibrium may exist at the throat of control valves and capacities may be greater than predicted by formulas, until test data on all principal designs of valves for various inlet conditions are available, it is believed that the formulas offer the most reliable method of valve sizing for this service. Valve internal areas obtained from the rational analysis are not exorbitantly large. In a recent installation, a $1^1/_2$-in-line-size valve, subjected to inlet conditions such that flashing could not occur until the fluid had passed the throat, did not have sufficient capacity. The rational analysis indicated that a 2-in. valve will be adequate for the service.

Alternative Designs of Heater Drain Systems

The objective of the design engineer is to provide the most economical piping arrangement that will pass the flow over the entire load range without operating difficulties, and be entirely free from any deleterious effect, such as erosion or vibration resulting from high water-steam mixture velocities. It is axiomatic that the piping be as free from bends and elbows as is compatible with flexibility requirements and the physical arrangement of equipment. Although always desirable from the viewpoint of the piping designer, the inclusion or omission of a drain cooler is dictated by the economies of the over-all plant.

Drain Piping Systems With Drain Coolers

Clearly, the use of a drain cooler in the drain system will restrict the amount of flashing and make possible the use of smaller valves and pipe. What has not been recognized generally is that it is possible to eliminate flashing completely, in systems employing drain coolers. This may be done, and actually has been done, although accidentally, at the Potomac River Generating Station, by utilizing the critical-pressure phenomena, and thereby sizing the pipe from the control valve to the receiver so small that the pipe-exit critical pressure is above the saturation pressure corresponding to the exit temperature from the drain cooler. Of course, this may be done without a drain cooler, but it appears impractical as the receiver would have to be located many feet below the source.

In order to carry out this design and eliminate flashing completely, there must be sufficient pressure differential available (source heater pressure minus pipe exit or critical pressure) to overcome friction in the piping, and the differential across the control valve. The pipe is sized by using Equation [8a], substituting for critical pressure the valve corresponding to drain-cooler exit temperature and solving for area. After the pipe is sized, the pressure drop due to friction and valve size may be determined by the usual criteria for liquid flow. As a number of variables, initial pressure, rate of flow, and pipe friction are involved, it may be impossible to carry out the design so that flashing is eliminated over the entire load range. For example, at very low flows it may be that flashing will not be eliminated completely owing to sizing the piping large enough to pass the flow at high load.

Drain Systems Without Drain Coolers

One objective which would be desirable to achieve, but which is not always feasible if regulating valves are located adjacent to the downstream receiver, would be to size the piping so that flashing does not occur before the throat of the control valve as this will result in a minimum valve size. This necessitates some static head on the valve and it must be located below the source. The curve[4] in Fig. 1 shows the head required in feet of liquid above the initial saturation pressure for the valve throat pressure to correspond to the initial saturation pressure over the range from zero to 150 psia. In order to determine the total static head required on the valve, the friction drop in feet of liquid in the piping from the source heater to the valve must be added to the value obtained from Fig. 1. If this is accomplished, the valve is sized as for liquid flow with the available pressure differential equaling the total static head minus the pressure drop in the piping before the valve.

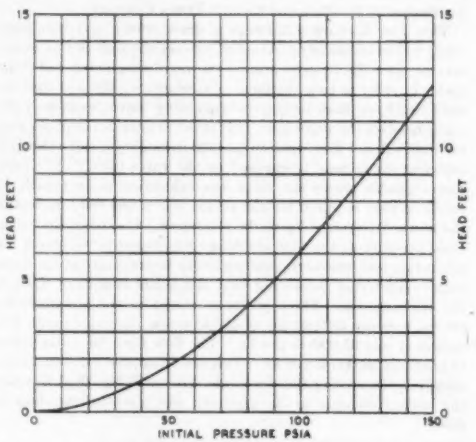

Fig. 1 Minimum Initial Static Head Required to Prevent Vaporization Before the Throat

The first step in determining the size of piping from valve outlet to the receiver is to investigate the possible existence of a critical pressure at the discharge end using Equation [8a]. As previously noted in the literature (3), from the point of view of restricting mixture velocities and thereby alleviating possible erosion difficulties, it may be advantageous to size the piping so that the pipe-exit critical pressure is greater than the receiving-heater pressure as the increase in specific volume of the mixture with decreasing pressure may actually result in a higher velocity for a larger pipe size. In order to find the pressure drop from control-valve outlet to the pipe exit, Equation [6a] may be used with a friction factor $4f = 0.012$ as reported previously in the literature (3, 4). The pressure p_1 at control-valve outlet is the unknown in this case.

The location of the control valve adjacent to the downstream

[4] A similar curve is presented in reference (4).

receiver with a straight run of pipe from the valve to the receiver is an arrangement that offers the least possibility of erosion in the piping, with the exception of the control valve. The pressure drop due to friction in the piping before the valve will increase its size above that required if it were located below the source heater with a static head of liquid on the inlet. On the other hand, the optimum size of piping between the two heaters will be less when the valve is located adjacent to the downstream heater. Furthermore, the valve internals, subjected to the flashing conditions, are of materials better able to resist the erosive action of the mixture than is the pipe.

In this case the pressure at the valve inlet and the size of piping from the source to the valve may be determined by using Equation [6a]. The piping from the valve to the receiving heater is sized as for the previous example.

The procedure for valve sizing is not as simple as before because the pressure at the valve throat is unknown. Reference to the curve plotted in Fig. 2[5] will give a first estimate of the valve throat pressure. This curve, which is calculated on the basis of saturated liquid at the control-device inlet, shows saturated-liquid critical pressures over the entire range from zero to 3226 psia. Several values of pressure less than the value from the

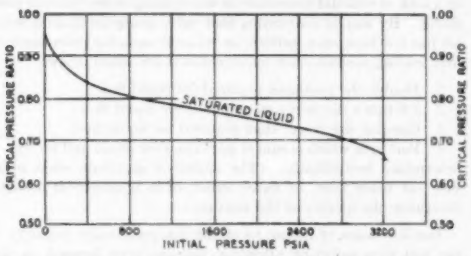

FIG. 2 CRITICAL-PRESSURE RATIOS FOR FLOW OF SATURATED LIQUID WATER COVERING PRESSURES TO CRITICAL POINT

curve may be assumed and substituted in Equation [10b] which is solved for a maximum value. The equation for critical pressure may be used to check the calculation. In the absence of any evidence on the discharge coefficients for a mixture of water and steam, the procedure that has been followed with success thus far is to divide the value of area obtained from Equation [10b] by the manufacturer's cold-water coefficient of discharge for the valve, and use the quotient as the total throat area required in the valve.

ACKNOWLEDGMENT

The author gratefully acknowledges the encouragement of Messrs. W. F. Ryan, B. C. Mallory, and L. E. Chadbourne, in preparing this paper, and the able assistance of Mr. G. E. Weir in checking the completed manuscript.

BIBLIOGRAPHY

1 "Thermodynamic Properties of Steam," by J. H. Keenan and F. G. Keyes, John Wiley & Sons, Inc., New York, N. Y., 1936.

2 "Fluid Flow Through Two Orifices in Series," by M. C. Stuart and D. R. Yarnall, *Mechanical Engineering*, vol. 58, 1936, pp. 481–484.

3 "The Flow of a Flashing Mixture of Water and Steam Through Pipes," by M. W. Benjamin and J. G. Miller, Trans. ASME, vol. 64, 1942, pp. 657–669.

4 "Flow of Boiling Water Through Orifices and Pipes," by W. T. Bottomley, Trans. Northeast Coast Institution of Engineers and Shipbuilders, vol. 53, 1936–1937, pp. 65–100.

5 "The Flow of Boiling Water Through Nozzles, Orifices, and Pipes," by J. G. Burnell, *Journal of the Institution of Engineers*, Australia, vol. 18, 1946, pp. 41–49.

6 "The Flow of Saturated Water Through Throttling Orifices," by M. W. Benjamin and J. G. Miller, Trans. ASME, vol. 63, 1941, pp. 419–429.

7 "Fluid Flow Through Two Orifices in Series—II," by M. C. Stuart and D. R. Yarnall, Trans. ASME, vol. 66, 1944, pp. 387–397.

8 "Discharge of Saturated Water Through Nozzles," by R. S. Silver and J. A. Mitchell, Trans. Northeast Coast Institution of Engineers and Shipbuilders, vol. 62, 1945–1946, pp. 51–72, D15-30.

9 "Discharge Capacity of Traps," by A. E. Kittredge and E. S. Dougherty, *Combustion*, vol. 6, September, 1934, pp. 14–19.

[5] A similar curve is presented in reference (2).

Discussion

J. G. MILLER.[6] As coauthor of a paper on this same subject, ref. (3) Bibliography, the writer is pleased to learn that others have been devoting some time and energy to the subject of flow of flashing mixtures. There is still much information needed on this subject, principally test data. The author has extended the analysis of the existing test information, and this will serve a useful purpose. It is hoped that others will be encouraged to study the problem from the standpoint of conducting some tests especially at the higher initial pressures.

Reference is made to certain of the test data provided in the paper (3) written by M. W. Benjamin and the writer, and in his Table 1 the author compares calculated end of line pressure with the value obtained on test. In the writer's opinion, the agreement on lines 1, 2, and 3 is very good. About line 4, the author makes the statement that there is evidently an error because the calculated critical pressure is much lower than the receiver pressure.

In the original paper in the discussion of the 14 cascade drain lines given under Table 4 (3), it was pointed out that not all of the lines had a critical pressure at the end. It should be noted that in line 4, Table 1, the calculated end pressure as given by the author is 20.2 psia, but that the downstream heater pressure is 45.8 psia and the measured pressure at the end of the line is 47.2 psia or slightly higher than the downstream heater pressure.

In any case, the measured pressure at the end of the line could not have been less than the downstream heater pressure. In the writer's opinion, it should be assumed in this case that the combination of (*a*) initial upstream pressure, (*b*) quantity of mixture flowing, and (*c*) the size of the pipe will produce a critical pressure of 20.2 psia, if the downstream heater pressure is low enough. In this case, however, the downstream heater pressure of 45.8 psia is 24.4 lb higher than the critical pressure as given in the calculated "end of line" pressure in Table 1.

W. J. KINDERMAN[7] AND D. ROBERT YARNALL.[8] This paper represents a significant contribution to the engineering application of pipe lines and valves to flashing mixtures of steam and water. The derivation of formulas yielding direct solutions in place of the rather laborious trial calculations involving critical-pressure determinations, particularly, promises to simplify future engineering application work in this field.

The cited case of the 2-in. regulating valve on a stage heater drain line, with the inlet pressure at the valve below the initial saturation pressure, appears to represent a case where the piping restrictions ahead of the valve establish the critical pressure which fixes the flow for all downstream pressures below this value. Positioning of the valve within this subcritical pressure range in-

[6] Superintendent of Production, Metropolitan Edison Company, Reading, Pa. Jun. ASME.

[7] Research Engineer Yarnall-Waring Company, Philadelphia, Pa. Mem. ASME.

[8] President, Yarnall-Waring Company, Past-President, ASME.

fluences the valve inlet and outlet pressures without changing the rate of flow.

As the author states, the formulas as applied to control valves are on the conservative side, and metastable flow conditions may result in much higher flow rates. The measured capacity of most steam traps, for example, are considerably higher than those indicated by the formula.

Regarding drain coolers, it may be interesting to note that the thermal capacity of comparatively small, long drain lines has an appreciable effect in cases of occasional discharge for short intervals, such as discharge from blow-off valves. Radiation from uninsulated long pipe lines such as steam-trap return lines, particularly in the smaller pipe sizes, likewise may be sufficient to increase materially the computed values.

C. S. L. Robinson.[9] The phenomenon described by the author is associated with the fact that the specific volume varies enormously from the single-phase liquid state to the two-phase mixture of water and steam. In other words, it depends on the compressibility of the fluid. Hence it is suggested that the complete derivative

$$dh = du + p\,dv + v\,dp$$

be considered in Equations [2] and [4], rather than $v\,dp$ alone. The latter is strictly equivalent to dh only for incompressible fluids.

Furthermore, is not the critical pressure essentially the pressure where sonic velocity is encountered as in other flow problems? This problem is complicated, however, by pipe friction and by the change of fluid state.

Author's Closure

The first paper offering test data for the flow of a flashing mixture in pipes (4) was presented by Bottomley in England. Unfortunately, this paper had only limited circulation in this country. The subsequent paper by Benjamin and Miller (3) which contained the results of tests on a number of drain lines, verified conclusively the single test by Bottomley and the theoretical predictions of earlier writers that a critical pressure could exist at the end of a pipe line conveying a flashing mixture. In addition, the Benjamin and Miller paper presented values of the friction factor confirming that obtained by Bottomley on his single test, and outlined a design procedure for minimizing erosion difficulties. The author is indeed gratified to have a discussion from the coauthor of that significant contribution.

With regard to Mr. Miller's statements concerning line No. 4 in the Benjamin and Miller paper (3) the impression that the author intended to convey when he stated that the pressure measurement was in error was that the line could not have a critical or end-of-line pressure above the pressure in the downstream heater because the calculated critical pressure was much less than the downstream heater pressure. Although it was realized that this line did not have a critical pressure, the data were presented in order to cover all of the test results listed in the Benjamin and Miller paper with end-of-line pressures higher than receiver pressures. Clearly, the end-of-line pressure could not be less than downstream heater pressure. Equally obvious is the fact that the end-of-line pressure, if actually measured at the end of line, could not be higher than the downstream heater pressure and the author adheres to his conclusion that the measurement was in error by 47.2 — 45.8 = 1.4 psi.

Mr. Miller's comment that the analysis of existing test data is extended in the paper possibly may create the impression that no new test results are presented. Although the comparisons of calculated and test results are intended primarily to show that the assumptions underlying the derivation of formulas are justified rather than to present new test results, the author submits that the data on the 2 in. valve at the Chesterfield Station, which admittedly is not of high precision, is the first information published on regulating valves for flashing flow service.

The author is in complete agreement with Mr. Miller that many test data are still needed on the subject. However, the data of Bottomley, Benjamin and Miller, and Burnell are conclusive enough with regard to flow in pipes to give ample experimental justification for the use of the formulas for the specific problem of designing heater drain piping. Additional data would be informative, particularly to fill the gap in the 2 in. to 3-in-pipe size range between the data of Bottomley and Benjamin and Miller on the one hand, and Burnell on the other, and to indicate the demarcation line below which the uniform mixture, average velocity assumption gives conservative results.

The author's experience at Stone & Webster Engineering Corporation in reviewing the design of existing heater drain systems has led him to the conclusion that the majority of cases in which the flow capacity of drain systems has been inadequate are due to a lack of rational procedure in valve sizing rather than in pipe sizing. By way of illustrating that valve sizing for flashing service has not been on a uniform or rational basis the procedures of four leading control-valve manufacturers are listed below:

1 Double the port area required for liquid flow.
2 1.6 times the port area required for liquid flow.
3 One line size larger than required for liquid flow.
4 Port area which is sum of port areas for liquid and for vapor determined individually. (The author is uncertain what pressure—at valve inlet, at valve outlet, or in between—is used to determine the quality of the mixture.)

Another cause of failure to obtain adequate valve capacity is the fact that sufficient attention has not been focused on the great importance of physical location of the control valve with respect to the source heater, both in terms of elevation and distance in equivalent feet of pipe. The reason for the importance of location is succinctly expressed in Messrs. Kinderman and Yarnall's statement (in regard to the 2 in. regulating valve at the Chesterfield Station) that the piping restrictions ahead of the valve establish the critical pressure which fixes the flow for all downstream pressures below this value.

As emphasized in the body of the paper, the valve-capacity formulas will always result in adequate valve sizes if due consideration is given to valve location in the drain line. However, because of the probable existence of metastable equilibrium it is also probable that the valves could be smaller than the sizes determined from the formulas and still be adequate for the service. The author believes, therefore, particularly in regard to heater drain systems, that the most acute need is for test information on valves of various internal designs, over the range of initial (saturation) pressures from 5 psia to 300 psia, and for various locations in the piping system.

The author is interested in the observation of Messrs. Kinderman and Yarnall that heat transfer from the fluid to the pipe or surroundings in the case of small, long lines such as blow-off discharge and steam-trap return lines may appreciably increase the capacity predicted on the basis of no heat transfer. In the cases that the author has considered, which have not included intermittent or unlagged flow systems, heat-transfer calculations have indicated that such effects would be negligible. Although such considerations on the part of the author by no means preclude the possibility of the correctness of the writer's observation, he wishes again to call attention to the experiments of Burnell (5) con-

[9] Central Technical Department, Shipbuilding Division, Bethlehem Steel Co., Quincy, Mass.

ducted on well-lagged, small-diameter pipes in steady operation. Burnell concluded that he obtained flow rates higher than theoretically predicted because of the failure of the fluid to attain a satisfactory approximation to the uniform mixture, average velocity state. Of course, for design purposes the existence of excess capacity is the significant fact and not the cause of the excess.

In examining Mr. Robinson's suggestion that the complete derivative

$$dh = du + pdv + vdp$$

be considered in Equations [2] and [4] rather than vdp alone, it is essential to note that Equation [1], the energy equation, is derived from the first law of thermodynamics, and Equation [2], the dynamic equation, is derived from Newton's law of motion. The first law of thermodynamics is a fundamental principle involving energy while the Newtonian Law is a fundamental principle involving force and motion. The equations resulting from the application of these two separate and distinct fundamental principles to fluid motion are identical only for the special case in which heat transfer and friction are neglected. Mr. Robinson evidently is basing his proposal on the fallacious premise that Equations [1] and [2] are always identical.

The invalidity of his suggestion may be illustrated clearly by replacing vdp in Equation [2] with $dh = du + pdv + vdp$ as he proposes. With this substitution a comparison of Equations [1] and [2] term by term implies the absurdity that the term containing the friction factor must be equal to the heat transfer[10] in the general case and for the case of no transfer of heat the term containing the friction factor must always be equal to zero.

Contrary to Mr. Robinson's statement that $dh = vdp$ only for incompressible fluids, for the special case of isentropic flow $dh = vdp$ for compressible fluids, whereas in all other cases in which the heat transfer is negligible

$$dh = vdp + \frac{fVV^2}{2Ag}\,dL$$

In response to Mr. Robinson's question concerning the relationship between critical pressure and sonic velocity, it is true for the uniform mixture, average velocity condition assumed that the velocity of the fluid at the critical pressure is the same as the local velocity of sound in the mixture.

In conclusion, the author wishes to express his appreciation to the discussers for their comments and additions to the paper.

[10] The heat transfer, dQ, in Equation [1] represents the flow of energy from a source external to the fluid system by virtue of the temperature difference between the source and the fluid system.

Report of Progress on Measurements of Friction Coefficients, Recovery Factors, and Heat-Transfer Coefficients for Supersonic Flow of Air in a Pipe

By JOSEPH KAYE,[1] J. H. KEENAN,[2] and W. H. McADAMS,[3] CAMBRIDGE, MASS.

Measured values are presented for friction coefficients, recovery factors, and heat-transfer coefficients for a stream of air flowing through a pipe at Mach numbers ranging from 2.5 to 1.2. The friction coefficients are in good agreement with those of Keenan and Neumann. At a diameter Reynolds number at inlet of about 1×10^6, which is intermediate between values observed by Keenan and Neumann, frictional effects of a very low order were observed. Maximum frictional effects occurred at a diameter Reynolds number at inlet of about 1.5×10^6. Friction coefficients are, in general, considerably lower than those for fully developed turbulent flow of incompressible fluids at the same values of the Reynolds number.

For laminar boundary layer, it appears that the recovery factor is in close agreement with the results of the Pohlhausen analysis, namely $(\mathrm{Pr})^{1/2}$ or 0.865. For turbulent boundary layer the recovery factor appears to vary from about 0.79 where the Mach number is 1.3 to about 0.865 where the Mach number is 2.2. It cannot be determined from the present tests whether this variation is primarily an effect of variation in Mach number, although it probably is.

The measured values of heat-transfer coefficient in the region of laminar boundary layer seem to be roughly in accord with the Pohlhausen analytical values for incompressible flow over a flat plate. In the region of greatest turbulence in the boundary layer, agreement with the McAdams correlation of data for turbulent flow in pipes is good. The major portion of the data obtained appears to be in the region of transition in the boundary layer from laminar to turbulent flow. Most of the observed values of heat-transfer coefficient are smaller by far than the corresponding ones for fully developed turbulent flow—the ratio of one to the other being as small as 1 to 10.

Nomenclature

The following nomenclature is used in the paper:

a = velocity of sound
c_p = specific heat at constant pressure
D = inside diameter of pipe
f = apparent friction coefficient, reference (1)[4]
g = acceleration given to unit mass by unit force
G = flow per unit area or mass velocity
h = coefficient of heat transfer, $q/(t_w - t_{aw})$
M = Mach number, V/a
Pr = Prandtl number, $c_p\mu g/\lambda$
q = rate of heat transfer per unit of wall area
r = recovery factor $(t_{aw} - t_m)/(t_0 - t_m)$
Re_D = diameter Reynolds number, $DG/\mu g$
Re_x = length Reynolds number, $xG/\mu g$
t_{aw} = adiabatic wall temperature, deg F
t_m = mean stream temperature, deg F
t_0 = stagnation temperature before nozzle, deg F
t_w = wall temperature, deg F
T_{aw} = adiabatic wall temperature, deg F abs
T_0 = stagnation temperature before nozzle, deg F abs
V = velocity
x = distance from nozzle-exit plane
λ = thermal conductivity
μ = viscosity
ρ = density
τ = shear stress at wall

Introduction

The literature of heat transmission contains very few data on heat flow from a wall to a gas stream moving at supersonic velocities. The present investigation is intended to provide some data of this sort for air flowing in a heated pipe. The short lengths of supersonic flow that can be attained and the rather high longitudinal gradients of pressure and temperature in the air stream make it desirable to determine as nearly as possible point values of the heat-transfer rate as distinguished from the values corresponding to a length of many times the pipe diameter which have commonly been measured for incompressible flow. In this investigation values were obtained for increments of length approximating 2 diam.

The coefficient of heat transfer for compressible flow is defined as the rate of heat flow per unit of surface area per unit of difference between the temperature of the wall and the temperature of an adiabatic wall alongside a stream having the same mean properties over the cross section (1).

Therefore it is necessary first to measure adiabatic wall temperatures. These are expressed in terms of the recovery factor, which is defined as the ratio of the excess of the adiabatic wall temperature over the mean stream temperature to the excess of the mean stagnation temperature over the mean stream temperature.

---

[1] Associate Professor of Mechanical Engineering, Massachusetts Institute of Technology. Jun. ASME.

[2] Professor of Mechanical Engineering, Massachusetts Institute of Technology. Fellow ASME.

[3] Professor of Chemical Engineering, Massachusetts Institute of Technology. Mem. ASME.

Presented originally at the Heat Transfer and Fluid Mechanics Institute Meeting, Berkeley, Calif., June 22–24, 1949. Contributed by the Heat Transfer Division and presented at the Fall Meeting, Worcester, Mass., September 19–21, 1950, of The American Society of Mechanical Engineers.

Note: Statements and opinions advanced in papers are to be understood as individual expressions of their authors and not those of the Society. Paper No. 50—F-13.

[4] Numbers in parentheses refer to the Bibliography at the end of the paper.

In order to determine the mean stream temperature at any section it is necessary to know the stagnation conditions at inlet, the heat transfer to the stream before the section in question, and the pressure at that section. The measurements of pressure at various sections along the test pipe for adiabatic flow yielded data on friction for a supersonic stream in a pipe.

The experimental data and details of computation have been omitted from this report to keep it reasonably concise. Recently a new apparatus for measuring the recovery factor, which has a supersonic nozzle of different design from the one reported here and a different means of reducing radial and longitudinal heat transfers in the lucite tube, has been under test. The experimental data obtained from both sets of apparatus will be reported in detail in subsequent publications.

Method

Preparation of Air Stream. Atmospheric air is raised to a pressure in excess of 100 psia in a steam-driven two-stage compressor. The air stream from this compressor is cleaned by filtering and by condensing out oil and water vapor. As indicated in Fig. 1, the air passes first thrcugh a precooler which is an ice bath for condensing out the major portion of the oil and water vapors. The condensate is vented to the atmosphere.

The remaining condensable constituents are almost completely removed by cooling the air down toward the temperature of dry ice (roughly to — 60 F). This is accomplished by means of a regenerative cooler designed by Prof. S. C. Collins. The air passes through one side of this regenerator to a bath consisting of dry ice in alcohol and then back through the other side of the regenerator.

Since the actual temperature decrease of the air stream in passing through the dry-ice bath is only a few degrees, the consumption of dry ice is relatively small. Almost all the cooling from the water-ice point to the dry-ice point takes place in the regenerator by heat transfer to the colder air stream returning from the dry-ice bath.

Condensation in the regenerator and in the dry-ice region is mostly to the solid phase. The regenerator must have sufficient volume, therefore, to permit frost formation for several hours under test conditions without prohibitive resistance to flow. At the end of such a period the regenerator must be purged by a flow of warm air.

The specific humidity of the air entering the test apparatus is of the order of 1.5×10^{-3}. The effect on the static pressure of any condensation shock resulting from the presence of this water vapor is estimated to be about 1 part in 100,000—an effect far smaller than the precision of measurement of static pressure.

In order to bring the air to the desired temperature at inlet to the test section, heaters were provided downstream from the regenerator, as shown in Fig. 1. The first of these, a shell-and-tube type, in which the source of heat is hot water, brings the temperature of the air to within about 5 deg F of the desired temperature. The second is a large water bath with controls operating an electrical heater in the bath so as to maintain the desired temperature within ±0.2 deg F.

Test Apparatus. Upon leaving the water bath, the air enters

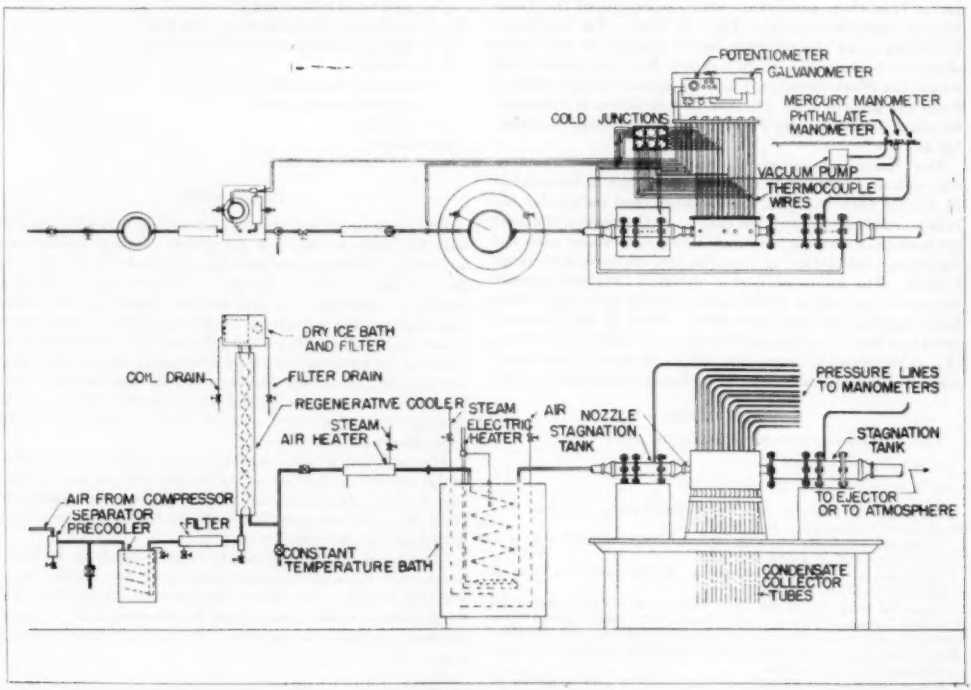

Fig. 1 Arrangement of Apparatus

a passage 3 in. diam, which is called the upstream stagnation tank. In this passage the stream is slowed down to a uniform low velocity by means of baffles and wire screening. Nine thermocouples distributed over a cross section of the stagnation tank were used to determine the temperature distribution and the mean temperature of the stream approaching the nozzle. The variation in temperature over the cross section was kept within 1 deg F. Although the stagnation-tank walls were insulated carefully, the thermocouples were shielded nevertheless against radiation to the walls. A pressure tap in the stagnation tank was connected to a manometer.

Upon leaving the stagnation tank the air passed into an axially symmetrical brass nozzle, Fig. 2, with a throat diameter of approximately $^1/_4$ in. and a divergence about $2^1/_4$ in. long to the test-pipe diameter of about $^1/_2$ in. The Mach number corresponding to the measured pressure at the inlet end of the test

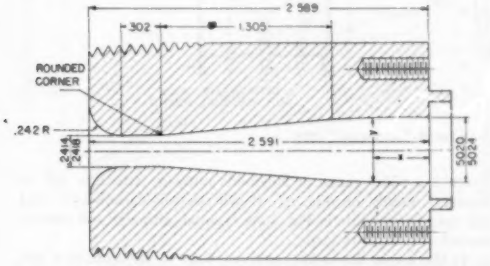

x —	0.000	0.245	0.399	0.502	0.569	0.617	0.656	0.689	0.742
y —	0.502	0.501	0.498	0.494	0.490	0.486	0.482	0.478	0.470

FIG. 2 CROSS SECTION OF NOZZLE

to radial flow of heat to a minimum. Longitudinal flow of heat is small in these tests because the wall temperature of the tube is nearly constant along its length.

The first tube made for adiabatic measurements was of textolite, a plastic-impregnated cambric wound on a mandril into cylindrical form. The inner surface was polished and appeared to be quite smooth. The textile structure of this material, however, raised doubts as to the actual smoothness of the surface and prompted the manufacture of a second tube of lucite, Fig. 3. Data were obtained with both the textolite and the lucite tubes.

Both the textolite and lucite tubes were made from thick-walled cylinders of about 1.5 in. OD and 0.5 in. ID. Pressure taps 0.020 in. diam and thermocouple wells 0.031 in. diam were provided at intervals of 2 in. (4 diam) along the tube length. The thermocouple wells extended to within $^1/_{32}$ in. of the inside wall. In between measuring stations the tube wall was machined down to a thickness of $^3/_{32}$ in. in order to reduce longitudinal heat transfer.

Between the nozzle and the test pipe a short brass tube was inserted. The quality of the inside surface at the junction between nozzle and collar and between collar and tube could be made as good as desired before assembling all three.

The test pipe for heat-transfer measurements is shown in Fig. 4. It consists of a brass tube of 0.502 in. ID and of 0.125 in. wall thickness. The inside surface of the tube was prepared by successive polishing operations interspersed with successive cleanings of the pressure-tap holes. The final result was a high polish with no detectable burrs at the pressure taps.

The tube was surrounded by a box with a cross section of about $7 \times 7^3/_4$ in. This box constitutes a steam jacket, the steam within which is the source of heat, and the condensate from which is used to measure the amount of heat flow to the air in the tube.

In order to measure the heat transfer for incremental lengths of the tube, the space around the tube is subdivided by thin brass

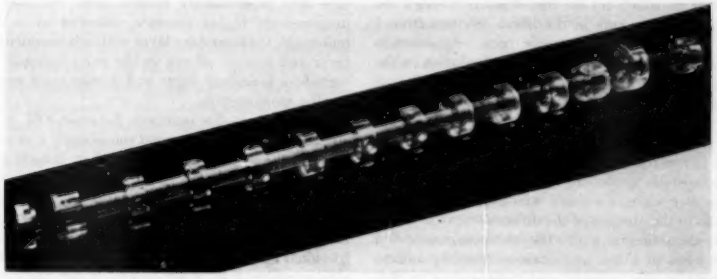

FIG. 3 LUCITE TUBE FOR ADIABATIC TESTS

pipe is about 2.6. The profile of this nozzle was designed by a method (2) which has proved satisfactory as a means of obtaining shock-free expansion. It is probable, however, that the method of characteristics will make possible a reduction in length in future nozzles, and, consequently, of boundary-layer thickness at nozzle exit.

The test pipe is of two different kinds depending upon whether the object of the test is to measure adiabatic wall temperatures or heat-transfer coefficients. For the adiabatic wall measurements the test pipe was made of a material of low thermal conductivity so as to reduce to a minimum the effects of longitudinal conduction of heat through the test-pipe wall. For the heat-transfer measurements, on the other hand, the test pipe was made of high-conductivity material so as to reduce the resistance

partitions set perpendicular to the axis of the tube at intervals of 1 in. and soldered to the tube wall. The condensate from the tube between any pair of partitions is caught in a trough of semicircular cross section from which it drains into a measuring tube. In order to protect this trough from condensation occurring on surfaces other than the test pipe, a cylindrical umbrella of semicircular cross section is suspended inside the steam jacket over the entire pipe and trough. Because of its low thermal conductivity, neoprene tubing was used to connect the trough and the condensate-metering tube. Each collecting tube was steam-jacketed so as to prevent condensation in the collecting tube itself.

At the center of each increment of length of test pipe a pressure tap connected to a manometer was provided. Immediately

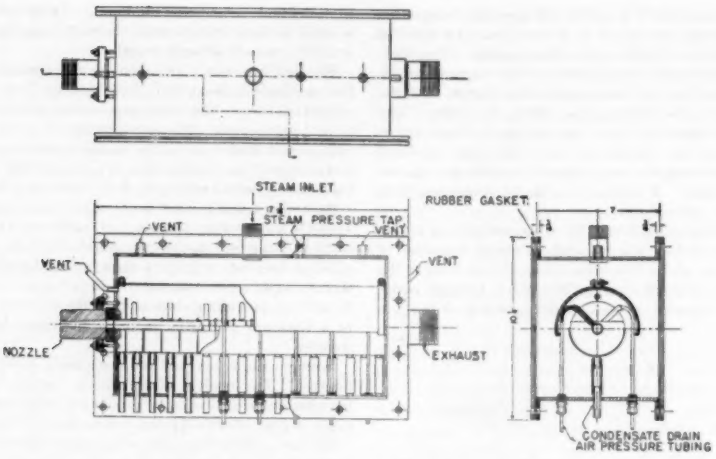

FIG. 4 TEST PIPE AND JACKET FOR HEAT-TRANSFER TESTS

downstream from the pressure tap a thermocouple was soldered into a circumferential groove in the pipe wall. Thermocouple leads were taken out of the jacket through soft packing between the jacket flanges.

A short hard-rubber tube between nozzle and test pipe served the same purpose as the short brass tube in the adiabatic tests and provided a degree of insulation between nozzle and test pipe as well.

The effect of longitudinal heat transfer was determined by means of blank runs in which no air was flowing through the test pipe. The condensation rate in the blank run was from 1 to 10 per cent of that in the heat-transfer runs. Appropriate correction was made of the observed rate of condensation in the heat-transfer runs.

In both the adiabatic and the heat-transfer experiments the air from the test pipe passed directly into a 4-in-diam downstream stagnation tank. Because of variation of friction factor with Reynolds number, it was found impracticable to fit a diffuser to the test pipe which would serve any useful purpose over the range of tests. In fact when a diffuser was used the flow was often less stable than in the absence of the diffuser.

The downstream stagnation tank, like the upstream one, served to bring the air stream to a low and uniform velocity and to provide measurement of the pressure and temperature in this condition. Comparison of upstream and downstream stagnation states provides an indication of over-all heat transfer.

The pressure in the downstream stagnation tank was maintained as low as desired by means of an ejector which pumped the air to an atmospheric exhaust.

TEST RESULTS

The test results fall into three categories, namely, friction data for adiabatic flow, recovery factors for adiabatic flow, and heat-transfer data. They will be discussed in that order.

Friction in Adiabatic Flow. Figs. 5 and 6 show the variation in pressure, expressed as a fraction of the upstream stagnation pressure, along the length of the test pipe for textolite and lucite, respectively. Each curve is labeled with the Reynolds number based on pipe diameter and mean-stream properties at the first test section. Since the tests for lucite were more numerous and covered a wider range of Reynolds number, attention will be focussed mainly on Fig. 6. It will be noted, however, that the data for textolite in Fig. 5 are in good, although not perfect, accord with those for lucite.

At the lowest Reynolds numbers, 0.48×10^5 to 0.70×10^5, Fig. 6 shows curves rising first to a maximum, falling to a minimum, and rising thereafter to the tube exit. These characteristics might be accounted for on the hypothesis of a thickening laminar boundary layer at inlet which constrains the supersonic core into progressively smaller cross sections and so causes a progressively higher pressure, followed by a transition to turbulence in the boundary layer with a consequent thinning of that layer and reverse effects in the core, followed by a thickening turbulent boundary layer and a core once more converging to smaller cross section.

At high Reynolds numbers, between 1.07×10^5 and 4.65×10^5, the pressure curves trend consistently upward in the direction of flow, although some evidence of an inflection which might be attributed to transition in the boundary layer may still be found near the inlet end. A shock appears near the outlet end for Reynolds numbers between 1.37×10^5 and 2.41×10^5 and is furthest upstream for 1.37×10^5. This indicates a maximum frictional effect at this Reynolds number. At still higher Reynolds numbers, 3.36×10^5 to 4.65×10^5, the pressure ratios near exit decline, giving evidence of a declining frictional effect with increasing turbulence in the boundary layer.

At intermediate Reynolds numbers, 0.81×10^5 to 1.03×10^5, the curves are quite different from those for higher and lower values, showing the pressure rising very gradually to a maximum near the tube outlet. This is evidence of an extraordinarily low frictional effect.

The behavior at low and at high Reynolds numbers seems to be consistent with well-known behavior of the boundary layer on a flat plate which develops first as a laminar layer of increasing thickness, decreases in thickness in the course of transition to turbulence, and then increases again. In both the laminar and the turbulent regions the frictional effect decreases with Reynolds number, but in the transition it may suddenly increase. As flow velocity increases the transition point moves upstream.

The curves for Reynolds numbers 0.81×10^5 to 1.03×10^5

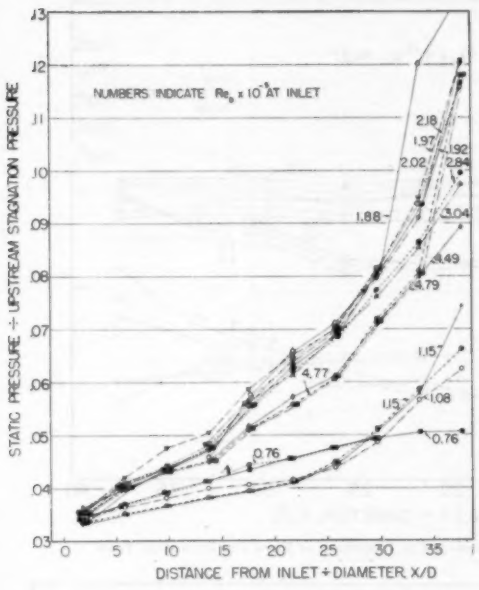

FIG. 5 LONGITUDINAL PRESSURE DISTRIBUTION IN TEXTOLITE TUBE

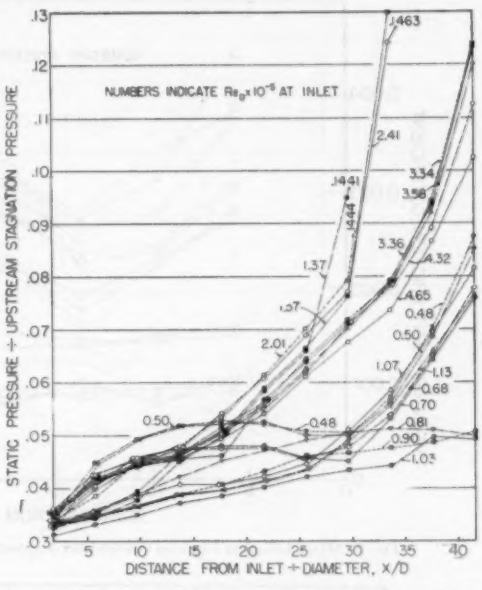

FIG. 6 LONGITUDINAL PRESSURE DISTRIBUTION IN LUCITE TUBE

however, seem to indicate a transition further downstream than those for lower Reynolds numbers. Although this characteristic has appeared in all the test results with three different tubes, namely, textolite, lucite, and brass, no satisfactory explanation has been found.

If the point of inflection in the curves for lower Reynolds numbers is evidence of transition from laminar to turbulent flow in the boundary layer, then the transition occurs further downstream than would be expected from observations of flow over flat plates. In terms of Reynolds number, with the distance from the leading edge as the characteristic length, the transition for incompressible flow over flat plates has been observed to occur at 0.9×10^5 to 1.1×10^6 (3). If the distance from the nozzle exit is used in place of this length, transition occurs in these tests at about 2×10^6 for the tests at low values of the diameter Reynolds number.

Figs. 7 and 8 show the variation of mean apparent friction coefficient along the length of the tube for textolite and lucite tubes, respectively. The apparent friction coefficient is intended to represent for any cross section of the stream the quantity

$$\frac{2\tau g}{\rho V^2}$$

where τ denotes the shear stress at the pipe wall, ρ the mean density, and V the mean velocity (1). In computing τ from the measured values of pressure along the tube length the assumption is made that the velocity is uniform over each cross section. (More strictly, the assumption made is that the mean velocity found from the flux of kinetic energy is identical with that found from the flux of momentum.) Since the velocity distribution changes considerably from section to section, particularly in the region of transition from laminar to turbulent boundary flow, this method of computation yields what has been called an apparent shear stress and an apparent friction coefficient. The mean apparent friction coefficient at any section is computed for the pressure change from the section nearest the inlet (approximately $1^1/_2$ diam from the nozzle exit) to the section in question.

As indicated by the previous figures, the accord between the data for the textolite tube and those for the lucite tube is good. The data for lucite being the more extensive, attention will be focused on Fig. 8. This shows the low frictional effect at inlet Reynolds numbers near 1×10^5, and the high values at inlet for lower and higher Reynolds numbers, particularly the lower. It shows that as the Reynolds number increases from 0.5×10^5, the mean apparent friction coefficient first decreases, then suddenly increases, and then decreases more gradually.

Along the right-hand margin of the figure values of the friction coefficient for fully developed turbulent flow of an incompressible fluid in a pipe are shown for the present range of Reynolds numbers. It appears that the observed values are lower than the familiar ones for incompressible flow, probably because of laminar conditions in the boundary layer for some distance downstream from the inlet.

Comparison with the data of Keenan and Neumann (1) shows very good qualitative agreement and good quantitative agreement. In general, the present tests show a declining mean friction coefficient over a greater length of the tube following the inlet section than do those of Keenan and Neumann, but both show a decline followed by a rise. Both show, also, values which are, in general, less than the Kármán-Nikuradse values for fully developed turbulent incompressible flow. Keenan and Neumann made tests at Reynolds numbers of about 0.5×10^5 and 3×10^5, but not at intermediate values. No comparison can be made, therefore, in the region where the present tests indicate the lowest frictional effect.

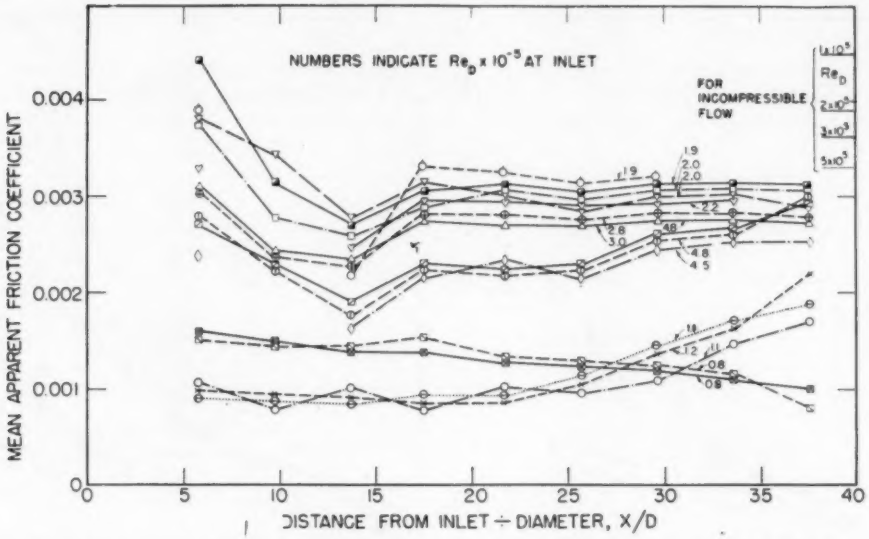

FIG. 7 MEAN APPARENT FRICTION COEFFICIENT AGAINST DISTANCE IN DIRECTION OF FLOW FOR TEXTOLITE TUBE

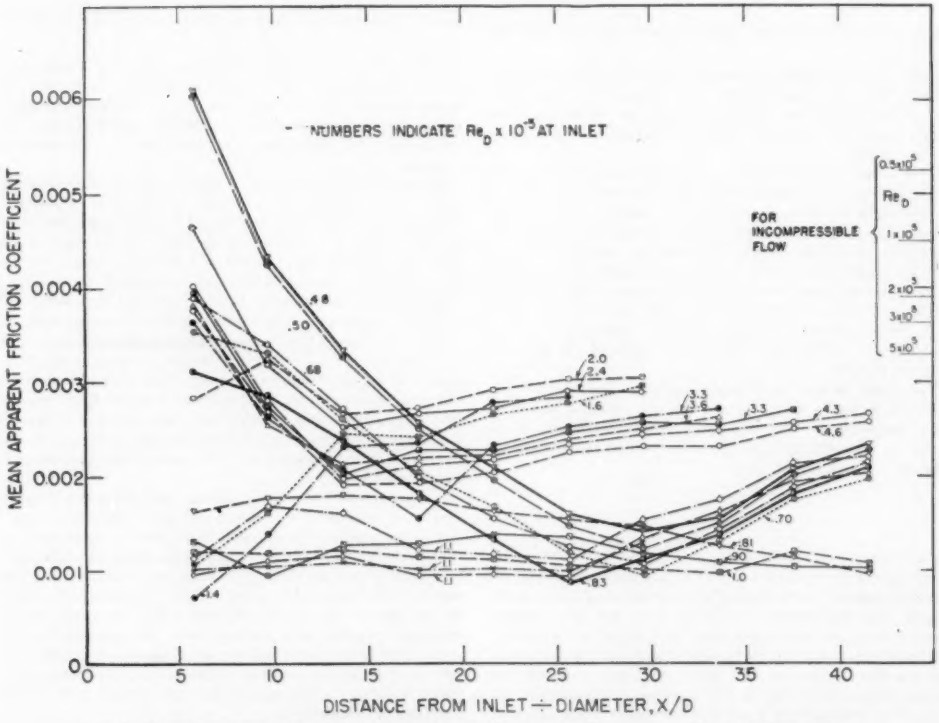

FIG. 8 MEAN APPARENT FRICTION COEFFICIENT AGAINST DISTANCE IN DIRECTION OF FLOW FOR LUCITE TUBE

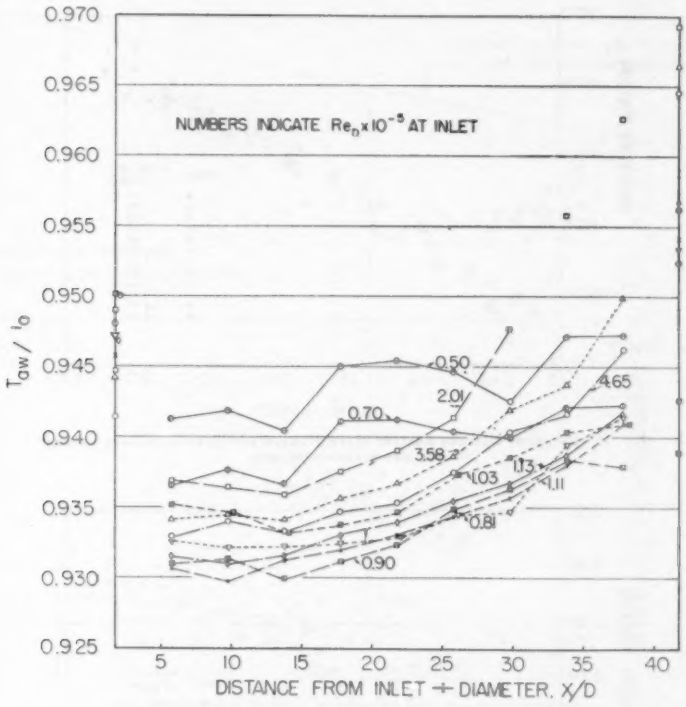

FIG. 9 LONGITUDINAL TEMPERATURE DISTRIBUTION IN LUCITE TUBE

Comparison with the data of Shapiro and Smith (4) for incompressible flow indicates that the minimum point in these curves is found at somewhat greater length Reynolds number than in the incompressible case.

These results must be considered tentative until further tests are made using nozzles of different design. Although it seems unlikely that the present nozzle introduces any shock effects, it is probable that a shorter nozzle can be made which will be equally free from shock effects but which will provide a stream with a thinner boundary layer at the inlet to the test pipe.

Recovery Factors. Fig. 9 shows the variation in temperature of the lucite-tube wall under adiabatic conditions. In order to insure against radial heat transfer, the upstream stagnation temperature was set at a value, roughly 100 F, for which the tube-wall temperature approximated room temperature. A high resistance to heat transfer across the small remaining differences in temperature was provided by a rock-wool blanket 12 in. thick.

The values of temperature at the end sections 1 and 11 are affected by longitudinal heat transfer from the adjacent warmer stagnation regions. The low conductivity of the tube wall and the relatively small temperature gradients over the central portion of the test pipe seem to justify confidence in the temperatures for sections 2 to 10.

The frictional characteristics discussed in the foregoing are reflected in these temperature curves. For example, the rise in temperature in a shock is evident in the curves for Reynolds numbers at inlet of 1.57×10^5 and 2.01×10^5.

In Figs. 10 and 11 the adiabatic wall temperatures are shown in the form of recovery factors plotted against Mach number. The recovery factor is here defined as the ratio of the excess of wall temperature over mean stream temperature to the excess of upstream stagnation temperature over mean stream temperature. The Joule-Thomson effect, which would affect the recovery factor by amounts up to 1 part in 100, depending upon how it is taken into account, is ignored.

The data for the textolite tube alone, Fig. 10, would be well represented by a single curve extending from a recovery factor of 0.875 at a Mach number of 2.4 to a recovery factor of 0.8 at a Mach number of 1.4. A single curve would not suffice if the data were plotted against Reynolds number. It is not clear, however, that Mach number is the important variable. A single curve would represent the data if the abscissa were Prandtl number because over the range of these tests the Prandtl number is very nearly a single-valued function of the Mach number.

Although Fig. 11, for lucite, shows excellent agreement with Fig. 10, for textolite, at each Reynolds number which appears in both figures, the data in Fig. 11 cannot be so well represented by a single curve. This is principally because of the introduction of lower Reynolds numbers than any appearing in Fig. 10.

Since the inlet temperature is nearly the same for each of the tests in Fig. 12, the magnitude of the Prandtl number is very nearly fixed by the magnitude of the Mach number. It becomes possible, therefore, to show in Fig. 11 a curve for the square root of the Prandtl number which is also the analytical value of the recovery factor for incompressible laminar flow past a flat

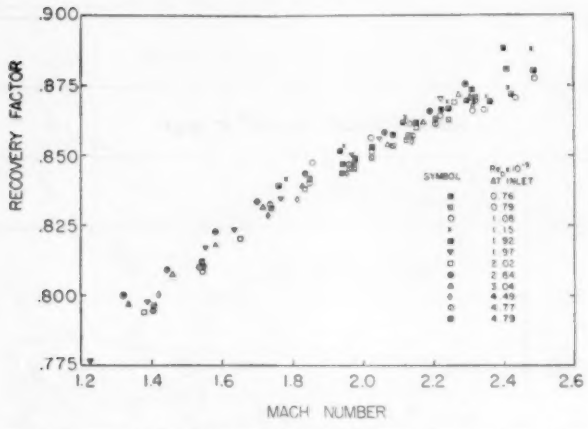

FIG. 10 RECOVERY FACTORS AGAINST MACH NUMBER FOR TEXTOLITE-TUBE VALUES FOR END STATIONS OMITTED

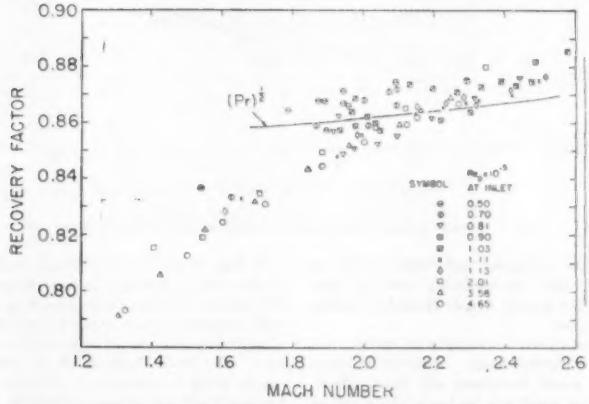

FIG. 11 RECOVERY FACTORS AGAINST MACH NUMBER FOR LUCITE-TUBE VALUES FOR END STATIONS OMITTED

plate (5). All recovery factors for tests at lower inlet Reynolds numbers and all recovery factors near the inlet end of the tube for all inlet Reynolds numbers show fairly good agreement with the curve of $(Pr)^{1/3}$. A curve lying 1/2 per cent higher than the curve of $(Pr)^{1/3}$ would seem to be indicated by a major portion of the data for which laminar conditions most probably prevail.

For high values of inlet Reynolds number and for sections near the downstream end of the tube, the experimental values for lucite fall along the same curve as those for textolite.

Analytical values of recovery factor for a turbulent boundary layer in subsonic flow over a flat plate include Ackermann's proposal (6) of the cube root of the Prandtl number (approximately 0.9 for these tests) and the higher values of Schirokov (7). The experimental value of McAdams, Nicolai, and Keenan (8) was approximately 0.89 for fully developed turbulent subsonic flow in a pipe. Eckert and Weise (9) show a similar value for flow of air parallel to a cylinder at high values of the length Reynolds number. It appears that the present values for supersonic flow with turbulent boundary layer bear no resemblance to the corresponding values for subsonic flow.

Coefficients of Heat Transfer. Heat-transfer coefficients in the form of Stanton numbers are plotted in Fig. 12 against length Reynolds number and in Fig. 13 against diameter Reynolds number. The heat-transfer coefficient is the heat flux per unit area per unit difference between the temperature of the wall and the temperature of an adiabatic wall alongside the same fluid stream.

The temperature of the adiabatic wall is computed from the mean stream conditions and a recovery factor taken from a curve through the data in Figs. 10 and 11.

The data in Figs. 12 and 13 are somewhat insensitive to minor variations in the selected value of the recovery factor because the difference between wall temperature and adiabatic wall temperature is relatively large. A difference of 0.01 in recovery

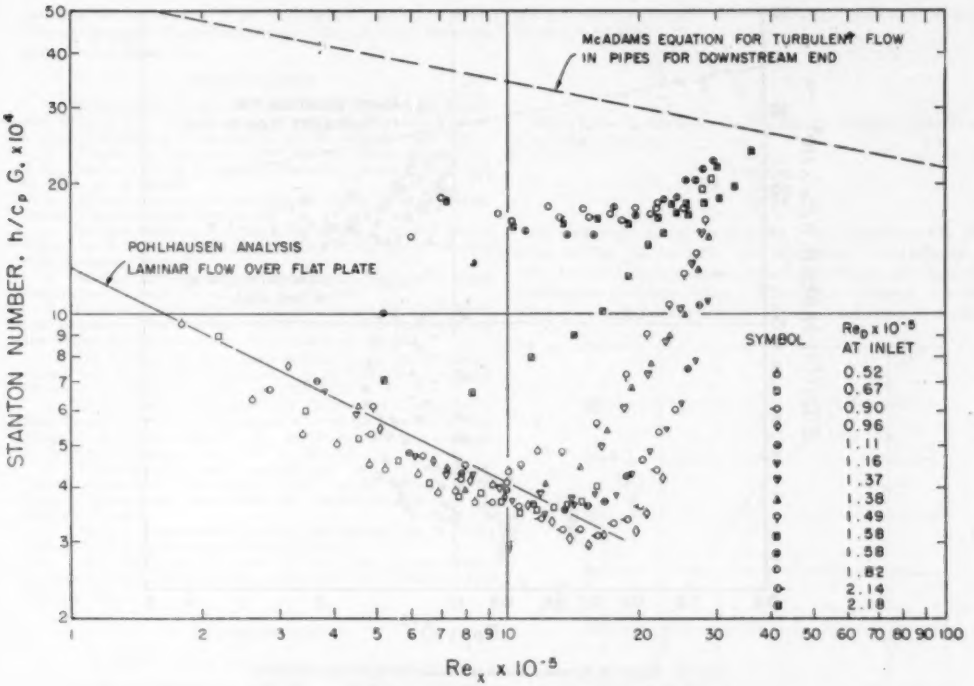

FIG. 12 STANTON NUMBER AGAINST LENGTH REYNOLDS NUMBER

factor, for example, will make a difference in heat-transfer coefficient of about 2 per cent.

Each point in Fig. 12 or Fig. 13 represents a measurement of steam condensed along one incremental length of the brass test pipe in Fig. 4. Points marked by identical symbols belong to the same test. In Fig. 12 upstream points are to the left and downstream to the right.

The points in Fig. 12 seem to form a series of curves which converge to the left and again to the right, but which spread widely in between. It is probable that the left-hand ends of the curves are converging on a curve similar to what might be found for laminar flow over a flat plate. The analytical equation of Pohlhausen (10) for this case is drawn on the chart. It seems to represent reasonably well points where convergence occurred.

In Fig. 12 is also shown the curve corresponding to the McAdams equation (11) for fully developed turbulent flow of an incompressible fluid. Since the McAdams equation is in terms of the diameter Reynolds number, it yields a separate curve on the abscissa of Fig. 12 for each station along the test pipe. The curve shown is for the station furthest downstream.

It appears that the data in Fig. 12 lie between a curve for laminar flow and a curve for fully developed turbulent flow. Most of the observed values of heat-transfer coefficient are smaller by far than the corresponding ones for fully developed turbulent flow—greatest departure being in the ratio of 1 to 10.

The points in Fig. 12 seem to offer more positive evidence of laminar conditions than do the friction-coefficient points in Figs. 7 and 8. Moreover, they seem to confirm, in a way, the low frictional effects for diameter Reynolds numbers of about 1×10^4. The two sets of points which follow the laminar curve furthest to the right in Fig. 12 are for this Reynolds number. For higher and lower Reynolds numbers transition begins earlier.

The value of the length Reynolds number at which transition begins appears to vary with the inlet diameter Reynolds number. The highest value of length Reynolds number at which transition begins is about 1.5×10^5. It should be remembered, however, that at the tube inlet, where the length Reynolds number is taken to be zero, the boundary layer is not of zero thickness because friction on the nozzle walls has already affected the stream. The effective length Reynolds number at the beginning of transition, therefore, will in this case be greater than 1.5×10^5.

In Fig. 13 the same data as in Fig. 12 are plotted against diameter Reynolds number. Here the points from a given test lie nearly on a vertical line, the slight variation in value of the abscissa being attributable to variation in the viscosity in the direction of flow. Upstream points lie to the right of downstream points.

For the tests at low Reynolds numbers, the value of the ordinate first decreases in the direction of flow, probably in accordance with laminar behavior, and then increases, probably upon entering the transition region.

For the tests at high Reynolds numbers, the coefficient rises slowly at the downstream end of the tube and seems to be approaching a limiting curve which presumably would be the curve for fully developed turbulent flow. The curve for the empirical equation of McAdams for fully developed turbulent incompressible flow is shown in Fig. 13. It seems to lie a little above where the limiting line of the present data would be. If the experi-

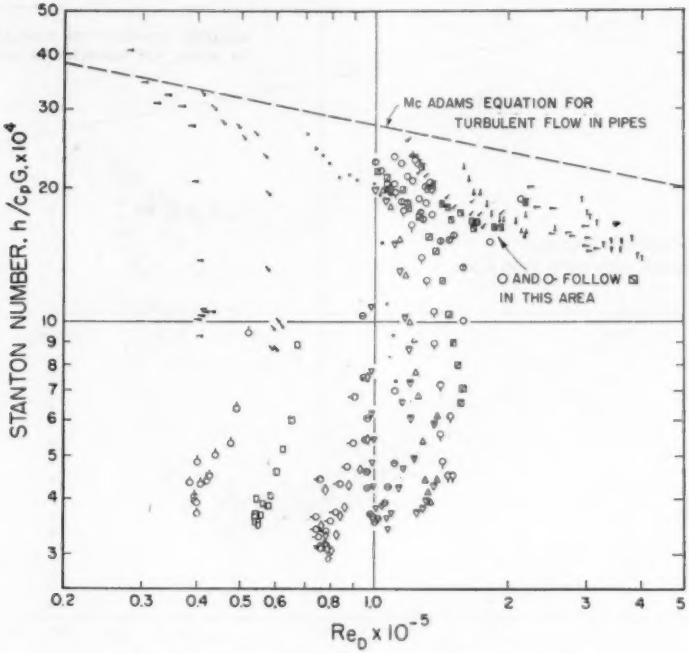

FIG. 13 STANTON NUMBER AGAINST DIAMETER REYNOLDS NUMBER

mental points were computed for values of the properties corresponding to the wall temperature instead of the mean stream temperature the points for the increment furthest downstream would lie approximately on the McAdams curve.

The dots with various flags shown in Fig. 13 represent measurements made with an unsuspected defect in the flow passage. The collar joining the nozzle and the test pipe was found to be eccentric by approximately 0.0005 in. after these tests were completed. It seems probable that this eccentricity caused shock waves to be set up in the test pipe with consequent thickening of the boundary layer and stimulating of incipient turbulence. It appears from the arrangement of these points that even for low Reynolds numbers, the coefficients at the downstream end of the tube have attained the values for fully developed turbulence.

CONCLUSIONS

The present measurements of friction coefficients and recovery factors for a stream of air in a pipe cover a range of Mach numbers from about 1.2 to about 2.5, and of diameter Reynolds numbers at inlet from 0.5×10^5 to 4.6×10^5. The measurements of heat-transfer coefficients cover the same range of Mach numbers, but a somewhat smaller range of Reynolds number at inlet, namely, 0.5×10^5 to 2.2×10^5.

The friction coefficients are in good agreement with those of Keenan and Neumann. At a diameter Reynolds number at inlet of about 1×10^5, which is intermediate between values observed by Keenan and Neumann, frictional effects of a very low order were observed. Maximum frictional effects occurred at a diameter Reynolds number at inlet of about 1.5×10^5. Friction coefficients are, in general, considerably lower than those for fully developed turbulent flow of incompressible fluids at the same values of the Reynolds number.

For laminar boundary layer, it appears that the recovery factor is in close agreement with the results of the Pohlhausen analysis, namely, $(Pr)^{1/2}$ or 0.865. For turbulent boundary layer the recovery factor appears to vary from about 0.79, where the Mach number is 1.3 to about 0.865, where the Mach number is 2.2. It cannot be determined from the present tests whether this variation is primarily an effect of variation in Mach number, although it probably is.

The measured values of heat-transfer coefficient in the region of laminar boundary layer seem to be roughly in accord with the Pohlhausen analytical values for incompressible flow over a flat plate. In the region of greatest turbulence in the boundary layer, agreement with the McAdams correlation of data for turbulent flow in pipes is good. The major portion of the data obtained appears to be in the region of transition in the boundary layer from laminar to turbulent flow. Most of the observed values of heat-transfer coefficient are smaller by far than the corresponding ones for fully developed turbulent flow—the greatest departure being in the ratio of 1 to 10.

ACKNOWLEDGMENTS

The following persons have contributed to this work in the course of their work as graduate students or as research assistants: Kenneth K. Klingensmith, Edwin Malloy, Jr., Richard M. Junge, Justin M. Margolskee, James DeWitt Wyant, William E. Helfrich, John W. Connors, Wallace L. England, William J. Larkin, Robert H. Shoulberg, and Gardner M. Ketchum. Prof. S. C. Collins provided the scheme and much of the equipment for

purifying the air stream. This investigation was sponsored as Contract Number N5-ori-07805 by the Office of Naval Research of the United States Navy.

BIBLIOGRAPHY

1 "Measurements of Friction in a Pipe for Subsonic and Supersonic Flow of Air," by J. H. Keenan and E. P. Neumann, *Journal of Applied Mechanics*, Trans. ASME, vol. 68, 1946, pp. A-91–100.

2 "Nozzles for Supersonic Flow Without Shock Fronts," by A. H. Shapiro, *Journal of Applied Mechanics*, Trans. ASME, vol. 66, 1944, pp. A-93–100.

3 "Modern Developments in Fluid Mechanics," by S. Goldstein, Oxford University Press, 1938, p. 326.

4 "Friction Coefficients in the Inlet Length of Smooth Round Tubes," by A. H. Shapiro and R. D. Smith, NACA Technical Note 1785, November, 1948.

5 "Modern Developments in Fluid Mechanics," by S. Goldstein, Oxford University Press, 1938, pp. 627–630.

6 "Plattenthermometer in Strömung mit grosser Geschwindigkeit und turbuleuter Grenzschicht," by G. Ackermann, *Forschung auf dem Gebiete des Ingenieurwesens*, vol. 13, 1942, pp. 226–234.

7 "Der Einfluss der Laminaren endschicht auf den wärmeaustausch bei hohen Geschwindigkeiten," by M. Schirokov, Technical Physics of the USSR, vol. 3, 1936, pp. 1020–1027.

8 "Measurements of the Recovery Factors and Coefficients of Heat Transfer in a Tube for Subsonic Flow of Air," by W. H. McAdams, L. A. Nicolai, and J. H. Keenan, Trans. American Institute of Chemical Engineers, vol. 42, 1946, pp. 907–925.

9 "Messungen der temperaturvertielung auf der oberfläche Schnell angeströmer unbeheitster körter," by E. Eckert and W. Weise, *Forschung auf dem Gebiete des Ingenieurwesens*, vol. 13, 1942, pp. 246–254.

10 "Modern Developments in Fluid Mechanics," by S. Goldstein, Oxford University Press, 1938, pp. 623–627.

11 "Heat Transmission," by W. H. McAdams, second edition, McGraw-Hill Book Company, Inc., New York, N. Y., 1942, p. 128, Equation [4c].

Discussion

W. B. Brown.[8] These are excellent heat-transfer data in a region where such data are badly needed. The Stanton numbers, shown in Fig. 12 of the paper, for the laminar region, however, are worthy of further discussion.

Study of Figs. 5 and 6 of the paper indicate a considerable pressure gradient in the free stream. This gradient is large enough to cause a change of 20 to 30 per cent in the heat-transfer coefficients from the Pohlhausen flat-plate value for the small $\mathbf{Re}_D$ values. The effect of the pressure gradient is conveniently specified by means of the Euler number, **Eu**, where

$$\mathbf{Eu} = -\frac{dp/dx}{\rho V^2} x$$

p = pressure
x = distance from stagnation point
ρ = density
V = free-stream velocity

If the Euler number is constant, then it has the same value as the exponent m in the equation

$$V = C^m$$

The equation for Nusselt number, **Nu**, in terms of **Eu** has been published by E. Eckert and O. Drewitz.[6] It is

$$\frac{\mathbf{Nu}}{\sqrt{\mathbf{Re}}} = \frac{\sqrt{\frac{\mathbf{Eu}+1}{2}}}{\int_0^\infty \exp\left(-\mathbf{Pr}\int_0^{\bar{\eta}} \bar{f}\, d\,\bar{\eta}\right) d\bar{\eta}}$$

where $\bar{f}$ is the function of Falkner and Skan as computed by D. R. Hartree,[7] and $\bar{\eta}$ is

$$\bar{\eta} = \sqrt{\frac{\mathbf{Eu}+1}{2}}\ y\sqrt{\frac{V}{\nu x}}$$

When **Eu** = 0, this gives the Pohlhausen relation. For **Pr** = 0.748, this relation is

$$\mathbf{St} = \frac{0.400}{\sqrt{\mathbf{Re}_x}}$$

By assuming a set of values of **Eu** from +0.05 to —0.09, the curve in Fig. 14, herewith, was calculated. The ordinate is h/h_p, where h is the actual heat-transfer coefficient and h_p is the Pohlhausen flat-plate value. When each observed Stanton number in the laminar region in Fig. 12 of the paper is divided

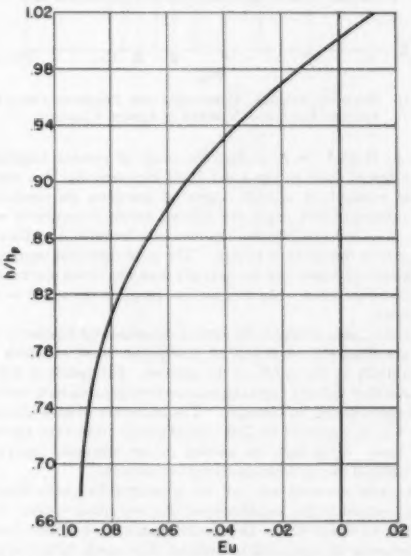

Fig. 14 Correction Factor for Pressure-Gradient Effect

by the ordinate of this curve for corresponding Euler numbers of the investigation, all the points are reduced to flat-plate values. Fig. 15 of the discussion shows a plot of the reduced values. The scatter of the data around the Pohlhausen curve is much less than in Fig. 12 of the paper. The agreement between theory and experiment is quite good when pressure gradient is considered. The Euler numbers for the investigation were computed from the formula

$$\mathbf{Eu} = -2f\frac{x}{D}$$

where f is given by results in Figs. 7 and 8 of the paper, and x/D equals $\mathbf{Re}_x/\mathbf{Re}_D$. $\mathbf{Re}_x$ appears in Fig. 12, and $\mathbf{Re}_D$ in Fig. 13.

[8] Lewis Flight Propulsion Laboratory, National Advisory Committee for Aeronautics, Cleveland Airport, Cleveland, Ohio.

[6] "Die Berechnung des Temperaturseldes in der laminaren Grenschicht schnell umstrometer, und unbeheitser Koerper," by C. Eckert and O. Drewitz, *Luftfahrtforschung*, vol. 19, 1942, pp. 189–196.

[7] "On an Equation Occurring in Falkner and Skan's Approximate Treatment of the Equations of the Boundary Layer," by D. R. Hartree, *Proceedings of the Cambridge Philosophical Society*, vol. 33, 1937, p. 223.

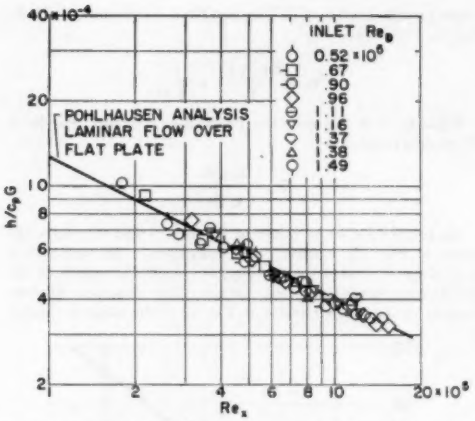

FIG. 15 STANTON NUMBER, CORRECTED FOR PRESSURE GRADIENT, AGAINST REYNOLDS NUMBER IN LAMINAR REGION

N. A. HALL.[8] In extending the scope of present knowledge of the flow of fluids in pipes and ducts, it is essential that experimental research of a high degree of precision be conducted. The authors of this paper are making available results of such work, and their contribution represents an important addition to background technical literature. The procedure and equipment are clearly described and the data are presented from several constructive viewpoints. As a report on progress the paper is well organized.

Several points in regard to further experimental studies in this field are apparent on review of this paper, most of which are undoubtedly in the minds of the authors. Ultimately it will be essential that velocity and temperature distributions both radially and longitudinally be obtained. The character of such distributions can be expected to differ significantly from that for subsonic flow. Such data are needed for an adequate analytical correlation of the material presented in this paper.

The tests reported are still for a limited Reynolds number range confined to the neighborhood of a transition region. It is desirable to extend this. The relative importance of inlet transition behavior as compared to subsonic flow needs further study.

The authors have gone to considerable effort to obtain shock-free flow in their tests. While this is essential in obtaining basic data, the question immediately arises as to the relation of such data to practical flow systems where shock patterns of some nature are certain to occur. In due course it will be necessary to include such effects in more complete descriptions of internal-flow behavior. This will require a more difficult analysis dealing with extensive flow behavior rather than local characteristics.

It is recognized that these tests represent only preliminary work. The correlation with previous relevant material is good, and the scope of further studies is clearly indicated.

H. A. JOHNSON.[9] The supersonic-flow data for friction and heat transfer presented by the authors is of much interest since reliable experimental information here is still meager and difficult to obtain. Recognizing that the definitions and form of presentation given in the paper will facilitate design for supersonic flow in pipes, there remains an evaluation referred to the isentropic-core flow up to the point where the boundary layer fills the pipe or shock occurs. This has been done by the writer in the following manner within the limits of information contained in the paper:

The local recovery factor referred to the center line or isentropic temperature T_c and defined by

$$r = (T_{aw} - T_c)/(T_0 - T_c)$$

was found to have local values of 0.895 ± 0.004 for the three lucite tube Reynolds numbers 1.03, 2.01, and 4.65×10^5, respectively. These values appeared quite independent of local isentropic Mach number (range 2.3 to 2.9) and local or pipe entrance Reynolds number, although the heat-transfer data indicate laminar, transition, and possibly turbulent boundary-layer flows. While the value 0.895 is too large compared with the theoretical laminary flat-plate value of $\mathbf{Pr}^{1/2}$ it is only a little less than the empirical turbulent flat-plate value of $\mathbf{Pr}^{1/3}$. Consequently, it can only be said that the suggestion persists that the recovery factor is independent of Reynolds and Mach number. A detailed analysis for an annular boundary layer may give added significance to this recovery-factor magnitude.

The Stanton number correlation data given in Fig. 12 of the paper were adjusted with reference to isentropic core flow for the two entrance Reynolds ($\mathbf{Re}_D$) values of 0.90 and 1.58×10^5. In the range of pressure ratios 0.03 to 0.10, the ratio of the two moduli are well represented by the relations

$$\mathbf{Re}_c/\mathbf{Re}_m = 23.3\ (P/P_0)^{0.343} \text{ and } \mathbf{St}_c/\mathbf{St}_m = 0.105/(P/P_0)^{0.312}$$

where subscript c designates core flow, and m the mean flow conditions as defined in the paper. Since the pressure distribution for the heat-transfer tests were not given, it was estimated from Fig. 6.

When compared with the local flat-plate correlation formulas

$$\mathbf{St} = 0.332/\mathbf{Re}^{1/2}\,\mathbf{Pr}^{2/3} \text{ for laminar flow}$$

$$\mathbf{St} = 0.0296/\mathbf{Re}^{0.2}\,\mathbf{Pr}^{2/3} \text{ for turbulent flow}$$

the agreement for $\mathbf{Re}_D = 0.90 \times 10^5$ was much the same as that shown in Fig. 12, except that the apparent transition, i.e., departure from the laminar-flow line, occurred at $\mathbf{Re}_{x_c} = 3 \times 10^5$. On the other hand, for $\mathbf{Re}_D = 1.58 \times 10^5$, using the test points with the larger values of Stanton modulus, the distribution of points was radically altered with nine downstream points showing a tendency toward decreasing values of Stanton modulus as expected for a turbulent boundary layer. However, these values all lie about 15 per cent below the turbulent flow line.

These evaluations are offered only to show that they are promising and warrant including the pressure distributions for the heat-transfer data and possibly a table of values for the nozzle stagnation temperature T_0 and pressure P_0 for each value of entrance Reynolds number $\mathbf{Re}_D$.

AUTHORS' CLOSURE

The authors wish to express their appreciation to Messrs. Brown, Hall, and Johnson for presenting material which enhances the value of the paper.

The results presented by Mr. Brown are very interesting and in line with some work which the authors have been doing recently in connection with the effect of pressure gradient on the recovery factors and friction coefficients for supersonic flow of air in a tube.

The results presented by Professor Johnson for local-recovery

[8] Professor, Mechanical Engineering, Head, Heat and Power Mechanical Engineering Department, Thermodynamics Division, University of Minnesota, Minneapolis, Minn. Mem. ASME.

[9] Associate Professor of Mechanical Engineering, University of California, Berkeley, Calif.

factors based on the isentropic core of the flow in the tube confirm the findings which the authors computed previously in a similar fashion.

The discussion by Professor Hall indicates the great need for further testing and analysis. The authors have obtained in the past year considerably more quantitative data; both these and the older data will soon be published in detail. In addition, extensive analytical work has been carried out to gain a better understanding of the phenomena occurring in supersonic flow of air in a tube.

Heat Transfer Through Gases at Low Pressures

By R. E. PECK,[1] W. S. FAGAN,[2] and P. P. WERLEIN,[3] CHICAGO, ILL.

The purpose of this study is to determine experimentally the heat transfer between two parallel vertical plates. The space between the plates is filled with a gas at low pressure, and the boundaries of this gas layer are enclosed by a solid heat insulator. The variation of this heat transfer with pressure, temperature difference, type of gas, and thickness of the gas layer is determined. The experimental result is compared with both theoretical and empirical equations.

This result is

Helium:

$$Nu = 8.0\ Gr^{0.04}\ (L/H)^{0.75}\ 10^{-3} < Gr < 5 \times 10^{3}$$
$$h = 9.2\ kP^{0.050} \qquad 1 < P < 760 \text{ mm Hg}$$

Air:

$$Nu = 14.1\ Gr^{0.032}\ (L/H)^{0.75}\ 10^{-1} < Gr < 5 \times 10^{3}$$
$$h = 17.1\ kP^{0.063} \qquad 1 < P < 100 \text{ mm Hg}$$

Note: P in mm Hg, h/k in ft^{-1}

Nomenclature

The following nomenclature is used in the paper:

- B' = coefficient of thermal expansion (deg^{-1})
- g = vector of earth's acceleration (length/time^2)
- Gr = Grashof number (0)
- H = height of the gas layer (length)
- h = over-all heat-transfer coefficient based on conduction and convection (energy/time area deg)
- k = coefficient of thermal conduction (energy/time length deg)
- L = thickness of gas layer (length)
- M = molecular weight of gas (mass/mass mol)
- Nu = Nusselt number (0)
- P = pressure (force/area)
- P_0 = pressure indicated by vacuum gage (force/area)
- q'' = rate of heat transfer per unit area normal to heat flow (energy/time area)
- q_T = heat transfer due to conduction, convection, and radiation (energy/time)
- q_N = net heat transfer through gas space due to conduction and convection (energy/time)
- q_E = heat transfer due to radiation and end effects (energy/time)
- R = universal gas constant (energy/mass mol deg)
- S = area of heat-transfer surface normal to heat flow (area)
- T_A = temperature of molecule after leaving a cold plate (deg)
- T_B = temperature of a molecule after leaving a hot plate(deg)
- T_0 = absolute temperature of vacuum-gage environment (deg)
- t_1 = cold-plate temperature (deg)
- t_2 = hot-plate temperature (deg)
- Δt = $t_2 - t_1$ (deg)
- W = ratio of specific heat at constant volume to universal gas constant (0)
- ν = kinematic viscosity (length^2/time)

Introduction

This problem may best be analyzed by study of the mechanisms of heat transfer at various pressure ranges. At "low" pressure, the mechanism is of molecular motion; at "high" pressure we have free convection dominating in the bulk of the gas stream; and at "intermediate" pressure, a combined effect of the two is noticed.

We may define pure thermal conduction in a gas as that mechanism by which moving particles of the gas transport thermal energy, yet the net mass flow through any area element in the space is zero. The classical kinetic theory predicted that this property of a gas should be independent of pressure. In 1872 Stefan (1)[4] experimentally showed independence of pressure for air from 428 to 760 mm mercury. Kundt and Warburg (2) showed independence for air from 0.5 to 19.5 mm, for carbon dioxide from 1.5 to 7.7 mm, and for hydrogen from 8.8 to 154 mm. All of the many subsequent investigators have confirmed the law experimentally, that the thermal conductivity of a gas is independent of pressure.

Kundt and Warburg (2) first noticed the variation of thermal conductivity with pressure at low pressure. Quantitative measurements were made by Brush (3) and Smoluchowski (4). Their results showed proportionality of thermal conductivity with pressure.

The next mechanism to be considered is that by which heat is conducted from a hot isothermal surface through a relatively stagnant layer of gas, enters the bulk of the gas stream which is in motion due to free convection currents, and then this energy is given up to a neighboring cold isothermal surface. The present knowledge of this case is summarized in a paper by Jakob (5). Semitheoretical equations are presented representing data of Mull and Reiher (6). The correlation was of Nusselt's number as a power function of the Grashof number. It was pointed out that these data disagree with those of others, such as Wilkes and Peterson (7). It was proposed that experimental elimination of end effects in Mull and Reiher's (6) work made their data valid, since elimination of end effects assured two-dimensional heat flow. Many references are given on this problem in Jakob's paper (5).

For very low pressures, where the mean free path of the molecules is much greater than the spacing between the plates, the heat transfer should be proportional to the pressure. An expression

$$q'' = (3^{1/2}/4)WP_0(R/M)^{1/2}(T_B - T_A)/(T_0^{1/2}) \quad [1]$$

was derived by Fagan (8). For air, this reduces to

$$q'' = 0.578\ P_0(T_B - T_A)/(T_0^{1/2}) \quad [2]$$

---

[1] Professor of Chemical Engineering, Illinois Institute of Technology.

[2] Associate Chemical Engineer, Argonne National Laboratory.

[3] Graduate Assistant in Chemical Engineering, Illinois Institute of Technology.

Contributed by the Heat Transfer Division and presented at the Fall Meeting, Worcester, Mass., September 19–21, 1950, of The American Society of Mechanical Engineers.

Note: Statements and opinions advanced in papers are to be understood as individual expressions of their authors and not those of the Society. Manuscript received at ASME Headquarters, June 16, 1950. Paper No. 50—F-16.

[4] Numbers in parentheses refer to the Bibliography at the end of the paper.

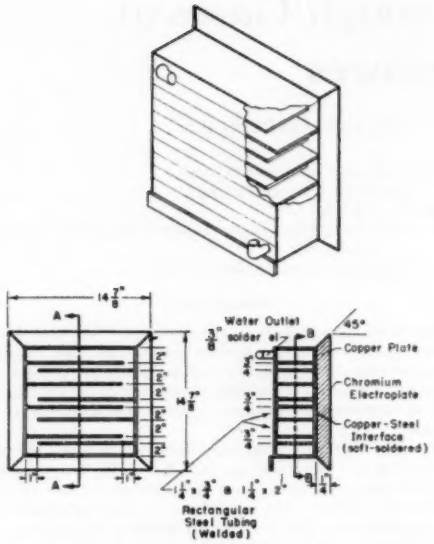

FIG. 1 COLD-PLATE ASSEMBLY

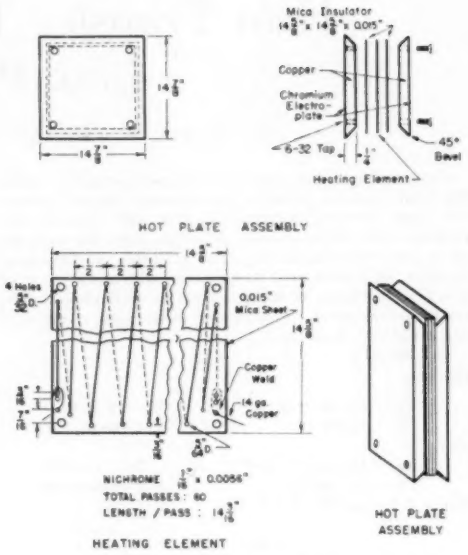

FIG. 2 HOT-PLATE ASSEMBLY

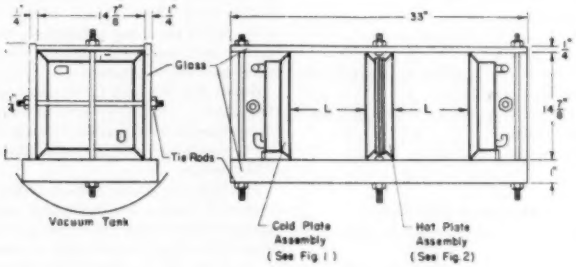

FIG. 3 HEAT-TRANSFER ASSEMBLY

where the dimensions are P_0 (microns Hg), T (deg R), and q'' (Btu/hr ft^2).

EXPERIMENTAL APPARATUS

The heat-transfer assembly (see Figs. 1, 2, and 3) was housed in a horizontal cylindrical steel tank, 3 ft long and 2 ft in diam. Heavily webbed steel blind flanges sealed the ends of the tank. The vacuum seal at the flanges was made by machining matching V-grooves into both tank flange and blind flange and compressing a lightly greased solid-rubber cord in the groove. The metal vacuum tank was painted inside and outside with several thin coats of glyptal lacquer. A short piece of steel pipe was threaded into the tank wall, and rubber tubing with an adjustable screw clamp was placed over the pipe to permit pressure adjustment.

An oil-diffusion pump was connected to the tank through a welded elbow. The foreside of the pump was connected to a mechanical pump through a globe valve. Copper tubing was soft-soldered on the outside of the welded elbow, and cooling water passed through it to act as a baffle and to prevent saturated oil vapor from entering the vacuum tank. All welds and soft-soldered joints were covered with hard wax. All pipe joints were screwed together with glyptal in the threads.

The pressure gages used were a closed end U-tube, an open end U-tube, a McCleod gage, and a Pirani gage. A glass trap was used for the Pirani bulb, and one was also used for the mercury gages. A rubber tape joint connected the gage manifold to the tank-gage connection.

The heat-transfer assembly consists of heating plates, cooling plates, and enclosure (see Figs. 1, 2, and 3). The glass enclosure was painted with glyptal lacquer to prevent transmission of radiation.

The heating element, Fig. 2, was nichrome ribbon wound on a drilled mica sheet with two mica sheets as insulators. This bundle was compressed between two copper plates to form the hot isothermal surfaces. The copper plates were chrome-plated to reduce radiation, and the edges of the plates were beveled to reduce conduction losses. The thermocouples were placed by drilling through the plate and soft-soldering the couple into a

small trench in the surface. The thermocouple wire was led out between the copper and mica. A precision potentiometer and ice-water cold junction were employed.

The cooling plates were beveled plated copper as before. Rectangular steel tubing was welded into a cooling-water raceway so that the water moved in nine horizontal passes through the tubing, Fig. 1. This raceway was soft-soldered to the copper plate. Thermocouples were installed similarly to the heating plates, except holes were drilled without piercing the water chamber.

The heat-transfer assembly, Fig. 3, was put together by standing the vertical cooling plates at opposite ends of the plate glass with the chromium surfaces facing each other. The heating plate was inserted midway between the cooling plates with its chromium surfaces facing those of its neighbors. The two side glass plates were placed vertically against the beveled metal surfaces, and the top glass plate was lowered into position, giving metal-to-glass contact at all points. The heating plate was held upright by holes drilled into the glass, inserting small screws in the holes, and placing the screw heads between the beveled surfaces, causing a positive bond. The plate glass was held compactly by two tie rods on each end passing through holes drilled in the glass. This whole heat-transfer unit was lifted into the steel vacuum tank.

The cooling water was introduced through a constant-head thermostatic bath, and the flow rate was measured by rotameters. Flexible seamless copper tubing was used to connect the cold plates to the external coolant circuit.

The power input to the heating plates was measured with a direct-current voltmeter and ammeter. This power was introduced through the vacuum tank by soft-soldered kovar-glass seals. All thermocouples were led out of the tank by compressing the wires between rubber-gasketed metal planes and applying hard vacuum wax to the compressed joint.

Experimental Technique

The experimental technique for a given run involved the achievement of a steady-state heat-transfer experiment in terms of all the operating parameters. A fine-bore capillary tube was inserted in the constant-leak opening to regulate the pressure. Pressure readings were taken on the particular gage which was applicable. The U-tubes and the McCleod gage were primary standards and needed no calibration. The Pirani gage was calibrated against the McCleod gage; the Pirani was trapped with liquid nitrogen, and the McCleod with acetone-dry ice. Since the Pirani gage will lose calibration with use, it was checked frequently with the McCleod. During all experimental runs, the Pirani was untrapped to indicate condensibles while acetone-dry ice was used to trap the mercury gages and to freeze out water. For the runs at ultimate vacuum, a closed-end glass tube was inserted in the leak connection, and the tube placed in liquid nitrogen to trap out any residual condensibles.

The thermocouples used were calibrated individually in an hypsometer at the steam point. The average value of the millivoltage was 4.259, the maximum deviation from the average was 0.004 mv or 0.09 per cent, and the average of the absolute value of the deviations was 0.002 mv. This corresponds to about 0.1 deg F. This calibration disagreed with the Leeds and Northrup calibration by 0.6 deg F, and the assumption was made that the deviation was proportional to the voltage over the experimental range. The ammeter used in the heater input measurements was calibrated against a laboratory standard ammeter, and the rotameters were calibrated by direct weighing of the discharge.

Data and Sample Calculation

A typical set of runs is given in Table 1.

The complete calculation for a run is typified by run No. 40. The hot-plate temperature was obtained by averaging the temperatures on one hot isothermal surface, averaging the temperatures on the other hot isothermal surface, and then averaging these mean values. This temperature, t_2, is 157.8 F. By similar determination of mean values, the cold-plate temperature, t_1, is 85.4 F. By subtraction, the temperature difference, Δt, is 72.4 F. The total heat transfer, q_T, is calculated by means of voltmeter and ammeter and is 100.4 Btu per hr.

The transfer due to radiation losses and conduction through the glass, q_g, is found from the runs at ultimate vacuum and $1^1/_2$ in. plate separation, where conduction through the gas is zero as per Equation [1]. Ultimate vacuum is such a pressure that the reading of the McCleod gage was zero and no deflection from zero could be observed on the Pirani needle when the gage was trapped with liquid nitrogen. Ultimate vacuum corresponds to less than 0.02 microns. It represents the best possible vacuum that could be obtained with the equipment. Runs Nos. 13, 14, and 15, those at ultimate vacuum and 1 ft separation are plotted, log q_T versus log t_2, and a curve of slight concavity is obtained. However, if log q_T versus log $(t_2 - 47.5)$ is plotted, a straight line is obtained. In all runs, the temperatures were adjusted to approximate those of runs Nos. 13, 14, and 15. For the case of $1^1/_2$-in. plate separation, 47.5 is replaced by 65.0. From Fig. 4, for t_2 equal 157.8, q_g equals 26.5 Btu per hr.

The transfer by conduction and convection, q_N, is found from $q_T - q_g$ and equals 73.9 Btu/hr. The pressure for this run is read on a closed-end U-tube and is 12 mm mercury. The heat-transfer surfaces measure $14^3/_4 \times 14^3/_4$ in. and the area, S, is $(2)(14^3/_4)^2/(144)$ equals 3.08 sq ft. The over-all heat-transfer coefficient of conduction and convection may be found

$$h = q_N/(S\Delta t) = (73.9)/(3.08\ 72.4) = 0.331 \text{ Btu/hr ft}^2 \text{ deg F}$$

The mean temperature of hot and cold plates is $(t_1 + t_2)/2$ equals 122 F. The thermal conductivity of air at this temperature is 0.01587 Btu/hr ft deg F, and the kinematic viscosity is 44.0 sq ft per hr. These were obtained from data (9) at 1 atm, assuming that k is independent of pressure and ν inversely proportional to pressure. The coefficient of thermal expansion,

TABLE 1 TEST DATA

Run number	28	34	37	39	40	41	43
Gas	Air	Air	Air	Air	Air	Air	Air
L (in.)	1.5	1.5	1.5	1.5	1.5	1.5	1.5
P (mm Hg)	$<2 \times 10^{-5}$	0.100	0.780	12	12	12	80
t_2 (deg F)	156.1	157.4	155.1	110.1	157.8	195.7	156.9
t_1 (deg F)	85.1	85.0	84.9	84.8	85.4	84.9	84.9
$t_2 - t_1$ (deg F)	71.0	72.4	70.2	25.3	72.4	110.8	72.0
q_T (Btu/hr)	25.72	71.39	88.7	37.0	100.4	161.5	110.0
q_g (Btu/hr)	25.76	26.37	25.4	8.91	26.53	44.4	26.15
q_N (Btu/hr)	−0.04	45.02	63.3	28.1	73.9	117.1	83.9
h (Btu/hr ft² deg F)		0.202	0.293	0.260	0.331	0.343	0.378
$(t_2 + t_1)/2$(deg F)			120	97	122	140	121
ν_m (ft²/hr)			672	40.9	44.0	46.4	6.57
k_m (Btu/hr ft deg F)			0.01581	0.01532	0.01587	0.01623	0.01584
Nu (0)			2.32	2.94	2.61	2.64	2.98
Gr (0)			0.217	22.0	52.1	69.5	2330

B' is 1/(122 + 460) equals 1/582 deg R. The plate separation, L, is $^1/_8$ ft. Nusselt and Grashof numbers are computed as follows:

$$Nu = hL/k = (0.331)(^1/_8)/(0.01587) = 2.61$$
$$Gr = L^3gB'\Delta t/\nu^2 = (^1/_8)^3(4.15\ 10^8)\ (72.4)/(582)(44.0)^2 = 52.1$$

The data on viscosity of helium is given by McAdams (10)

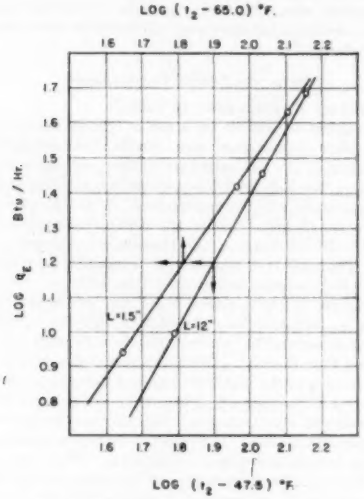

FIG. 4 ULTIMATE VACUUM HEAT TRANSFER

The mass density is taken from the ideal gas law and the thermal conductivity from Jakob (11).

RESULTS AND DISCUSSION

Fig. 5 shows the effect of temperature difference on heat transfer for $1^1/_2$-in. spacing. For air at atmospheric pressure the slope is usually given as 1.25. The slope found in this work was 1.18 which is somewhat low. In order to check the effect of separation on this slope, a series of runs was made at a 12-in. separation. The results are shown in Fig. 6 and the slope at this separation is still about the same. Runs at a $^3/_4$-in. separation gave the same value.

Fig. 7 shows the effect of pressure on the heat transfer, and Fig. 8 shows the effect of pressure on the heat-transfer coefficient. The results indicate that free convection plays only a small role in the case of helium. Curve C (which is pure conduction) is only slightly below curve D (which is the experimental value). In the case of air, convection plays a much greater part in the transfer of heat.

Fig. 9 shows the results plotted in dimensionless form. All the values for helium are at very low Grashof numbers due to the low density. As radiation and heat loss were determined at ultimate vacuum, the results at high pressure are only approximate but check fairly well with figures given in the literature.

In order to check the apparatus, considerable work was carried out at atmospheric pressure. The apparatus was very carefully insulated (12) and heat flow along the glass checked with thermocouples on the plates. Runs were made both above and below room temperature. These alterations caused less than 15 per cent deviation in any result. The coefficients for the 12-in.

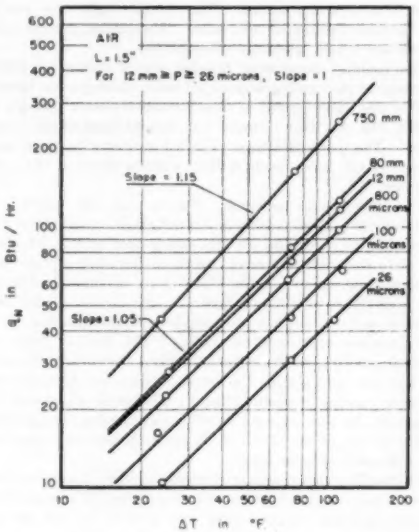

FIG. 5 VARIATION OF NET HEAT TRANSFER WITH TEMPERATURE DIFFERENCE

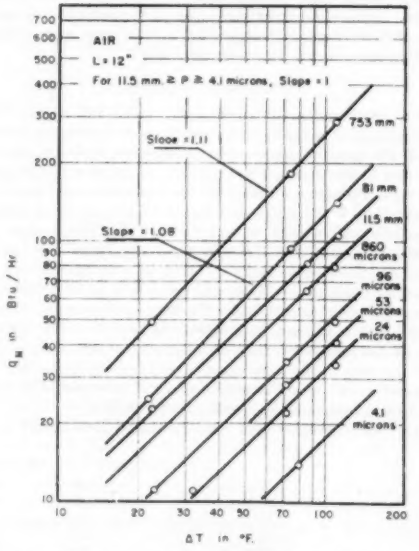

FIG. 6 VARIATION OF NET HEAT TRANSFER WITH TEMPERATURE DIFFERENCE

spacing showed the greatest deviation and thus are not too reliable. They are included, however, to show that heat transfer is substantially independent of the plate spacing.

The results obtained at atmospheric pressure are shown in

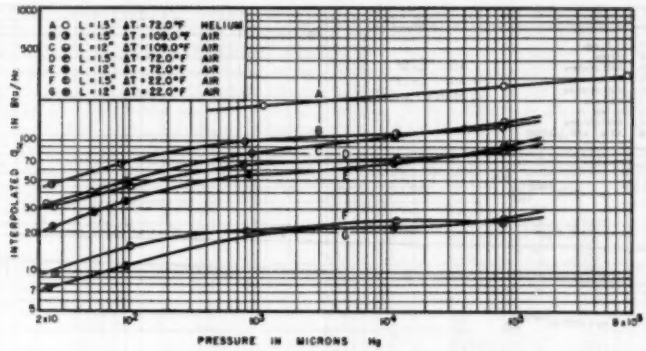

FIG. 7 VARIATION OF NET HEAT TRANSFER WITH PRESSURE

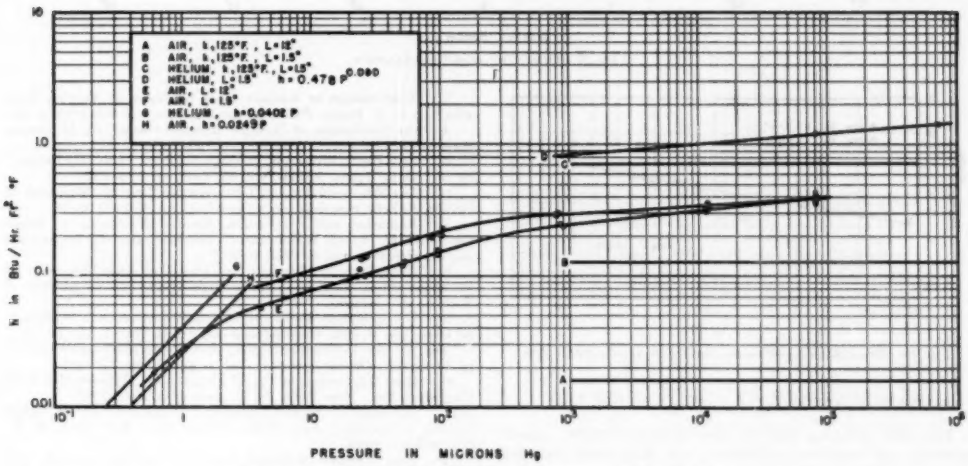

FIG. 8 VARIATION OF HEAT-TRANSFER COEFFICIENT WITH PRESSURE

Fig. 10. Convection plays a greater part in the heat transfer at higher pressures than it does at lower pressures, so the Grashof number has a higher power. This alteration causes the power of L/H to be lower as H is independent of L. Height H was not varied and is only used in order to make the equation dimensionless.

The atmospheric-pressure data for air may be represented by the equation

$$Nu = 1.38\,Gr^{0.178}\left(\frac{L}{H}\right)^{0.404} \quad \ldots\ldots\ldots\ldots [3a]$$

If it is desired to use the plate height H rather than plate separation L as the characteristic length, the equation may be rewritten

$$(Nu)_H = 1.38\,(Gr)_H^{0.178}\left(\frac{L}{H}\right)^{-0.068} \quad \ldots\ldots\ldots [3b]$$

or

$$(Nu)_H = 1.38\,(Gr)_H^{0.178} \quad \ldots\ldots\ldots\ldots [3c]$$

Equations [3a], [3b], and [3c] are equivalent. It must be stressed that no variations in H were experimentally studied. It was deemed inadvisable to introduce the Prandtl number as this modulus is about the same for both air and helium.

In dimensional form, this equation would be

$$h = 0.28\,(\Delta t)^{0.18}$$

for air at one atmosphere. Δt was varied from 15 to 115 deg F, and L was varied from 0.75 to 1.5 in. These results are 15 per cent higher than those given by Griffiths and Davis (13) and 30 per cent higher than those reported by Jakob (5).

CONCLUSIONS

Extrapolation of dimensionless correlations found in the literature to low Grashof numbers would lead to considerable error. Due to the low density of helium, its Grashof number would fall below 10^4 at atmospheric pressure.

The heat-transfer coefficient for helium can be given by the equation

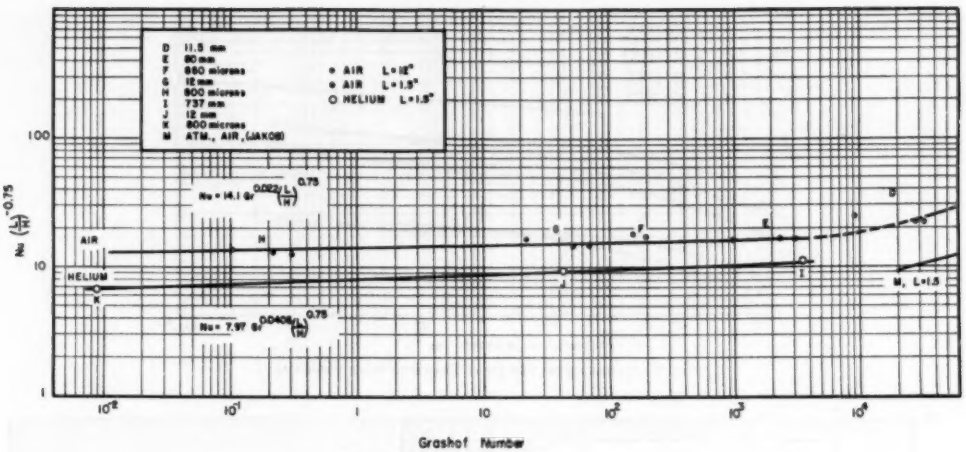

FIG. 9 DIMENSIONLESS CORRELATION

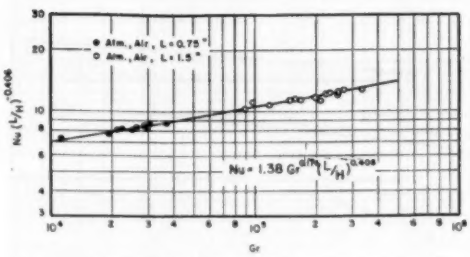

FIG. 10 DIMENSIONLESS CORRELATION FOR ATMOSPHERIC AIR

$$Nu = 8.0\, Gr^{0.04}(L/H)^{0.75} \qquad 10^{-2} < Gr < 5 \times 10^{3}$$

The only variables studied were distance between plates, pressure, and temperature difference. In dimensional form this equation could be written as

$$h = 9.2\, k P^{0.080} \qquad 1 < P < 760 \text{ mm Hg}, \ (h/k \text{ in ft}^{-1})$$

For air, the heat-transfer coefficient could be represented by the dimensionless equation

$$Nu = 14.1\, Gr^{0.022}(L/H)^{0.75} \qquad 10^{-1} < Gr < 5 \times 10^{3}$$

or in dimensional form

$$h = 17.1\, k P^{0.085} \qquad 1 < P < 100 \text{ mm Hg}, \ (h/k \text{ in ft}^{-1})$$

At higher pressures for air, the data show the film coefficient to be a function of the temperature difference.

At low Grashof numbers, the coefficient was independent of plate separation and temperature gradient.

BIBLIOGRAPHY

1 "Untersuchungen uber die Warmeleitung in Gase," by M. Stefan, *Wiener Sitzungsberichte*, vol. 65, 1872, p. 45.

2 "Uber Reibung und Waermeleitung in Verduennten Gasen," by A. Kundt and E. Warburg, *Annalen der Physik*, vol. 156, 1875, p. 177.

3 "Transmission of Radiant Heat by Gases at Varying Pressure," by C. F. Brush, *Philosophical Magazine*, vol. 45, 1898, p. 31.

4 "On Conduction of Heat by Rarefied Gases," by M. Smoluchowski, *Philosophical Magazine*, vol. 46, 1898, p. 192.

5 "Free Heat Convection Through Enclosed Plane Gas Layers," by M. Jakob, Trans. ASME, vol. 68, 1946, pp. 189–193.

6 "Der Warmeschutz von Luftschichten," by W. Mull and H. Reiher, *Beihefte zum Gesundeits-Ingenieur*, vol. 1, 1932, p. 28.

7 "Radiation and Convection Across Air Spaces in Frame Construction," by G. Wilkes and C. Peterson, *Heating, Piping and Air Conditioning*, vol. 9, 1937, p. 505.

8 "Heat Transfer Through Gas Layers at Low Pressure," by W. Fagan, PhD. thesis in chemical engineering, Illinois Institute of Technology, January, 1949.

9 "Die Zähigkeit als hydrodynamisch massgebende Stoffeigenschaften," by S. Erk, *Chemie-Ingenieur*, vol. 1, part 1, pp. 69–73.

"Die für die Wärmeübertragung wichtigsten Stoffeigenschaften," by M. Jakob, *Chemie-Ingenieur*, vol. 1, part 1, pp. 311–325.

10 "Heat Transmission," by W. McAdams, McGraw-Hill Book Company, Inc., New York, N. Y., second edition, 1942.

11 "Elements of Heat Transfer and Insulation," by M. Jakob and G. A. Hawkins, John Wiley & Sons, Inc., New York, N. Y., first edition, 1942.

12 "Heat Transfer Between Vertical Plates by Natural Convection," by P. Werlein, MS thesis in chemical engineering, Illinois Institute of Technology, June, 1949.

13 "The Transmission of Heat by Radiation and Convection," by E. Griffiths and A. Davis, Department of Scientific and Industrial Research, Special Report No. 9, London, England, 1922.

Discussion

M. JAKOB.[5] Considering recent usage of medium and extreme vacuum, it is gratifying that the authors contributed the results of careful experiments to our knowledge of the heat transfer under vacuum conditions. Their extension of experimentation to standard atmospheric pressure, however, seems to suffer under the often observed fact that an experimental device well designed for certain conditions, will be less appropriate under others.

At atmospheric pressure the authors obtained considerably higher values of heat transfer through air layers than had been observed by other investigators (Griffiths and Davis, Mull and Reiher). The reason for these deviations may be searched for in the heat loss of the system. It seems that the authors deter-

[5] Research Professor of Mechanical Engineering, Illinois Institute of Technology, Chicago, Ill. Mem. ASME.

mined the loss from their runs at "ultimate vacuum," where convection does not play any role, and that they deducted this loss from the total heat input. However, at atmospheric pressure, the glass plates closing the air layer against the air of the steel tank, will be at higher temperature than their environment and give up heat energy by convection which also should be subtracted from the heat input. Some of this heat energy is coming from the air enclosed, some may come over the beveled edges of the copper plates, and some from the hot nichrome ribbon of the heating element. Correcting for these losses, lower values of heat transfer through the air layers would have been obtained.

Authors' Closure

The readings taken in this investigation have their maximum error at atmospheric conditions. The high-pressure runs were included for comparison with other investigations. The Nusselt numbers were about 20 per cent above those of Griffiths and Davis. Their results were about 20 per cent above the values obtained by Mull and Reiher (6).

Runs were made above and below room temperature and the same results were obtained. However, better precision could be obtained in an apparatus build for atmospheric conditions.

62,000-Hp Vertical Six-Nozzle Impulse Turbines for the Bridge River Hydrodevelopment

By W. F. BOYLE[1] and I. M. WHITE,[2] SAN FRANCISCO, CALIF.

Information is presented concerning the historical background of the vertical impulse-type turbines installed at the Bridge River hydrodevelopment of the British Columbia Electric Railway Company, Ltd. This plant is of wide interest since few similar installations have been made. Data are presented to disclose the reason for selecting the 6-nozzle vertical turbine in comparison with other impulse-type turbines.

The Site and Station

THE initial conception of Canada's Bridge River Power Project at Shalalth, British Columbia, dates back to 1910, when Mr. Geoffrey M. Downton, a British Columbia land surveyor, stood on top of Mission Mountain and saw that the Bridge River was located very close to Seton Lake but well over 1000 ft higher in elevation. With his partner, Mr. P. D. Booth, he succeeded in interesting Vancouver businessmen in the formation of a company to develop the power, but nothing came of the venture owing to the fact that the site was 130 miles northeast of Vancouver and the power demand was then insufficient to justify the enormous expense.

In 1913, study of the Bridge River run-off was begun and since that time, engineers of the Dominion Water and Power Bureau have, to quote the B. C. Electric Railway Company, "made a systematic study, using the most modern stream-gaging equipment, including continuous water-stage recorders at various points on the main stem and its tributaries, in co-operation with our engineers. With these authentic hydrometric records, the company has been able to plan complete utilization of the water supply."

These studies revealed a power potential of 600,000 hp, and the long-range planning of B. C. Electric contemplates two tunnels through Mission Mountain and several penstocks feeding a group of 62,000-hp turbines.

The flow of Bridge River, in common with other streams in British Columbia, is subject to wide variation from the snow-melting high-water period in the summer to the low-water winter months when demand for electricity is at its peak. Accordingly, it was necessary to construct the Lajoie storage dam with a present capacity of 170,000 acre-ft and an ultimate capacity of 570,000 acre-ft, 40 miles upstream of the diversion dam which directs the water through a $2^1/_2$-mile-long tunnel, 14 ft 3 in. diam, carved out of the solid rock of Mission Mountain. Three individual 75-in-OD penstocks, 2100 ft long, carry the water from the tunnel mouth down to the powerhouse, where three 62,000-hp, 50,000-kva, 3-phase, 60-cycle, 13,800-volt turbine-generator units are now in operation. Transformers step up the voltage to 230,000 for transmission to the Vancouver power ring.

Extension of the development beyond the third unit, according to current plans, will not be undertaken until completion of other projects more favorable from the immediate economic viewpoint and in the light of other system considerations.

Application Engineering

It seems proper and fitting to the authors to state that Pelton, in its early studies of the Bridge River Development, strongly recommended a Francis turbine installation. It was considered that with proper design the expected favorable efficiency differential of the reaction over the impulse turbine, coupled with the setting loss which must be assessed against the latter, would more than offset the maintenance problems inherent in a reaction turbine using power water reportedly carrying a large quantity of fine abrasive silt.

To cope with the silt our reaction-turbine recommendation included an auxiliary seal water system to force clear water into the seals at an elevated pressure level and in sufficient quantity to insure that the silt-laden water would be prevented from passing through them. The amount of water required for this purpose would be such as to penalize the turbine efficiency between 1 and 2 per cent, and there would be an added increment of capital investment as well as attendant operating complication to reckon with. However, this innovation seemed justifiable in view of the generally well-understood requirement for radial clearances of the order of 0.015 in. between the stationary and rotating parts of a turbine of the size in question, and the definite possibility that the abrasive silt might quickly increase the seal clearance and reduce the turbine efficiency beyond the economic limit.

The B. C. Electric Company tenaciously insisted from the outset that the turbine should be of the impulse type for the admittedly fundamental reason that silt erosion has very little effect on the operating efficiency of the Pelton turbine and that repairs could be made by welding with the runner in place.

After careful consideration of the problem, we, of necessity, concurred with the Company on the premise that the very best impulse turbine from an efficiency standpoint might be favorably evaluated against a reaction design if the latter were debited with (*a*) the water requirements of the auxiliary sealing system, (*b*) the possible frequent and expensive runner and seal repairs, and (*c*) the economic losses growing out of interim efficiency depreciation between overhaul periods.

Once reconciled to the impulse-turbine solution, studies were made of the three basic versions: (*a*) The more popular horizontal single-nozzle, double-overhung type; (*b*) the horizontal double-nozzle, double-overhung type: and (*c*) the vertical multinozzle type.

At this point B. C. electric and its engineers, the Shawinigan Engineering Company, Ltd., Montreal, issued an inquiry and specification in June, 1946, calling for a 62,000-hp horizontal

---

[1] Vice-President and General Manager, The Pelton Water Wheel Company.

[2] Manager of Engineering, The Pelton Water Wheel Company. Mem. ASME.

Contributed by the Hydraulic Division and presented at the Annual Meeting, New York, N. Y., November 27–December 2, 1949, of The American Society of Mechanical Engineers.

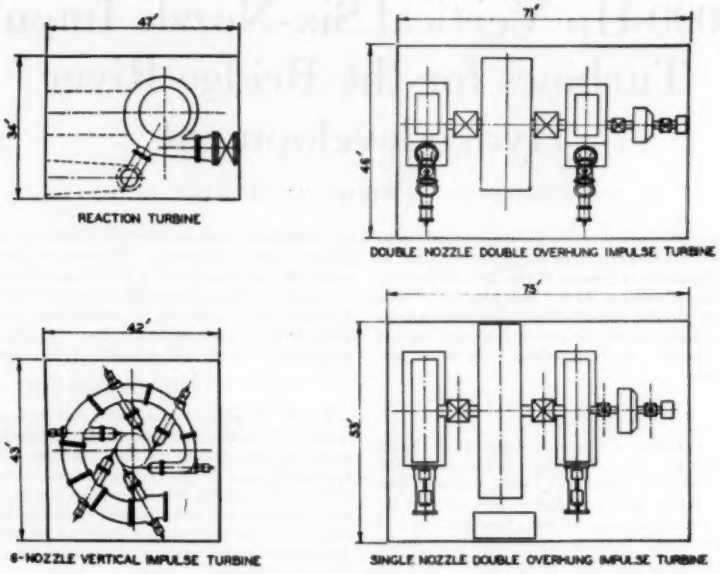

FIG. 1 SPACE REQUIREMENTS—62,000-HP TURBINE, 1118 FT HEAD

double-runner impulse turbine, and, alternatively, one of the vertical-shaft single-runner type. In response thereto Pelton and its Canadian associate, the Vancouver Engineering Works, Ltd., Vancouver, B. C., submitted proposals covering a single-nozzle, double-overhung turbine and, alternatively, a vertical four-nozzle machine. Not too long thereafter a contract was awarded to Pelton-V.E.W. for a four-nozzle vertical impulse turbine, the design conditions for which are enumerated in Table 1. As a matter of interest, Fig. 1 has been prepared to

TABLE 1 BASIC DESIGN DATA

Turbine rating: 62,000 hp; 1118 ft effective head; 300 rpm:	
Guaranteed efficiency, per cent	88
Predicted efficiency, per cent	89
Present gross head, ft	1226
Maximum gross head (future), ft	1360
Maximum effective head (future), ft	1171
Maximum surge head (future), ft	1465
Hydrostatic test pressure:	
Pounds per square inch	935
Head, ft	2160

show the space requirements of various types of 62,000-hp turbines.

TURBINE EFFICIENCY

Prior to obtaining the contract for the Bridge River turbines, it had been our policy to limit impulse-turbine efficiency guarantees to 85 per cent while predicting 87 per cent, so that it is needless to emphasize our respect for this contractual obligation which called for a best point guarantee of 88 per cent with a predicted maximum of 89 per cent. While we believed the attainment of these values to be well within the realm of possibility, we also appreciated, on the basis of past laboratory and field tests, that they represented the top limit and then only with an optimum fluid path.

The realization that losses throughout the fluid path must be minimized at all points resulted in the laying out of a one-year laboratory and field-testing program, using the widest range of model sizes in the history of our company, with more careful attention to detail than had heretofore ever been necessary.

Sobering also was our own not too favorable past experience with the vertical multinozzle turbine as well as such experience of the other turbine builders as had come to our attention.

In short, we approached this task determined to get the maximum bucket performance coupled with the ideal (*a*) casing, (*b*) nozzle, and (*c*) wheel-housing combination. That is to say, the best impulse turbine that we knew how to build was necessary to attain the guaranteed performance with sufficient margin to care for the contingencies inherent in a field test on so large a prime mover.

RESEARCH AND DEVELOPMENT PROGRAM

After a careful study of the several multiple-nozzle design possibilities it became clear, early in our initial work, that the 6-nozzle construction had many points in its favor over the 4-nozzle turbine which we had contracted to construct. Table 2 gives the key points of comparison as between the arrangements based upon laboratory testing with a horizontal single-nozzle turbine.

Past experience with vertical multinozzle turbines might prompt some hydraulic engineers to question the effect of the 60-deg nozzle spacing inherent in the 6-nozzle arrangement from the standpoint of possible interference between adjacent jets with deleterious effect on efficiency. This particular point was of no concern to us inasmuch as we had long ago established the fact that angularity between adjacent nozzles could be brought down to 55 deg without such interference.

Referring again to Table 2, it will be noted that the 6-nozzle proposition operating at 300 rpm produces, in effect, a lower

TABLE 2 BASIC COMPARISON 4 AND 6-NOZZLE DESIGNS

	4-Nozzle turbine	6-Nozzle turbine
Turbine rating: 62,000 hp; 1118 ft head; 300 rpm		
Specific speed per jet	5.77	4.71
Ratio: Runner diam / Jet diam	10.4	12.7
Efficiency, Pelton No. 17 bucket, per cent	87	88.75
Efficiency, Pelton No. 18 bucket, per cent	88.1	89.35
Relative strength of bucket attachment to wheel center	1	1.21

specific speed per jet. This is significant in that, aside from the indicated efficiency improvement, there is the added attraction of a more favorable space relationship in which to work out the design of bucket attachment to the wheel center.

At the time of the initial comparison of the 4 and 6-nozzle approaches, the results of our No. 18 bucket research were not available so that the $1^3/_4$ point potential efficiency gain with the No. 17 bucket loomed large in view of the 88 per cent guarantee.

All in all, efficiency and other considerations made obvious the necessity for an extensive vertical testing program whose object was, in effect, to examine all facets of the 4 and 6-nozzle designs.

The program was next broken into a group of major problems: (1) a series of casing studies to determine that fluid path which provided minimum losses between the turbine inlet and the individual jets; (2) a number of housing studies to establish that contour which would most effectively clear the water from the upper runner discharge; and (3) extensive efficiency tests to insure that the last tenth of a per cent was being extracted from the power fluid.

To facilitate study of the first major problem, a plastic nozzle piece was made to permit observation of the flow of water into the individual nozzles with different types of directing vanes and extension sections. A view of the plastic nozzle is shown in Fig. 2. Dye and small quantities of air were introduced into the

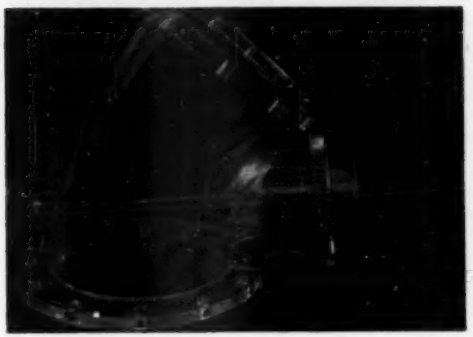

FIG. 2 LUCITE CASING SECTION FOR FLOW STUDY

water and indicated the flow pattern by forming small streaks that were photographed by time exposure.

The need for streamlined flow in the nozzle of an impulse turbine is generally well understood and extremely important, as turbulence causes the jet to lose shape or explode, with the result that a considerable quantity of power is lost before the water has an opportunity to act on the wheel.

The results of this phase of our experimental work proved gratifying in bringing about streamlined flow at the nozzle tips which in turn resulted in smooth cylindrical jets. Tests with curved vane sections such as are used in short-radius elbows, showed turbulence while, contrary to our past thinking, the best flow pattern was produced with a straight type of grid in the entrance to the individual nozzle. The superior performance of the relatively inexpensive straight vanes was, of course, favorable from a manufacturing viewpoint.

Study of the second major problem, that of directing the discharge water from the upper side of the runner, was begun by building two $^1/_8$-scale turbine models to the 6-nozzle configuration, with wheel housings of different sizes and contours and adaptable to several types of baffling for laboratory testing under a head of 100 ft, Fig. 3. In each case the wheel itself was a standard horizontal design mounted vertically so that one half of the discharge water is directed to the upper part of the housing and must return around the outside of the runner periphery without splashing back on it. In passing, the size and shape of the upper housing above the casing center line is extremely critical in this type of turbine.

Twenty-five different versions of housing shape and proportions and several baffle arrangements were tested with the two turbine models. Dummy jet deflectors and jet protectors were provided in all cases to simulate actual operating conditions. The deflectors were not used to control the turbine output but merely to show whether they might possibly be responsible for a splash condition detrimental to turbine efficiency.

After many months, this phase of the development program was completed and a peak efficiency of 89 per cent obtained with the No. 17 buckets.

The third major problem was investigated on the permanent bucket-efficiency-testing setup in the laboratory with a $^3/_{32}$-size model of jet-bucket relationship in an attempt to improve the single-nozzle efficiency beyond 88.75 and, after hundreds of test hours, was gratifyingly productive in that an improvement of 0.6 per cent was obtained, or a maximum of 89.35 per cent. Because the vertical and horizontal testing was, for practical reasons, done with wheels of different sizes, this improvement could not be verified in the Pelton laboratory under the 100-ft head available with the 6-nozzle configuration.

The vertical tests in the laboratory with a model $^1/_8$ the size of the Bridge River turbines proved operation up to a head of 500 ft. This is of course in accordance with Froude's law of similitude which established that the model head times the size ratio gives the full-size head for homologous design.

In order to prove definitely the operation of the full-size turbine, it was necessary to make arrangements for further testing under a head of approximately 250 ft. A special portable turbine dynamometer was constructed, and arrangements were made through the kindly co-operation of the Pacific Gas & Electric Company for testing at its Halsey powerhouse where the necessary head was available. The installation at Halsey is shown in Fig. 4. For these tests a new runner was made utilizing the No. 18 buckets. Comparative tests were made with runners previously tested in the laboratory so as to provide a check with the laboratory results. The maximum efficiency obtained under 250 ft head was 89.8 per cent. This represents model efficiency as high as ever obtained by the authors' company and is also believed to be as high as ever obtained on impulse tests in any laboratory.

The important point here is that the 250-ft head corresponded to an operating head of 1250 ft on the full-size turbine, or considerably above the design head of 1118 ft.

During the course of the vertical testing program a $^1/_{16}$ scale model was used to obtain comparative results at an accelerated rate on different types of housing shapes. These data facilitated the selection of the most appropriate type of housing shapes for testing with the $^1/_8$ scale model.

A new type of spherical valve was developed for the Bridge River turbines. Fig. 5 shows a 12-in. model in the Pelton labora-

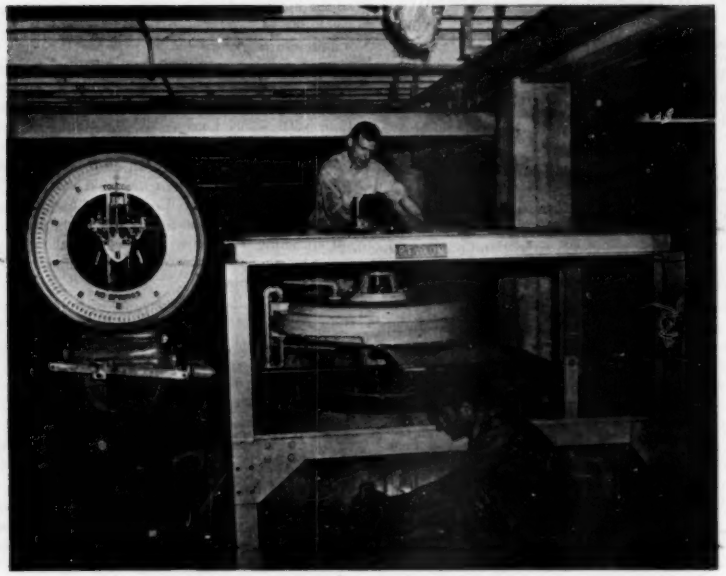

FIG. 3 LABORATORY VIEW SHOWING 70-HP 100-FT HEAD 450-RPM MODEL WITH DYNAMOMETER

FIG. 4 FIELD TEST MODEL ON LOCATION AT HALSEY POWERHOUSE OF PACIFIC GAS AND ELECTRIC COMPANY

tory where extensive tests were conducted. The valve is truly spherical with the seats on the plug and in the body located off center with respect to the flow passageway in such manner that rotation alone brings the plug seat into register with the body seat.

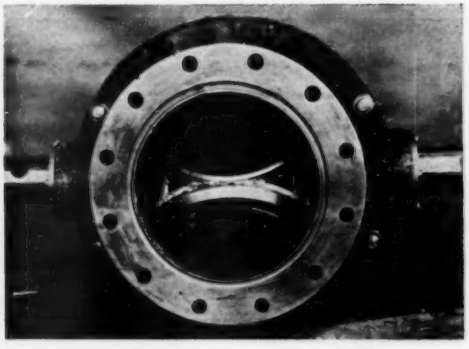

FIG. 5 12-IN. VALVE MODEL IN MEDIAN POSITION

In the open position the valve produces a cylindrical passageway equal to the diameter of the inlet.

The laboratory tests proved to be successful, and accurately foretold the results obtained on shop tests on the full-size valve. The latter, under a head of 935 psi, resulted in a leakage through the seat of only a few drops per min, which is exceptional for a 54-in. valve under high pressure. Laboratory experiments to determine the force required to pull the valve from its seat after removal of pressure indicated a required force of approximately 1 per cent of the available operating force. This was later confirmed on the test floor to the gratification of the engineering department, as we had feared the possibility that the spherical section of the valve body might contract and partly wedge the valve disk into the closed position.

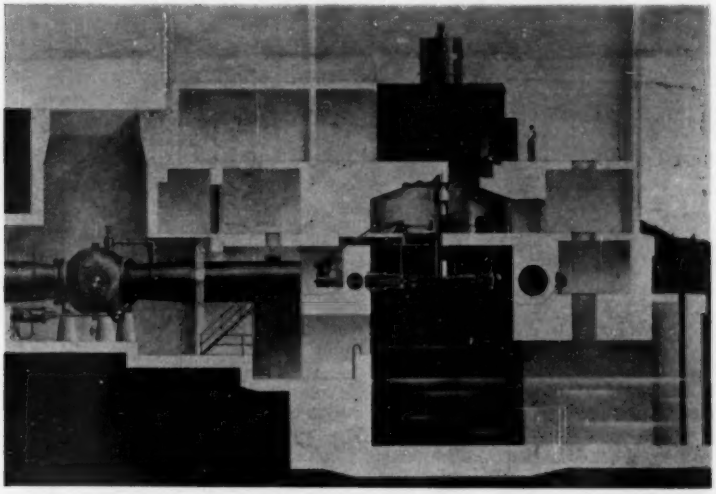

FIG. 6 SECTION THROUGH TURBINE-GENERATOR UNIT SHOWING 54-IN. SPHERICAL INLET VALVE

SOME COMMENTS ON THE TURBINE, CONTROL, AND INLET-VALVE DESIGN

The hydraulic contours of the Bridge River turbine have been made homologous, i.e., that all dimensions of the wetted surfaces have been stepped up from the model by applying a factor of 5. A mechanical structure has been built with inside dimensions conforming to the hydraulic fluid path and of sufficient strength to withstand a maximum surge of 1465 ft. The portion of the turbine wheel pit which must take the full impact of the deflected jets at times of load rejection have been reinforced to handle the load.

Figs. 6 and 7 illustrate the arrangement of the turbine and inlet valve in the powerhouse.

The combination turbine-generator unit is a short-coupled, three-bearing arrangement with two generator bearings and one turbine bearing. The top generator bearing is of the conventional thrust type and supports the total load of all of the rotating parts.

That the general powerhouse design has been skillfully worked out is illustrated by the fact that the floor levels have been so nicely related to the several operating levels of the turbine. For instance, the first floor directly under the generator floor is on the same level as the turbine pit, and therefore provides easy access to the servomotors which control the jet deflectors. The next, lower floor exposes the individual needle servomotors which are distributed around the turbine at a convenient level for maintenance and adjustment. The next, or lowest, floor provides access to the turbine wheel pit below the runner and to the base of the main shutoff valve.

Getting back to the Bridge River turbine, the speed and load control is accomplished by a very flexible governing system. The primary governor is a Woodward cabinet actuator located on the generator floor which directs the flow of oil to or from the servomotors in the turbine pit to control the position of the six interconnected deflectors. Normally each deflector operates in a position just outside of its jet. In the event of load rejection the deflectors rapidly enter the jets by control from the actuator, so that the entire hydraulic force is removed from the wheel and deflected into the wheel pit. The timing of the deflector, in the case of load rejection, is set for approximately 2 sec so as to hold the speed rise following load rejection to a low value.

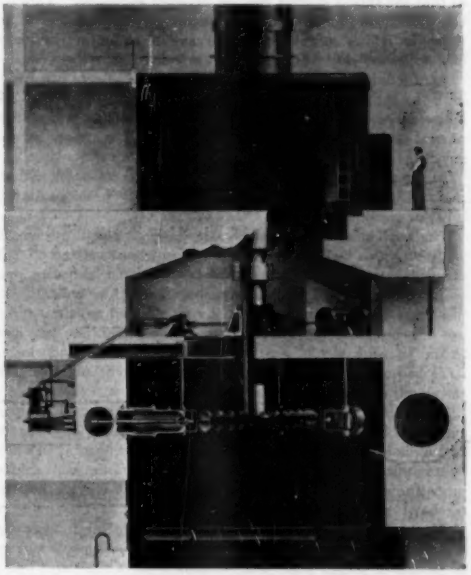

FIG. 7 CLOSE-UP SECTION THROUGH TURBINE-GENERATOR

Because the water in the penstock cannot be decelerated at such a high rate, interconnection is provided between the deflectors and the needles through jet controllers, so that movement of the deflectors, brings about a gradual closing of the individual

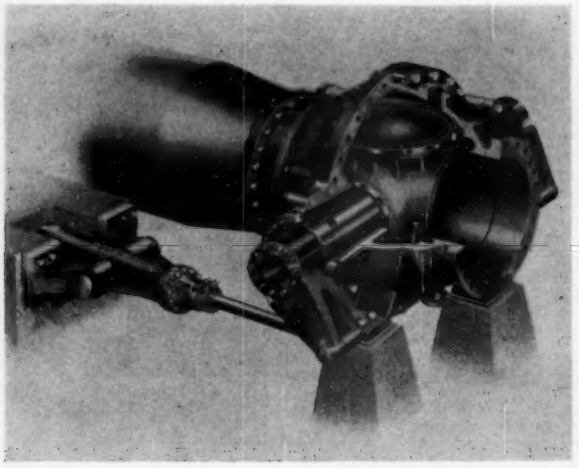

FIG. 8 54-IN. SPHERICAL VALVE IN OPEN POSITION

needles. Separate jet controllers are provided for each needle so that the timing of each may be adjusted separately. Through the utilization of individual jet controllers, it is possible to remove individual needles from service to maintain maximum efficiencies at light loads.

As the individual needles gradually close, at a rate consistent with the hydraulic characteristics of the penstock, the size of the deflected jets decreases until the wheel speed has returned to normal and the deflectors are removed from the stream by the governor.

In the case of a complete load rejection the deflectors will remain within the stream to the extent necessary to maintain stability at speed no-load.

The individual jet controllers are basically small governors, the pilot valve being responsive to deflector position rather than the conventional speed setting. A restoring mechanism is provided through an appropriately shaped cam to indicate the needle position at all times, and a conventional governor dashpot is included to prevent hunting. Adjustments are provided in the jet controller to regulate the rate of opening and closing so as to protect the pipe line properly. In addition, a compensating adjustment is provided to insure stability.

The main spherical-type inlet valve, Fig. 8, is essentially a direct step-up of the model valve after making proper allowances for the hydraulic loads imposed upon the full-sized structure. In order to minimize the torsional load throughout the plug stub shafts, operating cylinders have been attached to each end so that the torsional load is equally divided.

The seat on the plug is made adjustable to facilitate assembly and maintenance. The seat ring is movable on a plane surface to permit of proper alignment with the seat in the valve body. In initial assembly the plug seat is loose and the valve rotated to the closed position so that this seat will find its true position, after which it is secured.

MANUFACTURING PROBLEMS

The main structure of the turbine is the casing, Fig. 9, which is of cast steel and consists of eight nozzle and elbow sections. As previously emphasized, the inside hydraulic contour was established on the basis of the model design while the mechanical configuration was of necessity made consistent with practical manufacturing and shipping limitations.

Never before in western Canada have steel castings as heavy as the No. 1 nozzle, weighing 25,000 lb, been poured successfully. The entire casing weighed 150,000 lb, and its shop assembly and hydrostatic testing to 935 psi posed many interesting manufacturing problems to the staff of the Vancouver Engineering Works.

Of possible interest from both the manufacturing and maintenance viewpoints are the separate, replaceable, stainless-steel needle seats provided in conjunction with needle points of the same material.

The turbine runner, Fig. 10, is made up of 20 cast mild-steel buckets, each fastened to the forged-steel wheel center by two interference-fitted bolts. The bolts were carefully ground and selectively fitted to assure 0.0006 in. interference per in. of diameter in the bucket lugs and wheel center. Installation was made by a pulling operation, the bolt and hole being protected with white lead. The small bolts, $3^1/_4$ in. nominal size, were pulled in with an average load of 50 tons, whereas the large bolts, 4 in. nominal, required 75 tons.

A large number of fabricated parts went into the manufacture of the turbine. Principal among these is a structural member which covers the turbine wheel pit and provides support for the main turbine bearing.

FIELD TROUBLES

What appears to us to be definite proof of the basic soundness of the 6-nozzle impulse design has evolved, strangely enough, through bucket difficulties experienced after 10 months of operation, or more than 750,000,000 stress reversals, on the first turbine.

The forerunner of trouble was notice of a peculiar vibration and, about 12 hr later, when the unit could conveniently be shut down, an inspection was made which disclosed that one of the large bucket bolts was missing from one of the buckets. A check revealed that the bucket bolt in question fitted loosely into the hole and this, of course, caused considerable consternation.

In the course of the detailed inspection which followed immediately, small cracks were disclosed in a considerable number of the bucket lugs, generally located over the 4-in. boltholes at the point of highest loading.

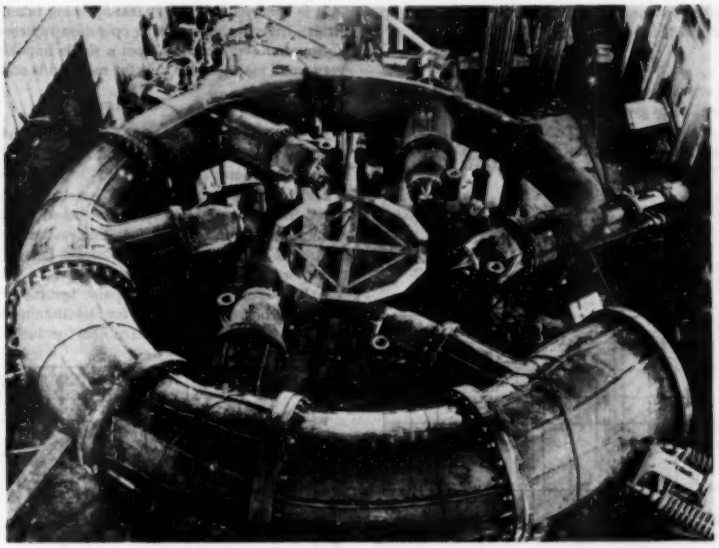

FIG. 9 SHOP ASSEMBLY OF TURBINE CASING AND NEEDLE NOZZLES

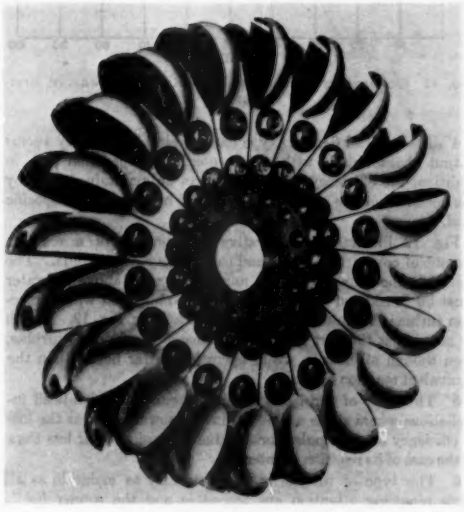

FIG. 10 ASSEMBLED TURBINE RUNNER

An extensive design and metallurgical investigation was put into motion at once and steps were taken to replace all defective or suspicious buckets. Examination by our metallurgists, confirmed by foundry personnel, revealed that the cracks were of foundry origin and had been in the buckets since the day they were cast.

Detailed examination of all of the cracks revealed that none had progressed even though, in the worst case, the stress-resisting cross section had been reduced to approximately one half, so that stress concentration around the edge of the crack must have produced stress effects of the order of 4 to 6 times normal design values.

The fact that such excessive stressing of the bucket lugs did not produce fatigue cracks throughout 750,000,000 operating cycles is construed as indicating a conservative and sound design.

As a result of this experience, the authors' company has completed a series of investigations in co-operation with all of its casting vendors which were designed to insure that all future bucket castings are made to the highest possible standard.

Under our new procurement technique the first bucket of every run is examined completely by breaking the lugs and cutting up the bowls to determine if the product is sound throughout.

All succeeding buckets are subjected to an elaborate inspection program utilizing magnaflux, x-ray, Zyglo, and the supersonic reflectoscope.

It is interesting to note that one particular bucket which passed inspection by magnaflux and x-ray contained a very serious crack.

INSTALLATION

The installation of the first Bridge River turbine-generator unit was made in record-breaking time considering the many obstacles that had to be overcome. Thus while the first nozzle section arrived in the powerhouse on August 6, 1948, the entire assembly was made and concreted into position by August 30.

The concrete work above the turbine floor was carried up to the generator level by September 13, and by September 28 the generator rotor was assembled in the stator. The combined turbine-generator assembly was completed on October 20, and the official starting date for the plant was October 23. The approximate time, $2^1/_2$ months, between the setting of the turbine casing and the initial operation of the turbine generator evidences exceptional speed in assembling a unit of this size, the

more so when allowance is made for the fact that the design was somewhat radical and hence unfamiliar.

Field Testing

In view of the urgent demand for power in the Pacific Northwest, it was impossible to give consideration to efficiency testing unit No. 1.

Shortly after installing the second unit, however, a Gibson efficiency test was conducted in accordance with the ASME Power Test Code.

Test reports are now available, and the results are shown, in comparison with predicted and guaranteed values, in Fig. 11. It is noteworthy that a maximum efficiency of 92 per cent was attained with better than 90 per cent between loads of 20,000 to 58,000 hp with all six nozzles in operation.

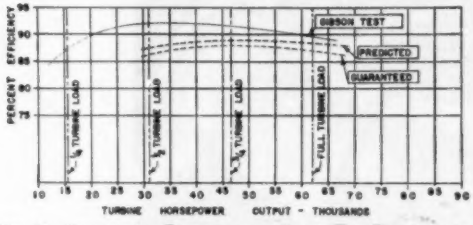

Fig. 11 Guaranteed, Predicted, and Gibson Test Performance

The test performance is gratifying to everyone concerned with the project in that the vertical, multinozzle impulse turbine has been justified by virtue of efficiency values much superior to results previously obtained in this country for turbines of the impulse type.

Maintenance

The vertical impulse turbine is fundamentally amenable to maintenance because the main bearing, deflector servomotors, deflector linkages, and needle servomotors are all readily accessible from the two turbine-operating floor levels.

A man door in the wheel-pit liner can be opened and planking installed on a structural-steel frame located about 7 ft below the runner. It is then possible to enter the wheel pit and have complete access to the runner, deflectors, needle points, and nozzles.

Apropos of maintenance, it was anticipated that serious erosion might be experienced due to the high silt content previously mentioned. This was particularly true in the case of the first turbine because the $2^1/_2$-mile-long tunnel had for some 20 years been supplying only a small unit, with the result that extensive silt accumulation, estimated at 50,000 tons, had built up.

During early operation a considerable portion of this silt was washed through the turbine. To minimize wear at the outset only two nozzles were used through the early weeks on the line. These two nozzles are the only ones that show an appreciable amount of wear in the first 10 months of operation. Some minor cavitation tendencies have been uncovered in a few of the buckets but careful grinding in these areas has reduced the tendency to the point where reasonably long life can be expected regardless of the fact that each bucket passes through a water stream 30 times per sec

It is believed that the 70,000 hp being taken from each of the Bridge River turbines now in operation represents the maximum horsepower ever obtained from a single impulse runner, and the very small maintenance thus far required is encouraging.

Conclusions

1 B. C. Electric's decision to install a vertical impulse turbine has been confirmed as sound by virtue of the proved high operating efficiency.

2 The basic 6-nozzle design has been demonstrated to be sound from a mechanical viewpoint because fatigue cracks failed to develop in spite of the fact that material defects produced stresses at critical points in the bucket lugs of between 4 and 6 times normal design values.

3 The 6-nozzle vertical impulse turbine permits of a compact powerhouse arrangement for installations in and beyond the head and capacity range of the subject turbine.

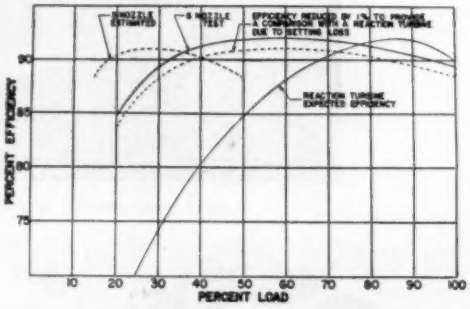

Fig. 12 Comparison of Impulse- and Reaction-Turbine Efficiency

4 The vertical 6-nozzle type has a desirable efficiency versus output characteristic with all six nozzles in operation and, in addition, the efficiency at low loads can be maintained high by the selection of the optimum number of nozzles for the specific load.

Fig. 12 illustrates comparative performance of a reaction turbine of comparable rating and the Bridge River turbine. The fact that the impulse turbine must be located above tailwater must be considered in making a direct comparison with a reaction turbine, hence the two curves indicated in Fig. 12. It will be noted that the part gate performance of the 6-nozzle turbine, even though all nozzles are in operation, is far better than the equivalent reaction turbine.

5 This type of turbine is admirably suited to high-head installations where silt is a problem in the power water as the loss in efficiency of an impulse turbine due to erosion is far less than in the case of its reaction counterpart.

6 This type of turbine is relatively easy to maintain as all parts requiring attention are accessible and the runner itself, considerably smaller than either one of the two runners of a conventional double-overhung type of turbine, is readily removed and replaced

An Improved Pneumatic Control System

By R. E. CLARRIDGE,[1] ROCHESTER, N. Y.

A pneumatic control system is being proposed which has one major advantage over conventional control systems. This advantage is that the control system can be used to start up a process automatically without overpeaking and, at the same time, maintain its control point when subsequent load changes occur. The control system is responsive to the rate of change of the control variable during the start-up period, and therefore good performance can be expected when the performance starts up under varying load conditions. It is suggested that on many applications a new criterion be used for adjusting the controller, namely, that the control point be reached on start-up with a minimum delay and without overpeaking.

Introduction

Most of the papers on automatic control in recent years have dealt with the three basic control responses, proportional, derivative, and reset, and their relationship to the reaction curves of various processes.[2, 3, 4, 5] Several methods have been suggested for relating the process characteristics, time lag, and reaction rate, to the magnitude of these three control responses. If process characteristics are known, optimum controller settings can be predicted. Therefore it would appear that this field has been fairly well explored.

In connection with these investigations, the determination of the constants of the control system has been based on the effect of a disturbance such as a load change. It has been assumed, in arriving at the optimum settings, that the best values were those which would produce the least deviation from the control point when a given load change was interposed on the system. In actual practice the quality of the control has been measured by (*a*) the maximum deviation from the control point, (*b*) the duration of the deviation from the control point, or (*c*) the integral of the absolute value of the instantaneous deviation, (*d*) the integral of the square of the value of the instantaneous deviation. Now, while there is no fault to find with this approach, it is the purpose of this paper to suggest a further analysis of control circuits and possibly other criteria for determining the best controller settings.

In the control problems of the process industries what is the major limitation of existing automatic controllers? Is it the fact that the control point is not maintained in a satisfactory manner? The answer seems to be "no" on those applications where automatic reset can be used, but it is a major factor when automatic reset cannot be used. In general, the automatic-reset response cannot be used satisfactorily in the controllers on a "batch" process. On these processes which are started up and terminated frequently, three options, as follows, are available, all of which may be unsatisfactory:

1 The controller may incorporate automatic reset and allow an undesirable overpeaking at the start-up.

2 The automatic-reset response may be eliminated, and the deviation, or offset, which occurs with load changes must be accepted.

3 Automatic reset may be used in the controller, and the process may be started up manually.

Now, of course, there is no truly continuous process, for all things must start and all things must end. However, this term is often used to characterize processes which have a relatively long-time period between start-up and shutdown. Owing to the length of these processes, automatic reset is often an essential feature of the automatic controllers. Since many of these continuous processes involve controllers which interact on each other, some of which may overpeak very badly on start-up, it is customary to start up these processes with manual control. Since manual control, even during start-up, requires constant attention, it is suggested that automatic start-up, even on continuous processes, would be of real merit.

Therefore let us examine the start-up characteristics of controllers with the three control responses to determine whether the control point can be maintained and overpeaking prevented.

The Start-Up Problem

The Proportional Controller. Assume that a controller with a proportional response has been adjusted so that the offset due to a load change is at the minimum value consistent with good controller stability. Also, that the process on which this controller is applied involves the heating of a material to a predetermined temperature and holding it at that value. While the load on the process can be at any value, it is necessary for our purpose to select one value for the comparison of our start-up performance. The load selected is that which requires the valve to remain half open after the temperature reaches the predetermined value in order to hold it at that value. If the load is at some other value during start-up, as would most often be the case, the start-up curves would be different but their characteristics would be comparable. Assume that the heat input to the process is proportional to the valve opening.

Under these conditions the temperature record of the instrument on start-up might be similar to that shown in Fig. 1(*a*). The overpeaking and slight subsequent transient oscillation will vary, depending upon the characteristics of the process and the throttling band, or sensitivity, of the controller. Now, without too much difficulty, the overpeaking shown in Fig. 1(*a*) can be avoided by broadening the throttling band, or lowering the controller sensitivity so that the valve starts to close at a lower temperature than in the previous case, Fig. 1(*b*). Viewing the results obtained from the start-up characteristic alone, it would appear that a considerable improvement has been made, for the overpeaking has been entirely eliminated. Note, however, that it has taken the controller a longer time to reach the control

---

[1] Application Engineering Department, Taylor Instrument Companies. Mem. ASME.

[2] "Optimum Settings for Automatic Controllers," by J. G. Ziegler and N. B. Nichols, Trans. ASME, vol. 64, 1942, pp. 759–768.

[3] "Process Lags in Automatic-Control Circuits," by J. G. Ziegler and N. B. Nichols, Trans. ASME, vol. 65, 1943, pp. 433–444.

[4] "Theoretical Considerations on the Optimum Adjustment of Regulators," by P. Hazebroek and B. L. van der Waerden, Trans. ASME, vol. 72, April, 1950, pp. 309–315.

[5] "The Optimum Adjustment of Regulators," by P. Hazebroek and B. L. van der Waerden, Trans. ASME, vol. 72, April, 1950, pp. 317–322.

Contributed by the Instruments and Regulators Division and presented at the Annual Meeting, New York, N. Y., November 26–December 1, 1950, of The American Society of Mechanical Engineers.

Note: Statements and opinions advanced in papers are to be understood as individual expressions of their authors and not those of the Society. Manuscript received at ASME Headquarters on October 5, 1950. Paper No. 50—A-100.

point and this may be objectionable. The major disadvantage of this method of eliminating overpeaking on start-up is that the offset, or deviation, which occurs due to subsequent load changes is considerably greater than that which would occur with the controller in the adjustment shown in Fig. 1(*a*). As a matter of fact, the magnitude of this offset, even with the controller in the adjustment shown in Fig. 1(*a*), often requires the addition of automatic reset to maintain the temperature sufficiently close to the desired value. Our conclusion, therefore, is that while the method eliminates overpeaking on start-up, it is not satisfactory.

Before proceeding further, the proportional band illustrated in Figs. 1(*a*) and (*b*) should be clearly defined. When the temperature is at one edge of this band, the valve is closed, and when it is at the other edge, the valve is open. The position of the temperature in this band at any time, therefore, indicates the opening of the valve.

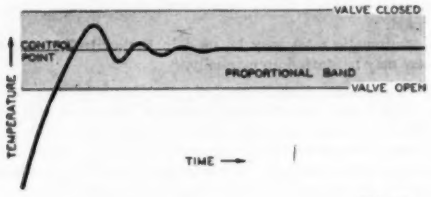

FIG. 1A

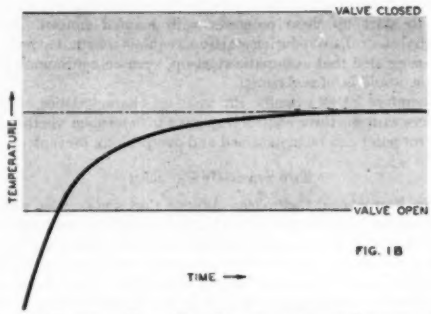

FIG. 1B

FIG. 1 TYPICAL START-UP CHARACTERISTICS—CONVENTIONAL CONTROLLER WITH PROPORTIONAL RESPONSE

Proportional-Plus-Derivative Controller. Let us now consider the start-up curves which might be obtained with a controller having proportional and derivative responses under similar conditions. If the sensitivity, or the proportional band of the controller, is unchanged from that illustrated in Fig. 1(*a*), and the magnitude of the derivative response is adequate, it is often possible to obtain a curve like that shown in Fig. 2(*a*), which is more stable. The derivative response closes the valve more rapidly than the proportional response, and reduces the rate of approach of the temperature to the control point. Therefore, with this added response, a start-up characteristic has been obtained which is considerably better than could be obtained with proportional response alone.

In this particular connection it might be well to note that as the derivative response is added to the proportional response of an instrument, the stability of the control is improved. An optimum value of the derivative response is reached so that further increase in its magnitude reduces the stability of the control. Now, if in this particular case the derivative response is increased further, a

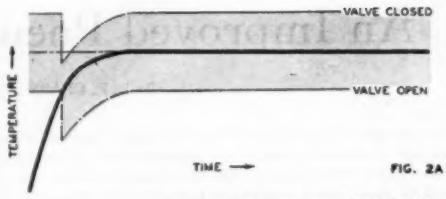

FIG. 2A

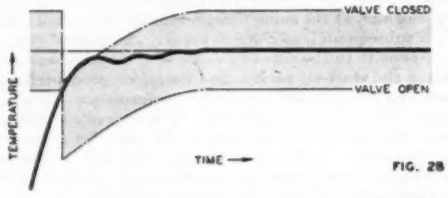

FIG. 2B

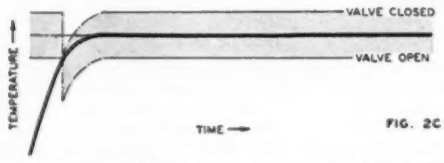

FIG. 2C

FIG. 2 TYPICAL START-UP CHARACTERISTICS—CONVENTIONAL CONTROLLER WITH PROPORTIONAL AND DERIVATIVE RESPONSE

curve somewhat like that shown in Fig. 2(*b*) may be obtained before the control becomes unstable. The sensitivity then can be increased and the performance of the controller will be similar to that shown in Fig. 2(*c*). Note that overpeaking has been eliminated and still the temperature approaches the control point without excessive rounding in. At the same time the proportional band has been narrowed so that the offset which occurs as a result of subsequent load changes will be reduced. Now, if the performance of a controller is to be judged by its start-up characteristics alone, the performance with proportional and derivative response cannot be excelled except by the use of derivative responses of higher order.

Proportional-Plus-Reset Controller. Now consider the start-up curve which might be obtained from a conventional controller with proportional and reset responses under these same conditions. The proportional band is unchanged, but the valve remains open until the temperature reaches the control point. Since no valve action occurs until this point is reached, the overpeaking is considerably greater than that which occurs with proportional response alone. While the control circuit illustrated in Fig. 5 will be discussed in greater detail subsequently, a brief review will show that under equilibrium or stable conditions, the pressures on both sides of the bellows unit are equal. When the instrument has been at the control point for an extended period, it is in equilibrium and the pressures are equal, locating the nozzle in a given position, which might be called the control-point position. Similarly, when the temperature has been above or below the control point for an extended period (shutdown condition), the pressures on both sides of the bellows unit are equal and the nozzle therefore assumes the position corresponding to the control point. Hence there is no action from the controller on start-up until the control point is reached at which time the baffle begins to affect the nozzle back pressure.

A typical curve is shown in Fig. 3 and it will be noted that as the temperature returns to the control point, the proportional

band shifts downward. It is this shifting of the band which restores the temperature to the control point after a load change. Therefore, by the addition of automatic reset to the controller, the control point is maintained under various load conditions, but the start-up characteristic becomes very poor.

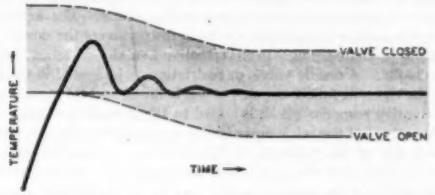

FIG. 3 TYPICAL START-UP CHARACTERISTICS—CONVENTIONAL CONTROLLER PROPORTIONAL PLUS AUTOMATIC-RESET RESPONSE

While no attempt has been made to illustrate the effect of narrowing or broadening the proportional band, or increasing or decreasing the reset rate, the curve shown in Fig. 3 approaches the optimum obtainable. The overpeaking is worse if the sensitivity is lowered, and the control becomes less stable if the sensitivity is raised. A slower reset rate would improve the stability slightly, but it would increase the time required to reach the control point. A faster reset rate would decrease the stability of the control.

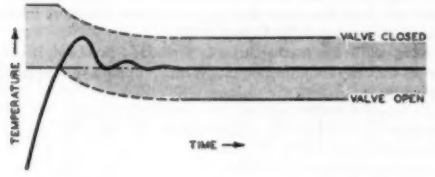

FIG. 4A

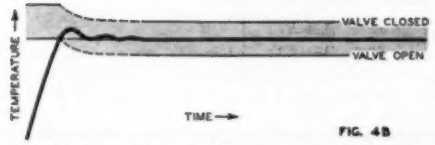

FIG. 4B

FIG. 4 TYPICAL START-UP CHARACTERISTICS—CONVENTIONAL CONTROLLER WITH PROPORTIONAL, DERIVATIVE, AND AUTOMATIC-RESET RESPONSE

Conventional Controller With Three Responses. If the derivative function is incorporated in a controller with the proportional and automatic-reset responses in the conventional manner, the performance of the instrument on start-up would approach that illustrated in Fig. 4(*a*). Note that with the same proportional band, the overpeaking is reduced and the stability is increased. In some instances this permits increasing the sensitivity and the improved performance illustrated in Fig. 4(*b*).

There is one main point which should be noted, namely, that as long as automatic reset is incorporated in the circuit in the conventional manner, the proportional band of the instrument remains above the control point until the temperature reaches it. Therefore the valve does not start to close until it is too late to prevent overpeaking. Hence, in order to eliminate the one evil, offset due to load changes, we must accept another evil, overpeaking on start-up. This premise has been so well accepted in the process instrument field that:

1 Automatic reset is not used when automatic start-up is required.

2 Processes are started up manually and subsequently thrown on automatic control.

CONTROL CIRCUITS AND EQUATIONS

Let us now examine the equations which apply to several control circuits to determine whether the conventional circuit cannot be improved materially. At the same time the equations should give us the relationship between the adjustments of the various instruments.

$(x - x_0)$ or dx = change in position of, or force developed by primary element—change in input to controller

$(P - P_0)$ or dP = change in output pressure of that portion of instrument or controller incorporating derivative action—change in input to reset relay—used only when reset follows derivative action

$(p - p_0)$ or dp = change in output pressure of complete controller—change in pressure to diaphragm-valve assembly

t = time—expressed in minutes

S = manual adjustment determining proportional relationship between $(x - x_0)$ or $(p - p_0)$; in conventional circuit illustrated in Fig. 5, controller sensitivity when x is expressed in inches and p is expressed in pounds per square inch. It will be shown that in the conventional circuit with three responses, the setting when determined in the normal way is not in reality the true value $\bar{S}$.

S' = manual adjustment determining proportional relationship between $(x - x_0)$ and $(P - P_0)$ in the proposed controller illustrated in Fig. 6; might be called controller sensitivity when x is expressed in inches and p is expressed in pounds per square inch, but it will be shown that it too is not the true value of sensitivity $\bar{S}$.

$\bar{S}$, $\bar{S}_a$, $\bar{S}_b$, $\bar{S}_c$ = in a controller with completely independent adjustments, reset and derivative responses need not be based upon magnitude of proportional response. For convenience, these three different constants are used to illustrate this point. This also allows the use of the conventional constants R and T in their usual sense having the dimensions of reciprocal minutes and minutes, respectively.

$\bar{R}$ = manual adjustment determining relationship between reset and the proportional response of a noninteracting controller; often called reset rate having dimension of reciprocal minutes.

R = manual adjustment determining relationship between reset and proportional response of conventional controller illustrated in Fig. 5. It will be shown that this value of R does not always equal true value of reset rate $\bar{R}$.

R' = manual adjustment determining relationship between reset and proportional response of proposed controller illustrated in Fig. 6. It will be shown that the value of R' is not identical with true value of reset rate of controller $\bar{R}$.

$\bar{T}$ = manual adjustment determining relationship between derivative and proportional response of a noninteracting controller; often called the derivative time having the dimension of minutes.

T = manual adjustment determining relationship between derivative and proportional response of conventional controller illustrated in Fig. 5. It will be shown that this value is not identical with true value of derivative time $\bar{T}$.

T' = manual adjustment determining relationship between derivative and proportional response of proposed controller illustrated in Fig. 6. It will be shown that this is not identical with true value of derivative time $\bar{T}$.

n = ratio between instantaneous pressure changes in output and input of reset relay when R equals zero.

Noninteracting Controller. Let us consider an ideal controller which has independent proportional, reset, and derivative responses. The equation expressing the response of this controller is

$$\frac{dp}{dt} = \bar{S}_a\bar{R}(x - x_0) + \bar{S}_b\frac{dx}{dt} + \bar{S}_c\bar{T}\frac{d^2x}{dt^2} \quad \ldots\ldots [1]$$

In designing mechanisms it is often more convenient and economical to use the proportional response

$$\left(\bar{S}_b\frac{dx}{dt}\right)$$

to obtain the reset and derivative responses. When this is done, $\bar{S} = \bar{S}_a = \bar{S}_b = \bar{S}_c$ and Equation [1] becomes

$$\frac{dp}{dt} = \bar{S}\left[\bar{R}(x - x_0) + \frac{dx}{dt} + \bar{T}\frac{d^2x}{dt}\right] \quad \ldots\ldots [2]$$

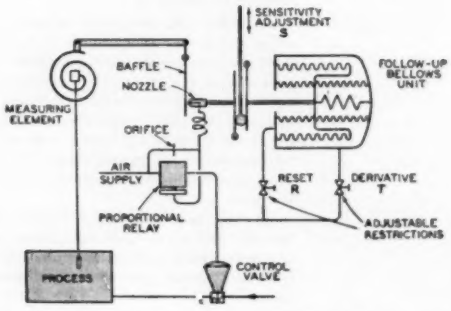

FIG. 5 SCHEMATIC DIAGRAM OF CONVENTIONAL CONTROLLER

Conventional Controller. This equation does not describe the pneumatic control circuits which are in widest use today. For example, in Fig. 5 a system is illustrated which might be considered typical of "motion balance" pneumatic control circuits. A primary element moves a baffle or flapper which opens or closes a nozzle, which, in turn, actuates a relay valve. The output pressure from this relay valve is connected to a diaphragm motor and may operate a valve or damper. This same output pressure from the relay valve operates on a bellows and spring assembly which is connected mechanically to the nozzle. The action of the relay valve is such that as the baffle uncovers the nozzle the output pressure changes in the direction to make the nozzle follow the baffle. A needle valve, or restriction, is indicated in the line to the right, or follow-up, side of the bellows, and this produces a derivative response which is added to the proportional response. The output of the relay valve is also connected to the opposite or reset side of the bellows. A needle valve, or restriction, must always be used in the reset line or the instrument will be unstable. The action of the pressure on the reset side of the bellows counteracts the follow-up action and as the two pressures are equalized, the variable is restored to the control point. There is a mechanical adjustment between the motion of the bellows and the motion of the nozzle so that larger or smaller nozzle motions can be obtained for a given output pressure. When the nozzle motion is small, the sensitivity is high; and when the motion is large, the sensitivity is low.

Now, an instrument of this sort does not exactly follow the simplified equations to be given. However, it does follow these equations closely if the motion of the baffle is great compared to that required to open and to close a fixed nozzle. Neglecting these minor idiosyncrasies, it will be seen that the derivative and reset responses from this controller are interrelated in a more involved way than indicated by Equation [2].

Now, while the mathematics is somewhat involved, it can be shown that the simplified equation which applies to this particular circuit is

$$(\text{Total})\frac{dp}{dt} = S\left[\frac{R}{1 - RT}(x - x_0) + \frac{1 + RT}{1 - RT}\frac{dx}{dt} + \frac{T}{1 - RT}\frac{d^2x}{dt^2}\right] \quad \ldots\ldots [3]$$

neglecting the actual baffle-nozzle sensitivity, relay valve capacity, circuit volume, etc. (For derivation of Equation [3], refer to Appendix.)

Equation [3] may be rewritten as follows

$$(\text{Total})\frac{dp}{dt} = \frac{(1 + RT)}{(1 - RT)}S\left[\frac{R}{1 + RT}(x - x_0) + \frac{dx}{dt} + \frac{T}{1 + RT}\frac{d^2x}{dt^2}\right] \quad \ldots\ldots [4]$$

Much can be learned from a brief study of Equations [3] and [4]. Note that if the derivative time T, or the reset rate R is set at zero (no derivative or no reset response), the equation assumes the same form as Equation [2]. However, when the controller incorporates both the reset and derivative responses, the coefficients of each term differ from those in Equation [2] and, therefore, the true reset rate $\bar{R}$, sensitivity $\bar{S}$, and derivative time $\bar{T}$, have different values from the apparent settings determined in the usual manner. In other words, the true reset rate $\bar{R}$ is actually $R/(1 + RT)$. The true sensitivity $\bar{S}$ is $(1 + RT)S/(1 - RT)$, and the true derivative time $\bar{T}$ is $T/(1 + RT)$.

Considering sensitivity first, note that if the product of RT is $^1/_4$, then the actual sensitivity is $^4/_3$ of the apparent sensitivity. It will be seen that the true sensitivity increases very rapidly as the product of RT increases, producing instability in the control. Furthermore, if the product of RT is equal to $^1/_4$, the true reset rate and derivative time are only $^4/_3$ of their apparent value,

while if RT were made equal to 1, the actual values of the reset rate and derivative time would be $^1/_2$ of their apparent value. Thus with this controller in normal adjustment, the actual reset rate $\bar{R}$ and derivative time $\bar{T}$ vary only slightly from the apparent values R and T.

The purpose of this portion of the discussion in connection with existing controllers is to show that in a conventional controller incorporating proportional, reset, and derivative responses, the magnitude of the control responses does not correspond to the actual instrument settings.

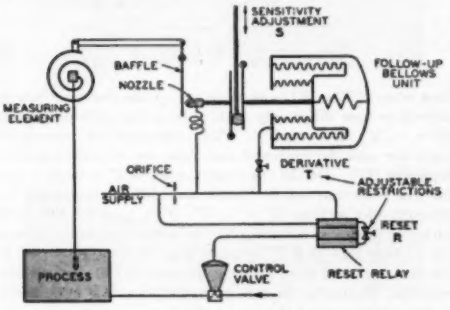

FIG. 6 SCHEMATIC DIAGRAM OF PROPOSED CONTROLLER

Proposed Controller. Refer to Fig. 6 illustrating a simple pneumatic circuit which offers certain advantages over the more conventional circuit in Fig. 5. Again the primary element operates a baffle which opens and closes a nozzle, fed from an air supply through a restriction. In this particular instance, the "follow-up" bellows operates from the nozzle back pressure to reduce the sensitivity of the mechanism. The nozzle movement is always proportional to the movement of the primary element, and by changing this movement of the nozzle for a given pressure change in the bellows, the proportional response or sensitivity of the controller is changed. An adjustable restriction is incorporated in the line leading to the follow-up bellows so that, while the pressure in the bellows is proportional to the movement of the baffle, the nozzle back pressure is proportional to the movement plus the rate of movement of the baffle. Note that the action of the nozzle and baffle, Fig. 6, differs from that of Fig. 5 in that the nozzle moves to follow the baffle on shutdown and remains at one extreme position or the other regardless of the length of the shutdown. In the example, if the temperature falls on shutdown, the baffle moves away from the nozzle and the nozzle follows it to its extreme left position. This position is unchanged until start-up occurs, and at that time the nozzle is affected by the baffle before the temperature reaches the control point. Since the derivative effect is incorporated into this portion of the control circuit, major pressure changes can be obtained from it before the control point is reached. This is not possible with the conventional controller, as illustrated in Fig. 5.

Now, if the output from this nozzle-baffle subassembly is fed into a relay valve which has a proportional response and adds the automatic-reset response, the output pressure from the entire controller will incorporate all three control responses.

The proportional response from the nozzle, baffle, and bellows combination is

$$(P - P_0) = S'(x - x_0) \quad \text{or} \quad \frac{dP}{dt} = S'\frac{dx}{dt} \qquad [5]$$

The derivative response from this section of the controller is

$$(P - P_0) = S'T'\frac{dx}{dt} \quad \text{or} \quad \frac{dP}{dt} = S'T'\frac{d^2x}{dt} \qquad [6]$$

The total output from this section of the controller is the input to the reset relay and it may be written as follows

$$\left.\begin{aligned} \text{(Total) } (P - P_0) &= S'\left[(x - x_0) + T'\frac{dx}{dt}\right] \\ \text{or} \\ \text{(Total) } \frac{(dP)}{(dt)} &= S'\left[\frac{dx}{dt} + T'\frac{d^2x}{dt^2}\right] \end{aligned}\right\} \qquad [7]$$

The proportional response output from the reset relay in terms of the input to the reset relay is

$$(p - p_0) = n(P - P_0) \quad \text{or} \quad \frac{dp}{dt} = n\frac{dP}{dt} \qquad [8]$$

The automatic-reset response of the reset relay is

$$\frac{dp}{dt} = nR'(P - P_0) \qquad [9]$$

and the total response from the reset relay expressed in the input to the reset relay is

$$\text{(Total) } \frac{dp}{dt} = n\left[\frac{dP}{dt} + R'(P - P_0)\right] \qquad [10]$$

Since we are interested in the output from the reset relay in terms of the input to the controller, rather than the input to the reset relay, this can be obtained by substituting Equation [7] in Equation [10]

$$\text{(Total) } \frac{dp}{dt} = n\left[S'\frac{dx}{dt} + S'T'\frac{d^2x}{dt^2} + R'S'(x - x_0) + R'S'T'\frac{dx}{dt}\right] \qquad [11]$$

which, on simplification, becomes

$$\text{(Total) } \frac{dp}{dt} = n\,S'\left[R'(x - x_0) + (1 + R'T')\frac{dx}{dt} + T'\frac{d^2x}{dt^2}\right] \qquad [12]$$

$$\text{(Total) } \frac{dp}{dt} = n(1 + R'\bar{T}')\,S'\left[\frac{R'}{1 + R'\bar{T}'}(x - x_0) + \frac{dx}{dt} + \frac{T'}{1 + R'T'}\frac{d^2x}{dt^2}\right] \qquad [13]$$

Note that the terms in the brackets in Equation [13] are identical with those in the brackets of Equation [4]. At the same time the proportional response of the controller has a different multiplier. This new multiplier includes n—the proportional response gain or amplification of the reset relay and a factor which includes the product of the reset rate and the derivative time.

If the proposed controller is to be adjusted so that it produces the same results on load changes as the conventional controller, it is reasonable to assume that the coefficients of each term of the equation must be set equal to each other. These coefficients may also be set equal to the coefficients in Equation [2] which describe an instrument with independent noninteracting adjustments of $\bar{S}$, $\bar{R}$, and $\bar{T}$. In fact, the values of $\bar{S}$, $\bar{R}$, and $\bar{T}$ in Equation [2] are the true values of the sensitivity, reset rate, and derivative time, while the values of S, R, and T in Equations [4], and S', R', and T' in Equation [13] are only apparent values. Note,

however, that these values are the measured values in both the conventional and the proposed controller when either $R = 0$ or $T = 0$.

Response	Actual coefficients	Coefficients in conventional controller	Coefficients in proposed controller
Proportional	$\overline{S}$	$= \frac{1 + RT}{1 - RT} S$	$= n(1 + R'T')S'$ ..... [14]
Reset	$\overline{SR}$	$= \frac{R}{1 - RT} S$	$= nS'R'$ ..... [15]
Derivative	$\overline{ST}$	$= \frac{T}{1 - RT} S$	$= nS'T'$ ..... [16]

By substituting the values of R' and T' obtained from Equations [15] and [16] in Equation [14], we obtain two solutions

$$nS' = \frac{S}{1 - RT}, \quad R' = R \text{ and } T' = T \ldots\ldots [17]$$

and

$$nS' = \frac{RTS}{1 - RT}, \quad R' = \frac{1}{T} \text{ and } T' = \frac{1}{R} \ldots\ldots [18]$$

(For detailed solution refer to the Appendix.)

The first solution, Equation [17] is not surprising, for it simply indicates that in the proposed controller the over-all apparent sensitivity nS' can be set at a higher value than in the conventional controller. The values of the reset rate and the derivative time are unchanged. To be specific, if the product of R and T is $^1/_4$, then the over-all apparent sensitivity nS' of the new controller must be $^4/_5$ of the apparent sensitivity S, of the conventional controller, in order to obtain the same recovery curves.

The second solution, Equation [18], however, is extremely interesting, for it indicates that there is another setting of the sensitivity, reset rate, and derivative time which will produce identical recovery curves. In this case the apparent over-all sensitivity setting nS' of the proposed controller is appreciably lower than the setting of the sensitivity S, in the conventional controller. Note that the reset-rate setting on the proposed controller is the reciprocal of the previous derivative time, and the derivative-time setting is the reciprocal of the previous reset rate.

To be specific and select definite values, let us again make RT equal to $^1/_4$. When this is done it will be seen that the new apparent over-all sensitivity nS' is $^1/_5$ of the value in the conventional controller, while the reset rate and the derivative time are 4 times their former value.

This low sensitivity, or widened proportional band coupled with the higher reset rate and derivative time, has great value. If overpeaking is to be prevented on start-up, the control action must be initiated long before the control point is reached. Since, in the proposed controller, action is initiated by the motion of the baffle before the control point is reached, the wide proportional band of the second solution, Equation [18], will almost certainly initiate action early enough to prevent overpeaking, while the narrower band of the first solution, Equation [17], may not. While the higher settings of reset rate and derivative time are also essential, the actual reset and derivative responses, like the proportional response, have no greater effect than in the conventional controller. (If this were not so, the instrument would produce unstable control.) Therefore the second solution is in reality a method of initiating the standard control responses long before the control point is reached on start-up so that the mechanism will approach an equilibrium before the control point is reached. At the same time it will be seen that if correct settings are chosen, the quality of the control, as judged by load changes, will not be impaired. Action of this sort, and hence automatic start-up, is not possible with the conventional controller.

The interrelationship between the apparent reset rate R' and the derivative time T', and the true or actual values $\overline{R}$ and $\overline{T}$, should be emphasized. Substituting Equation [14] in Equations [15] and [16]

$$\overline{R} = \frac{R'}{1 + R'T'} \text{ and } \overline{R} = \frac{R}{1 + RT} \ldots\ldots [19]$$

$$\overline{T} = \frac{T'}{1 + R'T'} \text{ and } \overline{T} = \frac{T}{1 + RT} \ldots\ldots [20]$$

Now when $R'T'$ or RT is small (e.g., $^1/_4$), the true reset rate and derivative time differ only slightly from the controller settings ($\overline{R} = {}^4/_5 R'$; $\overline{T} = {}^4/_5 T'$). This occurs with the conventional controller and the proposed controller set in accordance with Equation [17]. On the other hand, when $R'T'$ is large (e.g., 4), the true reset rate and derivative time differ considerably from the controller settings ($\overline{R} = {}^1/_5 R'$; $\overline{T} = {}^1/_5 T'$). This occurs with the proposed controller set in accordance with Equation [18]. Note that as $R'T'$ becomes large the true reset rate $\overline{R}$ is affected more and more by the adjustment of the derivative restriction. Similarly, the true derivative time $\overline{T}$ is more affected by the adjustment of the reset restriction.

Start-Up Characteristics of Improved Pneumatic Control System

Referring now to Fig. 6, let us consider the behavior of this controller on start-up. The important feature of this circuit is that in the portion involving the orifice, nozzle, and follow-up bellows, there is no automatic-reset response. Therefore, in this portion of the circuit the proportional band remains on both sides of the set point when the process is shut down.

Referring to Figs. 1 and 2, note the proportional band indicated by the shaded area extends on both sides of the set point whereas in Figs. 3 and 4, when automatic reset has been added, the control band is on the "wrong" side of the control point while the process is shut down. Therefore, in the proposed control circuit the orifice, nozzle, baffle, and bellows portion of the circuit behaves in a manner like that illustrated in Fig. 2 so that control action is obtained before the temperature reaches the control point. The proportional band in this section of the control circuit shifts downward due to the derivative action as soon as its lower edge is reached by the temperature. This initiates action of the reset relay before the control point is actually reached.

Now, since the pressure from this portion of the control system is led to the reset relay, rather than to a valve, the illustrated proportional band should be defined. This is the band which is shifted by the derivative response, and the position of the temperature in this band at any time indicates the pressure level applied to the input of the reset relay. In the selected example, the reset relay is not actuated until the temperature crosses the bisector of this band, but this adjustment is not necessary for satisfactory operation.

Referring to the proportional band of the reset relay, this remains above the set point until the input pressure to the reset relay changes. This portion of the circuit behaves in a manner similar to that shown in Fig. 3. The actual performance of the proposed controller is a unique combination of the derivative-controller performance of Fig. 2, and the reset-controller performance of Fig. 3. This controller may be considered a two-band controller, and in this respect it differs from the conventional controller of Fig. 4. Now the second solution, Equation [18], of

the previous equation states that the instrument sensitivity can be lowered, or its proportional band broadened appreciably, and still maintain the same quality of performance on load changes. The fact that the proportional band can be widened indicates that the process can be started up with a two-band instrument of this type without overpeaking.

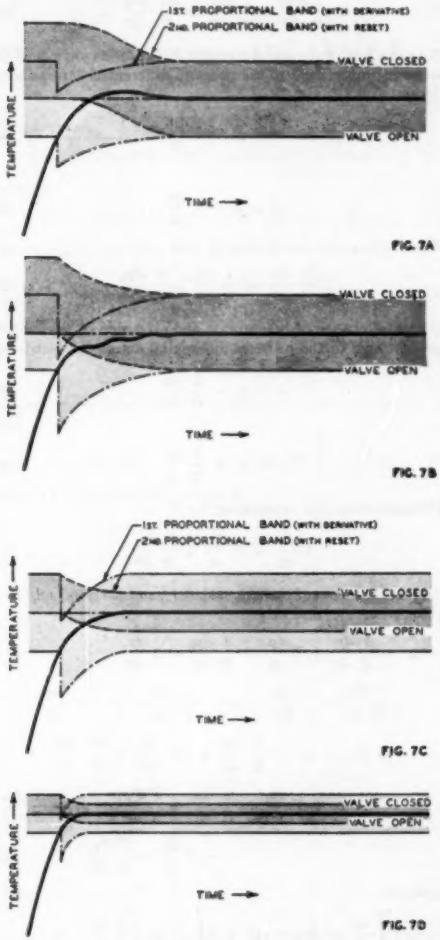

FIG. 7 TYPICAL START-UP CHARACTERISTICS—PROPOSED CONTROLLER WITH PROPORTIONAL, DERIVATIVE, AND AUTOMATIC-RESET RESPONSE

Fig. 7(*a*) illustrates the possible performance of an instrument of this type on an application similar to that described previously. Note that the proportional band in the derivative section of the circuit shifts downward as soon as the temperature reaches its lower edge. This results in pressure changes which actuate the reset relay and its proportional band before the set point is reached and the shifting of this control band is indicated. In this particular illustration the amplification, or gain n, is assumed to be equal to 1. In Fig. 7(*b*) the derivative time has been increased so that the responses occur more quickly with an accelerated action. This reduces the temperature rise more rapidly after it enters the control band and prevents overpeaking. If the derivative action is somewhat excessive, slight instability such as that illustrated may be experienced. Fig. 7(*c*) shows the performance which might be obtained if the gain, or amplification n, were equal to 2. If the temperature in this case approached the control point in the manner shown, it is quite possible that an increased sensitivity S' would produce a curve with less rounding in as illustrated in Fig. 7(*d*).

Now all of the curves have been drawn, assuming that the load on the control system was such that after the control point is reached the valve is 50 per cent open. If the load is lighter than this, the temperature approaches the control point more rapidly, the derivative effect is greater, and, if the instrument is in proper adjustment, overpeaking will still be prevented. On the other hand, if the load is heavy, the temperature approaches the set point more slowly, the derivative action is reduced, and excess time will not be required to reach the control point.

In all of the approach curves, proportional bands have been illustrated. A careful examination will show that they do not shift exactly as indicated, particularly in Figs. 3, 4, and 7. This is due to the difficulty in plotting the bands, especially when several control responses are involved. However, the illustrated bands may help understand the merit of the proposed control system.

CONCLUSIONS

The proposed pneumatic control system has one major advantage over conventional control systems. It can be used to start up a process automatically without overpeaking and at the same time maintain the control point when subsequent load changes occur. During the start-up period, the control system is responsive to the rate of change of the controlled variable before it reaches the control point and, therefore, good performance can be expected when the process starts up even under varying load conditions.

A controller of this type may be adjusted to provide excellent start-up characteristics, and yet its performance with load changes will not be impaired. This has been accomplished by the use of an improved control circuit which has the derivative function in a closed loop ahead of the automatic-reset function. A controller of this character has two proportional bands, the first being shifted by the derivative action, and the second by the automatic-reset action. Under all stable conditions the first band assumes a given position which in a normal controller would be expected to extend on both sides of the control point. While in the previous illustrations this band was bisected by the control point, under stable conditions, there may be cases when better performance will be obtained with the control point near one edge of the band. The second proportional band is not in a fixed position, but is shifted about the control point by the automatic-reset response. It is this shifting which restores the variable to the control point when load changes occur. On start-up this band is always on the opposite side of the control point from the controlled variable so that if it were not for the first proportional band, corrective control action would not be started until the control point was reached and, therefore, overpeaking would be very bad. In the improved control system the use of a wide proportional band, coupled with higher values of the derivative time and reset rate, shifts the automatic-reset proportional band before the control point is reached, and in this manner prevents overpeaking on start-up.

In the new control system there are two sets of values of sensitivity S', reset rate R', and derivative time T', which will pro-

duce the same response to a load change as a single setting of these values on the conventional controller. In one set of values S' differs slightly from the corresponding setting in the conventional controller, while R' and T' are unchanged. While the proposed controller, even with this setting, has better start-up performance than the conventional controller, due to its two-band characteristic, the improvement is not nearly as marked as when the second set of values is used. In this set of values the proportional band is widened and S' is a fraction of the corresponding setting on the conventional controller, while R' and T' are several times their existing values. To be specific, if in the conventional controller the best results are obtained where the product of RT is $^1/_4$, as suggested by Ziegler and Nichols, identical performance on load changes can be obtained with the setting of the sensitivity of the proposed controller at $^1/_3$ of its previous value, and that of the reset rate and derivative time at 4 times their values in the conventional controller. This reduced sensitivity, coupled with the high derivative time and reset rate will prevent overpeaking on most applications.

There are many other values of S', R', and T', which lie between those mentioned. These values will produce stable control, but the performance following a load change will differ. Still, this performance may be entirely satisfactory, while the performance of the controller on start-up may be considerably improved. It is suggested that these values of S', R', and T', be more fully investigated on actual processes and on analogs to determine the values which produce the best start-up characteristics. As a suggested criterion, the controller performance is best on start-up when the control point is reached with a minimum delay without overpeaking. On many applications, it would appear that this criterion should be used to adjust the controller rather than the performance following a load change.

The proposed control system would seem to have great merit on many batch, semicontinuous, and continuous processes. It has the advantage of the proportional plus derivative responses on start-up, and the advantage of the proportional plus automatic-reset responses on load changes.

Acknowledgment

The author wishes to thank Messrs. N. B. Nichols and W. I. Caldwell of the Taylor Instrument Companies, and also Mr. R. D. Webb, Union Carbide and Carbon Corporation, for their courtesy in reading the paper and their constructive criticisms.

Appendix

Derivation of Equation [3]

Equation [3] applying to the conventional controller can be developed on the following assumptions, referring to Fig. 5:

p_i = pressure on right or follow-up side of bellows
p_r = pressure on left or reset side of bellows
p = output pressure of controller

Since the nozzle follows the baffle in the controller under normal conditions

$$p_i - p_r = S(x - x_0) \quad [21]$$

Differentiating Equation [21]

$$\frac{dp_i}{dt} - \frac{dp_r}{dt} = S\frac{dx}{dt} \quad [22]$$

Multiplying Equation [22] by $(1/R) + T$

$$\frac{1}{R}\frac{dp_i}{dt} + T\frac{dp_i}{dt} - \frac{1}{R}\frac{dp_r}{dt} - T\frac{dP_r}{dt} = \frac{S}{R}\frac{dx}{dt} + ST\frac{dx}{dt} \quad [23]$$

Differentiating Equation [22]

$$\frac{d^2p_i}{dt^2} - \frac{d^2p_r}{dt^2} = S\frac{d^2x}{dt} \quad [24]$$

Multiplying Equation [24] by T/R

$$\frac{T}{R}\frac{d^2p_i}{dt^2} - \frac{T}{R}\frac{d^2p_r}{dt^2} = \frac{ST}{R}\frac{d^2x}{dt^2} \quad [25]$$

Now the rate of change of pressure on the follow-up side of the bellows is proportional to the pressure differential across the restriction

$$p - p_i = T\frac{dp_i}{dt} \quad [26]$$

or

$$p = p_i + T\frac{dp_i}{dt} \quad [27]$$

Differentiating and multiplying by $1/R$

$$\frac{1}{R}\frac{dp}{dt} = \frac{1}{R}\frac{dp_i}{dt} + \frac{T}{R}\frac{d^2p_i}{dt^2} \quad [28]$$

The rate of change of pressure on the reset side of the bellows is proportional to the pressure differential across the restriction

$$p - p_r = \frac{1}{R}\frac{dp_r}{dt} \quad [29]$$

or

$$p = p_r + \frac{1}{R}\frac{dp_r}{dt} \quad [30]$$

Differentiating and multiplying by T

$$T\frac{dp}{dt} = T\frac{dp_r}{dt} + \frac{T}{R}\frac{d^2p_r}{dt^2} \quad [31]$$

Adding Equations [21], [23], [25], [27], and [28], and subtracting Equations [30] and [31]

$$\begin{aligned} p_i - p_r + \frac{1}{R}\frac{dp_i}{dt} + T\frac{dp_i}{dt} - \frac{1}{R}\frac{dp_r}{dt} - T\frac{dp_r}{dt} \\ + \frac{T}{R}\frac{d^2p_i}{dt^2} - \frac{T}{R}\frac{d^2p_r}{dt^2} + p + \frac{1}{R}\frac{dp}{dt} - p - T\frac{dp}{dt} \\ = S(x - x_0) + \frac{S}{R}\frac{dx}{dt} + ST\frac{dx}{dt} + \frac{ST}{R}\frac{d^2x}{dt^2} \\ + p_i + T\frac{dp_i}{dt} + \frac{1}{R}\frac{dp_i}{dt} + \frac{T}{R}\frac{d^2p_i}{dt^2} - p_r - \frac{1}{R}\frac{dp_r}{dt} \\ - T\frac{dp_r}{dt} - \frac{T}{R}\frac{d^2p_r}{dt^2} \quad [32] \end{aligned}$$

Simplifying

$$\left[\frac{1}{R} - T\right]\frac{dp}{dt} = S(x - x_0) + S\left[\frac{1}{R} + T\right]\frac{dx}{dt} + \frac{ST}{R}\frac{d^2x}{dt^2} \quad [33]$$

Multiplying by $R/(1 - RT)$

$$\frac{dp}{dt} = S\frac{R}{(1 - RT)}(x - x_0) + S\left(\frac{1 + RT}{1 - RT}\right)\frac{dx}{dt} + S\frac{T}{(1 - RT)}\frac{d^2x}{dt^2} \quad [34]$$

which is Equation [3] in the paper.

Derivation of Equations [17] and [18]

Equations [17] and [18] may be developed from Equations [14], [15], and [16] in the paper in the following manner:

Substituting the value of R' and T' from Equations [15] and [16] in Equation [14], it becomes

$$\frac{1+RT}{1-RT}S = nS' + \frac{RTS^2}{(1-RT)(1-RT)nS'} \quad [35]$$

Simplifying by multiplying by $(1-RT)(1-RT)nS'$

$$(1+RT)(1-RT)nS'S = (1-RT)(1-RT)(nS')^2 + RTS^2 \quad [36]$$

which becomes

$$(1-RT)^2(nS')^2 - (1-R^2T^2)nS'S + RTS^2 = 0 \quad [37]$$

factoring

$$[(1-RT)nS' - RTS][(1-RT)nS' - S] = 0 \quad [38]$$

Setting each factor equal to zero

$$nS' = \frac{S}{1-RT} \quad [39]$$

and

$$nS' = \frac{RTS}{1-RT} \quad [40]$$

Substituting Equation [39] in Equations [15] and [16] of the paper

$$R' = R \quad \text{and} \quad T' = T, \text{ when } nS' = \frac{S}{1-RT} \quad [41]$$

which is Equation [17] of the paper.

Substituting Equation [40] in Equations [15] and [16] of the paper

$$R' = \frac{1}{T} \quad \text{and} \quad T' = \frac{1}{R}, \text{ when } nS' = \frac{RTS}{1-RT} \quad [42]$$

which is Equation [18] of the paper.

Discussion

J. Johnston, Jr.[4] In order to initiate control-valve response sufficiently early to prevent over-peaking, it would appear necessary to assign a definite value to the proportional band of the primary controller. Where a control point may be set at any position over the entire range of the instrument, a proportional band of 200 per cent should be necessary. Is this true? If not, what proportional-band range is incorporated in the design of the subject controller?

Author's Closure

In the first commercial instrument incorporating the improved control circuit, the first proportional band is 200 per cent as suggested. In this particular instrument (not illustrated in the paper S' remains fixed and nS', the over-all instrument sensitivity, is adjusted by varying n. In other designs incorporating this principle, S' need not be fixed and the first proportional band need not be 200 per cent. It is only necessary that the value of S' be low enough (e.g., the first proportional band be wide enough), to initiate action in the second section of the circuit in time to prevent overpeaking on the application under control.

[4] Engineering Service Division, Engineering Department, E. I. du Pont de Nemours & Company, Inc., Wilmington, Del.

Principles of Foundation Design for Engines and Compressors

By W. K. NEWCOMB,[1] PAINTED POST, N. Y.

This paper discusses the elastic character of the ground and shows that foundations for reciprocating machines can be treated as spring-supported masses, the machine and foundation representing the mass, and the ground the spring. Such elastic systems have natural periods of vibration; if the frequency of unbalanced inertia or other exciting force is near the natural frequency of the foundation, resonance will occur producing excessive vibration. Examples of this phenomenon are given and tests on foundations having resonance are described. Also, the nature of inertia forces found in reciprocating machines is explained. Examples of good and bad foundation design are shown and a rational method for foundation design is outlined.

Introduction

THIS paper is an attempt to rationalize foundation design. It is written by a designer and builder of reciprocating machines, one not in the foundation business, and it therefore reflects the observations of a mechanical engineer rather than a civil engineer or expert on soil mechanics.

Foundations for reciprocating machines differ from foundations for buildings or similar structures since dynamic rather than static loads are involved. With a static load, only the bearing capacity of the soil need be considered, and there are various well-known rules to follow. With a dynamic load, however, these rules do not apply, since the frequency of the forces and danger of resonance with attendant excessive vibration must govern foundation design.

Elastic Character of Ground

Although ground characteristics and subsoil elasticity have been discussed or mentioned in engineering literature (1, 2, 3, 4, and others)[2] from time to time, their relationship to the principles of foundation design has not been emphasized adequately nor thoroughly understood. As a result, the elastic character of the ground is not always recognized. The following examples show this characteristic:

An oil-storage tank was observed to settle when filled and rise to its original position when emptied. The test was made with a transit and repeated several times with the same results. There was a definite relation between load and deflection which is typical of elastic materials.

The elastic character of the ground is also shown by a soil-deflection test at another site. A loading platform with 2 sq ft bearing area was loaded gradually. The deflections obtained are plotted in Fig. 1, curve AB. With 1500 lb per sq ft load, the deflection B, was 0.30 in. This load was maintained for 72 hr and no further deflection took place. Then the load was removed quickly, and the deflection changed to 0.25 in., C. The load was applied quickly, and the deflection went to 0.305 in., D, which is very close to the original deflection, B. The line BC therefore represents the load-deflection characteristics of this ground.

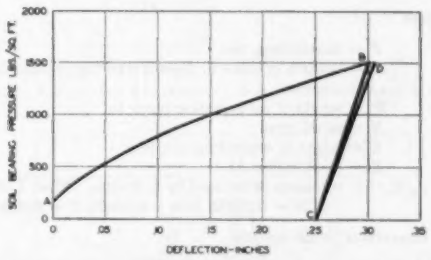

FIG. 1 LOAD-DEFLECTION TEST OF WET SAND AND CLAY SOIL

Because of this elastic nature of the ground the foundation and subsoil form an elastic system consisting of a mass (foundation block and machine) supported by a spring (subsoil). If such an elastic system is excited by periodic forces having a frequency near the natural frequency[3] of the elastic system, resonance will occur producing excessive vibration.

Forces Acting on Foundations

It is not always possible to obtain perfect balance in reciprocating machines and, as a result, unbalanced periodic forces may exist. These forces are caused by acceleration and deceleration of the piston or other reciprocating parts. Also, centrifugal forces and torque reactions are sometimes factors. Fig. 2 shows the inertia forces in a typical single-cylinder engine or compressor resulting from this acceleration and deceleration. At top dead center (in a vertical machine), the acceleration and resulting inertia force are maximum in the direction away from the crank. At bottom center they are maximum in the opposite direction.

This inertia force F, which acts along the axis of piston or crosshead as shown in Fig. 2(*a*), can be expressed mathematically as a Fourier series[4] as follows

$$F = 0.0000284\ WRN^2\ (\cos\theta + A\cos 2\theta + B\cos 4\theta + C\cos 6\theta + \ldots) \quad [1]$$

---

[1] Mechanical Engineer, Ingersoll-Rand Company. Mem. ASME.

[2] Numbers in parentheses refer to the Bibliography at the end of the paper.

Contributed by the Oil and Gas Power Division and presented at the Oil and Gas Power Conference, Baltimore, Md., June 12–16, 1950, of THE AMERICAN SOCIETY OF MECHANICAL ENGINEERS.

NOTE: Statements and opinions advanced in papers are to be understood as individual expressions of their authors and not those of the Society. Manuscript received at ASME Headquarters, March 20, 1950. Paper No. 50—OGP-5.

[3] Natural frequency, the frequency at which an elastic system tends to vibrate after being displaced from the equilibrium position and released.

[4] Reference (5) and other texts on engine dynamics.

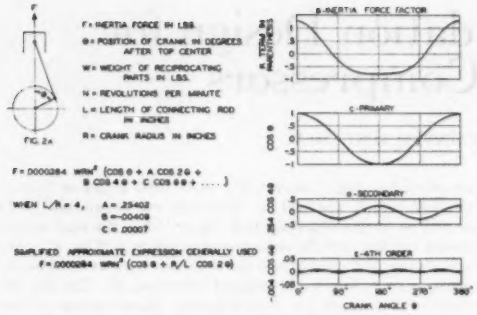

FIG. 2 INERTIA OR ACCELERATION FORCES IN CRANK AND CONNECTING-ROD MECHANISM

where

F = inertia force, lb
θ = position of crank in degrees after top or outer dead center
W = weight of reciprocating parts, lb
N = speed, rpm
L = length of connecting rod, in.
R = crank radius, in.
A, B, C = constants determined by L/R ratio. When $L/R = 4$, $A = 0.25402$, $B = -0.00409$, $C = 0.00007$

Equation [1] is also written

$$F = 0.0000284\ WRN^2\ K \quad \ldots\ldots [2]$$

K is called the inertia force (acceleration) factor and represents the terms in parentheses in Equation [1]. Values of K for different L/R ratios are found in most mechanical-engineering handbooks.

The inertia force F is represented graphically in Fig. 2(b), where K is plotted against crank angle. Note at outer dead center ($\theta = 0$) that K is maximum having a value of 1.250 (when $L/R = 4$). As the crank rotates, K decreases to zero, then becomes negative, reaching a maximum negative value of −0.750 at bottom dead center ($\theta = 180°$). When K is positive, the inertia force F acts away from the crankshaft; when negative it acts toward the crankshaft.

Examination of Equation [1] or [2] shows that the inertia force F varies directly with the reciprocating weight, directly with the stroke (or crank radius) and with the square of the speed.

The first term of the part of the equation in parentheses, that is, "cos θ," Equation [1], represents the "primary" inertia force which has one complete cycle per revolution of the crankshaft as shown in Fig. 2(c). The second term, "A cos 2θ," represents the "secondary" inertia force and is much smaller; it has two complete cycles per revolution, Fig. 2(d). The next term is the fourth order with four cycles per revolution, but it is very small and is usually neglected. There are also 6th, 8th, and higher orders, but they are likewise very small and can be neglected. For foundation design we need only consider the primary and secondary forces, and the simplified approximate form of the inertia-force equation is generally used.

Here the inertia force F is expressed as

$$F = 0.0000284\ WRN^2\left(\cos\theta + \frac{R}{L}\cos 2\theta\right) \quad \ldots\ldots [3]$$

The primary inertia force F' and secondary inertia force F'' become

$$F' = 0.0000284\ WRN^2 \cos\theta \quad \ldots\ldots [4]$$

$$F'' = 0.0000284\ WRN^2\frac{R}{L}\cos 2\theta \quad \ldots\ldots [5]$$

The primary and secondary forces having different frequencies have different effects on vibration and must be dealt with individually. Since they vary sinusoidally, the maximum values are used for foundation and vibration calculations. The maxima occur when $\cos\theta = 1$ and $\cos 2\theta = 1$, and the primary and secondary forces then become

$$\text{Primary,}\quad F'_{max} = 0.0000284\ WRN^2 \quad \ldots\ldots [6]$$

$$\text{Secondary,}\quad F''_{max} = \frac{R}{L}F'_{max} \quad \ldots\ldots [7]$$

In single-crank machines both primary and secondary inertia forces are unbalanced. With two cranks at 180 deg the primary force of one crank is opposed to the primary force of the other crank and completely balances it if the reciprocating weights of the two cylinders are the same. The resultant primary force will then be zero. However, the secondary forces act in the same direction and add. With two cranks at 90 deg, the secondaries are balanced and primaries partly balanced. With 3 or more equally spaced cranks, both primary and secondary forces are balanced. However, while the forces may be balanced, couples can be produced by the forces acting along the axes of the dif-

TABLE 1 UNBALANCED INERTIA FORCES AND COUPLES FOR DIFFERENT CRANK ARRANGEMENTS

CRANK ARRANGEMENTS	FORCES		COUPLES	
	PRIMARY	SECONDARY	PRIMARY	SECONDARY
SINGLE CRANK	F' WITHOUT COUNTERWTS. 0.5 F' WITH COUNTERWTS.	F''	NONE	NONE
TWO CRANKS AT 180° IN LINE CYLINDERS	ZERO	$2F''$	FD WITHOUT COUNTERWTS. $\frac{FD}{2}$ WITH COUNTERWTS.	NONE
TWO CRANKS AT 180° OPPOSED CYLINDERS	ZERO	ZERO	NIL	NIL
TWO CRANKS AT 90°	1.41 F' WITHOUT COUNTERWTS. 0.707 F' WITH COUNTERWTS.	ZERO	1.41 $F'D$ WITHOUT COUNTERWTS. 0.707 $F'D$ WITH COUNTERWTS.	$F'D$
TWO CYLINDERS ON ONE CRANK CYLINDERS AT 90°	F' WITHOUT COUNTERWTS. ZERO WITH COUNTERWTS.	1.41 F''	NIL	NIL
TWO CYLINDERS ON ONE CRANK OPPOSED CYLINDERS	2F' WITHOUT COUNTERWTS. F' WITH COUNTERWTS.	ZERO	NONE	NIL
THREE CRANKS AT 120°	ZERO	ZERO	3.46 $F'\frac{D}{2}$ WITHOUT COUNTERWTS. 1.73 $F'D$ WITH COUNTERWTS.	3.46 $F'\frac{D}{2}$
FOUR CYLINDERS CRANKS AT 180°	ZERO	$4F''$	ZERO	ZERO
FOUR CYLINDERS CRANKS AT 90°	ZERO	ZERO	1.41 $F'D$ WITHOUT COUNTERWTS. 0.707 $F'D$ WITH COUNTERWTS.	$4.0F'D$
SIX CYLINDERS	ZERO	ZERO	ZERO	ZERO

F' = PRIMARY INERTIA FORCE IN LBS.
$F' = .0000284\ RN^2W$
F'' = SECONDARY INERTIA FORCE IN LBS.
$F'' = \frac{R}{L}F'$
R = CRANK RADIUS, INCHES
N = R.P.M.
W = RECIPROCATING WEIGHT OF ONE CYLINDER, LBS
L = LENGTH OF CONNECTING ROD, INCHES
D = CYLINDER CENTER DISTANCE

ferent cylinders. Table 1 shows unbalanced forces and couples obtained with some common crank arrangements.

Resonance in Foundations

Since the foundation is an elastic system, these periodic forces (and to a lesser extent the couples) tend to induce vibration. If the frequency of the exciting force is near the natural frequency of the foundation, resonance will occur and may cause excessive vibration.

Fig. 3 shows a gas-engine-driven compressor foundation having resonance within the operating speed range. While adequate concrete yardage was used (four times that generally necessary for a machine of this type), it was not placed effectively. The

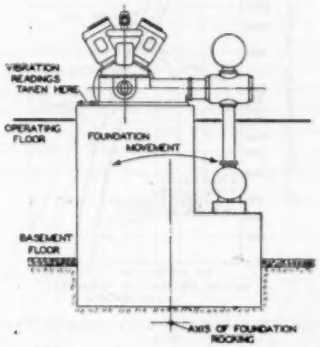

Fig. 3 Foundation Having Resonance in Operating Speed Range

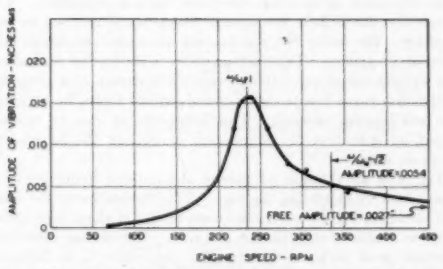

Fig. 4 Vibration Test Showing Resonance in a Foundation

ground was soft, and the result was excessive vibration. Vibration measurements showed that the foundation rocked back and forth about an axis slightly below the base as marked in Fig. 3. This movement was caused by horizontal secondary forces in the compressor.

The horizontal movement at top of the foundation is plotted in Fig. 4. Note that at 354 rpm the amplitude of vibration is 0.0045 in. As the speed decreases the amplitude increases, reaching a maximum of 0.016 in. at 236 rpm, although the inertia force (which varies as the square of the speed) is 56 per cent less than at 354 rpm. Below 236 rpm the amplitude drops off sharply. In this particular machine the unbalanced force was 10,800 lb (secondary) at 354 rpm, and 4800 lb at 236 rpm.

The vibration peaking in this manner is typical of an elastic system. As there were two complete vibrations per revolution due to unbalanced secondary forces, the natural frequency is 472, the vibrations per minute occurring at 236 rpm, the resonant speed.

An engine or compressor foundation can be represented graphically as a spring-supported mass with a dashpot to provide damping as shown in Fig. 5. When the mass, spring characteristics, and damping are known, also the magnitude and frequency of the exciting force, the amplitude of the resulting vibration can be determined.

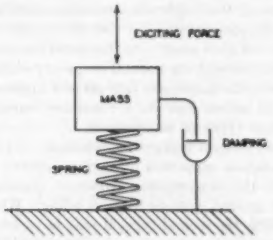

Fig. 5 Foundation Represented as a Spring-Supported Mass

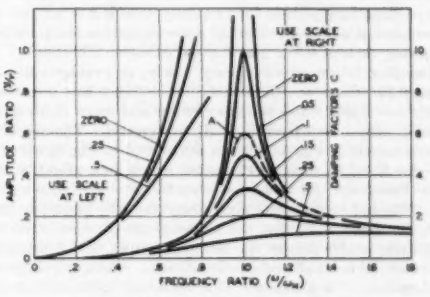

Fig. 6 Vibration-Resonance Curves

Fig. 6 shows typical resonance curves for the elastic system represented in Fig. 5. Here "amplitude ratio" is plotted against "frequency ratio" for different damping factors.[5] Note that

$$\text{Amplitude ratio,}^{6}\ \frac{y}{r} = \frac{\omega^2/\omega_n^2}{\sqrt{(1-\omega^2/\omega_n^2)^2 + (2\,c\,\omega/\omega_n)^2}} \qquad [8]$$

when

y = actual amplitude
r = free amplitude, the amplitude with which the foundation mass would vibrate if it were not restrained
c = damping factor, viscous damping assumed
ω = frequency of exciting force
ω_n = natural frequency of foundation

$$\text{Free amplitude, } r = 35{,}200\,F/W\omega^2, \text{ in.} \qquad [9]$$

[5] Damping is the reduction in amplitude of vibration due to friction or viscosity, etc. Viscous damping is assumed where the damping is proportional to the square of the velocity (6). When the damping is sufficient to just prevent vibration, $c = 1$. When $c = 0$, the amplitude of vibration at resonance becomes infinite.

[6] Reference (7) and other texts on vibration.

where

F = maximum value of primary or secondary inertia force, whichever is being considered, lb
W = combined weight of foundation and machine, lb
ω = frequency of inertia force F, in cycles per min (cpm)

An examination of Fig. 6 shows the amplitude ratio is zero, when the frequency ratio is zero, which means there is no vibration when the machine is standing still. Then, as the speed of the machine and frequency and magnitude of the exciting force are increased, the amplitude increases, reaching a maximum at or near the frequency ratio of 1 (for the smaller damping factors such as $c = 0.25$ or less). At this speed the periodic exciting force is in resonance with the natural frequency of the foundation. At higher speeds the amplitude falls off and approaches the free amplitude. Let us see how these resonance curves can be applied to different types of foundations.

There are two general types of foundations; (*a*) the resiliently mounted foundation supported on springs, rubber, cork or felt, etc., and, (*b*) the conventional concrete foundation poured directly on the ground, with or without piling. While this paper mainly deals with the second type, it may be of interest to point out some differences between them so as to emphasize the characteristics of the latter. To be effective, the resilient foundation must have a natural frequency well below the frequency of any exciting force so that the frequency ratio is 2 or 3.[7] On the other hand, it is desirable that the conventional foundation have a frequency ratio of 0.5 or less to avoid excessive vibration.

Damping factors of soil c, vary widely, an average value (1) being 0.25. However, the foundation in Fig. 3 had a damping factor $c = 0.082$, which is unusually low and was a result of the rocking action displacing little of the ground. The vibration measurements of this foundation are plotted in Fig. 6, curve A, showing that the actual performance agrees with vibration theory. Fortunately, it is not necessary to know the damping factor of the soil because in a good foundation the frequency ratio is 0.5 or less. Note that the damping has little effect on the amplitude in this part of the resonance curve, and if neglected the error will be small and on the safe side. Thus, to predict the performance of a foundation it is necessary to know only the "free amplitude," "natural frequency," and the "magnitude" and "frequency" of the "exciting forces."

Factors Affecting Natural Frequency of a Foundation

In theory a foundation can have six degrees of freedom. That is, it may vibrate in six different ways as shown in Fig. 7, or a combination of them. However, in the actual foundation the movement is generally either horizontal or vertical, depending on which force predominates or is near resonance. The horizontal natural frequency is usually the same as the vertical natural frequency. The natural frequency in rocking is influenced by the dimensions of the foundation. For shallow foundations the rocking natural frequency will be very nearly the same as the vertical natural frequency. For high foundations (also deep foundations) it will be much lower. The approximate natural frequency of a foundation can be determined from the static deflection as described later in Equation [10] or expressed in terms of soil-bearing pressure as shown in Fig. 8.[8] Here the natural frequencies for two different soils are given. Note that the softer ground has the lower natural frequency. The graph also shows how the natural frequency is affected by soil loading; the lower the soil bearing pressure, the higher the natural frequency. This fact provides a means for controlling the natural frequency. If the natural frequency of a proposed foundation is too low, it can be raised, within limits, by reducing the soil bearing pressure. This improvement can be accomplished by spreading the foundation or placing the foundation block on a mat.

Fig. 9 is an example of raising the natural frequency of a foundation by extending the base. This foundation is the same one shown in Fig. 3, but a reinforced mat, 2 ft thick, was added to tie to another foundation on one side. This change raised the resonant peak ($\omega/\omega_n = 1$) from 236 rpm, curve A, to 346 rpm, and substantially reduced the amplitude as shown in curve B. The new natural frequency is 692 vibrations per min and is a big improvement over the original foundation.[9] Curve A (same as Fig. 4), shows amplitude of the original foundation for comparison.

[7] References (7, 8).

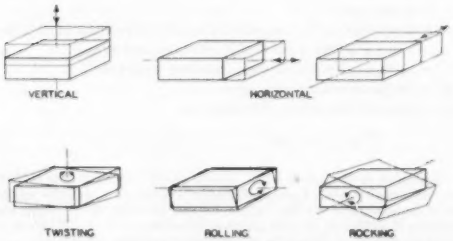

Fig. 7 Vibration of Foundations, Six Degrees of Freedom

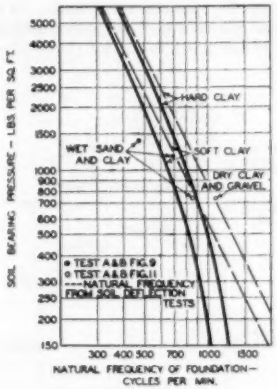

Fig. 8 Natural Frequency of Foundation on Two Types of Soil

[8] Fig. 8, while empirical, is based on published data on soils. The upper ends of the curves, where the soil bearing pressure is high, approach the natural frequencies calculated from static deflection (1). The lower ends of the curves where the soil bearing pressure is low, approach the natural frequency of the ground determined by vibrator tests, such as (2). Thus it takes into account the fact that the ground acts like a spring having appreciable mass. Reference (4) gives additional information on natural frequency of foundations.

[9] The shape of the resonance curves in this test indicates substantially linear soil-deflection characteristics although other investigators (3) find nonlinearity. This difference may be the result of size or shape of foundation or magnitude of deflection of the soil. The broken line in curve B is superimposed vibration about another axis.

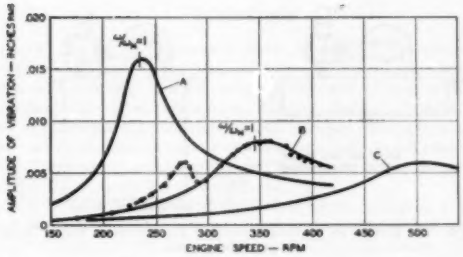

FIG. 9 RAISING NATURAL FREQUENCY BY EXTENDING FOUNDATION BASE

The revised foundation was satisfactory for all speeds up to 300 rpm. Further improvement could be obtained by extending the base on the other side. Curve C, Fig. 9, shows results expected if the foundation had been placed originally on an adequate mat, so as to provide a lower soil bearing pressure and obtain a higher natural frequency.

Fig. 10 shows an example of resonance in a compressor foundation.

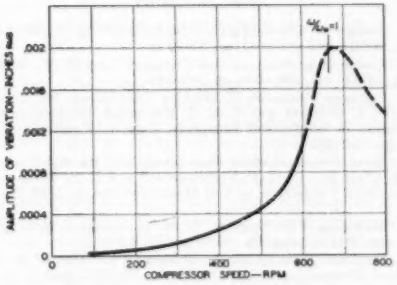

FIG. 10 RESONANCE IN COMPRESSOR FOUNDATION

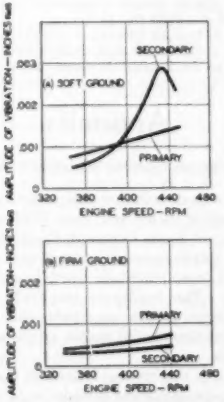

FIG. 11 RESONANCE IN ENGINE FOUNDATION

The effect of soft and firm ground under identical foundations is shown in Fig. 11. Fig. 11(*a*) shows the results of a vibration test where a foundation intended for firm ground was placed on soft ground. Here the natural frequency was too low, producing resonance and excessive vibration at 434 rpm. In Fig. 11(*b*), the engine and foundation were exact duplicates, but the ground was firm. A much higher natural frequency (beyond the range of the test) was obtained and vibration was nil.

The desirability of low soil loadings for soft ground, such as wet sand and clay, cannot be overemphasized. A common mistake in the design of engine and compressor foundation is to follow the soil bearing pressures allowed by building codes such as Table 2. These soil bearing pressures are much too high for dynamic loads. Soft clay or wet sand, for instance, is considered suitable for 2000 lb per sq ft under building footings, but an engine or compressor foundation on this soil and with this bearing load will have a natural frequency of 490 vibrations per min (from Fig. 8), which is suitable only for a low-speed machine.

TABLE 2 EXAMPLES OF ALLOWABLE SOIL BEARING PRESSURES FOR STATIC LOADS

	Lb per sq ft
Quicksand or alluvial soil	1000
Soft clay, sand, loam, silt	2000
Firm clay, sand and clay	4000
Hard clay	6000
Compact sand and gravel	8000
Shale and hard pan	16000
Rock	20000 and higher

NOTE: For dynamic loads only a fraction of these soil bearing pressures can be used depending on frequency of forces present.

The fact that high or deep foundations have a lower natural frequency in rocking than shallow foundations has already been mentioned. A comparison of typical shallow and high foundations shows that the natural frequency of the latter may be reduced to one half, unless special precautions are taken. When necessary to install engines or compressors on high foundations a mat should be used to lower the soil loading and raise the natural frequency. The block on which the machine rests can be relatively small, the only requirement being that it is sufficiently strong and rigid to provide adequate support and maintain proper alignment of the machine and transmit the vibration forces to the mat.

PILING

When poor soil is encountered, piling is often desirable. It is beyond the scope of this paper to discuss the detailed use of piles as this subject belongs to the foundation specialist. However, piles properly used will raise the natural frequency of the foundation, especially the vertical natural frequency if driven to firm ground. When substantial horizontal inertia forces are encountered and piling is necessary, the use of batter piles is important to keep the natural frequency high. A foundation supported on piles should always be checked for natural frequency on the assumption that the earth may shrink away leaving the foundation supported on columns. This can be done by determining the "static deflection" caused by a horizontal force equal to the total weight of the foundation and machine. There is a convenient relation between the static deflection and the natural frequency as follows

$$\omega_n = 188 \sqrt{\frac{1}{\delta}} \qquad [10]$$

where

ω_n = natural frequency, vibrations per min
δ = static deflection, in.

Fig. 12 shows natural frequency plotted against static deflection.

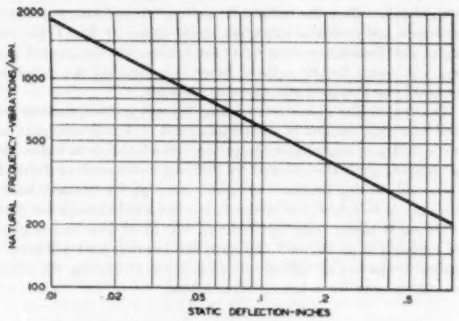

FIG. 12 RELATION BETWEEN STATIC DEFLECTION AND NATURAL FREQUENCY

DESIGNING FOUNDATIONS

Manufacturers' foundation drawings show foundations suitable for firm soils such as well-cemented sand and gravel or hard clay. When softer ground is encountered, additional precautions must be taken. Many foundation problems can be solved by placing the foundation block on a mat, the size of which is determined by the magnitude and frequency of the unbalanced forces and the character of the ground. In other cases piling can be used effectively. It is good practice to refer the design of all special foundations to a foundation expert, one familiar with soil dynamics.

In designing the foundation for an engine or compressor, or any machine having periodic forces, the procedure to follow should be:

1 Determine the magnitude and frequency of the unbalanced forces. This information is generally supplied by the manufacturer of the machine. The frequency of the unbalanced forces establishes what the natural frequency of the foundation must be to avoid resonance and obtain a vibrationless installation. The natural frequency should be at least twice the frequency of any substantial unbalanced force. Expressing it another way, the frequency ratio should be less than 0.5.

2 Determine the character of the soil by borings, deflection tests, and, if possible, dynamic tests (2, 3, 6). The maximum allowable bearing pressure required to obtain the natural frequency found in item 1 can be developed from these data or an approximate value can be read directly from Fig. 8.

3 Pick off the amplitude ratio from Fig. 6.

4 Assuming some allowable amplitude of vibration such as 0.002 in., determine the free amplitude.

5 Knowing the magnitude and frequency of the unbalanced force, item 1, and the free amplitude, item 4, the total mass of the machine and foundation can be found. But the foundation must be proportioned so as not to exceed the maximum allowable soil bearing pressure determined in item 2.

THE IDEAL FOUNDATION

Fig. 13 shows examples of good and bad foundation design. Avoid high or deep foundations. If the latter type must be used be sure to provide a generous mat. The ideal foundation is shallow (but sufficiently rigid to maintain alignment) and is spread out to obtain a low soil bearing pressure and place a large

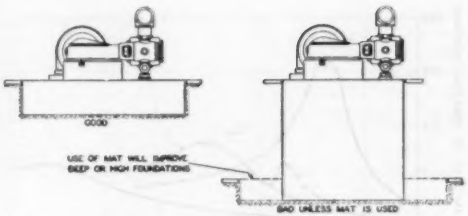

FIG. 13 EXAMPLES OF GOOD AND BAD FOUNDATIONS FOR A HORIZONTAL COMPRESSOR

surface in contact with the ground. This construction insures a high natural frequency which is necessary for vibrationless operation.

ACKNOWLEDGMENTS

The author wishes to express his appreciation to members of the Ingersoll-Rand Company staff for assistance with the preparation of this paper. Also, to Mr. F. E. Rasmers for data on soil deflection, and to Mr. W. P. Kinneman for suggestions on use of piling.

BIBLIOGRAPHY

1 "Design of Diesel-Engine Foundations," by K. H. Larkin, Trans. ASME, vol. 64, 1942, pp. 341–350.

2 "Geophysical Study of Soil Dynamics," by R. K. Bernhard, Trans. AIME, vol. 138, 1940, pp. 326–344.

3 "Dynamic Principles of Machine Foundations and Ground," by J. H. A. Crockett and R. E. R. Hammond, Proceedings of The Institution of Mechanical Engineers, London, England, vol. 160, 1949, pp. 512–523.

4 "Resonance of Machine Foundations and the Soil Coefficients Which Affect It," by G. P. Tschebotarioff and E. R. Ward, Second International Conference on Soil Mechanics, vol. 1, 1948, pp. 309–313.

5 "Balancing of Oil Engines," by W. K. Wilson, J. B. Lippincott Company, Philadelphia, Pa., 1929, pp. 7–10.

6 "Dynamic Tests by Means of Induced Vibrations," by R. K. Bernhard, Proceedings of the ASTM, vol. 37, 1937, part 2, pp. 634–645.

7 "Mechanical Vibrations," by J. P. Den Hartog, second edition, McGraw-Hill Book Company, Inc., New York, N. Y., 1940, p. 59, p. 74, etc.

8 "Theory of Elastic Engine Supports," by D. S. Rosenzweig Trans. ASME, vol. 61, 1939, pp. 31–36.

9 "Reduction of Ground Vibrations into Structures," by J. H. A. Crockett and R. E. R. Hammond, Institution of Civil Engineers, Structural Paper no. 18, London, England, 1947.

Appendix

INSTRUMENTS USED TO MEASURE VIBRATION

The vibration tests described in this paper were made with the Type 761A vibration meter and Type 762B vibration analyzer made by the General Radio Company, Cambridge, Mass. These instruments are inertia-operated crystal type and measure the root-mean-square (rms) amplitude which is plotted in the different illustrations. The maximum amplitude from the mean position is 1.414 times the rms amplitude, while the total over-all displacement (sometimes called double amplitude) is 2.828 times the rms amplitude.

The test, shown in Fig. 10, was made with the foregoing vibration-measuring instruments and recorded with a Brush Development Company oscillograph.

Discussion

P. E. HALL.[10] The author is to be commended for having sufficient interest in the over-all phases of the field of compressor engineering to have done an obviously extensive amount of research in a line not strictly his own. It is only through a broadening of interest such as this that both the designer and the user of equipment become conversant with the problems of each other. This blending of understanding can only result in better machines and more intelligent machine use.

The following discussion reflects exclusively the viewpoint of a practicing civil engineer who is engaged in the design and building of compressor stations and who knows little of the design procedures on machines.

The writer agrees that earthern materials are pseudoelastic in character, ranging from the very stiff, such as rock, to the semifluid, such as the marsh lands of the Gulf Coast of Texas and Louisiana. Unfortunately, most of the compressor foundations with which the writer has been familiar were located in the softer soils; so that the peculiarities of this type will be discussed in detail.

When soft soils are loaded with an applied force appreciable displacement of the original contact plane between soil and foundation occur; however, soil and foundation remain in contact. This displacement is caused by a simultaneous but varying degree of compression occurring in the successive layers of a vertical column of earth beneath the load.

The degree of compression is a maximum at the contact plane and finally becomes zero at some point below this plane. The point of zero compression varies with types of soil and severity of loading, but a good approximation of its location may be obtained from a study of the equations of the French elastician Boussinesq, together with a laboratory analysis of a soil sample.

One may wonder why all the ado about this insignificant point. It takes on great significance when it is realized that at least 50 per cent of the volume of earth from the contact plane to the point of zero stress is in essentially in-phase motion with the concrete supporting the engine and as such must be considered as a part of the weight resisting engine movement. It follows logically that the soil nearest the contact plane will be the part most perfectly in phase with the concrete foundation.

One may satisfy himself on the validity of the foregoing description of action by building two engine blocks having the same weight. One of the blocks should have a minimum contact area with the earth. The second should have less block but an extended mat to increase the contact area. He will find that under vertical cyclic forces only, the second foundation will have greater stability. The increase in stability will be greater than can be accounted for by considering only the decrease in unit soil loading.

Experience has shown one further piece of evidence which supports the theories expressed herein. The writer has had occasion to design compressor foundations in gasoline plants where the extended mat was the conventional 20 to 30 in. in thickness. On later compressor additions much thinner mats were used, but the mats were stiffened by use of haunched beams anchored to the block and extended to the extremities of the mat. The second mats were not particularly lighter than the conventional ones but much stiffer. When the additional units were put into operation it was found that the new stiffer mats were much more satisfactory than conventional designs. The writer feels that the stiffer mats allowed less out-of-phase vibration of the participating earth than the initial design.

[10] Special Representative, Peerless Oil and Gas Company, Houston, Texas.

Equation [10] of the paper may be put into the following form which generally is easier to handle with the data a structural engineer obtains for his design from the soils laboratory

$$f_s = \frac{1}{2\pi}\sqrt{\frac{KAg}{W + W_s}} \quad \ldots\ldots\ldots\ldots [10a]$$

where

f_s = natural frequency, cycles per sec (cps)
K = subgrade modulus, lb per cu ft.
A = area of foundation contact plane, sq ft
g = 32.2 ft/sec/sec
W = weight of engine plus concrete foundation, lb
W_s = weight of soil which participates in vibration, lb

The natural frequency of a foundation in rotation may be expressed by the following equation

$$f_\theta = \frac{1}{2\pi}\sqrt{\frac{1}{I_b + I_s}\left[\frac{KAa^2}{3} - (W + F_b)h\right]} \quad \ldots\ldots [10b]$$

where

f_θ = natural frequency, cps
I_b = mass moment of inertia of engine and foundation, referred to center of rotation, slug (ft)^2
I_s = mass moment of inertia of soil mass which vibrates with block referred to center of rotation
K = same as [10a]
A = same as [10a]
a = one half cross-sectional width of mat, ft
W = same as [10a]
F_b = resultant vertical force due to displacement of contact plane when earth is compressed (generally negligible)
h = height of center of mass above center of rotation, ft

When these frequencies are known it is then possible to ascertain the maximum dynamic pressures transmitted to the foundation by the vertically unbalanced force by means of the following equation

$$P_s = \frac{F}{A} \times \frac{1}{1 - \dfrac{\omega^2}{(f_s)^2}} \quad \ldots\ldots\ldots\ldots [10c]$$

where

F = weight of unbalanced parts, lb
A = area of soil contact plane, sq ft
ω = circular frequency of unbalanced force, cps
f_s = same as Equation [10a]

The maximum dynamic pressures transmitted to the foundation by the unbalanced couple M may be found by the following equation

$$P_\theta = \frac{MKa}{\frac{1}{3}KAa^2 - (W + F_b)h} \times \frac{1}{1 - \dfrac{\omega^2}{(f_\theta)^2}}$$

where f_θ equals natural frequency of foundation in rotation in cycles per second.

By evaluating these formulas with data pertinent to a particular problem, it is possible to plot natural frequencies versus imposed vibration frequencies to see if dangerous resonance occurs. It is also possible to plot the value of dynamic pressure transmitted to foundation. According to Terzaghi, the dynamic

pressure should be multiplied by a factor of 3 to 5 to obtain equivalent static pressure that will cause the same settlement.

Table 1 of the paper presents useful data for use on power engines only. Unfortunately most vibrational problems are encountered with the angle-type reciprocating compressor which is not mentioned. Table 1 covers the case of unbalanced forces in one plane only, while the angle compressor produces cyclic unbalanced forces in two planes at right angles to each other. When the resultant unbalanced force exerted on the main bearing is plotted in polar co-ordinates it is easy to see that it varies widely both in magnitude and direction during one revolution. Not only does one obtain vertical forces, tending to shake the foundation, but horizontal forces as well. In modern pipe-line practice, compression ratios are low. This condition produces rather massive compressor pistons which increase the horizontal unbalanced forces. It is suggested that if the manufacturer would submit such polar co-ordinate plots to the designer of foundations, more effort would be expended toward designing stable foundations. It has been the writer's experience that manufacturers are extremely reluctant to release such information owing to their thought that the diagram might reflect adversely on their design. This is an unfortunate condition for it is well recognized that perfect balance is not practical, and it is better to plan for the actual condition rather than to minimize it.

In designing extended mat foundations on soft soils, the critical design stress is frequently overlooked because it occurs during construction. The usual construction procedure is to pour the mat immediately after excavation to seal off any ground water and to provide a dry floor for erection of block and wall forms. The blocks are generally poured consecutively from one end of the mat to the other. Rarely is all the concrete poured before the engines arrive. In order that handling of the engines may be minimized, they are generally moved from car to the engine block or as near there as possible in one move.

Visualize the following condition which actually happened: An extended mat for five compressors had been poured for one week, three adjacent engine blocks had been completed and forms were set for the remaining two; all five engines arrived the same day. Heavy timber cribbing was placed between the three blocks, and all five engines skidded together to occupy the space of the three blocks. Is there any wonder that the mat cracked? This procedure, incidentally, is widely practiced in construction.

T. H. MEEK.[11] The similarity between spring supports and soil or pile-supported foundations for machines has been generally recognized for some time. Foundations for high-speed machines of ordinary size are usually mounted on a resilient base, and the foundation design is simplified by information furnished by the manufacturers of the resilient materials. The design of foundations for large reciprocating machines of a relatively low speed has not generally employed the spring-support theory because of the lack of a rational method for obtaining and using the information required in the time available. Consequently, the design of the latter type of foundations has depended entirely on the designer's knowledge of successful installations and his judgment concerning the many variables with which he has to deal. The time element involved makes it nearly impossible for a construction design engineer to indulge in any research on his problem. The author's method of design, by eliminating the unnecessary mass of computations required for mathematically exact results, and the necessity for elaborate soil investigations, promises to correct this condition.

The author's selection of a frequency ratio of 0.5 or less is substantiated by vibration tests made on various soils. The use of less should be emphasized, as published reports of vibration tests indicate that excessive vibration and settlement occur in a frequency range from $^1/_2$ to $1^1/_2$ times the natural frequency of the soil.

As the magnitude and frequency of the exciting forces are, or should be, furnished by the manufacturer of the machine, the structural engineer is interested only in the free amplitude and natural frequency.

Step 1 in the design of the foundation is simple and depends only upon the frequency ratio selected.

Step 2 in the design to determine the natural frequency is the main problem in the design. Under ordinary circumstances the designer will have static-load tests and soil borings for his use in determining the type and quality of the soil. This information is to permit him to interpret the information shown in Fig. 8 of the paper. We believe the diagram for the information, shown in Fig. 8, is essential, and that vibration tests as a check on the interpretation of the soil tests and the results obtained from the diagram are desirable. It would seem to be a simple matter to develop a mechanism of reasonable accuracy that could be used for this purpose by ordinary soil-testing personnel. There is, however, considerable reason to doubt the dependability of the information upon which Fig. 8 has been plotted. All of the published data that have come to our notice give much higher values than those shown for the natural frequency of the soil, as determined by vibration equipment at both high and low loadings and by dynamite shots. The results obtained for natural frequencies, computed from direct tests of static deflections, give much lower values, and their accuracy is open to question. The static deflection, as measured in conjunction with the static-load test, is a very small figure when measured by conventional equipment and when determined under ordinary field conditions.

In addition to that, Fig. 1 of the paper is typical of the deflection under a static-load test, and the reading on the line AB would not be the proper figure to use for this purpose. The lines BC and CD would give a figure showing the resilience of the soil, and accurate determinations of this figure in the field would not be practical. The use of the deflection as indicated by line AB might explain the very large difference between natural frequencies, determined by this method, and those determined by vibration equipment. It also should be remembered that the deflection under static loads on cohesive and cohesionless soil occurs for entirely different reasons. The information shown in Fig. 8 is undoubtedly conservative and may lead to overdesigning, since adequate information of its accuracy is not available to permit adjustment of the other factors of safety to conform. Experimental data in the operating range of soil pressures, from approximately 1000 to 2500 lb per sq ft, are needed for the use of the design.

Step 3 in the design, the determination of amplitude ratio from Fig. 6, is a simple operation. It may be noted, however, that for any selected frequency ratio, the amplitude ratio will always be the same. This figure also illustrates the desirability of holding the frequency ratio to a minimum.

Step 4 in the design is also a simple matter if the allowable amplitude of vibration is known. It is obvious that the range of this allowable amplitude must be determined before the designer can proceed farther. As the free amplitude is directly proportional to the allowable amplitude selected, there is an enormous range possible in this part of the design.

Step 5 in the design is purely a mathematical computation of the size of the foundation and its proper proportioning which any designer entrusted with this type of problem should be able to do satisfactorily.

Compressor foundations bearing on the soil are usually more

[11] Staff Engineer for Structures, Carbide and Carbon Chemicals Division, Union Carbide and Carbon Corporation, South Charleston, W. Va.

satisfactory than those supported by piling, but there are times when the use of piling is unavoidable. The computations for the natural frequency of a foundation supported on piles can be made mathematically exact in accordance with the formula given by the author if certain assumptions are made. It is these assumptions that make a prediction of the action of the foundation on piles very difficult. It is necessary to assume that the piles will be fixed in the soil at a certain depth which varies in standard specifications from 5 ft to 10 ft, depending on the quality of the soil. It is also necessary to make an assumption regarding the joint at the juncture of the pile and the foundation, whether it is a free joint or a sliding joint, as used in design of structures for earthquake resistance. When we consider that the static deflection varies as the cube of the unsupported length of the pile, and the unsupported length of the pile for a sliding top is only one half of that for a free top, it is evident that the static deflection, and, consequently, the natural frequency, can vary over a wide range. There is very little experimental data available concerning the action of piles under either lateral or vibrating forces; consequently, batter piles, and any other practical methods of stabilizing the foundation, are used where piles are unavoidable. It should be remembered that the use of batter piles, and some of the other methods of stabilizing foundations for reciprocating machines, may create a new problem by transmission of the vibration to resonant structures in the vicinity with disastrous results.

The importance of this problem and the value of the author's contribution to the profession may be illustrated by our own experience as our division alone of the Union Carbide and Carbon Corporation has installed more than 100 machines in the last 15 years with horsepowers ranging from 800 to 1500 and speeds varying from 125 rpm to 330 rpm.

J. D. Swannack.[12] In the Diesel field, the manufacturer supplies plans for a standard foundation, by experience found to be satisfactory on "firm soil." Whether or not the soil is "firm" is usually discovered when vibration complaints develop. Too many of us who even appreciate a rational design lack soil-stiffness data, such as illustrated in Fig. 1 of the paper.

The author's free amplitude concept is useful.

Our experience with high foundation, such as Fig. 3, tends to confirm the present remarks. Particularly since the war, our company has found the basement type of power plant in favor. This results in a concrete block about 10 ft wide, 12 ft high, and 25 ft long under a medium-size Diesel-alternator set. Primary forces and couples and sidewise shaking forces sometimes produce appreciable foundation rocking. A calculation of free amplitude always shows larger than measured values, indicating operation below resonance, but still too close to it. Speed limitations of the engines are such that we have never been able to go up through and beyond resonance to establish the natural frequency. Still referring to this same size of foundation and engine, it can be added that at 257 rpm practically no vibration troubles occurred, but at 300 rpm occasional vibration complaints began to appear.

These foundations have static loadings of 1000 to 1600 lb per sq ft. While the previous remarks refer to primary forces, it should be mentioned that in a few cases we have had large secondary vibrations. Reference to Fig. 8 explains this situation.

Many foundations involve over 200 sq ft of base area. In the author's opinion, what size of test-loading area would generally give data reliable for the much greater area? Is it possible to obtain reliable data from the floor of the excavation before the concrete "pouring"—supposing the digging to have been done by power machinery; or should a pit be dug previously by hand?

[12] Chief Design Analyst, Fairbanks, Morse & Company, Beloit, Wis. Mem. ASME.

G. P. Tschebotarioff.[13] The writer's considered conclusion is that there is at present no practicable way of determining, in advance of construction, the dynamic soil constants so as to permit the accurate prediction of the natural frequency of the foundation-soil system. Neither does there appear to be any possible promise in the near future for the development of a generally practical or useful procedure for that purpose. All proposals to that end which the writer has encountered so far invariably omit some essential factor and oversimplify the problem from a soil mechanics point of view. The present paper is no exception to that general rule. For instance, Fig. 8 of the paper suggests that the natural frequency of a foundation can be predicted for a certain type of clay merely as a function of the bearing pressure which is exerted by the foundation on the soil. This is an oversimplification too. The size of the contact area between the foundation and the soil also has a great influence on the natural frequency of the foundation-soil system, irrespective of the intensity of the contact pressure between the foundation and the soil. In addition, the load-deflection curve during a soil load test for loading and unloading does not consist of straight lines *BC* and *CD*, as shown in Fig. 1, but forms a "hysteresis loop" as shown in Fig. 14 herewith. The average slope of the loop will be quite different if only partial unloading *EF* is performed.

Certain facts upon which the writer and one of his associates have elaborated in greater detail elsewhere,[14] will be reviewed.

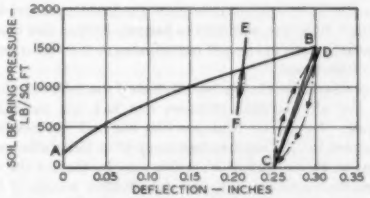

Fig. 14 Load-Deflection Test of Wet Sand and Clay Soil

The conventional natural frequency equation for undamped vibrations reads

$$\omega_n = \frac{1}{2\pi}\sqrt{\frac{k}{M}} \qquad [11]$$

where

ω_n = natural frequency of vibrating system
M = mass of vibrating system
k = linear spring coefficient of support

Lorenz[15] performed experiments with vibration-producing machines of the German Research Society of Soil Mechanics ("*Degebo*") and subsequently transformed Equation [11] of this discussion to read

$$\omega_n = \frac{1}{2\pi}\sqrt{\frac{k' Ag}{W_s + W_e}} \qquad [12]$$

[13] Associate Professor of Civil Engineering, Princeton University, Princeton, N. J.

[14] "The Resonance of Machine Foundations and the Soil Coefficients Which Affect It," by G. P. Tschebotarioff and E. R. Ward, Proceedings of the Second International Conference on Soil Mechanics and Foundation Engineering, Rotterdam, Holland, vol. 1, 1948, pp. 309–313.

[15] "New Results of Dynamic Investigations of Foundation Soil," by H. Lorenz, *Zeitschrift des Vereines deutscher Ingenieure*, vol. 78, March, 1934, pp. 379–385.

where

A = contact area between base of vibrator machine and soil
$k' = k/A$ = dynamic modulus of soil reaction, or volume spring coefficient
g = acceleration of gravity
W_v = weight of vibrator machine, including its foundation
W_s = weight of vibrating soil

In subsequent studies, Lorenz assumed that the dynamic modulus of soil reaction k' was a constant. With the help of this assumption and of experiments with vibratory tests on footings of different sizes, Lorenz claimed to have evaluated the mass of the soil which vibrated together with the foundation.

However, at about the same time another series of similar but entirely independent experiments had been performed in Soviet Russia by Barkan.[16,17] Some of his carefully performed preliminary tests indicated beyond any doubt that the coefficient k' was not a constant at all but that it varied with the intensity of the contact pressure on the soil as well as with the size of the contact area of the foundation. In addition, this coefficient changed with the speed at which the load was applied and removed. The latter finding was of particular importance since it showed that there is no practical way of determining this coefficient from static test loadings for the purpose of using it later in relation to dynamic phenomena—especially if resonance magnified contact soil pressures to an unknown extent. These findings appear entirely logical and invalidate the basic assumption made by Lorenz. However, similarly to Lorenz, Barkan also concluded that a certain mass of the soil participates in the vibration of the machine foundation.

This is where the matter rested during the following fourteen years. For all practical purposes one had run up against a blank wall. No matter what one did, one had two unknowns in one equation for the natural frequency of a foundation-soil system, that is, the coefficient k', which may be termed the volume spring coefficient of the soil, and the effective weight of the soil participating in the vibration.

To clarify this situation, the writer attempted to combine in graphical plots the known variables of actually recorded cases of resonance. Some interesting relationships were obtained from the plot which related natural frequencies to the size of the contact areas at a log-log scale.[18] A direct comparison of these values, however, was not justifiable since the unit contact pressures on the ground varied in all cases. Then Lorenz's equation was transformed to read as follows

$$\omega_n = \sqrt{\frac{A}{W_v}} \times \frac{1}{2\pi} \sqrt{\frac{k'g}{1 + \frac{W_s}{W_v}}} \qquad [13]$$

or

$$\omega_n = \frac{\omega_{nr}}{\sqrt{p}} \qquad [14]$$

where

$p = W_v/A$—average unit pressure on ground

ω_{nr} = "reduced natural frequency" or natural frequency at an average unit pressure on ground equal to unity; in this case to 1 ton per sq ft.

Fig. 15 herewith[19] shows the plot, at a log-log scale, of the reduced natural frequency ω_{nr} against the size of the contact area of the foundation with the soil. For the same area, the softer soil naturally produced a somewhat lower natural frequency than a stiffer soil. However, for the same type of soil the effect of the size of the contact area was strongly pronounced.

The two points obtained by the author are also indicated in Fig. 15. The one point which refers to dry clay and gravel might possibly correspond fairly closely to the "Degebo" sandstone test and give a line parallel to the ones obtained previously; but the second point, which refers to wet clay and sand, definitely is out of line. This fact only emphasizes the need for a continued and organized effort to obtain and correlate further data of this type. Fig. 15 should be taken only as an indication of a possible method to be employed in such correlations.

It should be recognized that there is no such thing as a natural frequency of a certain type of soil. If there are no other structures in the vicinity, the natural frequency of a foundation-soil system will depend on (*a*) the type of soil; (*b*) the size of the contact area between the soil and the footing; and (*c*) the unit pressure exerted by the foundation over that contact area. However, the presence in the immediate vicinity of other adjoining buildings or of other machinery foundations is likely to influence the natural frequency in a manner which it is impossible to evaluate numerically in advance of construction. At least it is impossible to do so at the present stage of development of our knowledge. Theoretical considerations or small-scale laboratory experiments cannot solve this problem. Maybe full-scale observations, if carried out systematically, will permit us to develop later rational semiempirical procedures on the basis of data supplied by more numerous field observations, but at the present

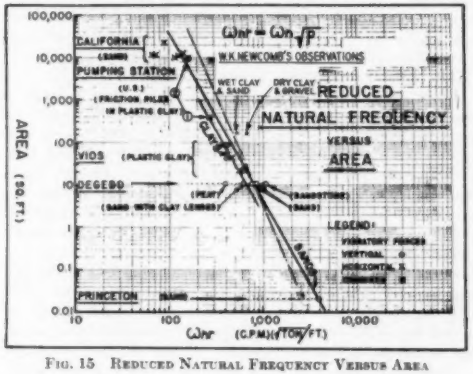

FIG. 15 REDUCED NATURAL FREQUENCY VERSUS AREA

time a sound engineering approach should consist in the recognition of facts as they are, namely, that there will always be a danger present, especially in the case of low-speed reciprocating machinery, that the actual operating speed may coincide either with the primary or the secondary natural frequency of the foundation-soil system.

In a previous paper,[14] a case is described when an effective remedy of a very severe case of resonance of foundations of pumping-station compressors, operating at 300 rpm, was ob-

[16] "Experimental Study of Vibrations of Mat Foundations Resting on Cohesive Saturated Soils," by D. D. Barkan (in Russian with English abstract), Transactions, Institute for Engineering Foundation Research (VIOS), Moscow, USSR, 1934.

[17] "Field Investigations of the Theory of Vibration of Massive Foundations Under Machines," by D. D. Barkan, Proceedings of the First International Conference on Soil Mechanics and Foundation Engineering, vol. 2, 1936, pp. 285–288.

[18] Reference 14 of this discussion, fig. 1.

[19] Reference 14 of this discussion, Fig. 3.

tained as a consequence of the lowering of the ground water table by a couple of feet within the depth of the foundation mat. This increased by some 7 per cent the effective weight of the foundation by removing part of the buoyancy effect and therefore moved the peak of the natural frequency of the foundation-soil system away from the operating speed of the machinery.

The writer has been informed recently of another similar case when objectionable vibrations at resonance of another compressor foundation, operating at 300 rpm, were stopped by decreasing its weight. This was obtained by tying part of the operating floor rigidly to the foundation and by isolating the remainder of the floor. The engineer of the company which brought that case to the writer's attention inquired as to his suggestions for the development of some procedure for the rough estimation of the natural frequency of such foundations so that one might predict in advance of construction any possible resonance. The writer is grateful for this opportunity to bring up for general discussion the suggestion which he made then.

The proposal is that one should build massive foundation blocks with hollow spaces at their four corners in such a way that if necessary, some of these spaces could be filled with sand or low-strength concrete to change the mass of the foundation to the extent necessary to move the peak of the primary or secondary natural frequency of the foundation-soil system away from the operational speed of the engines with which it may have happened to coincide. It is the writer's opinion that this procedure is the only one which at present holds a promise of success since it is not possible accurately to predict natural frequency. Further, it is believed that this procedure could be adapted to cope with any type of objectionable vibratory motion.

Author's Closure

Mr. Hall points out the value of extended mats and the importance of stiffening members. This construction tends to raise the natural frequency. Also, the large mat by virtue of increasing the mass of earth that moves with the foundation decreases the free amplitude. The extended mat type of foundation is very effective in resisting couples because of its large polar moment of inertia which increases as the fourth power of the length and breadth.

Mr. Hall's statement that manufacturers are reluctant to release polar diagrams of the unbalanced forces in their engines or compressors is misleading. Polar diagrams give only the combined inertia and centrifugal forces acting on the foundation and are not much help to the foundation designer. As this paper points out, the foundation designer must know the primary and secondary components as each one has a different effect on the foundation. Polar diagrams do not show these components. The author, therefore, prefers the tabular method of expressing the unbalance. This method gives all the information needed, and it is accurate and convenient to use. Here maximum values of the primary and secondary forces in the horizontal and vertical planes are expressed. This method is used by the author's company and is generally followed by the industry.

Table 1 shows only some of the more simple crank arrangements. Gas-engine-driven compressors were not included because of the great variety of cylinder and crank arrangements possible. Also the compressor cylinders usually have greater reciprocating weights than the power cylinders and sometimes have different strokes and L/R ratios[30] so that a general expression representing the unbalance is impractical.

Mr. Meek's remarks on piling are appreciated. While the experimental data that are available on pile-supported foundations are limited, he confirms that they have the same characteristics as elastically supported masses. Mr. Meek also emphasizes the desirability of having the "frequency ratio" of the foundation less than 0.5. The author has found the most successful foundations for large heavy-duty machines have a frequency ratio around 0.3.

The high and narrow Diesel alternator set foundations described by Mr. Swannack, like the foundation in Fig. 3, have relatively low natural frequencies in rocking. However, the natural frequency can be raised and stability improved by placing the block on an extended mat. The rigidity of the mat will be increased by the use of stiffening members as advocated by Mr. Hall. Where several units are placed side by side rocking can be prevented by using a common mat and by tying the foundations together at the top with heavy I-beams placed just below operating floor.

The author will not attempt to answer Mr. Swannack's question about the size of test-loading area necessary to obtain reliable results; this is a question for the expert on soil mechanics. Terzaghi and Peck[31] discuss this subject and show that a number of factors have to be considered before reliable results can be obtained. The load-deflection test in Fig. 1 was presented mainly to illustrate the elastic character of the ground.

The author does not share Professor Tschebotarioff's pessimism on the hopelessness of determining the natural frequency of a foundation in advance of construction. In fact, his concept of reduced natural frequency provides another good method to assist the foundation designer. The foundation designer does not need a highly accurate figure on the natural frequency because an approximation is generally satisfactory and certainly much safer than entirely neglecting the factor of resonance as is too often done.

Professor Tschebotarioff points out in Fig. 14 that the slope EF is steeper than BC or CD. This means that the natural fre-

[30] See Equation [1].

[31] Soil Mechanics in Engineering Practice, by Karl Terzaghi and Ralph B. Peck, John Wiley & Sons, Inc., New York, N. Y., 1948, pp. 426–428.

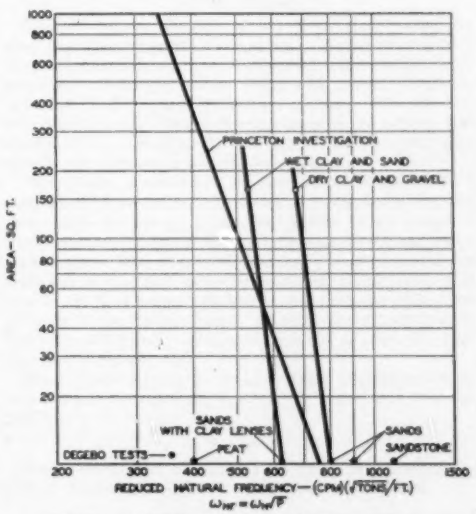

Fig. 16 Natural Frequencies of Foundations

quency calculated from *BC* or *CD* would be lower than that obtained from *EF* and the error is on the safe side.

The method of comparing foundations on the basis of Reduced Natural Frequency proposed by Professor Tschebotarioff has much to offer. However, the author believes the professor would obtain more consistent results if he did not try to compare foundations of 0.02 sq ft area with foundations of 20,000 sq ft area and expect to draw a straight line between these two points. The author suggests more weight be given to the points in Fig. 15 labeled "wet clay and sand" and "dry clay and gravel" which represent the results of the resonance test shown in Fig. 11(*a*) and Fig. 11(*b*), respectively. In these tests, like Degebo's, the vibration was vertical and the points obtained should not be confused with Professor Tschebotarioff's data which are the result of "horizontal" or "combined" vibratory forces. When horizontal forces are involved the foundation will rock (unless very shallow) at a lower natural frequency than obtained with vertical forces.

This may explain why points 1 and 2, Fig. 15, lie so far to the left of the point labeled "wet sand and clay." If these data are plotted as shown in Fig. 16 of this closure the author believes more consistent results will be obtained. Several foundations checked for natural frequency by the two methods, Fig. 8 and Fig. 16, show close agreement.

In conclusion the author wishes to thank Mr. Hall, Mr. Meek, Mr. Swannack, and Professor Tschebotarioff for their participation in the discussion. Their remarks have materially added to the value and usefulness of the paper.

Analysis of the Exhaust Process in Four-Stroke Reciprocating Engines

By J. D. STANITZ,[1] CLEVELAND, OHIO

This analysis determines the influence of engine design and operating variables upon the effectiveness of the exhaust process. This effectiveness is measured by the calculated pressure ratio (cylinder pressure, divided by exhaust-manifold pressure) near the end of the exhaust stroke. The variables that have an imporant effect upon this pressure ratio are the gas-velocity parameter (which is a ratio including the engine speed, piston displacement, exhaust-valve area, exhaust-valve flow coefficient at maximum valve lift, etc.) and the effective exhaust-valve closing angle. The variables that have an unimportant effect are the pressure ratio at the effective exhaust-valve opening angle (which, however, does become important for highly supercharged engines), the effective exhaust-valve opening angle, the engine compression ratio, the ratio of crank throw to connecting-rod length, and the ratio of specific heats. The maximum value recommended for the gas-velocity parameter is 0.325. From this value the minimum exhaust-valve area can be calculated directly for any given engine speed, displacement volume, etc. For large values of the gas-velocity parameter the exhaust valve should be closed as late as possible. For most current engine-operating conditions the correct exhaust-valve area does not depend upon the intake-valve area or upon the ratio of intake- to exhaust-manifold pressure (except for highly supercharged engines).

Nomenclature

The following nomenclature is used in the analysis (any consistent set of units may be used for the dimensions):

A_e = nominal exhaust-valve area
A_p = piston area
a_0 = speed of sound at T_0
c = exhaust-valve flow coefficient
c_{avg} = average flow coefficient for sine-curve approximation of c versus θ curve
c_{avg}' = average flow coefficient for actual c versus θ curve
c_{max} = flow coefficient at maximum valve lift
D = nominal valve diameter
f_1, f_2, f_3 = volume ratios defined by Equations [11a], [11b], and [11c]
g = acceleration of gravity
L = valve lift
m = weight of gas in cylinder at crank angle θ
P = pressure ratio, p/p_e
P_{cr} = critical pressure ratio, $\left(\frac{\gamma+1}{2}\right)^{\gamma/(\gamma-1)}$
P_m = intake-manifold pressure ratio
P_0 = pressure ratio at θ_0
P_{340} = pressure ratio at 340 deg ATC
p = cylinder pressure at crank angle θ
p_e = exhaust-manifold pressure
R = gas constant
r = compression ratio
S = average piston speed
s/l = ratio of crank throw to connecting-rod length
T = absolute gas temperature in cylinder at crank angle, θ
T_0 = absolute gas temperature at θ_0
t = time
V = cylinder volume at crank angle θ
V_{cl} = clearance volume
V_D = piston-displacement volume
Z = parameter defined by Equations [5a] and [5b]
γ = ratio of specific heats
Δ = finite increment
θ = crank angle (in radians unless otherwise specified)
θ_0 and θ_c = effective exhaust-valve opening and closing angles, respectively
θ_0' and θ_c' = actual exhaust-valve opening and closing angles, respectively
φ = gas velocity parameter, $\frac{V_D}{2c_{max} A_e a_0}$
ω = angular velocity of engine, $\frac{d\theta}{dt}$

Introduction

Efficient cylinder charging of four-stroke reciprocating engines depends (among other things) upon effective scavenging of the exhaust gases during the exhaust stroke. This analysis determines the influence of engine design and operating variables upon the effectiveness of the exhaust process. This effectiveness is measured by the calculated pressure in the cylinder near the end of the exhaust stroke. In general, the lower this pressure the more efficient is the cylinder charging.

The cylinder pressure near the end of the exhaust stroke is determined by the numerical solution of a differential equation that relates the change in cylinder pressure to the change in piston position and to the flow rate through the exhaust valve. This equation is so developed that the calculated results are applicable to most four-stroke reciprocating engines and may be used to arrive at general conclusions regarding the relative importance of the various factors affecting the exhaust process. The range of factors investigated is sufficient to cover any practical case that might arise.

This analysis was made at the Lewis Flight Propulsion Laboratory of the NACA and is the basis for NACA Technical Note No. 1242 (1).[2]

Analysis

Assumptions. The assumptions necessary to calculate the cylinder pressure during the exhaust process are as follows:

---

[1] Head, Applied Compressor and Turbine Analysis Section, Lewis Flight Propulsion Laboratory, National Advisory Committee for Aeronautics. Jun. ASME.

Contributed by the Oil and Gas Power Division and presented at the Oil and Gas Power Conference, Baltimore, Md., June 12–16, 1950, of The American Society of Mechanical Engineers.

Note: Statements and opinions advanced in papers are to be understood as individual expressions of their authors and not those of the Society. Manuscript received at ASME Headquarters, March 20, 1949. Paper No. 50—OGP-4.

[2] Numbers in parentheses refer to the Bibliography at the end of the paper.

1 The mixture of gases in the cylinder can be treated as a perfect gas.

2 The process under consideration can be treated as isentropic.

3 The flow rate through the exhaust valve can be calculated by the ordinary formula for steady flow through a nozzle (with experimental values of the exhaust-valve flow coefficient).

The third assumption requires that the exhaust-manifold pressure be known and, therefore, because the pressure variations caused by inertia effects in long exhaust pipes cannot be predicted accurately, the exhaust manifold must be sufficiently large or the exhaust pipes sufficiently short so that the exhaust-manifold pressure remains approximately constant during the exhaust process.

Differential Equation. The differential equation used to calculate the cylinder pressure during the exhaust process is developed from the equation of state for a perfect gas

$$pV = mRT \quad [1]$$

which, after differentiation with respect to θ, becomes

$$\frac{1}{p}\frac{dp}{d\theta} = \frac{1}{m}\frac{dm}{d\theta} + \frac{1}{T}\frac{dT}{d\theta} - \frac{1}{V}\frac{dV}{d\theta} \quad [2]$$

The left side of Equation [2] is given by

$$\frac{1}{p}\frac{dp}{d\theta} = \frac{1}{P}\frac{dP}{d\theta} \quad [3]$$

where the pressure ratio P is defined as

$$P = \frac{p}{p_s}$$

The first term on the right side of Equation [2] is combined with Equation [1] and with the identity

$$\frac{dm}{d\theta} = \frac{1}{\left(\frac{d\theta}{dt}\right)}\frac{dm}{dt} = \frac{1}{\omega}\frac{dm}{dt}$$

to give

$$\frac{1}{m}\frac{dm}{d\theta} = \frac{RT}{pV}\frac{1}{\omega}\frac{dm}{dt} \quad [4]$$

The flow rate through the exhaust valve, dm/dt in Equation [4], is related to the pressure ratio P, by the usual equation for flow through a nozzle (see assumptions). The following form of the equation is convenient for this analysis

$$\frac{dm}{dt} = -2c\,A_s\,pZ\left(\frac{\gamma g P^{(1-\gamma)/\gamma}}{RT}\right)^{1/2} \quad [5]$$

where the minus sign indicates flow out of the cylinder and where, for sonic velocity in the throat of the valve ($P > P_{cr}$)

$$Z = \frac{P^{(\gamma-1)/2\gamma}}{2}\left(\frac{2}{\gamma+1}\right)^{(\gamma+1)/2(\gamma-1)} \quad [5a]$$

and, for subsonic velocity in the throat of the valve ($P < P_{cr}$)

$$Z = \frac{P^{(\gamma-1)/2\gamma}}{2}\left[\frac{2}{\gamma-1}\left(P^{2/-\gamma} - P^{(\gamma+1)/-\gamma}\right)\right]^{1/2} \quad [5b]$$

The critical pressure ratio P_{cr} is related to γ by

$$P_{cr} = \left(\frac{\gamma+1}{2}\right)^{\gamma/(\gamma-1)} \quad [6]$$

Combining Equations [4] and [5] gives

$$\frac{1}{m}\frac{dm}{d\theta} = -\frac{2c\,A_s\,Z}{\omega V}\left(\gamma g R T P^{(1-\gamma)/\gamma}\right)^{1/2} \quad [7]$$

but

$$TP^{(1-\gamma)/\gamma} = T_0\,P_0^{(1-\gamma)/\gamma} = \text{const} \quad [8]$$

and

$$a_0 = (\gamma g R T_0)^{1/2}$$

so that Equation [7] becomes

$$\frac{1}{m}\frac{dm}{d\theta} = -\frac{2c\,A_s\,a_0}{\omega V}\,ZP_0^{(1-\gamma)/2\gamma} \quad [9]$$

The second term on the right side of Equation [2] is obtained from the differential of Equation [8]

$$\frac{1}{T}\frac{dT}{d\theta} = \left(1 - \frac{1}{\gamma}\right)\frac{1}{P}\frac{dP}{d\theta} \quad [10]$$

The third term on the right side of Equation [2] is given by

$$\frac{1}{V}\frac{dV}{d\theta} = \frac{f_2}{f_1 + f_2} \quad [11]$$

where

$$f_1 = \frac{V_{cl}}{V_D} = \frac{1}{r-1} \quad [11a]$$

$$f_2 = \frac{V - V_{cl}}{V_D} \quad [11b]$$

and

$$f_3 = \frac{d}{d\theta}\left(\frac{V}{V_D}\right) \quad [11c]$$

The factors f_2 and f_3 are functions of the crank angle and the ratio of crank throw to connecting-rod length s/l. Values of these factors can be obtained from engineering handbooks, (2) for example.

The differential Equation [2], when combined with Equations [3], [9], [10], and [11], becomes

$$\frac{dP}{d\theta} = \frac{-\gamma P}{f_1 + f_3}\left(\frac{2c\,A_s\,a_0}{\omega\,V_D}\,ZP_0^{(1-\gamma)/2\gamma} + f_3\right) \quad [12]$$

Exhaust-Valve Flow Coefficient c. The exhaust-valve flow coefficient for any given valve lift is determined under steady-flow conditions by measuring the air-flow rate through the valve for a fixed pressure drop across the valve and port. The flow coefficient is then defined as the measured flow rate divided by the calculated rate based upon the nominal valve area. The nominal valve area is the same for all valve lifts and is equal to $\pi D^2/4$. The value of D selected for the valve diameter is immaterial inasmuch as the product $c\,A_s$ used in the calculations is independent of the diameter, provided that the values of c and A_s are based upon the same diameter.

A description of valve flow-test methods and apparatus is given by Wood and others (3). The conventional method for plotting the data produces a curve of valve flow coefficient c against the ratio of valve lift to valve diameter L/D. Such a curve is presented in Fig. 1 for engine A, which is a typical high-speed, poppet-valve aircraft engine. From Fig. 1 a curve of flow coefficient against engine crank angle can be plotted if the variation in valve lift with crank angle is known. Such a curve is plotted in Fig. 2 for engine A.

The flow coefficients obtained under steady-flow conditions

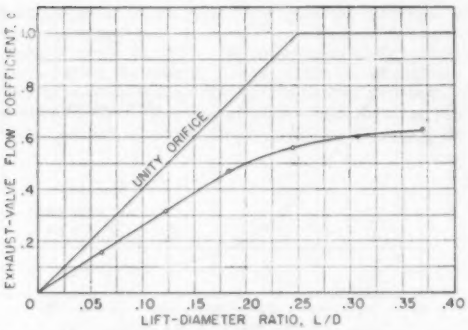

FIG. 1 CHANGE IN EXHAUST-VALVE FLOW COEFFICIENT WITH LIFT-DIAMETER RATIO
(Engine A; nominal valve diameter, 1.625 in.)

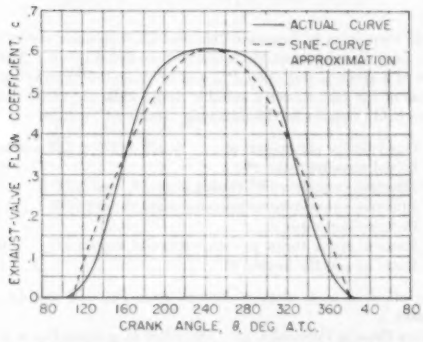

FIG. 2 COMPARISON OF ACTUAL EXHAUST-VALVE FLOW-COEFFICIENT CURVE WITH SINE-CURVE APPROXIMATION; ENGINE A

can be used to calculate the pressure ratio P, during the exhaust process (intermittent-flow conditions) because (*a*) the steady and intermittent-flow coefficients of poppet valves are not appreciably different (4) (except for low pressure drops across the valve and port, in which case the magnitude of the flow coefficient is unimportant anyway); and (*b*) the flow coefficients of exhaust valves do not vary appreciably with the pressure drop across the valve (5).

In order to express the variation in exhaust-valve flow coefficient with engine crank angle, a sine-curve approximation for the exhaust-valve flow coefficient can be fitted closely to the actual flow-coefficient curve of nearly all high-speed, four-stroke, reciprocating engines. For those few engines with a variation in exhaust-valve flow coefficient that cannot be approximated by a sine curve, the quantitative results of this analysis do not apply, although most of the trends and conclusions probably do. In order to fit the sine curve to the actual flow-coefficient curve, it is assumed as follows:

1 The value of the flow coefficient at the maximum valve lift is the same in both cases.

2 The total area under the curve of flow coefficient plotted against crank angle is the same in both cases.

From assumption 1

$$c = c_{max} \sin\left[\pi\left(\frac{\theta - \theta_b}{\theta_e - \theta_b}\right)\right] \quad [13]$$

The values of the "effective" opening and closing angles θ_b and θ_e, respectively, depend upon assumption 2, and upon the "actual" opening and closing angles θ_b' and θ_e'. The values of θ_b and θ_e for a specific engine are found as follows:

The area under the curve of the actual flow coefficient plotted against crank angle is

$$\text{area} = c_{avg}'\,(\theta_e' - \theta_b') \quad [14]$$

where c_{avg}' is the average flow coefficient (6). From Equation [13] the area under the approximate flow-coefficient curve is

$$\text{area} = \int_{\theta_b}^{\theta_e} c_{max} \sin\left[\pi\left(\frac{\theta - \theta_b}{\theta_e - \theta_b}\right)\right] d\theta$$

$$= \frac{2}{\pi}\, c_{max}\,(\theta_e - \theta_b) \quad [15]$$

From assumption 2 the two areas given by Equations [14] and [15] are equal so that

$$\theta_e - \theta_b = \frac{\pi}{2}\,\frac{c_{avg}'}{c_{max}}\,(\theta_e' - \theta_b') \quad [16]$$

For a symmetrical cam

$$\theta_b = \theta_b' + \frac{(\theta_e' - \theta_b') - (\theta_e - \theta_b)}{2} \quad [17a]$$

and

$$\theta_e = \theta_e' - \frac{(\theta_e' - \theta_b') - (\theta_e - \theta_b)}{2} \quad [17b]$$

By substitution of Equation [16] into Equations [17*a*] and [17*b*]

$$\theta_b = \theta_b' + \frac{(\theta_e' - \theta_b')}{2}\left(1 - \frac{\pi}{2}\,\frac{c_{avg}'}{c_{max}}\right) \quad [18a]$$

and

$$\theta_e = \theta_e' - \frac{(\theta_e' - \theta_b')}{2}\left(1 - \frac{\pi}{2}\,\frac{c_{avg}'}{c_{max}}\right) \quad [18b]$$

In order to apply the numerical results of this analysis to a specific engine, knowledge of the valve timings θ_b' and θ_e' and the coefficients c_{avg}' and c_{max} is necessary. A comparison of the actual flow-coefficient curve with the approximate flow-coefficient curve given by Equation [13] is shown in Fig. 2 for engine A. It will be noted that the actual and the effective opening and closing angles are nearly equal.

By substitution of Equation [13], the differential Equation [12] finally becomes

$$\frac{dP}{d\theta} = \frac{-\gamma P}{f_1 + f_2}\left\{Z\,\frac{P_0^{(1-\gamma)/2\gamma}}{\varphi}\sin\left[\pi\left(\frac{\theta - \theta_b}{\theta_e - \theta_b}\right)\right] + f_2\right\} \quad [19]$$

where the gas-velocity parameter φ is defined as

$$\varphi = \frac{\omega\, V_D}{2\, c_{max}\, A_v\, a_0} \quad [20]$$

NUMERICAL PROCEDURE AND ACCURACY OF RESULTS

The variation of pressure ratio P, with crank angle θ, is determined by the differential Equation [19]. This equation cannot be integrated directly, and an approximate point-by-point solution is necessary. The change in P with θ, obtained from

Equation [19], is multiplied by a small angular increment $\Delta\theta$ to obtain the change in pressure ratio ΔP that occurs during the angular increment. The resulting pressure $(P + \Delta P)$ at the new angle $(\theta + \Delta\theta)$ is therefore obtained and the new slope $(dP/d\theta)$ at the new angle can be calculated by Equation [19]. This procedure is repeated from the effective exhaust-valve opening angle to 340 deg ATC. (The pressure ratio P_{340} has been selected in this analysis as indicative of the effectiveness of the exhaust process.)

An angular increment $\Delta\theta$ equal to 10 deg was used in the approximate numerical solution of Equation [19] (except during the first 10 deg of valve opening, during which period smaller angular increments were used). The effect of the magnitude of $\Delta\theta$ upon the calculated value of P_{340} is indicated in Fig. 3.

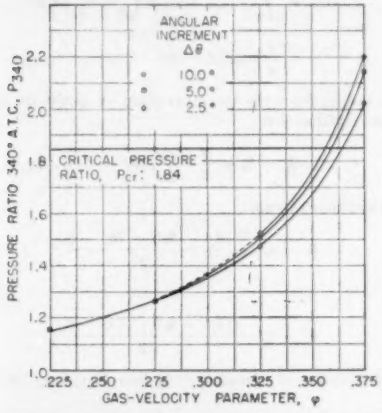

FIG. 3 EFFECT OF ANGULAR INCREMENT USED IN POINT-BY-POINT SOLUTION ON PRESSURE RATIO 340 DEG ATC

(Effective opening angle, 110 deg ATC; effective closing angle, 5 deg ATC; initial pressure ratio, 9.33; compression ratio, 7.5.)

For low values of φ the error in P_{340} for $\Delta\theta$ equal to 10 deg is of no consequence. However, for high values of φ, which result in high values of P_{340}, the error in P_{340} for $\Delta\theta$ equal to 10 deg is significant although not important (with regard to the order of magnitude of P_{340}). In general, large values of P near the end of the exhaust stroke result in large changes in P with θ; this condition, for $\Delta\theta$ as large as 10 deg, results in values of P_{340} somewhat lower than would be obtained by an exact solution of Equation [19].

A sample calculation is plotted in Fig. 4 for engine A, using both the actual and the approximate values of the flow coefficient as plotted in Fig. 2. No significant difference in the curves exists and the values of P_{340} are the same. Some difference might have been expected at 340 deg ATC had the effective closing angle θ_c occurred closer to top center, in which case the discrepancy between flow coefficients would have been greater for the crank angles just ahead of 340 deg ATC, as indicated in Fig. 2.

RESULTS AND DISCUSSION

In this analysis the effectiveness of the exhaust process is indicated by the calculated pressure ratio 340 deg ATC (P_{340}). The lower this pressure ratio, the more effective is the exhaust process. (The angle 340 deg ATC was selected rather than top center because, in general, the intake valve is not open or has not been open sufficiently long at 340 deg ATC to affect the calculated value of the pressure ratio.)

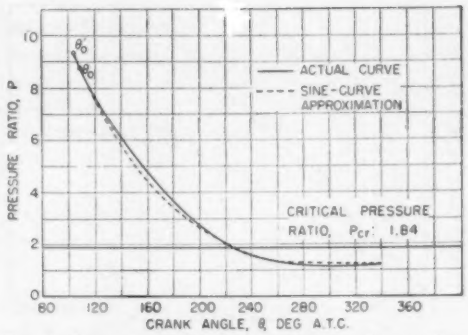

FIG. 4 COMPARISON OF CALCULATED PRESSURE RATIOS USING ACTUAL AND APPROXIMATE EXHAUST-VALVE FLOW COEFFICIENTS FOR ENGINE A

(Effective opening angle, 109 deg ATC; effective closing angle, 21 deg ATC; initial gas-pressure ratio 9.33 at the actual opening angle, 104 deg ATC; compression ratio, 7.5; gas-velocity parameter, 0.296.)

An inspection of Equation [19] and its derivation shows that P_{340} must depend upon the seven factors listed below. The effect of a given factor upon P_{340} was investigated by varying the value of the factor over a suitable range while the other factors were held constant at the following "standard" values:

1 Gas-velocity parameter, φ ..... 0.225, 0.275, 0.325, and 0.375
2 Initial pressure ratio, P_0 ..... 9.33
3 Effective exhaust-valve closing angle, θ_c, deg ATC 5
4 Effective exhaust-valve opening angle, θ_b, deg ATC 110
5 Compression ratio, r 7.5
6 Ratio of crank throw to connecting-rod length, s/l 0.25
7 Ratio of specific heats, γ 1.31

The effect of each of these factors upon P_{340} will now be discussed.

Gas-Velocity Parameter, φ. The effect of φ upon P_{340} is given in Figs. 5 to 7. This effect is shown to be important and in all cases increased values of φ result in increased values of P_{340}.

The importance of φ is demonstrated if c_{max} (in Equation [20]) is replaced by its equivalent, $(\pi/2)c_{avg}$, where c_{avg} is the average flow coefficient for the sine-curve approximation. If this substitution is made, Equation [20] becomes

$$\varphi = \frac{S\,A_p}{a_0\,c_{avg}\,A_v} \qquad [20a]$$

where

$$S\,A_p = \frac{\omega}{\pi}\,V_D$$

in which S is the average piston speed and A_p is the piston area. The gas-velocity parameter in this form (Equation [20a]) has been found to have an important effect upon volumetric efficiency when applied to the intake process (6, 7). It is reasonable that it should be important when applied to the exhaust process.

From Equation [20a], φ appears to have the characteristics of a Mach number (gas velocity divided by the speed of sound) in which $S[A_p/(c_{avg}\,A_v)]$ is considered to be an average (hypothetical) gas velocity through the exhaust valve during the exhaust stroke.

Representative values of the gas-velocity parameter φ are given in Table 1 for several military aircraft engines at take-off

speeds (maximum engine speed). The values are based upon a value for a_0 of 2500 fps.

Initial Pressure Ratio, P_0. The effect of the initial pressure ratio on P_{340} is given in Fig. 5. The range of P_0 is considered sufficient to cover conditions encountered in throttled engines (low values of P_0) and in supercharged engines (high values of P_0). From an analysis of various indicator cards, the standard value

TABLE 1 GAS-VELOCITY PARAMETERS FOR SEVERAL MILITARY AIRCRAFT ENGINES AT TAKE-OFF SPEED

Engine	Average piston speed S, fps	Ratio of piston area to exhaust-valve area, A_p/A_v	Average flow coefficient for sine curve approximation c_{av_E}	Gas-velocity parameter, φ
A	50.0	5.72	0.387	0.296
B	47.7	4.04	0.280	0.275
C	46.7	4.90	0.314	0.292

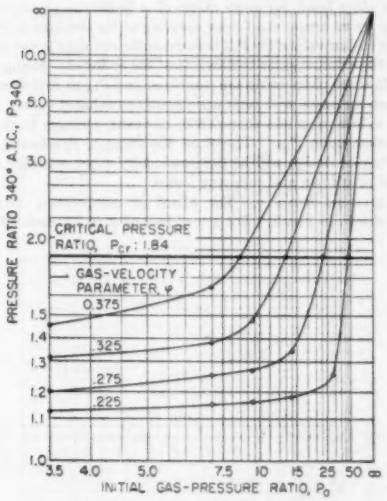

(a) Effective closing angle, θ_c, 5 deg ATC

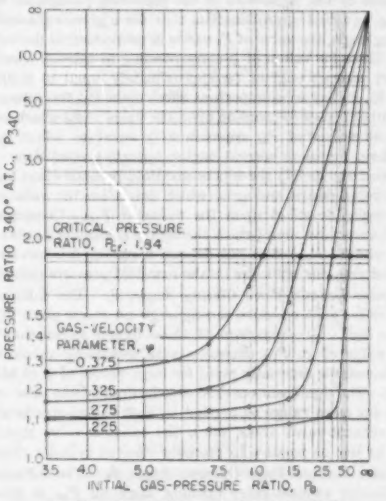

(b) Effective closing angle, θ_c, 20 deg ATC

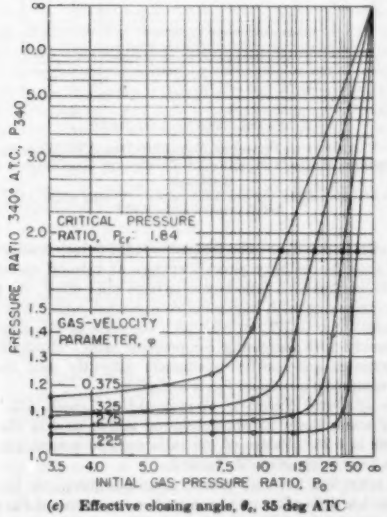

(c) Effective closing angle, θ_c, 35 deg ATC

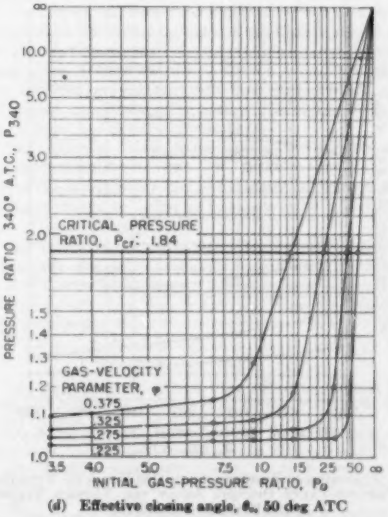

(d) Effective closing angle, θ_c, 50 deg ATC

FIG. 5 VARIATION IN PRESSURE RATIO 340 DEG ATC WITH INITIAL-PRESSURE RATIO FOR VARIOUS VALUES OF GAS-VELOCITY PARAMETER

(Effective opening angle, 110 deg ATC; compression ratio, 7.5)

of 9.33 for P_0 at 110 deg ATC was estimated to correspond to a value of P_m (ratio of intake-manifold pressure to exhaust pressure) roughly equal to 1.6.

From Figs. 5(*a*) to 5(*d*) it appears that, for the lowest gas-velocity parameters (0.225 and 0.275), P_0 has only a small effect on P_{340} for values of P_0 up to 12 or higher (depending upon the value of θ_0), which corresponds to values of P_m approximately equal to 2.1 or higher. (This value of P_m was obtained from the value of 1.6, mentioned in the preceding paragraph, by assuming, as a first approximation, that for a given exhaust-valve opening angle, the value of P_0 varies in proportion to the value of P_m). Even for values of φ corresponding to take-off speeds for military aircraft engines (φ approximately equal to 0.300, see Table 1), P_0 has an unimportant effect upon P_{340} for values of P_0 up to 10 or higher (depending upon the value of θ_0) which corresponds to values of P_m approximately equal to 1.7 or higher. Therefore, for most current engine operating conditions ($\varphi \leq 0.300$ and $P_m \leq 1.7$) the intake-manifold pressure ratio and the intake-valve design and area, which determine the value of P_0, have negligible effect upon the value of P_{340}. Consequently, the exhaust-valve area (which through φ is selected to give a desired value of P_{340}) does not depend upon the intake-valve design and area nor upon the intake-manifold pressure ratio P_m.

Effective Exhaust-Valve Closing Angle, θ_c. The influence of the effective exhaust-valve closing angle on P_{340} is given in Figs. 5(*a*) to 5(*d*). A comparison of these figures shows that for a given value of φ, P_{340} decreases with increasing values of θ_c. This decrease is especially rapid for large values of φ (0.325 and 0.375). The significant conclusion to be drawn from these curves is that for large values of φ (that is, high engine speeds and/or small exhaust-valve areas, etc.), the exhaust valve should be closed as late as possible to promote efficient cylinder charging.

Effective Exhaust-Valve Opening Angle, θ_0. The influence of the effective exhaust-valve opening angle on P_{340} is given in Fig. 6. In this figure the value of P_0 is assumed to vary with θ_0 according to

$$P_0 V_0^{\gamma} = \text{const}$$

where P_0 is equal to 9.33, when θ_0 is equal to 110 deg ATC.

For low values of φ (0.225 and 0.275), later opening of the exhaust valve (larger values of θ_0) results in lower values for P_{340} because the exhaust valve is farther open at 340 deg ATC. (Note that the effective exhaust-valve closing angle is fixed.) On the other hand, for large values of φ (higher engine speeds or smaller valve areas, etc.) later opening of the exhaust valve results in higher values for P_{340} because sufficient time is not available for the exhaust gases to flow out of the cylinder. For φ equal to 0.325 these phenomena are combined and P_{340} at first decreases and then increases with later opening of the exhaust valve.

For values of φ less than 0.350, however, changes in θ_0 have little effect upon P_{340}. Therefore the value of θ_0 selected for a given engine design will be determined by other considerations, such as blowdown and pumping losses.

Compression Ratio, r. The effect of compression ratio on P_{340} is shown in Fig. 7. For low values of φ (0.225 and 0.275), r has no effect upon P_{340}. For φ equal to 0.325 (which is somewhat higher than for military aircraft engines at take-off speed, see Table 1), compression ratio begins to have some effect, the value of P_{340} decreasing with increasing compression ratio. For very high values of φ (0.375, for example), the value of P_{340} decreases considerably with increasing compression ratio. However, for the maximum gas-velocity parameters currently used the effect of compression ratio on P_{340} is negligible.

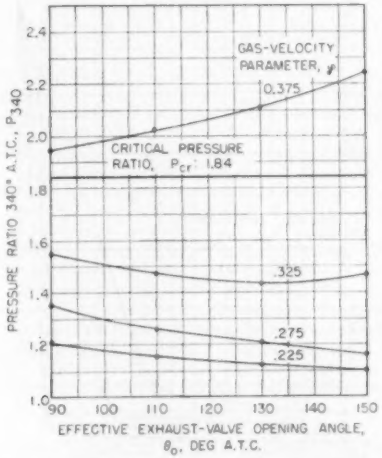

FIG. 6 VARIATION IN PRESSURE RATIO 340 DEG ATC WITH EFFECTIVE EXHAUST-VALVE OPENING ANGLE FOR VARIOUS VALUES OF GAS-VELOCITY PARAMETER

(Effective closing angle, 5 deg ATC; compression ratio, 7.5; initial pressure ratio has been varied with effective exhaust-valve opening angle according to isentropic relation between pressure and volume, value being 9.33 at crank angle of 110 deg ATC.)

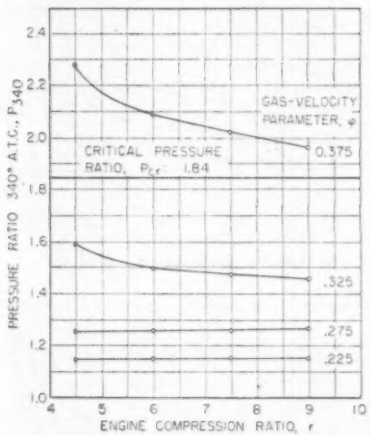

FIG. 7 VARIATION IN PRESSURE RATIO 340 DEG ATC WITH ENGINE COMPRESSION RATIO FOR VARIOUS VALUES OF GAS-VELOCITY PARAMETER

(Effective opening angle, 110 deg ATC; effective closing angle, 5 deg ATC; initial pressure ratio, 9.33.)

Ratio of Crank Throw to Connecting-Rod Length, s/l. The ratio of crank throw to connecting-rod length used in the calculations is 0.25. Values of the ratio used in several military aircraft engines are given in Table 2.

The ratio does not vary greatly among engines and, because the ratio has little effect on piston motion, no curves of P_{340} have been calculated for different values of s/l.

Ratio of Specific Heats, γ. The effect of γ on the pressure ratio P_{340} is shown in Fig. 8 for φ equal to 0.275 and 0.375. For

TABLE 2 RATIO OF CRANK THROW TO CONNECTING-ROD LENGTH FOR SEVERAL MILITARY AIRCRAFT ENGINES

Engine	Crank throw s, in.	Connecting-rod length l, in.	Ratio of crank throw to connecting-rod length, s/l
A	3.000	10.000	0.300
B	3.438	13.750	0.250
C	3.000	12.312	0.244

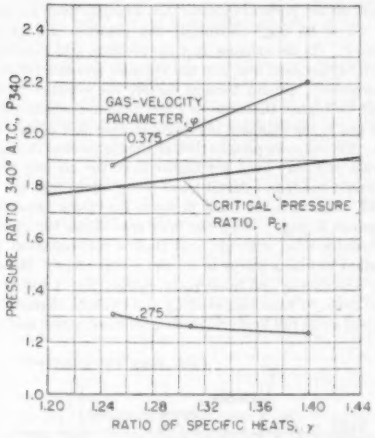

FIG. 8 VARIATION IN PRESSURE RATIO 340 DEG ATC WITH RATIO OF SPECIFIC HEATS FOR TWO VALUES OF GAS-VELOCITY PARAMETER (Effective opening angle, 110 deg ATC; effective closing angle, 5 deg ATC; initial pressure ratio, 9.33; compression ratio, 7.5.)

the lower value of φ, P_{340} decreases slightly with increasing values of γ; and for the higher value of φ, P_{340} increases with increasing values of γ. Therefore, for φ less than 0.325 (approximately) the effect of γ on P_{340} is negligible. The value of 1.31 used in this analysis is approximately the average value of γ for exhaust gases at the temperatures existing during the exhaust process (8).

Importance of Factors Affecting Exhaust Process. As a result of the foregoing analysis, the factors affecting the exhaust process can be classified as important or unimportant for satisfactory cylinder charging, as follows:

(*a*) Important factors that have an appreciable effect upon P_{340} and must therefore be considered when designing for efficient cylinder charging:

1 Gas-velocity parameter, φ.
2 Effective exhaust-valve closing angle, θ_e.

(*b*) Unimportant factors that have a negligible effect upon P_{340} for current engine operating conditions ($\varphi \leq 0.300$):

1 Initial pressure ratio, P_0 (except for high values of P_0, that is, for highly supercharged engine, $P_m \geq 1.7$).
2 Effective exhaust-valve opening angle, θ_0
3 Compression ratio, r.
4 Ratio of crank throw to connecting-rod length, s/l.
5 Ratio of specific heats, γ.

Recommended Value of Gas-Velocity Parameter, φ. The gas-velocity parameter φ, interrelates the exhaust-valve size with the engine speed, the displacement volume, and the exhaust-valve flow coefficient at maximum valve lift. Thus, if a maximum value of φ can be recommended, the minimum exhaust-valve size for a given engine speed can be determined.

The maximum allowable value of φ depends upon the allowable value of P_{340}, which for satisfactory cylinder charging depends upon the value of P_m. The greater the value of P_m (that is, the higher the supercharging), the greater the allowable value of P_{340} without appreciable adverse affects upon volumetric efficiency. Also, for a given value of P_{340} the value of φ depends upon θ_e (see Fig. 5). However, it appears from the calculated results of this analysis, that the value of P_{340} increases rapidly for values of φ greater than 0.325. The recommendation is therefore made that the maximum value of φ be no higher than 0.325 and that the desired value of P_{340} be obtained for this value of φ by selecting the proper value of θ_e.

APPLICATION OF RESULTS

The computed results of this analysis can be used to estimate the pressure ratio at 340 deg ATC for any four-stroke reciprocating engine (provided the exhaust manifold is sufficiently large or the exhaust pipes sufficiently short that the exhaust-manifold pressure remains constant during the exhaust process). The pressure ratio P_{340} is of interest because high values indicate high cylinder back pressures at intake-valve opening and therefore may explain low values of volumetric efficiency.

As an example, the pressure ratio in engine A at 340 deg ATC during the exhaust stroke will be estimated (from the plots) for P_0 equal to 9.33 and for an engine speed of 3200 rpm. Under these conditions the value of φ is 0.316. Also, θ_e', is 26 deg ATC, θ_0' is 104 deg ATC, c_{avg}' is 0.373 (compared with 0.387 for c_{avg}, see Table 1), and c_{max} is 0.608, so that θ_e computed by Equation [18*b*] is 21 deg. From 5(*b*) the calculated value of P_{340} is found to be 1.22. (The value of θ_0 is not considered, because this analysis has shown it to have a negligible effect upon P_{340}.)

CONCLUSIONS

As a result of this analysis, the following conclusions are drawn:

1 The factors that have an important effect upon the pressure ratio near the end of the exhaust stroke are the gas-velocity parameter and the effective exhaust-valve closing angle.

2 The factors that have an unimportant effect upon the pressure ratio near the end of the exhaust stroke (for current engine operating conditions) are the initial pressure ratio at the effective opening angle (which, however, does become important for highly supercharged engines), effective exhaust-valve opening angle, engine compression ratio, ratio of crank throw to connecting-rod length, and ratio of specific heats.

3 The maximum value recommended for the gas-velocity parameter is 0.325.

4 For large values of the gas-velocity parameter, the exhaust valve should be closed as late as possible to promote efficient cylinder charging.

5 For most current engine operating conditions the correct exhaust-valve area does not depend upon the intake-valve area.

6 For most current engine operating conditions the correct exhaust-valve area does not depend upon the intake-manifold pressure ratio.

BIBLIOGRAPHY

1 "An Analysis of the Factors That Affect the Exhaust Process of a Four-Stroke-Cycle Reciprocating Engine," by J. D. Stanitz, NACA Technical Note No. 1242, 1947.

2 "Mechanical Engineers' Handbook," by L. S. Marks, fourth edition, McGraw-Hill Book Company, Inc., New York, N. Y., 1941.

3 "Air Flow Through Intake Valves," by G. B. Wood, Jr., D. U. Hunter, E. S. Taylor, and C. F. Taylor, *SAE Journal*, vol. 50, June, 1942, pp. 212–220 and 252.

4 "Steady- and Intermittent-Flow Coefficients of Poppet Intake Valves," by J. D. Stanitz, R. E. Lucia, and F. L. Masselle, NACA Technical Note No. 1035, 1946.

5 "Study of Exhaust-Valve Design From Gas Flow Standpoint."

by Seng-Chiu Hu, *Journal of the Aeronautical Sciences*, vol. 11, 1944, pp. 13–20.

6 "The Effect of Inlet-Valve Design, Size, and Lift on the Air Capacity and Output of a Four-Stroke Engine," by J. C. Livingood and J. D. Stanitz, NACA Technical Note No. 915, 1943.

7 "Effect of Changing Manifold Pressure, Exhaust Pressure, and Valve Timing on the Air Capacity and Output of a Four-Stroke Engine Operated With Inlet Valves of Various Diameters and Lifts," by J. C. Livingood and J. V. D. Eppes, NACA Technical Note No. 1366, 1947.

8 "Thermodynamic Data for the Computation of the Performance of Exhaust-Gas Turbines," by Benjamin Pinkel and L. R. Turner, NACA Wartime Report No. E-23, 1945.

Discussion

P. H. Schweitzer.[3] The author has performed an interesting mathematical analysis of the exhaust process which permitted him to draw some significant conclusions. There is some question as to how accurate and how generally valid those conclusions are. In the absence of apparent mathematical errors the results are believed to be accurate within the validity of the original assumptions. The writer has no objection to the three assumptions listed by the author, but does question the realism of one silent and one semisilent assumption.

The silent assumption is that during the exhaust process the pressure in the cylinder is uniform, i.e., the same at every part of the cylinder at any given instant. This assumption abrogates the existence of the so-called Kadenacy effect or, specifically, the kinetic energy of the gas column inside of the cylinder. That, in general, cannot be considered negligible. It is frequently so pronounced that it produces a considerable vacuum in the cylinder during the exhaust process.[4] The Kadenacy effect is predicated upon the existence of a pronounced pressure gradient within the cylinder, the magnitude of which, in turn, depends on the rate of opening of the exhaust valve. The latter is admittedly slower in four-stroke-cycle engines, but surely not negligible. The latest Kadenacy-type engine that has been developed by Worthington has exhaust valves that do not differ substantially from four-stroke-cycle valves.

The other assumption is that the pressure in the exhaust pipe is constant during the exhaust process. This may be called a semisilent assumption because a remark following assumption 3 refers to it. In no practical engine can it be assumed that the pressure in the exhaust pipe remains constant. In the exhaust pipe of a single-cylinder engine the pressure fluctuates more or less as a sine curve between positive and negative pressures due to the fundamental and reflected pressure waves.[5] In a multicylinder engine the reflected pressure waves are fairly well dissipated, but a still worse disturbance is encountered, namely, the interference from neighboring cylinders.

Take the case of an 8-cylinder engine where the exhaust blowdown in cylinder x is followed by a blowdown in cylinder $(x + 1)$. Both exhaust branch pipes connect with a common manifold. Shortly after the blowdown of cylinder x started and is in good progress, the adjacent cylinder blows down and sends a puff of exhaust into the branch pipe of cylinder x. The blowdown process gets interrupted and reversed by this blowdown in cylinder $(x + 1)$. What happens can be visualized from Fig. 9 of this discussion, which refers to an 8-cylinder two-stroke-cycle engine with a firing order of 1-6-5-2-8-3-4-7. If each cylinder would exhaust through a separate well-tuned exhaust pipe, each cylinder would have exhaust and cylinder pressure fluctuations as shown by the lines marked "without interference," which are satisfactory. However, if the cylinders exhaust into a common manifold, all the cylinders will not behave alike. Consider for instance, cylinder No. 3. Shortly after its exhaust blows down, (exactly 45 deg crank angle later) the adjacent cylinder No. 4 blows down. The pressure wave that is generated finds the exhaust and intake ports of cylinder No. 3 largely open for the next 140 — 45 = 95 deg. Naturally the pressure will propagate right into it. In the exhaust duct the pressure gets a sudden kick as shown by the solid line, and the cylinder pressure follows suit. In consequence, around bottom center, the exhaust-duct pressure will be higher than the cylinder pressure which will force exhaust gas in the cylinder, involving reverse flow in the exhaust branch. The cylinder pressure is high during most of the scavenging period and may even get higher than the air box pressure, which would result in exhaust gases being forced into the intake manifold. The exhaust back pressure fluctuates between plus 4 and minus 3 psig. When the inlet port closes the cylinder is only partially filled with air, and that is contaminated by the combustion products swept in by the reverse flow. Because of its poor scavenging and inadequate charge, No. 3 will be a hot cylinder liable to have ring-sticking and cylinder deposits. The shortage of air at full load will cause poor combustion and smoke.

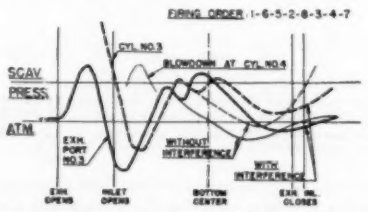

Fig. 9 Pressure Fluctuations During Exhaust

One may think that conditions are not that bad in a four-stroke-cycle engine where the piston pushes out the exhaust. However, under certain conditions, they can be even worse. During deceleration and going downhill, the butterfly is almost closed. The combustion pressure rise is very small. Consequently there will be a vacuum in the cylinder during part of the exhaust period. In a popular eight-in-line engine, No. 4 and No. 3 exhaust valves are open simultaneously for a period of about 80 crank deg. Obviously, the exhaust of cylinder No. 4 will blow straight into cylinder No. 3. It is even sucked in by the prevailing vacuum. And that is not all! There is a valve overlap of 38 crank deg, during which the inlet valve is also open. At the time the No. 4 piston is at bottom center, No. 4 and 3 exhaust valves and No. 3 intake valve are open. So the exhaust of cylinder 4 blows into cylinder 3, through the cylinder, through the intake valve, into the carburetor. Instead of running on air the car is running on exhaust gas.

The answer to these anomalies is the proper shaping of the exhaust manifolds. We have been studying exhaust manifolds for the Navy for 3 years and have learned a great deal which will be reported on in due time. We have developed aspirator-type manifolds that create, instead of a back pressure, a vacuum in the exhaust ports, and, instead of bucking, they help scavenge the cylinder. Some of these manifolds give better performance than no manifold at all.

Coming back to the present paper, the writer wonders why the author restricted his analysis to four-stroke-cycle engines. His

[3] Professor of Engineering Research, The Pennsylvania State College, State College, Pa. Mem. ASME.

[4] "Taking the Mystery Out of the Kadenacy System of Scavenging Diesel Engines," by P. H. Schweitzer, C. W. Van Overbeke, and L. Manson, Trans. ASME, vol. 68, 1946, pp. 729–734.

[5] "Exhaust Pipe Phenomena," by G. F. Mucklow, The Manchester Association of Engineers, vol. 21, 1942; abstract *The* (British) *Motorship*, January, 1943.

analysis is equally applicable to two-stroke-cycle engines, except that the consequences of the cited simplifying assumptions then become more conspicuous. On the other hand, to derive his general conclusions, he could have used a constant flow coefficient for the exhaust valve of approximately 0.63, as can be seen from his Fig. 1, by dividing the lower line with the upper line.

C. F. TAYLOR.[6] The relation of valve capacity to engine performance is so important and has received so little intelligent attention, that this paper is a welcome addition to the meager literature on this subject.

Although work done at M.I.T.[7] indicates that computed pressure losses through poppet valves (based on steady-flow coefficients) agree well with pressures measured in actual engine operation, some engine measurements compared with the computed results given in the paper would be valuable. In this connection, Fig. 10 of this discussion, based upon recent work at M.I.T., should be of interest. This figure shows actual measurements of volumetric efficiency as a function of the exhaust-valve parameter ϕ as defined in the subject paper.

The tests forming the basis of Fig. 10 were made with exhaust valves of various sizes at various lifts, and apparently correlate well on the basis of the flow parameter ϕ, regardless of how a given value of this parameter was obtained. These curves show maximum volumetric efficiency at values of ϕ at or below that recommended as a maximum by the author. This agreement helps to confirm the computations and also indicates that pressure ratio at 340 deg is a good indication of the influence of the exhaust process on volumetric efficiency.

With 50-deg valve overlap and a ratio of inlet-to-exhaust pressure greater than 1, the high volumetric efficiencies shown in Fig. 10 at low values of ϕ, are due to flow of fresh mixture through the exhaust valve during the overlap period and should not be interpreted as indicating a proportionate increase in air available for combustion. Bearing this in mind, the curves with overlap indicate a maximum desirable value of ϕ about as recommended by the author.

For the tests shown in Fig. 10, the inlet-valve flow capacity, A_iC_{max}, was made larger than the flow capacity of the largest exhaust valve at its highest lift. This condition was purposely chosen so that inlet-valve effects would be minimized. In this connection, it should be emphasized that conclusion 5 of the paper, to the effect that the correct exhaust-valve area does not depend upon the inlet-valve area, applies only to the range of valve sizes in general use. For example, it is obvious that if the inlet-valve flow capacity is very small, little will be gained by providing a large exhaust-valve capacity. Eppes, Livengood, and Taylor[8] give some information on the effects of varying the ratio of inlet-to-exhaust-valve flow capacity, but more work on this problem is needed.

Another point to be remembered is that exhaust-valve capacity affects not only volumetric efficiency, but also the mean effective pressure lost between the point of exhaust-valve opening and the beginning of the inlet stroke. This loss in pressure can be computed and also can be measured from an indicator card. It could be expressed conveniently as the ratio of lost mean effective pressure to cylinder pressure at exhaust-valve opening. In cases where the lost mean effective pressure is large, the conditions which give lowest pressure at 340 deg might not be the conditions giving optimum engine performance. Curves of lost mep/P_b, for the conditions covered by the paper, would be of great interest.

T. C. TSU.[9] In 1943 the writer analyzed the inlet and exhaust processes of four-stroke-cycle engines, and the findings were

[6] Professor of Automotive Engineering, Massachusetts Institute of Technology, Cambridge, Mass.

[7] "A Mathematical Analysis of the Intake and Exhaust Processes of the Internal Combustion Engine," by Tsung-Chi Tsu, Thesis, M.I.T. Library, 1944.

[8] "The Effect of Changing the Ratio of Exhaust-Valve Flow Capacity to Inlet-Valve Flow Capacity on Volumetric Efficiency and Output of a Single-Cylinder Engine," by J. V. D. Eppes, J. C. Livengood, and C. F. Taylor, NACA Technical Note No. 1365, October, 1947.

[9] Associate Professor of Engineering Research, The Pennsylvania State College, State College, Pa. Mem. ASME.

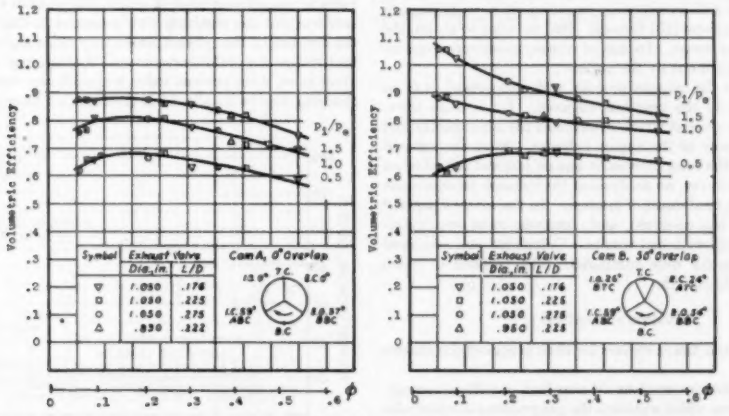

FIG. 10 EFFECT OF EXHAUST-VALVE CAPACITY ON VOLUMETRIC EFFICIENCY—C.F.R. ENGINE, $3^1/_4 \times 4^1/_2$

(Compression ratio = 4.92; inlet valve 1.40 in. OD, 0.277 in. lift, $AC_{avg} = 0.404$; $T_i = 120$ F, $p_e = 30$ in. Hg abs, $F = 0.078$, best power spark advance Data from "Effect of Exhaust-Valve Lift and Size on Volumetric Efficiency," thesis by D. H. Frantz, Jr., 1948, on file in M.I.T. Library.)

subsequently published.[10] Although the author used a somewhat different approach, his Equation [12], except for notation and arrangement, is the same as the writer's equation of the exhaust process.[10] It is gratifying that the author has presented his paper before the Society, for, in the writer's opinion, it is highly desirable that such theoretical analysis should be brought to the attention of the practical engine designer in an acceptable manner.

According to the writer's investigations, Equation [5a] in the author's paper is unnecessary. It is a common belief that the gas velocity through an engine valve cannot exceed the local velocity of sound, which occurs at the "throat" of a gas stream when the pressure ratio becomes equal to or greater than the critical pressure ratio

$$\left(\frac{\gamma+1}{2}\right)^{\gamma/(\gamma-1)}$$

γ being the ratio of specific heats. While this is true in the case of the inlet valve, it is not so in the case of the exhaust valve where the gases are forced out by the cylinder pressure during blowdown.

In the exhaust stream, the "throat" does not necessarily occur at the valve. When the critical pressure ratio is exceeded, the throat occurs ahead of the valve, and the velocity at the valve becomes supersonic. In the writer's work,[10] many exhaust processes were calculated without imposing any condition such as the author's Equation [5a], and the calculated indicator diagrams were almost in perfect agreement with the experimental ones. Earlier work by the writer[11] indicated that when a condition such as the author's Equation [5a] was used in the calculations, the agreement between calculated and experimental indicator diagrams was much inferior. Further discussion of this point can be found in Appendix C of the later paper.[10]

With respect to the variation of exhaust-valve flow coefficient with crank angle, the author has used a sine curve to approximate the actual curve. This does not appear to be necessary. Since the calculation has to be done point by point, the use of a sine curve does not simplify the calculations. As a matter of fact, it complicates the calculations since one would have to go through the author's Equations [13] through [18b] in order to obtain the approximated sine curve. Its use, of course, introduces some inaccuracies as pointed out by the author.

The analysis of the exhaust process, while important, is of no immediate value to the practical engineer. He is more interested in the inlet process which determines the air capacity and volumetric efficiency of the engine cylinder. Since the exhaust process precedes the inlet process, it has an indirect influence on air capacity. However, an analysis of the exhaust process alone does not yield the final result of interest. In the writer's paper,[10] the inlet process was analyzed, and numerous cases were calculated and compared with test results. Calculated and measured volumetric efficiencies were compared. The problem of valve overlap was also dealt with.

Author's Closure

The author thanks the reviewers for their prepared discussions of this paper.

Professor Schweitzer questions "the realism of a silent assumption" in the analysis which supposes the gas pressure is essentially uniform throughout the cylinder at any given instant during the exhaust stroke, and which thereby ignores the Kadency effect. The Kadency effect, as Professor Schweitzer points out, results from the kinetic energy of the moving gas column in the cylinder and this kinetic energy becomes significant only for large ratios of effective valve area to piston area and for very rapid rates of valve opening. In four-stroke reciprocating engines it appears that both of these conditions are lacking and the Kadency effect need not be considered.

Professor Schweitzer also questions the realism of one "semi-silent assumption" that supposes the exhaust-manifold pressure remains "approximately" constant during the exhaust stroke. As stated in the paper this assumption requires that the exhaust pipe be sufficiently short (and this was intended to imply short, individual exhaust stacks at each exhaust valve) or the exhaust manifold must be sufficiently large (and this was intended to imply large "volume," so that the exhaust manifold acts much like a surge tank). While these exhaust-manifold design characteristics do not exist in a great many engine installations at present, it is suggested that these characteristics are realistic, practical, and desirable for many engine installations and that many of the difficult manifold problems which Professor Schweitzer has been studying for the last 3 years could be avoided by using the above mentioned exhaust-manifold design characteristics. For unsupercharged engines these exhaust-manifold design characteristics establish, in effect, exhaust conditions corresponding to no manifold at all; a desirable condition, as Professor Schweitzer implies in his discussion. The author looks forward to reports on the interesting work that Professor Schweitzer is now doing on the exhaust-manifold problem.

The experimental data presented by Professor Taylor in Fig. 10 are a valuable contribution to the subject of the paper.

As requested by Professor Taylor, the following additional information is reported concerning the lost mean effective pressure due to blowdown and pumping losses:

The optimum exhaust-valve opening angle from the viewpoint of cylinder charging may not be the optimum exhaust-valve opening angle for power output. At low engine speeds, if the exhaust valve is opened near bottom center, the cylinder charging may be excellent but the resulting high pressures in the cylinder during the first half of the exhaust stroke may cause high pumping losses that reduce the brake horsepower. At high engine speeds, on the other hand, if the exhaust valve is opened very early, the cylinder charging may be excellent but the resulting blowdown losses dur-

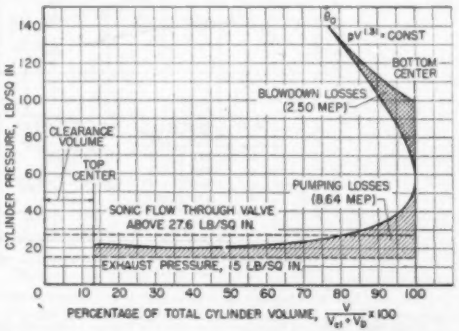

Fig. 11 Change in Cylinder Pressure With Percentage of Total Cylinder Volume Showing Blowdown and Pumping Losses

(p_x, 15 psi; θ_x, 5 deg ATC; p_0, 140 psi; θ_0, 110 deg ATC; φ, 0.325; r, 7.5.)

[10] "Theory of the Inlet and Exhaust Processes of Internal Combustion Engines," by Tsung-Chi Tsu, NACA Technical Note No. 1446.

[11] "A Mathematical Analysis of the Intake and Exhaust Processes of the Internal Combustion Engine," by Tsung-Chi Tsu, ScD thesis, Massachusetts Institute of Technology, 1944.

ing the last half of the power stroke may reduce the brake horsepower.

The blowdown losses and the pumping losses are indicated in Fig. 11. These losses have been obtained from the calculated p against θ curves for an exhaust pressure of 15 psi and are plotted in Figs. 12 and 13. The blowdown losses, which occur between θ_0 and 180 deg, are plotted in Fig. 12. As expected, these losses are higher for the lower values of φ and the earlier exhaust-valve opening angles because more gas escapes from the cylinder under these conditions and less work, therefore, is done by the gases on the piston.

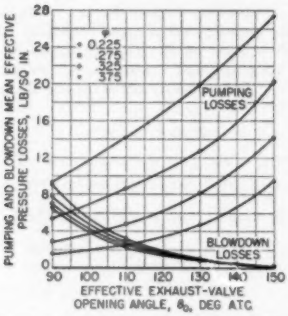

FIG. 12 CHANGE IN PUMPING AND BLOWDOWN LOSSES WITH EXHAUST VALVE OPENING ANGLE
(p_s, 15 psi; θ_s, 5 deg ATC; p_0 equals 140 psi when θ_0 equals 110 deg ATC; r, 7.5.)

The pumping losses, which occur between 180 and 360 deg (exhaust stroke) are also plotted in Fig. 12. As might be expected, these losses are higher for the higher values of φ and for the later exhaust-valve opening angles.

Any change in φ or in θ_0 that decreases the blowdown losses will increase the pumping losses. For each value of φ, therefore, an optimum value of θ_0 must exist for which the losses are a minimum. These optimum values of θ_0 are shown in Fig. 13 in which the total losses (blowdown and pumping) are plotted against θ_0 for various values of φ.

The author does not agree with Professor Tsu's comments concerning supersonic velocity at the valve when the critical pressure ratio is exceeded across the valve. For critical pressure

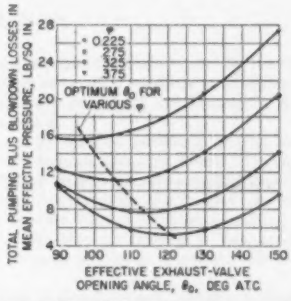

FIG. 13 CHANGE IN TOTAL PUMPING PLUS BLOWDOWN LOSSES DURING THE EXHAUST PROCESS WITH EXHAUST-VALVE OPENING ANGLE
(p_s, 15 psi; θ_s, 5 deg ATC; p_0 equals 140 psi when θ_0 equals 110 deg ATC; r, 7.5.)

ratios sonic velocity always occurs at a throat which has been established by test to exist downstream from the valve seat (just as the throat, or vena contracta, exists downstream from a thin-plate orifice). If the throat is downstream from the valve, the velocity at the valve is subsonic and unaffected by the exhaust manifold pressure when the critical pressure ratio is exceeded across the valve.

Professor Tsu is correct in stating that the sine-curve approximation for the flow coefficient against crank-angle relation is not necessary. Some other curve, more nearly equal to the average of a large number of such curves from typical engines, could have been used. However, to fit this average curve to the curve of a particular engine would still entail a set of equations similar to Equations [13] through [18b].

Design of Lanchester Damper for Elimination of Metal-Cutting Chatter

By R. S. HAHN,[1] WORCESTER, MASS.

A Lanchester damper for eliminating chatter of boring quills is shown. The rate of decay of free vibrations of the quill is found to be of importance in chatter. The free vibrations of a single-degree-of-freedom system with a viscously coupled Lanchester damper attached are analyzed, yielding a chart from which the optimum coupling can be determined. The damping characteristics of thin air films are discussed.

Nomenclature

The following nomenclature is used in the paper:

K = spring constant of quill, lb per in.

$M = \frac{K}{\omega^2}$ = equivalent lumped mass of quill, lb-sec^2 per in.

c = dashpot strength, lb-sec per in.

m = inertia weight mass, lb-sec^2 per in.

x_1, x_2 = co-ordinates of M and m

$\omega = \sqrt{\frac{K}{M}}$ = natural undamped angular frequency, radians per sec

$A_1 = \frac{c(M+m)}{Mm}$

$A_2 = \omega^2$

$A_3 = \frac{c}{m}\omega^2$

s_1, s_2, s_3 = roots of characteristic equation

u = real part of complex root

v = imaginary part of complex root, damped natural frequency

$q = \frac{c}{m}\frac{K}{M} + \frac{2}{27}\left[\frac{c}{m}\left(1+\frac{m}{M}\right)\right]^3 - \frac{1}{3}\frac{K}{M}\frac{c}{m}\left(1+\frac{m}{M}\right)$

$p = \frac{K}{M} - \frac{1}{3}\left[\frac{c}{m}\left(1+\frac{m}{M}\right)\right]^2$

δ = logarithmic decrement

K_1 = const

D = plug diameter, in.

L = plug length, in.

h = radial clearance, in.

α, β, γ = empirical exponents

Introduction

Those who are concerned with the machining of metals with single-pointed tools are often confronted with a self-excited vibration, commonly termed chatter, during the cutting process. This difficulty is especially acute where the rigidity of the tool or work-holding structure is relatively small such as when boring long holes with a single-pointed tool mounted at the free end of a boring bar or quill.

The differential equation governing this phenomenon is apparently still unknown although Arnold (1)[2] has given some attention to the subject of metal-cutting chatter. However, the system behaves somewhat in a manner corresponding to the solutions of van der Pol's or Rayleigh's equation (2). In view of the pronounced effect of damping in these equations we may well expect damping to play an important role in metal-cutting chatter.

The purpose of this paper is to describe a damper for boring quills. The damper described herein is essentially a Lanchester damper with viscous coupling. Brock (3) has given the optimum conditions for the Lanchester damper under forced vibration. The optimum conditions under free vibrations will be given here.

Quill Construction

Fig. 1(*a*) shows a typical quill with the inertia weight fitted into a hole bored in the end of the quill. Fig. 1(*b*) shows the equivalent two-degrees-of-freedom system. The mass M and spring K correspond to the quill (cantilever beam). It has been found that the thin air film surrounding the inertia weight m, behaves essentially viscously and is represented by c in Fig. 1(*b*). The problem consists essentially of finding the value of c that will cause the mass M to have its greatest logarithmic decrement under free vibration.

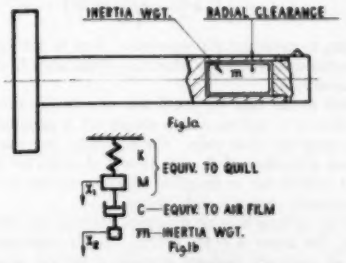

Fig. 1 Diagram of Boring Quill With Lanchester Damper and Equivalent Lumped-Parameter System

Analysis of Lanchester Damper

Writing the dynamical equations for the system shown in Fig. 1(*b*) we get

$$\left.\begin{aligned} M\frac{d^2x_1}{dt^2} + Kx_1 - c\left(\frac{dx_2}{dt} - \frac{dx_1}{dt}\right) &= 0 \\ m\frac{d^2x_2}{dt^2} + c\left(\frac{dx_2}{dt} - \frac{dx_1}{dt}\right) &= 0 \end{aligned}\right\} \quad \ldots\ldots [1]$$

---

[1] Research Engineer, The Heald Machine Company. Mem. ASME.

Contributed by the Production Engineering Division and Research Committees on Metal Cutting Data and Bibliography, and Cutting Fluids, and presented at the Fall Meeting, Worcester, Mass., September 19–21, 1950, of The American Society of Mechanical Engineers.

Note: Statements and opinions advanced in papers are to be understood as individual expressions of their authors and not those of the Society. Manuscript received at ASME Headquarters, March 29, 1950. Paper No. 50—F-11.

[2] Numbers in parentheses refer to the Bibliography at the end of the paper.

Eliminating x_2 gives a third-order equation for the motion of M, which has the following characteristic algebraic equation

$$s^3 + \frac{c(M+m)}{Mm}s^2 + \frac{K}{M}s + \frac{Kc}{Mm} = 0 \quad \text{.....[2a]}$$

or

$$s^3 + A_1 s^2 + A_2 s + A_3 = 0 \quad \text{.....[2b]}$$

Thus the motion of M is given by

$$x_1 = C_1 e^{s_1 t} + C_2 e^{s_2 t} + C_3 e^{s_3 t} \quad \text{.....[3]}$$

For practical values of the coefficients of Equation [2a], one root s_1 will be a negative real number, and s_2 and s_3 will be complex with negative real parts. It turns out for the values encountered in practice that s_1 is large and consequently the first term of Equation [3] disappears very rapidly.

Accordingly, the rate of decay of the mass M is governed essentially by the real part of the complex roots.

Writing the expression for the roots of Equation [2] with the aid of Cardan's formulas we get

$$s_1 = \left[-\frac{q}{2} + \sqrt{\frac{p^3}{27} + \frac{q^2}{4}}\right]^{1/3} + \left[-\frac{q}{2} - \sqrt{\frac{p^3}{27} + \frac{q^2}{4}}\right]^{1/3} - \frac{A_1}{3} \quad \text{.....[4]}$$

$$s_{2,3} = \left(-\frac{1}{2} \pm i\frac{\sqrt{3}}{2}\right)\left[-\frac{q}{2} + \sqrt{\frac{p^3}{27} + \frac{q^2}{4}}\right]^{1/3} + \left(-\frac{1}{2} \pm i\frac{\sqrt{3}}{2}\right)\left[-\frac{q}{2} - \sqrt{\frac{p^3}{27} + \frac{q^2}{4}}\right]^{1/3} - \frac{A_1}{3} \quad \text{.....[5]}$$

Thus the real part of the complex roots is

$$u = -\frac{1}{2}\left(-\frac{q}{2} + \sqrt{\frac{p^3}{27} + \frac{q^2}{4}}\right)^{1/3} - \frac{1}{2}\left(-\frac{q}{2} - \sqrt{\frac{p^3}{27} + \frac{q^2}{4}}\right)^{1/3} - \frac{A_1}{3} \quad \text{.....[6]}$$

We wish to maximize this expression, since it will then correspond to the case where the vibration of the mass M dies out at the greatest rate.

One will notice that the coefficient of s in Equation [2a] is independent of c, and m, and is simply ω^2, a parameter which depends upon the quill only. Consequently, one can consider u as being a function of A_1 and A_3 with A_2 fixed for any given quill. A surface can be imagined which is constructed by plotting u vertically over the A_1A_3-plane.

It will be obvious that no optimum value of the inertia mass m exists; the larger m is the better. On the other hand, there will be an optimum dashpot strength c for any given mass. Consequently, Equation [6] should be maximized with respect to c. This will lead to extremely complicated equations. In order to avoid these, one may differentiate Equation [6] with respect to the coefficient A_3 and equate to zero, which places the following condition on the coefficients A_1, A_2, and A_3

$$\frac{p^3}{27} + \frac{q^2}{4} = 0 \quad \text{.....[7a]}$$

or putting in the values of p and q

$$A_3 = -2\left(\frac{A_1^3}{27} - \frac{A_1A_2}{6}\right) \pm \sqrt{\left(\frac{A_1^3}{27} - \frac{A_1A_2}{6}\right)^2 - \left[\frac{A_2^3}{27} - \frac{1}{3}\left(\frac{A_1A_2}{6}\right)^2\right]} \quad \text{.....[7b]}$$

From physical considerations A_3 must be real. Consequently, the discriminant of Equation [7b] must be positive or zero giving the condition

$$A_1 \geq \sqrt{3A_2} \quad \text{.....[8]}$$

Applying the limiting case with the equal sign in Equation [8] to Equation [7b] gives

$$A_3 = \frac{1}{27}A_1^3 \quad \text{.....[9]}$$

If this equation is plotted on the A_1A_3-plane with logarithmic co-ordinates the straight line labeled $m/M = 8$ results (see Fig. 2). Equation [7b], when plotted, holding the frequency ω constant, generates the two downward diverging branches of the curves shown in Fig. 2. By taking successive values for the frequency, a series of nesting surfaces $u = f(A_1A_3)$ is formed, and the loci of the maxima are indicated as the family of curves shown in Fig. 2.

In practice it usually happens that Equation [8] is not satisfied, which simply means there is no maximum in u with respect to A_3. The function u does, however, have a maximum with respect to the dashpot strength c. Under these conditions the maximum value of u was found by plotting u against c from

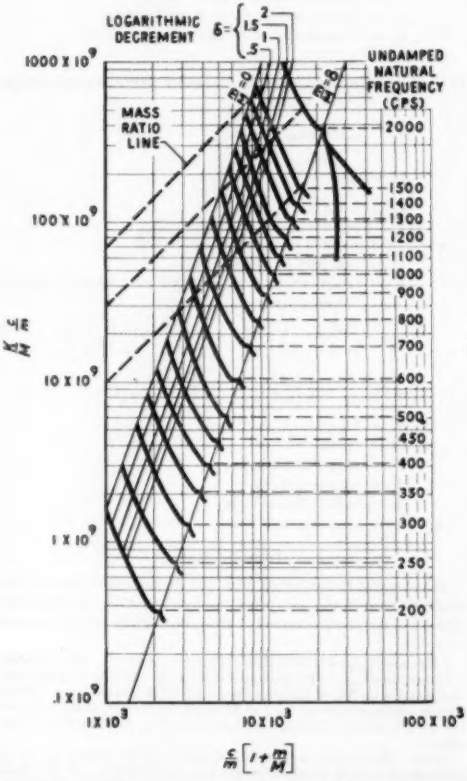

FIG. 2 CHART SHOWING "LOCI OF MAXIMUM DAMPING COEFFICIENT" FOR VARIOUS FREQUENCIES AND INERTIA WEIGHTS

Equation [6] for arbitrary values of the mass ratio m/M from 0 to 8. By virtue of the fact that the ratio A_2/A_1 is independent of c, these plots of u versus c represent a section through the surface $u = f(A_1A_2)$ along a line whose slope is

$$\frac{A_2}{A_1} = \frac{\omega^2}{1 + \frac{m}{M}} \quad \ldots\ldots [10]$$

as shown in Fig. 3 by the white lines radiating from the origin. Connecting the points of maximum altitude (measured along one of the radiating lines) gives the white line in Fig. 3 labeled "locus of maxima with respect to c." The model shown in Fig. 3 was turned upside down in order to cast a shadow and show the topography more clearly, so that the origin is at the upper right-hand corner.

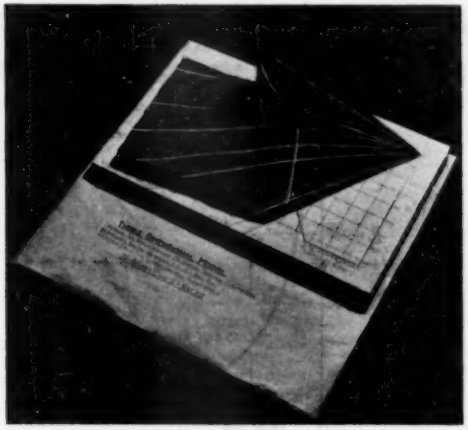

FIG. 3 THREE-DIMENSIONAL MODEL OF SURFACE $u = f(A_1A_2)$ SHOWING RELATION BETWEEN DAMPING COEFFICIENT (ALTITUDE) AND VARIABLES A_1 AND A_2

For each frequency of the quill there corresponds a model similar to that in Fig. 3. If these are nested as mentioned before, and the locus of maxima with respect to c drawn on the A_1A_2-plane, Fig. 2 results. The crevice at the upper left-hand corner of the model, Fig. 3, is represented by the already mentioned downwardly diverging branches of the curves in Fig. 2. The region between these lines represents real roots of Equation [2a] and corresponds to damping in excess of critical damping so that no oscillations occur.

In using the chart, Fig. 2, the characteristics of the K, M system are usually known, and also the largest inertia weight m that will fit in the quill. Consequently the known parameters when inserted into Equation [10] give the slope of the desired radiating white line in Fig. 3. On the logarithmic scale in Fig. 2 this slope corresponds to the ordinate intercept as shown by taking logarithms of Equation [10]. Because of the fact that the abscissa scale starts at 1×10^3 instead of 1, it is necessary to introduce the factor 10^3 in order to find the ordinate intercept, thus

$$\text{Ordinate intercept} = \frac{\omega^2 \times 10^3}{1 + \frac{m}{M}} \quad \ldots\ldots [11]$$

In addition, the slope in Fig. 2 is unity since A_1 and A_2 are to the first power in Equation [10]. Consequently the lines corresponding to the white radiating lines in Fig. 3, are lines having a 45-deg slope in the log-log field of Fig. 2 and the intercept just given. The intersection of one of these "mass-ratio" lines with the curve corresponding to the given frequency determines a point whose abscissa gives the optimum value of A_1, i.e., the value of A_1 for which the vibration of M dies out at the greatest rate. The optimum value of c is immediately calculated from A_1 by

$$c_{\text{optimum}} = \frac{m}{1 + \frac{m}{M}} A_{1_{\text{optimum}}} \quad \ldots\ldots [12]$$

and the problem of determining the optimum viscous coupling between m and M (Fig. 1b) is solved.

When Equation [6] was plotted in the vicinity of the maximum of u, it was very easy also to calculate the imaginary part of the complex root thus

$$v = \frac{\sqrt{3}}{2}\left(-\frac{q}{2} + \sqrt{\frac{p^3}{27} + \frac{q^2}{4}}\right)^{1/3} - \frac{\sqrt{3}}{2}\left(-\frac{q}{2} - \sqrt{\frac{p^3}{27} + \frac{q^2}{4}}\right)^{1/3} \quad \ldots\ldots [13]$$

which is of course the damped angular natural frequency. The logarithmic decrement δ is given by

$$\delta = \frac{2\pi u}{v} \quad \ldots\ldots [14]$$

Accordingly, lines of constant logarithmic decrement can be drawn in Fig. 2 as shown.

SPECIAL CASES

If $m \to \infty$ the system becomes the usual free vibration with damping of a one-degree-of-freedom system. Equation [2] reduces to

$$s^2 + \frac{c}{M}s + \frac{K}{M} = 0 \quad \ldots\ldots [15]$$

and

$$u = -\frac{c}{2M} \qquad v = \sqrt{\omega^2 - \left(\frac{c}{2M}\right)^2}$$

This corresponds to cutting the model in Fig. 3 with the plane $A_2 = 0$. If the model were turned around it would be seen that u rises linearly from the origin with a slope of $1/2$ as indicated by Equation [15], until

$$\omega = \frac{c}{2M}$$

which corresponds to the wedge-shaped void entering the upper left-hand corner of the model, Fig. 3.

The case where $c \to \infty$ corresponds to traveling out the radiating white lines, Fig. 3, which rise first to a maximum and then fall asymptotically to zero.

If $m \to 0$ the damping exponent is zero and the surface in Fig. 3 intersects the A_1A_2-plane along a line having the following slope

$$\frac{A_2}{A_1} = \frac{\omega^2}{1 + \frac{m}{M}} \to \omega^2$$

The limiting condition, where critical damping begins to

occur, may be obtained from Equations [8] and [9]. Writing out Equation [8] gives

$$\frac{c}{M}\left(1+\frac{m}{M}\right)=\sqrt{3}\,\omega$$

Eliminating A_1 between Equations [8] and [9] gives

$$\frac{c}{M}=\frac{\sqrt{3}}{9}\,\omega$$

Combining these two expressions we get $m/M = 8$ as representative of the threshold of critical damping. In other words, critical damping cannot be attained unless $m/M = 8$.

Dashpot Design

In order to design the quill shown in Fig. 1(*a*) it is necessary to know what clearance is proper. Therefore the relation between the dashpot strength c and the radial clearance h must be found. By laboratory tests, an empirical relation between the dashpot strength c, the radial clearance h, the length L, and diameter D of the inertia weight has been determined and was found to be of the form

$$c = K_1\frac{D^a L^\beta}{h^\gamma}$$

where the damping medium is air. It turned out that c varied inversely as $h^{2.75}$ whereas for simple viscous behavior h^3 would be expected. Accordingly, it is reasonable to depict the behavior as shown in Fig. 1(*b*) as primarily viscous.

In these tests a stationary bushing was arranged to engage a plug fastened to the end of a cantilever beam. By tapping the beam and observing its logarithmic decrement, the dashpot strength c could be calculated using the results of Young (4), for various clearances, and for various diameters and lengths of the inertia weight m.

In the case of horizontal rotating quills, it is advisable to keep the radial clearance small. For example, the clearance space around the cylindrical inertia weight could be filled with oil, and the same dashpot strength c obtained but with much greater clearance. By using air, the optimum dashpot strength c is obtained with very much smaller clearance than with oil. This is advantageous because of the effect of centrifugal force on the inertia weight. Due to the combined action of gravity and centrifugal force, the inertia weight tends to center itself in the quill at low speeds. Above a certain speed, centrifugal force overbalances gravity and the weight is pulled to one side and held there, thus becoming inoperative. Fig. 5 shows the relation between the speed and radial clearance at which centrifugal force just balances gravity. The region above the curve is unstable in that the weight is pulled against the side of the hole by centrifugal force. The region below the curve is stable wherein the weight tends to float in the hole. It is seen that the smaller the clearance, the greater the permissible speed and hence the preference for air as a damping medium rather than oil.

Experimental Work

Several quills were set up similar to that in Fig. 1(*a*), and a series of inertia weights were made which fitted the hole in the quill with various radial clearance ranging from 0.00025 in. to 0.0075 in. These weights were successively inserted into the quill, and an oscillogram of the free vibration of the quill was made from which the logarithmic decrements were readily measured. Fig. 4 shows the decrements plotted against radial-plug clearance along with the short vertical lines indicating the

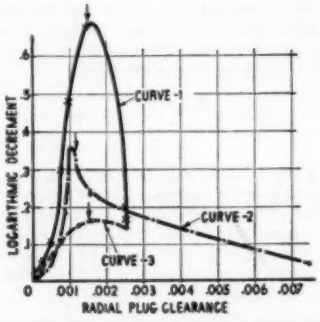

Fig. 4 Curve Showing Variation of Logarithmic Decrement With Plug Clearance; Short Vertical Lines Representing Optimum Clearance as Calculated

(Curve 1, Quill 1¹/₂ in. diam × 6 in. long; inertia weight, 54 g. Curve 2, Quill 1¹/₂ in. diam × 8¹/₂ in. long; inertia weight, 110 g. Curve 3, Quill 1¹/₂ in. diam × 8¹/₂ in. long; inertia weight, 58 g.)

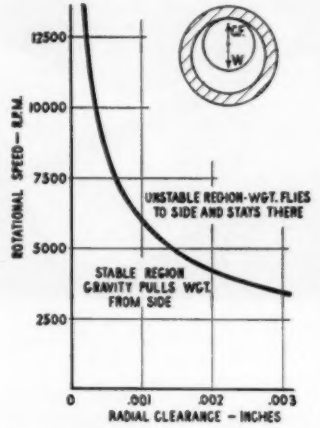

Fig. 5 Relation Between Rotational Speed and Plug Clearance Separating Stable Region From Unstable Region of Operation

calculated value of the optimum clearance as found by the foregoing theory. It is seen that the agreement between calculated and experimental values is fairly good.

Conclusions

Although the theory has been applied to boring quills in this paper, it is believed that it applies equally well for Lanchester dampers which are to be applied to any vibrating structure where the free vibration is to be damped out faster. By measuring the stiffness where the damper is to be attached, and the frequency, the equivalent "lumped-parameter" system is found, and the procedure as outlined may be carried through.

Acknowledgment

The author wishes to express his appreciation to Messrs. R. A. Heald and A. F. Townsend for supporting this work, to Mr. R. C. Griffith for counsel and co-operation in carrying it out, Mr.

P. Backman, Miss Irene Rakauskas also of The Heald Machine Company, and Mr. Henry Esen, student at the Worcester Polytechnic Institute, for their aid in making the numerical calculations and charts.

BIBLIOGRAPHY

1 "The Mechanism of Tool Vibration in the Cutting of Steel," by R. N. Arnold, Proceedings of The Institution of Mechanical Engineers, vol. 154, 1945, pp. 261–284.

2 "Introduction to Non Linear Mechanics," by N. Kryloff and N. Bogoliuboff, Princeton University Press, Princeton, N. J., 1943, p. 5.

"Introduction to Non-Linear Mechanics," by N. Minorsky. Published by J. W. Edwards, Ann Arbor, Mich., 1947.

3 "A Note on the Damped Vibration Absorber," by J. E. Brock, *Journal of Applied Mechanics*, Trans. ASME, vol. 68, 1946, p. A-284.

4 "Vibration of a Beam With Concentrated Mass, Spring and Dashpot," by Dana Young, *Journal of Applied Mechanics*, Trans. ASME, vol. 70, 1948, p. A-71.

Residual Grinding Stresses in Mild Steel

By J. FRISCH[1] and E. G. THOMSEN,[2] BERKELEY, CALIF.

A method for determining residual surface stresses is presented. For their determination, it is necessary to remove small layers from the part which has been bent by the residual stresses in the unrestrained state and to measure the resulting change in deflection and thickness of metal removed. Etching with a weak nitric acid and water solution was found to be a satisfactory method for removing surface metal without introducing additional stresses. Mild-steel bars were ground with a medium-soft grinding wheel in a surface grinder. The depth of surface layer containing residual stresses extended to approximately 0.012 in. to 0.018 in. below the surface for grinding cuts ranging in depth from 0.0003 in. to 0.003 in. The thickness of the layer containing residual stresses increases with increasing depth of grind. The maximum residual stress occurs on the surface and, for all depths of grinds, was considerably above the yield point of the original material. The maximum surface stresses when grinding mild steel within the foregoing range of depth of cut decreases with increasing depth. It is believed that this phenomenon can be explained by the possible partial recrystallization of the surface grains because of the higher surface temperatures obtained with heavy cuts.

Nomenclature

The following nomenclature is used in the paper:

H = height of test bar after grinding, in.
Δh = thickness of any infinitesimal layer, in.
h = distance from ground surface to any layer Δh, in.
h_n = depth of region containing residual stresses, in.
f = total deflection of test bar, in.
Δf = change in deflection, in.
L = one-half distance between knife-edges of deflection-measuring device (Fig. 4), in.
R = radius of curvature, in.
M = bending moment, lb-in.
ΔM = change in bending moment, lb-in.
I = moment of inertia, in.[4]
c = distance from neutral axis to outer fiber, in.
E = modulus of elasticity, psi
σ = total residual stress in any layer Δh, psi
σ' = residual stress in any layer Δh after removal of material above Δh, psi
$\Delta\sigma_N'$ = stress induced due to removal of axial force, psi
$\Delta\sigma_B'$ = stress induced due to removal of bending moment, psi
$1, 2 \ldots m \ldots n$ = subscripts denoting location of layers

Introduction

In many metal-working processes, as, for example, rolling, drawing, and forging, the metal must be deformed permanently to attain the desired shape of the product. Such permanent deformation is called plastic deformation and requires application of loads sufficiently high to overcome the resistance to plastic deformation of the metal. If the deformation process is carried out below the recrystallization temperature of the metal, it will become stronger, requiring increasing loads to sustain plastic deformation during the deformation process. Under these conditions, the metal is said to be work-hardened, and modern theories on plasticity of metals attempt to describe the work-hardened state mathematically in terms of the stress or strain path employed during the deformation process and the work-hardening properties of the metal.

Plastic deformation or permanent deformation is a nonreversible process and, upon release of the forming loads, the part will remain in the deformed state. This is fortunate for it can be readily seen that all forming processes rely on this principle. Associated with plastic deformation, however, is a small elastic deformation, resulting in storage of elastic energy or potential energy during the deformation process. This energy is conservative and, upon release of the forming loads, tends to go to zero, as evidenced by a small change in shape of the deformed part, in practice, known as springback. This elastic energy is a function of the work-hardened state of the metal and increases with increasing work-hardening. If the forming process results in a uniformly work-hardened state throughout the part, the elastic energy is likewise uniformly distributed and reduces to zero upon release of the forming load if the part is unrestrained. The part under these conditions can be considered to be stress-free, except for a slight nonuniformity in the deformed grains or grain boundaries themselves.

While complete relaxation of the stored elastic energy can be visualized in permanently deformed parts, the deformation process is seldom carried out in such a way that the state of work-hardening is uniformly distributed throughout the part. Consequently, the elastic energy distribution is also nonuniform, and the part will not be stress-free when the forming load has been released. These stresses remaining in the part are called residual stresses and, under certain applied loads in service, may lead to failure of the part under conditions normally ascribed as safe when residual stresses are absent. The general detrimental effect of residual stresses, especially when in the form of tensile stresses at surfaces of parts subjected to alternating stressing, is well recognized and much time and effort is expended in stress-relieving parts by thermal treatments or offsetting these tensile stresses by inducing compressive stresses such as in shot-peening.

Machining Stresses

A machining process, whether shaping, milling, turning, or grinding, is essentially a plastic-deformation process. The waste metal is removed in the form of chips, and both the chip and the work surface from which it is removed are severely plastically

[1] Instructor in Engineering Design, University of California. Jun. ASME.

[2] Associate Professor of Mechanical Engineering, University of California.

Contributed by the Production Engineering Division, and the Research Committees on Metal Cutting Data and Bibliography, and Cutting Fluids, and presented at the Fall Meeting, Worcester, Mass., September 19–21, 1950, of The American Society of Mechanical Engineers.

Note: Statements and opinions advanced in papers are to be understood as individual expressions of their authors and not those of the Society. Manuscript received at ASME Headquarters, June 20, 1950. Paper No. 50—F-10.

deformed. Consequently, a portion of the surface is in a state of severe work-hardening which will cause induced stresses in the machined part after the completion of the cutting process. If the shape of the part is such that partial relief of the stresses can occur, the part will warp or spring back, which is a well-known phenomenon observed by the man in the shop.

While it is generally known that machining induces residual stresses in machined parts, they are usually ignored because of lack of information concerning their magnitude. A particular case in point in which machining stresses are disregarded is in the experimental determination of residual stresses by the relaxation method. The usual method employed here involves the removal of successive layers of metal by machining from the stressed part and subsequent calculations of the stresses from the resulting deformations. The investigator in the very process of measuring stresses is, therefore, inducing new stresses of unknown magnitude which may lead to erroneous test data. It is the purpose of this paper to show that, even in the process of taking light cuts by grinding, the residual surface stresses may have a magnitude of two- to threefold the yield-strength value of the virgin material and, since the stressed layer extends an appreciable distance below the machined surface, the residual machining stresses may be of importance.

A survey of the literature reveals that little attention has been given to the problem of residual machining stresses. An exception to this is the experimental work reported by Henriksen (1, 2),[1] which represents a remarkable piece of work on residual machining stresses. The author has investigated a large number of machining conditions employing single-point cutting tools and has found that the residual stresses are quite dependent on the machining processes involved. It is only unfortunate that the results reported by Henriksen are given in terms of force in pounds per unit width of the test piece and are not readily convertible to stress, because of the unknown depth of the stressed layer and the unknown stress distribution in this layer. Henriksen has assumed a uniform stress distribution for some materials and reports a residual stress of 125,000 psi for a machined SAE 1020 steel. Glickman and Stepanov (3) investigated residual stresses, caused by taking heavy grinding cuts, in which the work was severely heated during the grinding process. These investigators used the theory of determination of stresses developed by Davidenkow (4) and Shevadin, which in principle was also adopted by the authors of the present paper.

Glickman and Stepanov found surface stresses in low-carbon steel of the order of 25,000 psi under the condition mentioned. The stresses are very low as compared with the results obtained in the present investigation and probably are due to surface heating and consequent annealing of part of the stressed layer.

Theory of Determination of Residual Stresses

If a straight metallic bar of rectangular cross section is subjected to such loads that stresses are induced in one of its surfaces, the stressed surface of the unrestrained bar will become curved upon release of the load. Furthermore, if the induced stresses are tension stresses and are constant at any particular depth in the stressed layer, the bar will assume a concave curvature of radius R when viewed from the stressed surface. It is the purpose of this section to develop equations for determination of the residual stresses in the bar after release of load, but in the restrained configuration, i.e., the bar is straight, which approaches the condition of a semirigid body with induced surface stresses.

Let the depth of the bar be H, as shown in Fig. 1, and the stressed layer of unknown stress distribution be h_s, then the deflection will be f as measured over a length $2L$ in the central portion of the bar; $2L$ is selected as a length less than the bar length in order to eliminate end effects. If consecutive layers of thickness Δh are removed from the bar until h_s is eliminated completely, it is possible to reconstruct the original stress distribution in this stressed layer from the observed changes in deflection of the bar. The following analysis deals with longitudinal stresses only, and it has been assumed that the effects of possible transverse and thickness stresses, if present, are negligible.

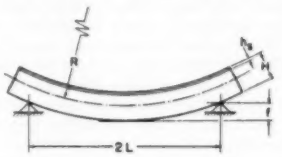

Fig. 1 Configuration of an Initially Straight Bar After Grinding

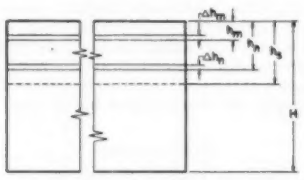

Fig. 2 Location of Layers Δh_m and Δh_n Below Surface of Bar Containing Residual Stresses

Let σ_n be the original stress, in the infinitesimal layer Δh_n, which is n arbitrary infinitesimal layers of thickness Δh below the surface of the original bar. Then σ_n is assumed to be constant throughout the layer Δh_n. If all stressed layers above Δh_n have been removed, the original stress will have changed to σ_n', because of the redistribution of stresses due to the removal of the layers above Δh_n. In order to visualize the effect of the removal of any layer upon the stress σ_n in layer Δh_n, consider the removal of layer Δh_m at depth h_m as shown in Fig. 2. Let σ_m' be the stress in layer Δh_m at the time this layer is removed. The removal of this layer causes two changes upon the stress in Δh_n:

1 A stress $\Delta\sigma_N'$, which is induced because of the removal of an axial force.

2 A stress $\Delta\sigma_B'$, which is induced because of the removal of a bending moment.

Therefore the original stress in layer Δh_n is composed of the stress σ_n' in the layer at the time of its removal plus the sum of the stresses induced in this layer because of the removal of all previous stressed layers. Symbolically this can be written as

$$\sigma_n = \sigma_n' + \sum_{0}^{n-1}(\Delta\sigma_N' + \Delta\sigma_B') \quad \ldots\ldots [1]$$

The stresses $\Delta\sigma_N'$ and $\Delta\sigma_B'$ induced in layer Δh_n when removing Δh_m can be calculated as follows: The axial force released with layer Δh_m is

$$\sigma_m' \Delta h_m = -\Delta\sigma_N'(H - h_m) \quad \ldots\ldots [2]$$

The (—) sign is used because the force removed with the layer

[1] Numbers in parentheses refer to the Bibliography at the end of the paper.

is a tension force which reduces the opposing compression force in the remaining bar. Thus

$$\Delta\sigma_N' = -\sigma_m'\left(\frac{\Delta h_m}{H - h_m}\right) \quad [3]$$

The stress $\Delta\sigma_B'$ can be found from the release of the bending moment given by

$$\Delta\sigma_B' = -\frac{\Delta M_m \times c_n}{I} \quad [4]$$

where

$$\left.\begin{aligned} \Delta M_m &= \sigma_m'\Delta h_m\left(\frac{H - h_m + \Delta h_m}{2}\right) \\ \Delta M_m &= \frac{2E}{L^2}\,\frac{(H - h_m)^3}{12}\,\Delta f_m \end{aligned}\right\} \quad [5]$$

$$c_n = \frac{H - 2h_n + \Delta h_n + h_m}{2} \quad [6]$$

$$I = \frac{(H - h_m)^3}{12} \quad [7]$$

and

ΔM_m = change in bending moment
Δf_m = change in deflection
c_n = moment arm = distance from center of layer Δh_n to neutral axis of remaining bar below it
I = moment of inertia of remaining section
$2L$ = length of bar between knife-edges

A graphical presentation of the foregoing state of stress is shown in Fig. 3.

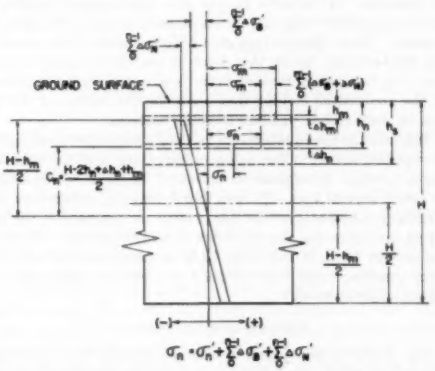

FIG. 3 STATE OF STRESS OF BAR CONTAINING RESIDUAL SURFACE STRESSES AT TIME OF REMOVAL OF LAYER Δh_m

Substituting Equations [5], [6], and [7] into [4] results in

$$\Delta\sigma_B' = -\frac{E}{L^2}(H - 2h_n + \Delta h_n + h_m)\Delta f_m \quad [8]$$

and the original stress in layer Δh_n as given by Equation [1] becomes

$$\sigma_n = \sigma_n' - \sum_0^{n-1}\left[\sigma'\left(\frac{\Delta h}{H - h}\right) + \frac{E}{L^2}(H - 2h_n + \Delta h_n + h)\,\Delta f\right] \quad [9]$$

In order to evaluate σ_n', it is necessary to remove layer Δh_n and to note the resulting change in deflection. The change in moment is given by

$$\left.\begin{aligned} \Delta M_n &= \sigma_n'\Delta h_n\left(\frac{H - h_n + \Delta h_n}{2}\right) = \frac{2E}{L^2}\,\frac{(H - h_n)^3}{12}\,\Delta f_n \\ \sigma_n' &= \frac{E(H - h_n)^3}{3L^2}\left(\frac{\Delta f}{\Delta h}\right)_n\left(1 + \left(\frac{\Delta h_n}{H - h_n}\right)\right) \end{aligned}\right\} \quad [10]$$

Substituting Equation [10] into [9] will give the equation of residual stress in any layer Δh_n, provided Equation [10] is substituted for σ' in Equation [9] by deleting subscripts n. Thus

$$\sigma_n = \frac{E}{L^2}\left[\frac{(H - h_n)^3}{3\left(1 + \frac{\Delta h_n}{H - h_n}\right)}\left(\frac{\Delta f}{\Delta h}\right)_n - (H - 2h_n + \Delta h_n)\,f_{n-1} - \sum_0^{n-1}\left\{\frac{(H - h)^3}{3\left(1 + \frac{\Delta h}{H - \Delta h}\right)}\left(\frac{\Delta f}{\Delta h}\right)\left(\frac{\Delta h}{H - h}\right) + h\,\Delta f\right\}\right] \quad [11]$$

If all stressed layers have been removed and Δh_n was the last layer, then the calculated stress of σ_{n+1} by use of Equation [11] for the layer Δh_{n+1} should reduce to zero. This latter calculation therefore serves as a check on the accuracy of the calculations or experimental technique employed in removing and measuring layers. It is of interest also to note that Equation [11] simplifies considerably if it is desired to obtain the surface stress only. In this case $\Delta h_n = \Delta h_1$ is the first layer, $h_n = \Delta h_1$ and f_{n-1} is zero, thus Equation [11] reduces to

$$\sigma_1 = \frac{E}{3L^2}\left(\frac{H^3}{1 + \frac{\Delta h_1}{H - \Delta h_1}}\right)\left(\frac{\Delta f}{\Delta h}\right)_1 \quad [12]$$

The stress in this first layer can be obtained with precision by obtaining the slope of the deflection versus depth-of-layer curve at the surface and letting $\Delta h \to 0$, thus

$$\sigma_1 = \frac{E}{3}\left(\frac{H^3}{L^2}\right)\left(\frac{df}{dh}\right)_{\text{surface}} \quad [13]$$

where

$\left(\frac{df}{dh}\right)_{\text{surface}}$ = slope of deflection as a function of depth of layer at $h = 0$, or surface of bar

EXPERIMENTAL TECHNIQUE

The specimens for this investigation were machined from $^1/_8$-in. × 1-in. SAE 1020 hot-rolled bars having a yield strength and tensile strength of 38,000 psi and 59,000 psi, respectively. These bars were cut in 12-in. lengths and machined all over to $^1/_8$-in. × $^3/_8$-in. cross sections, leaving approximately 0.005 in. on all sides as grinding allowance. After machining, the bars were given a full annealing treatment at 1600 F in an electric furnace, followed by a careful surface-grinding operation on all sides of the specimens. The depth of grind for any pass was kept below 0.0005 in. in order to minimize distortion from grinding, and it was necessary to take alternate cuts on opposite surfaces in order to obtain a straight bar. The surface grinding was followed by another full anneal at 1600 F in a hydrogen-atmosphere furnace in order to eliminate surface scaling during annealing. The 12-hr cooling period in this furnace provided essentially

stress-free bars as was ascertained by etching one surface of several bars which resulted in no observable deflection.

One bar at a time was placed on a carefully ground magnetic chuck of a Thompson surface grinder. The grinding wheel (3/4 in. wide × 12 in. diam) was a Norton alundum wheel of medium grain size, grade, and structure with a vitrified bond (specification No. 38A46-J8VBE). The spindle speed of the grinder was 1800 rpm, and the grinder was allowed to come to operating temperature by letting it run for 1 hr before commencing the experiment. The grinding wheel was dressed with a diamond dresser for each specimen in order to assure constant cutting conditions.

Before grinding the specimens were measured in a supermicrometer to an accuracy of 0.0001 in., and the initial deflection was recorded in the deflection-measuring device shown in Fig. 4.

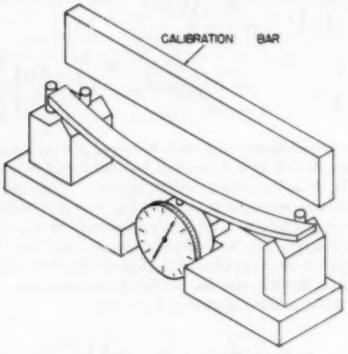

FIG. 4 DEFLECTION MEASURING DEVICE

Deflection measurements were obtained with a dial gage having a least count of 0.0001 in. The table feed of the grinder was set to an approximate value of 30 fpm and was kept constant for all tests. The depths of cut ranged from 0.0003 in. to 0.003 in. and were determined from measurements of the bar after the grinding operation. The grinding cuts consisted of one cut on the forward movement of the table, grinding approximately one half of the 3/4-in. width of the test bar and removing the remainder on the next forward motion. An adequate flow of Cimcool (1:100) cutting fluid was maintained over the work during the grinding operation.

After grinding, the specimens were cleaned thoroughly, the thickness was measured at 1-in. intervals throughout their length, and the initial deflection was obtained on the deflection-measuring device. Care was exercised in performing all measurements at approximately the same temperature, in order to minimize errors in measurements resulting from temperature changes.

The original stress distribution of the stressed layer below the ground surface can be calculated from Equation [11] for all depths, providing the change in deflection resulting from the removal of each layer is known. In order to remove these layers, without inducing additional stresses, it was decided to use an etching technique. The ground surface was kept moist with a freshly made acid solution of 5 to 15 per cent nitric acid in distilled water at atmospheric temperature, by applying the etchant constantly with a cotton swab. Layers of the order of a few 0.0001 in. at a time were removed in this fashion, and the change in deflection and the remaining thickness of the bar were measured after each etch. When all stressed layers were removed, the specimen returned to its original shape before grinding. Several additional layers removed after this resulted in no change in deflection and indicated that the bar was stress-free.

Several typical deflection curves as a function of depth of layers removed for several grinding conditions are shown in Fig. 5. The first point on each curve at zero depth of etch represents the deflection of an originally straight bar having been deformed by grinding. The deflection is zero when the entire stressed layer has been removed, i.e., the bar has assumed initial configuration

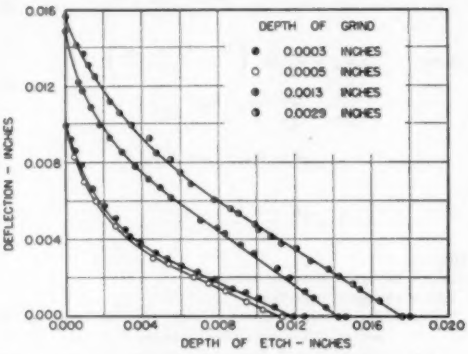

FIG. 5 CURVES SHOWING DEFLECTION OF MILD-STEEL GROUND BARS AS A FUNCTION OF DEPTH OF ETCH

before grinding. It may be noted that the deflection f as used in Equation [11] is taken as zero after grinding and reaches its maximum value when the entire stressed layer h_1 has been removed. While these curves give definite values of the depth of the total stressed layers, they must be considered as approximate only, for the actual stressed layer is somewhat greater because of the preferential etching that occurs on the surface of the test bar for deep etches, yielding irregular surfaces.

Inasmuch as the equations for residual stresses previously given are applicable only if the radius of curvature R of the deformed bar is constant throughout its measured length, it was necessary to check several bars. It was found that the radius was substantially constant over the bar, except for the ends of the bar, where the radius was approximately 4 per cent greater. By using the central 10 in. of the 12-in. bars for measurements only, the error resulting from nonconstancy of radius of curvature was substantially reduced.

RESULTS AND DISCUSSION

Fig. 6 shows the results of a stress analysis for two cutting conditions. The stresses were calculated by inserting the necessary quantities, evaluated from the experimental curves in Fig. 5, into Equation [11]. The introduction of experimental errors into the calculated stresses was minimized by using the faired curves drawn through the experimental points. It is evident from this figure that the surface stress induced by grinding is appreciably above the original yield point of the material, thus indicating considerable cold work. Furthermore, the depth of the deformed layer is larger than the thickness of the metal removed by grinding, thus indicating that an appreciable amount of deformation work in metal cutting may go into the workpiece itself. This fact has been neglected in analyses on chip formation in metal cutting (5, 6), but should be incorporated in future theoretical refinements.

The dependence of the depth of the stressed layer on the depth of grind is shown in Fig. 7. Heavier cuts than 0.003 in. per pass

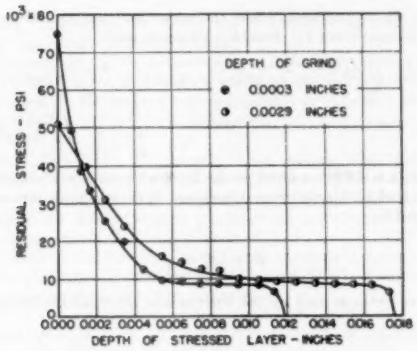

FIG. 6 RESIDUAL-STRESS DISTRIBUTION BELOW GROUND SURFACE OF MILD-STEEL BARS

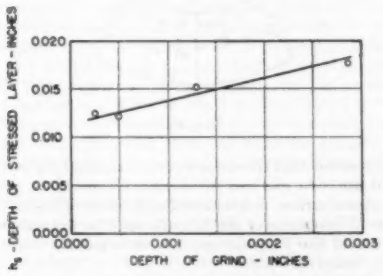

FIG. 7 INFLUENCE OF DEPTH OF GRIND ON DEPTH OF SURFACE LAYER OF MILD-STEEL BARS CONTAINING RESIDUAL STRESSES

were not deemed advisable for the workpiece became slightly blued, indicating that a momentary high surface temperature existed on the surface in spite of ample cooling with a cutting fluid. The experimental range of depth of cut therefore was not wide enough to determine at what depth of cut the thickness of the deformed layer becomes constant.

The maximum surface stresses resulting from various depths of grind are given in Fig. 8. These stresses were calculated by introducing the experimentally determined initial slopes of the deflection versus depth-of-etch curves into Equation [13]. The determination of these slopes can be established quite accurately by etching a few layers from the specimens and plotting the resulting changes of deflection as a function of thickness of metal removed. While it would be possible in theory to establish this slope by the removal of a single infinitesimal layer, in practice it is advisable to remove several layers, for it is difficult to ascertain the precise thickness of the layer removed.

The experimental points in Fig. 8, through which a solid curve was drawn, were obtained with the experimental procedure of dressing the grinding wheel between each grind and grinding in one direction only, as outlined previously. It is seen that the maximum surface stress decreases with increasing depth of grind. This in part can be explained by the greater surface heating obtained with deep cuts, resulting in possible partial recrystallization of the deformed grains.

It is of interest to note that two additional experimental points plotted in Fig 8 do not conform to the general trend described in the foregoing. The experimental procedure was varied by grinding one half of the surface of the specimen on the forward stroke of the table and the remainder on the return stroke. It appears from this that grinding sequences may have an important influence on the magnitude of the induced stresses.

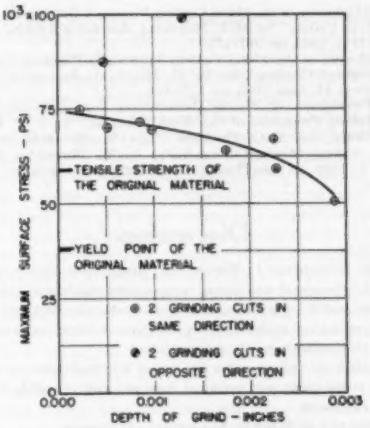

FIG. 8 MAXIMUM SURFACE STRESS INDUCED BY GRINDING MILD-STEEL BARS FOR VARIOUS DEPTHS OF GRIND

CONCLUSIONS

1 Grinding mild steel, SAE 1020, to a depth of 0.0003 to 0.003 in. in a surface-grinding operation resulted in maximum surface stresses well above the original yield point of the material.

2 The maximum surface stresses are smaller for heavy cuts than for light cuts.

3 The depth of the surface layer of the work deformed by grinding increases with the depth of cut.

4 The thickness of the surface layer of the work deformed by grinding is appreciably greater than the thickness of metal removed in the grinding process.

5 The maximum surface stresses can be calculated simply by the equations developed in this paper and the experimentally determined initial slopes of the deflection as a function of depth of etch curves.

6 Etching specimens with a 5 to 20 per cent nitric acid in water etchant is a satisfactory method of eliminating surface layers on mild steel without inducing new stresses.

7 The determination of the total depth of a deformed surface layer by grinding requires a large number of etches and results in a roughened final surface. Residual stresses and depth of deformed metal of the work material in consequence of this will be somewhat in error near the bottom of this layer when determined by the technique described in this paper.

BIBLIOGRAPHY

1 "Zerspannung und Eigenspannung," by E. K. Henriksen, Ingeniorvidenskabelige Skrifter, Copenhagen, Denmark, 1937.

2 "Residual Stresses in Machined Surfaces," by E. K. Henriksen, Trans. Danish Academy of Technical Sciences, No. 7 Copenhagen, Denmark, 1948.

3 "Residual Stresses Caused by Grinding," by L. A. Glickman and V. A. Stepanov, *Journal of Technical Physics*, USSR, vol. 16, 1946, pp. 791–802.

4 "A Study of Residual Stresses Due to Bending," by N. N. Davidenkow and E. M. Shevadin, *Journal of Technical Physics*, USSR, vol. 9, 1939, pp. 1112–1124.

5 "Mechanics of the Metal Cutting Process, I Orthogonal Cutting and a Type 2 Chip," by M. E. Merchant, *Journal of Applied Physics*, vol. 16, May, 1945, pp. 267–275.

"Mechanics of the Metal Cutting Process, II Plasticity Condition in Orthogonal Cutting," by M. E. Merchant, *Journal of Applied Physics*, vol. 16, June, 1945, pp. 318–324.

6 "Correlation of Plastic Deformation During Metal Cutting With Tensile Properties of the Work Material," by J. T. Lapsely, R. C. Grassi, and E. G. Thomsen, Paper No. 49—A-21, presented at the Annual Meeting, New York, N. Y., November 27–December 2, 1949, of THE AMERICAN SOCIETY OF MECHANICAL ENGINEERS.

Discussion

E. K. HENRIKSEN.[4] The writer, presumably being the first who ever measured machining stresses and emphasized their significance and detrimental effects, must, naturally, feel very happy by the widening understanding for this subject, as witnessed, among other things, by the present paper.

The authors' reference to the writer's introduction of the resultant stress value p in terms of force per unit of width, calls for a brief comment.

The use of p in lb per in. has several advantages:

(*a*) It constitutes directly the correction for machining stresses required when using the relaxation method for experimental determination of residual stresses in general.

(*b*) It gives a resultant value for the total stress-inducing effect of any cutting method.

(*c*) Its determination does not require any long time, and this enables the investigator to cover a larger area in a given time.

(*d*) It allows a direct comparison between the stress-inducing effect of various methods and conditions of cutting.

The writer's assumption of a uniform stress distribution over the work-hardened layer is tentative only, just for obtaining a simple approximation, and it is easy to see how the results would be changed if a somewhat different stress distribution were to be considered.

There is reason to point out that the method of stress analysis given by Davidenkow and Shevadin and used by the authors, is incomplete, because it does not give the values of the stresses over the cross section outside of the work-hardened layer (see accompanying Fig. 9, or the writer's previous work[5,6,7]). The

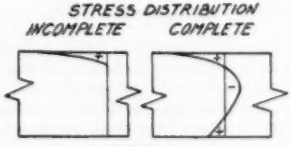

FIG. 9

first complete solution to this problem is presumably the one given by F. Staeblein[8] who developed his formula by calculus methods (the reader is warned of a misprint in the original text on page 92, 2nd column, where the upper limits of two integrals should read d, not δ). Staeblein's formula reads

$$\sigma(x) = \frac{x^3}{6}\frac{d_K(x)}{dx} + \frac{2}{3}x\,[K(x) - K(d)] + \frac{d-x}{3}K(d) - \frac{1}{3}\int_x^d K(\lambda)d(\lambda)$$

where x is the co-ordinate to the layer with stress $\sigma(x)$ (see Fig. 10 herewith), d is the original thickness, K is a curvature function, defined by

$$K = kE = \frac{E}{R}$$

The methods used by the authors and the Staeblein formula

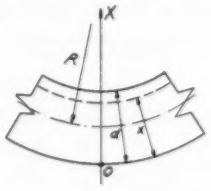

FIG. 10

have in common that the stresses are determined by a curvature versus depth curve and that the stress in the first layer, adjacent to the original surface, is determined by the slope of this curve.

In the development of the formulas used by the authors, the writer would like to point out two discrepancies which, fortunately, cancel each other.

When σ_n is the original stress in the nth layer, and σ_n' is the final stress in the same layer, just before its removal, and $\Delta\sigma_N'$ and $\Delta\sigma_B'$ the stresses induced by the removal of previous layers, then we must have

$$\sigma_n' = \sigma_n + \sum_0^{n-1}(\Delta\sigma_N' + \Delta\sigma_B') \quad \ldots\ldots\ldots [14]$$

Further we must have

$$\sigma_m'\Delta h_m = \Delta\sigma_N'(H - h_m) \quad \ldots\ldots\ldots [15]$$

because the removal of an axial tensile stress σ_m' must induce a new tensile stress σ_N' (which is the same as a reduction of a compressing force).

It is of some interest to compare the authors' findings with those of the writer. From the curves in Fig. 6 of the paper the writer has computed the following resultant stress values p:

Depth of cut, in.	Resultant stress value p, lb per in.
0.0003	212
0.0029	300

i.e., a heavier cut induces a higher resultant stress. These values are considerably below those found by the writer for square-end tools, but they are of the same order of magnitude as found generally for side-cutting tools during good cutting conditions.

Consequently, when using the relaxation method for determining residual stresses in general, it is doubtful whether there is anything gained by grinding.

The maximum stress σ as found by the authors, amounting to 50,000–75,000 psi, is below the values published by the writer

[4] Professor in Charge, Department of Material Processing, Sibley School of Mechanical Engineering, Cornell University, Ithaca, N. Y. Mem. ASME.

[5] Authors' Bibliography (1), Fig. 7.

[6] Authors' Bibliography (2), Fig. 9.

[7] "Residual Stresses in Machined Surfaces," by E. K. Henriksen, Paper No. 50—SA-27, presented at the June, 1950, meeting, St. Louis, Mo., of THE AMERICAN SOCIETY OF MECHANICAL ENGINEERS, Fig. 7.

[8] "Spannungsmessungen an einseitig abgeloeschter Knueppeln," by F. Staeblein, *Kruppsche Monatshefte*, vol. 12, 1931, pp. 93–99.

(round 100,000 psi), except for the special grinding procedure using two cuts in opposite directions.

The depth of the stress-carrying layer, as found by the authors (0.012–0.018 in.) is well above some of the values (0.002–0.005 in.) listed by the writer,[9] but considerably below other values (round 0.05 in. as found by T. G. Digges).

H. R. Letner.[10] The account of the authors' research is of particular interest to the Industrial Fellowship on Grinding Wheels at Mellon Institute which has been conducting a similar study of the residual stresses resulting from grinding. Most of our measurements have been made on 2-in. × 2-in. × $^1/_4$-in. specimens of an oil-hardening tool steel having a nominal composition of 0.90 C, 1.25 Mn, 0.50 Cr, and 0.50 W. Deflections are measured by optical interferometry.

There are many points of agreement between the data presented by the authors and our own. For example, in a particular surface-grinding operation on annealed specimens, using a wheel of the same grit and grade as the authors', operating at a peripheral speed of 6000 fpm, and employing a work speed of 50 fpm, a cross-feed of 0.050 in. at each end of the table traverse and no cutting fluid, residual curvatures parallel to traverse are obtained which correspond to the same range of deflections shown in Fig. 5 of the paper. As a result of the same grinding operation, the depth of the stressed layer is found to increase in a regular fashion from 0.003 in. for a depth of cut of 0.0005 in. to 0.014 in. for a cut of 0.0031 in. While this is a slightly greater spread of values than that shown in Fig. 7 for a similar range of unit downfeeds, the results completely substantiate the authors' conclusion that the thickness of the deformed layer is appreciably greater than the depth of cut.

We have used both machine lapping and chemical etching in a 5 per cent solution of concentrated nitric acid in ethyl alcohol to remove thin layers of the ground surfaces. Data obtained by the latter method resemble those in Fig. 5 which, incidentally, show the self-consistency characteristic of carefully made measurements; however, there is one point of departure. We have never experienced the sharp discontinuities exhibited by the curves in Fig. 5 as they approach the abscissa. Instead, our curves have either reached or approached a minimum in a smooth fashion. This causes the first term in Equation [11] of the paper to approach zero smoothly. As a result, the residual-stress curves similar to those in Fig. 6, level off at slightly negative (compressive) values as indeed they must in order to maintain equilibrium of forces in the bar. Ideally, the curves in Fig. 5 should approach the abscissa asymptotically. Practically, small errors in the zero correction for intitial deflection prior to grinding or small amounts of residual stress left by the mechanical and thermal preparation of the specimen can cause the curves to reach a minimum either slightly above or slightly below the axis. Since it is the slope of the curve and not the actual value of the deflection which is important in determining the residual stress by means of Equation [11], this departure from ideal behavior, if not too large, does not have a serious effect on the calculated stress.

M. C. Shaw.[11] The authors have presented a very interesting picture of the residual stresses encountered when annealed mild steel is ground. The observed decrease in the surface stress with increased wheel depth of cut is particularly interesting. While greater instantaneous temperatures are actually reached with the larger depths of cut, it is questionable whether this increased surface temperature could produce recrystallization and thus account for the smaller surface stresses. The temperature gradient extending from the ground surface into the workpiece is very great, and the temperature of the work surface will fall to the bulk temperature of the work in a fraction of a second after a cut is taken. Inasmuch as recrystallization is a time-temperature reaction, it seems unlikely that the surface temperature will remain at a sufficiently high level for the necessary time to enable appreciable recrystallization to occur. The observed phenomen might alternately be explained in terms of the size effect. As the layer of metal removed in a cutting operation decreases in depth, the mean shear stress on the shear plane is observed to increase. This effect is particularly pronounced in the case of grinding where the slope of the shear stress - depth of cut curve becomes very steep. For example, we have observed[12] the following shear strengths for mild-steel at depths of cut of 500, 200, and 20 μ in., respectively: 0.13×10^6, 0.21×10^6, and 1.9×10^6 psi. The actual grit depths of cut corresponding to the wheel depths of the data points in Fig. 8 of the paper, range from about 80 to 450 μ in. It is thus evident that the shear stresses involved in the lighter cuts were many times as great as those in the heavier cuts, and this could well account for the greater surface residual stresses observed with the lighter cuts. The relatively low surface stress reported by Glickman and Stepanov[13] was obtained under very severe grinding conditions and may be explained by the correspondingly low value of shear stress that would be involved in chip formation under such circumstances.

In a surface-grinding operation of the type described in this paper, severe grinding conditions may be achieved at a relatively large wheel depth of cut and small table speed, or a high table speed and relatively small depth of cut, or combinations of these two conditions. The actual mean grit depth of cut is the controlling variable responsible for the degree of severity of a grinding condition and hence is a better variable to use when presenting grinding data than the wheel depth of cut.

The fact that surface stresses in excess of the bulk yield point of a material are found in grinding and other machining operations is another observation which indicates that metals in thin layers have entirely different properties from those of the same metal in bulk. The yield stress of a metal in a given condition is not a material constant in the sense that Young's modulus of elasticity is, but depends upon the size of the specimen. For engineering structures of ordinary size, the variation in yield stress with the size of the structure is negligible. However, when thin layers of metal are involved, the variation in yield stress with specimen thickness is great. If this were not so, it would not be possible to obtain surface stresses of the order of twice the bulk yield point of the material as shown in Fig. 8. If the yield stress were constant for metal layers of all thickness, the metal in the surface would flow plastically until the stress dropped to the bulk yield stress. Actually, the surface stress is probably relieved by plastic flow in this manner but only until it reaches the yield stress for a layer of the appropriate thickness.

Fig. 6 of the paper may thus be used to estimate the thickness of a layer which just exhibits the bulk yield stress by noting the thickness for which the residual stress is equal to the bulk yield stress. This is seen to correspond to a layer of about 0.003 in. in Fig. 6. Thus it might be concluded that the metal in the outer 0.003 in. is stressed to the yield point of the metal for the corresponding thickness (which yield point varies with thickness approximately as shown by the curves in Fig. 6 up to

[9] Authors' Bibliography (2), pp. 86–87.

[10] Fellow, Mellon Institute of Industrial Research, University of Pittsburgh, Pittsburgh, Pa.

[11] Associate Professor of Mechanical Engineering, Massachusetts Institute of Technology, Cambridge, Mass. Mem. ASME.

[12] These tests will be described in detail in a forthcoming ASME paper.

[13] Authors' Bibliography (3).

0.003 in.); the metal below this level has residual stresses which are less than the local yield stress of the metal. While the presence of surface stresses in excess of the tensile strength of the metal in bulk is initially a startling observation, which suggests that great damage has been rendered by the responsible machining process, the situation is seen to be far less drastic when it is realized that these high surface stresses correspond to the yield stress of the metal for the appropriate thickness. Nevertheless, the presence of surface tensile stresses near the yield point can seriously affect the life of a part which is used under conditions that enable cracks to grow from the surface as in the case of cyclically loaded specimens and those subjected to a corrosive atmosphere.

While the authors have shown clearly that the etching technique employed did not introduce extraneous stress in the case of the thoroughly annealed specimen of low-carbon steel, we cannot be certain that stresses were not introduced when the same material was etched in the presence of a substantial stress gradient at the surface. There is no apparent way of separating the grinding stresses from those which may have been introduced by the etching technique. In this connection, a general note of warning regarding the use of the etch method of removing layers may be in order. Lihl[14] has extensively studied the stress introduced into a surface when layers are removed by etching with acids. The back reflection x-ray technique was employed in this work using a cobalt anode and powdered gold as a calibrating material. In the specimens used, there was no stress gradient at the surface. It was found that the stress introduced by the acid was always compressive in nature and was generally from 10,000 to 20,000 psi. The amount of stress introduced increased with the hardness of the specimen and the alloy content. Stress was produced regardless of the concentration of the acid used and whether or not an electric current was passed. In the case of electrolytic polishing, the etching stress decreased with increased current density. Lihl's explanation of these compressive etch stresses involves an increase in volume associated with the solution of the materials which normally precipitate in the grain boundaries of steel. This explanation is in agreement with the observed increase in magnitude of the etch stress with degree of heat-treatment and decreased grain size, and also the observed absence of etch stresses with pure electrolytic iron. Assur, Davidenkow, and Terminasov[15] have also reported the absence of etch stresses in annealed pure aluminum.

From the foregoing brief discussion of etch stresses, two observations might be made: (1) The introduction of compressive etch stresses of from 10,000 to 20,000 psi are to be expected with heat-treated steel specimens, and such stresses should certainly be taken into account if the work reported is to be extended in this direction, which is of considerably greater industrial interest than the grinding of thoroughly annealed material. (2) A method of ascertaining the influence of a high surface stress upon the production of etch stresses is still to be found and until then, we cannot be sure that etching does not introduce stress in the presence of a stress gradient even though the material in bulk is thoroughly annealed and exhibits no etch stress in the absence of surface stress.

L. P. Tarasov.[16] The procedure employed and the results obtained in this painstaking study of grinding stresses will be of great interest to those concerned with the physical effects of various types of machining processes. Since very little information has been published on grinding stresses, these results will be widely quoted and hence it is important to determine whether the conclusions drawn by the authors are valid over a wide range of grinding conditions or are more or less restricted to the particular conditions used in their work.

Several years ago, we obtained some curvature data which can be used to examine this point. Some of the experimental conditions were quite different from those of this paper, as can be seen from the following tabulation:

	Frisch and and Thomsen	Tarasov
Test bar:		
Material	SAE 1020	Oil-hardening tool steel
Hardness	Soft (annealed)	Hard (Rockwell C60)
Length	12 in.	6 in.
Width	3/4 in.	7/8 in.
Thickness	0.24 in.	0.18 to 0.13 in.
Wheel:		
Specification	38A46-J8VBE	38A46-J8VBE
Diameter	12 in.	8 in.
Width	3/4 in.	1/2 in.
Surface speed	5650 sfpm	6000 sfpm
Grinding conditions:		
Unit down-feed	0.0003 to 0.0029 in.	0.0001 to 0.0020 in.
Unit cross-feed	3/4 in., at end of of forward stroke	0.050 in., at end of each stroke
Table speed	30 fpm	60 fpm
Type of grinding	Wet	Dry

The differences in test conditions most likely to be important from the standpoint of the results were the hardness of the test bars and the unit cross-feed. Some subsidiary experiments showed that the nature of our results was not affected by changing from dry to wet grinding.

Before a test bar was ground, the wheel was diamond-dressed so as to leave it in a fairly sharp condition. Successive layers were then ground off at a unit downfeed which was kept the same for a given test bar. The deflection was measured prior to grinding and then after each layer was ground off, in a manner similar to that used by the authors. The deflections were corrected when necessary for any slight deflection that may have been present prior to grinding, and they were then recalculated to give the equivalent deflection for a strip with an effective length of 10 in. and a thickness of 0.240 in. Thus our deflection data can be compared directly with those in the paper.

It can be seen from Fig. 11 of this discussion that the deflections after each of the first few downfeeds varied in an unpredictable manner, and that the deflections became reasonably constant only after several consecutive downfeeds following dressing. Experience has shown us that a freshly dressed wheel face may be in a very unstable condition so that any grinding data obtained immediately after dressing may be unreliable, regardless of whether the data are for strip curvature or for some other variable, like wheel wear. For this reason we have generally found it necessary to do a certain amount of preliminary grinding after dressing, before starting the test run.

Accordingly, the average deflection for a given unit downfeed was obtained only from those measurements which were reasonably consistent with each other, i.e., after the first few downfeeds. These average deflections are plotted against unit downfeed in Fig. 12, herewith, the values being shown as hollow circles. The two duplicate points shown were obtained with additional test strips. All the points lie very close to a straight line passing near the origin.

The comparable curve for the authors' data, passing through

[14] "Changes in the State of Stress of Metal Surfaces as a Result of Etching," by F. Lihl, *Archiv. fur Metallkunde*, vol. 1, 1946, p. 16.

[15] "Residual Stresses in Straight Tension," by E. L. Assur, N. N. Davidenkow, and Y. S. Terminasov, *Journal of Technical Physics* (USSR), vol. 19, 1949, p. 1107.

[16] Norton Company Research Laboratories, Worcester, Mass.

the solid circles, was obtained from the deflections prior to etching as given in Fig. 5 of the paper. This curve, unlike ours, does not go anywhere near zero deflection, the lowest value being just

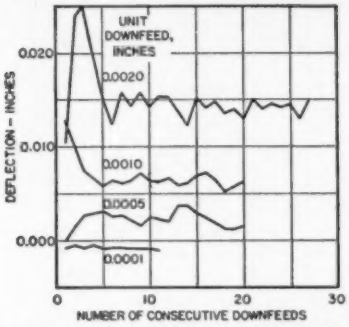

FIG. 11 DEFLECTION OF TEST BAR FOR VARIOUS UNIT DOWNFEEDS AS FUNCTION OF NUMBER OF DOWNFEEDS AFTER WHEEL WAS DRESSED

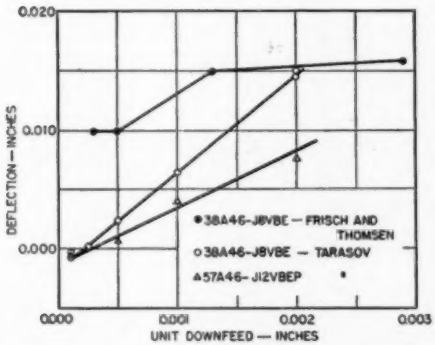

FIG. 12 EFFECT OF UNIT DOWNFEED UPON DEFLECTION OF TEST BAR

under 0.010 in. The marked difference between the two curves can be attributed only to the considerable differences in experimental conditions. The fact that authors obtained such high deflections even with the lowest downfeeds is perhaps due to the combined use of a wheel which had just been dressed and of a very large unit cross-feed. This combination may well have resulted in a dull wheel face which would give rise to a much higher deflection than would a sharp wheel. Whether this is the correct explanation would have to be determined by further experimentation. In our own case, where the unit cross-feed was much smaller and the steel was hard, the deflection was very low at the smallest unit downfeeds even when the wheel was freshly dressed.

There is considerable evidence to corroborate our belief that the deflection normally approaches zero as the grinding conditions are made progressively more gentle (as by decreasing the unit downfeed), and that the authors' results, wherein the deflection still remains high when the unit downfeed is made very low, are due to a special set of circumstances. For example, the line passing through the triangles in our Fig. 12 shows that similar results were obtained when we used a 57A46-J12VBEP wheel in place of the 38A46-J8VBE wheel previously discussed. We have other data which show that when the unit downfeed is kept the same, the deflection decreases toward zero as progressively softer wheels are used. All this is in accord with well-established practical experience that to grind a thin strip flat it is necessary to use gentle grinding conditions. To put it another way, were high deflections normal for very small unit downfeeds, it would be difficult indeed to grind thin stock flat.

Since the authors' deflection data appear to be valid only for their experimental conditions, it follows that the stress values which they have computed may be similarly limited in their applicability. When grinding conditions are such as to lead to far lower deflections than the authors happened to attain, we suspect that the stressed layer would be considerably shallower than indicated in Fig. 7 of the paper, and that the maximum surface stress would be correspondingly lower than shown in Fig. 8. The data presented in this paper are not sufficient to warrant the conclusion that maximum surface stresses are smaller for heavy cuts than for light cuts, unless this statement is restricted to the particular grinding conditions that were used. Only further experimentation, which we hope the authors will be in a position to undertake, will show the extent to which the authors' conclusions about the magnitudes and depths of grinding stresses can be generalized.

AUTHORS' CLOSURE

The authors wish to express their appreciation for the interest shown in the paper by Professor Henriksen, Dr. Letner, Professor Shaw, and Dr. Tarasov.

Professor Henriksen points out that the stress analysis neglects the stress in the bar which was not work hardened. This is not the case, for Equation [11] is general and gives the stress in any layer of the entire cross section of the bar. Furthermore, the objection to the plus sign in Equation [1] is not warranted inasmuch as Equation [1] is a general algebraic equation giving the state of stress in any layer n providing the proper interpretation of sign is given to $\Delta\sigma_N'$.

The authors are appreciative to know that Dr. Letner's results on grinding although obtained with different materials are in qualitative agreement with the data reported in this paper. The authors agree with Dr. Letner that the curve of deflection as a function of layers removed should approach the abscissa asymptotically, but presently cannot account for this nonideal behavior of the material.

The authors do not fully agree with Professor Shaw in his interpretation of the effect of size of chip removed on the residual stress in the work surface, for it is in disagreement with the results reported by Henriksen (2). Henriksen showed that the residual stress in terms of force p (lb per unit width) was practically independent of size of chip removed in machining with a single-point cutting tool. While the force p is not directly related to the residual stress in the deformed layer because of the unknown stress distribution and the depth of this layer containing the stress, the authors believe that these results are at least qualitatively correct.

The authors further believe that the original yield point (or bulk yield point) of the work material does not apply to the deformed layer inasmuch as it has been modified by the process of plastic deformation. Consequently it is presently impossible to separate the influence of size of chip removed and plastic deformation of the work material on the residual stress.

The authors agree with Professor Shaw that etching stresses may be induced during the process of removing layers from the surface of the work piece, but do not believe that the effect of these induced stresses would be great since the thickness of such

layers containing etching stresses would be of the order of magnitude of the grain size of the material.

The authors agree with Dr. Tarasov that their test conditions do not necessarily conform to grinding practice and the stresses shown in the paper may not be obtained in practice. The results show, however, the importance of proper wheel dressing, correct wheel selection, etc., in grinding in order to minimize residual stresses in the workpiece.

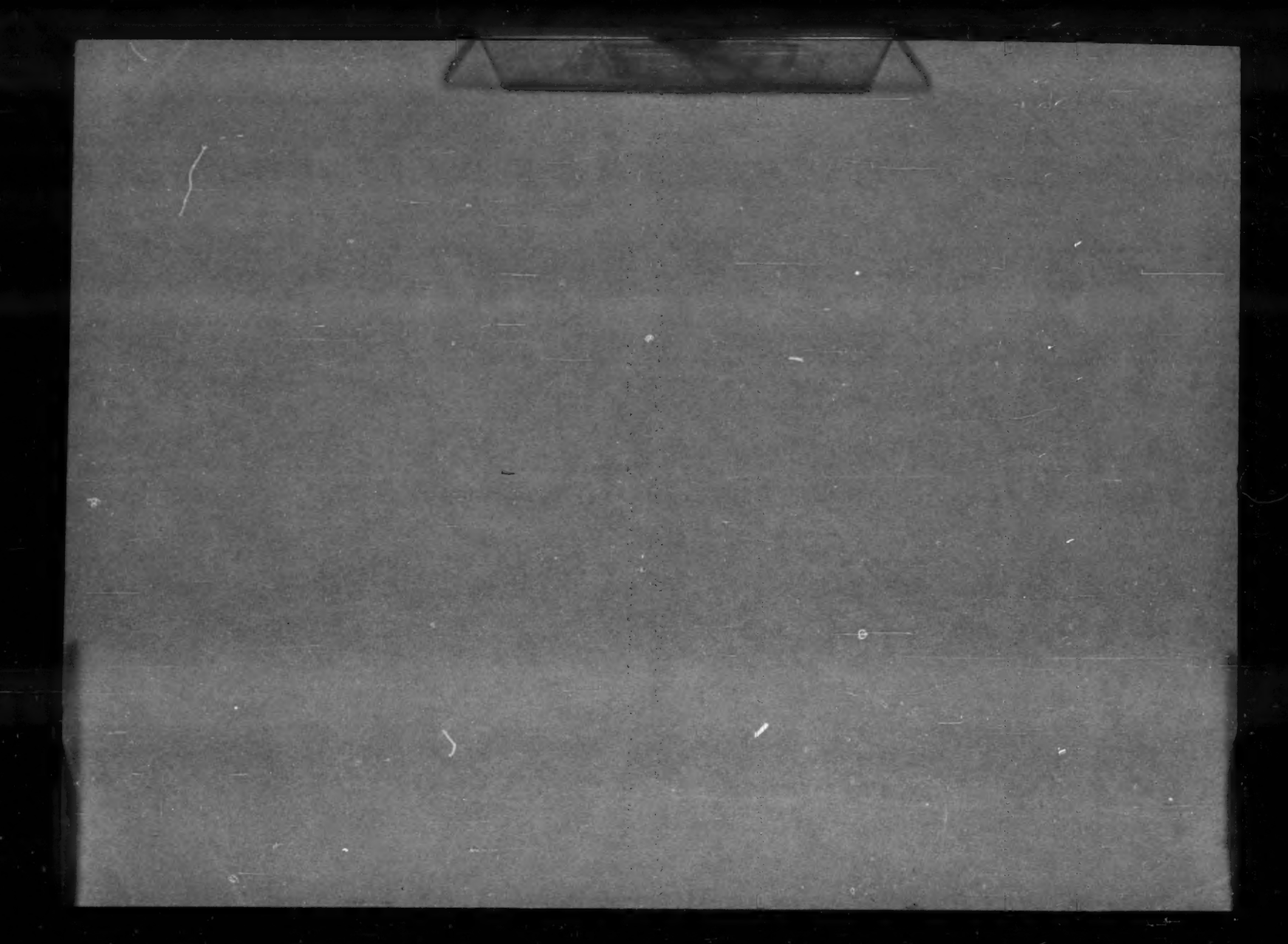

AN ASME PAPER

Its Preparation, Submission and Publication, and Presentation

To a large degree the papers prepared and presented under the ASME sponsorship are evidence by which its professional standing and leadership are judged. It follows, therefore, that to qualify for ASME sponsorship, a paper must not only present suitable subject matter, but it must be well written and conform to recognized standards of good English and literary style.

The pamphlet on "AN ASME PAPER" is designed to aid authors in meeting these requirements and to acquaint them with rules of the Society relating to the preparation and submission of manuscripts and accompanying illustrations. It also includes suggestions for the presentation of papers before Society meetings.

CONTENTS

Price 35¢. No discount allowed. *A remittance must accompany all orders for $2.00 or less. U.S. Postage Stamps are acceptable.*

THE AMERICAN SOCIETY OF MECHANICAL ENGINEERS
29 West 39th Street, New York 18, N. Y.